SLIDING WEAR OF NITRIDED STEELS

A thesis submitted for the degree of
Doctor of Philosophy

by

Hirotaka Kato

Department of Materials Technology,
Brunel University

August 1993

ABSTRACT

The unlubricated sliding wear behaviour of gas nitrided, plasma nitrided, and ferritic nitrocarburized BS970,905M39 (EN41B) steels was investigated systematically from an engineering point of view. Commercial nitriding processes were employed, and the wear studies were carried out using a pin-on-disc machine over a wide range of sliding speeds and applied loads. The worn specimens and wear debris were examined by several techniques; including optical and electron microscopy and X-ray analysis.

A sharp wear rate transition between mild and severe regimes was identified by varying the load for both untreated and gas nitrided steels. The wear rate was reduced by gas nitriding by up to two orders of magnitude, depending on the sliding condition. Moreover, gas nitriding expanded the mild wear region toward higher loads and sliding speeds. In the mild regime an oxidative wear mechanism operated, contrasting with the metallic wear in the severe regime. Wear maps for untreated and gas nitrided steels have been constructed, which show the dominant regimes of the wear mechanisms.

A "wear-face-limited" gas nitrided pin test showed that the benefit of the treatment was lost once the effective surface layer was completely worn away. It is suggested that hardness has a crucial role in determining the wear rate through nitrided diffusion layers. A thick and porous compound layer produced by gas nitriding showed a poor wear behaviour owing to its brittleness, while a thin nitrocarburized ϵ-Fe_3N compound layer exhibited a low wear rate.

There was no significant difference between the nitrided steels in terms of transition load and wear rate. However, the wear lives of the nitrided layers were dependent on their case depth. Severe wear should be avoided in engineering component design, and operating conditions should ensure that only mild wear occurs. Both the hardness profiles and the cost performance of nitriding processes should be considered in the selection of nitriding treatments.

CONTENTS

Chapter 1: Introduction

Wear is one of the main processes leading to the limitation of the useful life of engineering products. Wear also reduces operating efficiency by increasing the power losses, oil consumption, and the rate of component replacement[1]. In particular, sliding wear is one of the most commonly encountered industrial problems, sometimes leading to scuffing or galling which is a very severe type of wear. Although our understanding of wear mechanisms has been improving, wear is such a complex phenomenon that there is no reliable general law for its solution[2]. This is probably due, in part, to the very large number of variables which can influence wear behaviour; including the type and mode of loading, interaction rate and time, component geometry, material properties, and environmental factors including temperature and lubricant properties.

Czichos[3] has suggested that friction and wear are not only determined by the material properties but by the characteristics of the engineering system. Improvements for wear may be obtained by changing operating parameters, lubricant and conditions of the wear surface, or by optimizing the wear counterface combination. However, besides the problems associated with design of components, operating conditions, etc., the selection of materials for use in situations involving wear is, of course, very important[4,5].

Wear-resistant materials for engineering components may be obtained by the use of appropriate bulk materials, but this is often expensive or inconvenient. Since friction and wear are essentially surface phenomena, the presence of a suitable surface layer of material may have a crucial effect. To achieve the desired wear properties of materials, therefore, the application of surface treatments is the most attractive method, leaving the substrate to be chosen for its structural properties and ease of manufacture and also for economic benefit[6,7].

A great variety of surface treatments have been developed over the years for improving wear properties[8], and new surface treatment techniques are becoming available faster than the rate of our understanding of their precise wear characteristics[9]. There is, therefore, a problem in how to use a surface treatment properly for tribological components, and for this solution a fundamental study on the wear behaviour of surface treatments is necessary.

Among a large number of surface treatments developed, nitriding is one of the most widely used processes to improve the wear properties of engineering components[8]. The process of nitriding involves a ferritic thermochemical treatment in which nitrogen is diffused into a steel surface, at a temperature usually within the range 480-570°C. After nitriding, a thin compound layer, called white layer, and a relative thick diffusion layer are produced on the component surface. The surface layers have high hardness, depending on the process temperature and the substrate alloying elements. A significant advantage of nitriding is less distortion than in comparison with carburizing, because of the relatively low processing temperatures. The two main methods of nitriding are gas and plasma processing. Nitrocarburizing is a variation of nitriding in which nitrogen and carbon are introduced into a steel to produce mainly a surface compound layer with only a thin diffusion layer in a relative short treatment time.

There exist some reported studies on the wear behaviour of gas nitrided, plasma nitrided and nitrocarburized steels, which show that nitriding and nitrocarburizing processes improve wear properties. However, as will be discussed in the following chapter, most work has shown only the high wear resistance of nitrided steel under a narrow range of load and sliding speed, and little is known about the wear mechanisms in terms of examinations of wear debris and worn components. Moreover, a number of different and conflicting results about the effects of nitriding processes on the wear behaviour have been reported, and there is a tendency to demonstrate the good wear properties of only the favourite process that has been developed by the researchers. Another feature of the literature is that the evidence about the effects of compound layers on wear behaviour is also contradictory.

The overall aims of this program of work are to understand the wear behaviour of nitrided steels systematically, and to study the wear mechanisms by a number of material characterization techniques. The scientific objectives of this study are as follows:

(1) To investigate the effects of load and sliding speed over a wide range, in order to establish a

wear mechanism map for a nitrided steel.

(2) To compare the wear behaviour between different nitriding processes.

(3) To investigate the effect of the compound layer and the hardness variation in the diffusion layer.

In order to focus on the wear characterization of nitrided steels and not on the development of nitriding processes, three commercial nitriding processes, i.e. gas, plasma nitriding and nitrocarburizing, were employed in this study.

Chapter 2: Literature Survey

2.1. Scope of literature review

The main aim of this literature survey is to review and discuss the literature on the following subjects:

(1) Nitriding in surface treatments for wear resistance (section 2.2.)

(2) Processes and metallurgical properties of nitriding (section 2.3.)

(3) Wear characteristics of nitriding (section 2.3.6.)

(4) Wear mechanisms of materials in sliding situations (section 2.4.).

In order to restrict the survey to a reasonable size, the nature of nitriding is considered mainly from a tribological point of view, and also the wear mechanisms described are limited to metallic materials.

2.2. Classification of surface treatments for wear resistance

Surface treatments for wear resistance can be divided into two broad categories; those in which the hardened surface is produced by heat treatment, usually accompanied by the diffusion of elements, e.g. carbon or nitrogen, into the surface and, those in which a layer of hard material is formed or deposited on the surface[8]. The two categories are:

(1) Surface heat treatments

(2) Surface coatings.

The former involves thermal hardening, carburizing, nitriding, boronizing and metallizing (e.g. V, Nb), and the latter involves electro-deposition, chemical-deposition, chemical vapour deposition (CVD), physical vapour deposition (PVD), spraying and welding processes.

James and coworkers[10], considering surface treatments used in engine components, attempted to classify a very wide range of the processes by the method in which the surface layer was formed. The three basic divisions are:

(1) Material added to a surface

(2) Surface chemistry altered

(3) Surface microstructure altered.

Nitriding is one of those surface treatments that alter the surface composition. Other surface treatments that alter the surface chemistry are carburizing, boronizing and metallizing. These processes involve the diffusion of an element into the substrate material. Processes involving welding, thermal spraying, CVD or electrodeposition are good examples of a new material being added to the surface. Finally surface treatments that involve microstructural changes usually incorporate some thermal processing, such as hardening by quenching. Carburizing described as altering the surface composition involves combinations of the changes of both surface composition and material structure.

Recently, Bell[11] has proposed an alternate classification of surface treatments, and the classification is described as:

(1) Thermal treatment
(2) Thermochemical treatment
(3) Plating and coating
(4) Implantation.

He has also shown the typical thicknesses of surface layers of the various surface treatments (Fig.2.1). 'Plating and coating' in Bell's classification correspond to those treatments involving addition of material to the surface, and 'thermal treatment' and 'thermochemical treatment' correspond to those treatments that change the surface microstructure and those treatments that change the surface chemistry, respectively. 'Implantation' involves ion implantation processes, which have only been recently developed for wear applications. Obviously in this classification, nitriding and carburizing belong to thermochemical treatments.

On the other hand, Wilson[12] has divided surface treatments into two groups from a tribological point of view:

(1) Short-life surface treatments
(2) Long-life surface treatments.

The former treatments are those which have a life shorter than the life of the component, and form thin, relatively soft and preferably ductile layers on the surface. These processes are widely used to aid running-in wear in the initial stage of engineering service, and the layers are worn away rapidly and have limited lives. Phosphate coatings, tin coatings and coatings due to oxidation are examples of short-life surface treatments. On the other hand, long-life surface treatments are expected to last for the full life of the component, and these processes generally give a high hardness to the surface. Thus nitriding, which increases the surface hardness of steels, is regarded as a long-life surface treatment.

2.3. Nitriding

2.3.1. Introduction

From a metallurgical standpoint, thermochemical surface treatments can be divided into two groups; ferritic treatments and austenitic treatments[13]. The austenitic treatments are those processes whereby the non-metal, usually carbon and/or nitrogen, is diffused into the austenitic phase (e.g. carburizing), and ferritic treatments, whereby the non-metallic elements are diffused into the ferrite phase (e.g. nitriding). These surface treatments have been very widely used for engineering components to improve not only wear properties but also fatigue strength.

Nitriding is a ferritic thermochemical treatment in which nitrogen is diffused into a steel surface, at a temperature usually within the range 480-570°C. Consequently no austenite-ferrite transformation occurs on cooling to room temperature, and quenching is not required to develop surface hardness. The method was first used at the end of the 1920s[14], and since then its application has continuously spread because the process has been further developed.

The properties produced by nitriding can be summarized as follows[15]:

(1) High surface hardness and wear resistance, together with reduced risk of scuffing and galling.
(2) High fatigue strength, and low fatigue notch sensitivity because of the residual compressive stress[16].
(3) Improved corrosion resistance for non-stainless steels.

Together with these properties, there are many advantages in nitriding as follows[8]:

(1) Less distortion than in carburizing due to the relatively low processing temperatures employed.
(2) High resistance to tempering and retention of hardness up to 500°C.
(3) Cheap process compared with other surface coating techniques (e.g. thermal spraying, PVD, welding).

A disadvantage is, however, the long treatment time caused by the slow diffusion process at a low temperature, when a deep case depth is required.

2.3.2. Principle

To understand nitriding processes, it is important to consider the iron-nitrogen equilibrium diagram (Fig.2.2 [17]). The eutectoid reaction ($\gamma \rightarrow \alpha + \gamma'$) occurs at approximately 590°C. As nitriding is carried out at temperatures within the ferrite phase field, the processes have to be employed below the eutectoid temperature. At the nitriding temperatures commonly used, the maximum solubility of nitrogen is only 0.1 wt%. When the nitrogen content exceeds this value, γ'-nitride is formed, the chemical formula of which is Fe_4N. If the nitrogen content exceeds about 6 wt%, the γ'-nitride starts to change into ϵ-nitride ($Fe_{2-3}N$). Below 500°C, ζ-nitride begins to form as the nitrogen content increases further. The nitrogen content of this phase is about 11 wt% and its chemical formula is Fe_2N.

As nitrogen diffuses into the surface of steel in nitriding, the solubility limit is soon reached and these iron-nitrides are formed. When observing these in the metallurgical microscope, the γ' and ϵ-nitrides can be seen as a white surface layer, called the 'white layer' or 'compound layer'. As the thickness of this layer builds up, nitrogen diffuses from it into the underlying steel to form iron-nitrides at the ferrite grain boundaries and along certain crystallographic planes and, by reaction with alloying elements in steel, forms finely dispersed alloy-nitrides[18].

The high surface hardness which is obtained after nitriding is mainly due to distortion of the ferrite structure by finely precipitated alloy-nitrides, and partly due to the inherent hardness of the nitrides. Therefore those elements that form nitrides, such as Al, Cr and Mo, have a significant effect on increasing the surface hardness. Al, closely followed by Ti, has the greatest effect, and then come Cr, Mo and V (Fig.2.3) [15].

The hardened case which is usually 0.2-0.7 mm thick has a peak hardness of Hv 700-1100, depending on the process temperature and alloy content, and the hardness of the cross-section decreases gradually with increase in distance from the surface. The effective case depth is defined by the distance from the surface to the layer having a specific required hardness. BS (British Standard) 6479 defines the required hardness as Hv 550[19]. The effect of treatment time on the case depth is derived from the simple formula for diffusion;

$$D = k\sqrt{t} \qquad \text{(Eq.2.1)}$$

where D is the case depth, k a constant and t the treatment time[16]. The case depth is also a function of process temperature and alloy content. As the process temperature increases, the case depth increases, however the surface hardness decreases due to precipitate coarsening (Fig.2.4) [15].

2.3.3. Methods of nitriding

There are three main methods for nitriding; gas nitriding, plasma nitriding and salt-bath nitriding.

However, salt-bath nitriding is usually referred to as ferritic nitrocarburizing, in which both nitrogen and carbon are introduced into a steel. Thus the salt-bath method will be described under the heading "nitrocarburizing".

2.3.3.1. Gas nitriding

Gas nitriding is carried out in an ammonia atmosphere at a temperature usually within the range 490-530°C[8]. Part of the ammonia dissociates catalytically at the surface of the hot steel, and some of the nascent nitrogen is absorbed by the steel[15]:

$$2NH_3 \rightarrow 2[N]_{Fe} + 3H_2 \qquad \text{(Eq.2.2)}$$

The nascent atomic nitrogen is diffused into the surface of the steel, while molecular nitrogen is completely inert under the temperature and pressure conditions of nitriding[16]. The residual ammonia content of the exit gas is determined by means of an absorption burette using water[20]. Increased temperature results in increased dissociation. Gas nitriding is carried out in heat-resisting steel retorts in pit or batch type furnaces, generally electrically heated for good temperature control.

This method was established a long time ago, and is still widely used for engineering components. Although long treatment times are recognized as the major limitation of conventional gas nitriding process, a further problem, particularly with the nitriding of such engineering components as crankshafts, is the formation of a compound layer (white layer), which is usually removed before use in order to avoid spalling of this layer in service. The cost of removal of the compound layer by chemical or mechanical methods has been estimated to approach that of the nitriding treatment itself.

Bell and coworkers[21] showed that a gas nitriding process which involves a control of the nitriding potential by using NH_3/H_2 mixtures enables the formation of the compound layer on steel to be prevented. The nitriding potential defined as

$$a_N = P(NH_3) \,/\, P(H_2)^{3/2} \qquad \text{(Eq.2.3)}$$

was reduced by diluting the ammonia with hydrogen to minimize the amount of the compound layer formed. Moreover, it was shown that the hardness, case depth and fatigue properties obtained from this treatment are directly comparable to the properties resulting from conventional gas nitriding for the same cycle times. While this treatment has been shown to be effective in reducing the amount of compound layer on a component in its nitrided condition, it has not been used commercially because it calls for continuous precise control of the atmosphere. Clayton and Sachs[22] have proposed that by changing the nitriding atmosphere from ammonia to a mixture of nitrogen and hydrogen at the end of the nitriding cycle, the compound layer can be substantially changed to iron in 2-4 hours.

2.3.3.2. Plasma nitriding

Plasma nitriding, which has alternatively been called 'ion nitriding' or 'glow discharge' nitriding in the technical literature[23], was developed in Germany in the 1930s. However, it was not until the early 1970s that this process was used commercially, because of the relatively expensive equipment and the diversified technology which is essential if the process is to be carried out correctly. Owing to further development work during recent years, the use of the process has been widely accepted for engineering components, for example automotive parts[24,25]. It can be used to surface harden most grades of tool steel[26], stainless steels[27,28] and powder metal components[29].

The plasma nitriding process makes use of an ionized gas which serves as a medium for both heating and nitriding[15]. The parts to be treated are placed in the reaction furnace and cathodically charged to a potential in the rang 400-1500 V, with respect of the wall of the furnace, which acts as the anode. At the working pressure of about 10-1000 Pa, a glow discharge of the reaction gases, nitrogen and hydrogen, is created. The gases become ionized with the result that positive ions having a high kinetic energy bombard the components, the parts become heated to the required temperature, and at the same time nitrogen is introduced into the surface of the parts.

The process control parameters in plasma nitriding are the composition of the gas mixture, pressure, voltage, current density and cathode temperature. The last is usually within the range 450-550°C and is controlled by the power input.

To obtain an uniform nitriding depth and an uniform compound layer thickness, it is important that these process parameters must be selected empirically. The depth of hardening with plasma nitriding is greater than that of conventional gas nitriding since the heating up time for plasma nitriding is appreciably shorter. In actual practice, the treatment times are up to approximately 60 hours.

The plasma nitriding technique offers a number of advantages over conventional gas nitriding as follows[30]:

(1) Reduced treatment times arise because of a more rapid saturation of the surface owing to the enhanced mass transfer through the plasma.

(2) Reduced energy consumption is achieved both because the treatment time is reduced and also because only the cathode is heated; heat loss occurs only by radiation through the vacuum to the cold chamber wall.

(3) Reduced gas consumption with about 95% saving is claimed, because a low-pressure atmosphere is employed.

(4) No environmental hazard arises, e.g. no toxic wastes requiring disposal and no risks of explosion[31].

(5) High alloy steels such as ferritic and austenitic stainless steels can be nitrided without removing the adherent oxide films on the surface prior to nitriding, because the surface is kept clean by the

process of ion bombardment[13].

2.3.4. Nitrocarburizing

Nitrocarburizing is a variation of nitriding which involves the diffusion of mainly nitrogen, but also some carbon, into the surface with the formation of a thin (~25 μm) compound layer (white layer). This layer consists predominantly of ϵ-carbonitride, the formation of which is favoured by the presence of carbon[32]. The surface compound layer has an important role to prevent the metal-to-metal adhesive contact so that it improves scuff resistance and wear properties[33]. In addition, the presence of a small amount of porosity in the compound layers helps to retain oil under boundary-lubricated conditions[32,34]. Beneath the surface layer there is a diffusion zone up to 0.5 mm thick, containing finely dispersed nitrides, which increase the hardness and the fatigue strength of the material.

As most applications of nitrocarburizing make use of the properties of the ϵ-carbonitride layer and not the hardness of the underlying steel, the process is normally used on plain carbon steels and cast irons as well as alloy nitriding steels[16]. Compared to pure nitriding, where the γ'-nitride is predominantly formed, the presence of carbon during nitrocarburizing stabilises the ϵ-nitride so that it will form at much lower nitrogen activity than in the absence of carbon[32]. This results in faster growth of the compound layer due to the much wider solubility range of carbon and nitrogen in the ϵ-phase enabling a steeper concentration gradient than in the γ'-phase (Fig.2.5 [35]).

Nitrocarburizing is used particularly in the motor industry for applications such as camshafts, crankshafts, rocker arms, valve guides and distributor pinions. Other important applications are parts of hydraulic machines such as valves and pump bodies[33]. As the process offers a relatively cheap method of improving the wear performance of steels, it has become widely used over the last few decades.

This process is usually carried out at 570°C in either a salt both containing a mixture of sodium cyanide and cyanate or in a gas mixture containing ammonia and a carburizing gas. There are a number of variations of the basic nitrocarburizing processes which are known by their trade names, e.g. Tufftride and Nitrotec. In some variations a sulphide is added to the salt bath and these process variations are known as Sulfinuz and Sursulf.

2.3.4.1. Salt-bath nitrocarburizing

The earlier nitrocarburizing processes were based on molten cyanide salt baths. The salt bath nitrocarburizing is almost as old as the gas nitriding method.

The salt mixtures initially used contain mainly sodium cyanide (NaCN) and a few percent of carbonate (Na_2CO_3) and cyanate (NaCNO)[36]. By aging the bath at 570°C, the cyanide oxidizes to cyanate by contact with the atmosphere as shown in equation 2.4:

$$2NaCN + O_2 = 2NaCNO \qquad \text{(Eq.2.4)}$$

The cyanate thus produced then dissociates:

$$4NaCNO = Na_2CO_3 + 2NaCN + CO + 2\underline{N} \qquad (Eq.2.5)$$

The carbon monoxide breaks down according to the reaction:

$$2CO \rightarrow CO_2 + \underline{C} \qquad (Eq.2.6)$$

From these reactions the nitrogen and carbon diffuse into the surfaces of parts to be treated.

Up to the middle of the 1950s, salt-bath nitrocarburizing was used only on a very restricted scale and then mainly for short-period treatments (10-30 min). If longer process periods were used, pitting occurred on the steel surfaces and the results of the nitrocarburizing were not predictable due to variation in the cyanate content at different levels in the bath. During the last few decades, it has become possible to obtain better control of the cyanate content by injecting air into the bath. This method, which was developed by Degussa in Germany, is called the Tufftride process[15].

Another similar process, called Sulfinuz, was developed in France to aid the cyanate formation by adding sodium sulphide (Na_2S). During this process, sulphur is also introduced into the surface of parts, and this surface compound layer increases the anti-scuffing properties[37].

Since 1970 the concern about the environmental aspects of heat treatment processes with cyanide-based baths, which give rise to toxic effluent and sludge, has increased. The cyanide content is no longer acceptable, following the tightening of anti-pollution measures by the authorities concerned. Consequently, some salt-bath techniques with reduced toxicity levels have been developed. The patented Sursulf process[38], which was developed by Hydromechanique et Frottement Centre in France, has been marketed for use as an alternative to both the Tufftride and Sulfinuz treatments. Sursulf is based on a bath made up entirely from cyanide-free salts which includes lithium and sulphur. Another important function of the sulphur in the bath is to produce sulphur compounds in the surface layers of parts to produce lubricating properties[33].

Soon after the Sursulf method appeared on the market, another cyanide-free process called New Tufftride or Tufftride TF1[36] was developed in Germany.

In all of these salt-bath processes, components are preheated to 350-400°C and transferred to the nitrocarburizing salt bath at 570°C. Treatment times are usually in the range 1-3 hours. There are a very large number of applications for salt-bath nitrocarburizing processes to improve the resistance to scuffing and adhesive wear[33].

2.3.4.2. Gas nitrocarburizing

Gas nitrocarburizing has been developed from the classical ammonia gas nitriding as an alternative to the salt-bath methods. There are many types of processes based on various gas mixtures[8]:

(1) endothermic gas / ammonia (Nitemper)
(2) hydrocarbon gas / ammonia / oxygen
(3) carbon dioxide / ammonia / nitrogen.

The patented Nitemper process involves a treatment at 570°C in a sealed quench furnace supplied with a mixture of 50% ammonia gas and 50% endothermic gas. The treatment time is usually 2 to 3 hours followed by quenching in oil. The endothermic gas generated from natural gas contains methane (CH_4) and carbon monoxide[20], both of which can provide carbon in accordance with the following reactions:

$$CH_4 = [C]_{Fe} + 2H_2 \qquad \text{(Eq.2.7)}$$

$$2CO = [C]_{Fe} + CO_2 \qquad \text{(Eq.2.8)}$$

Investigations carried out by Bell and Lee[39] with a Nitemper atmosphere system, indicated that when the ammonia addition was controlled to a residual value of 32%, it was possible with a 3 hours treatment to develop a compound layer of 18 μm thickness, with a hardness value of Hv 650 for a low-carbon steel. It was also shown that the compound layer inherits the matrix carbon content of the steel being treated as well as obtaining carbon from the treatment atmosphere, thereby developing a nitrogen/carbon ratio of 5·4. X-ray diffraction analysis confirmed the structure of the layer to be a close-packed hexagonal ϵ-carbonitride, which was derived from the ϵ-nitride phase by replacing some of the nitrogen atoms with carbon.

Dawes and coworkers[40] showed that a compound layer can be produced on non-alloyed steel at sub-atmospheric pressures using ammonia-hydrocarbon atmospheres. The atmosphere used was a 50% ammonia, 50% methane gas mixture, to which 0-2% oxygen was added. It was found that increasing the oxygen content increased the thickness of the compound layer. One of the advantages of this process is the ability to replace an endothermic gas generator by using methane, which is equivalent to the gases produced by the generator.

Wells and Bell[41] have performed trials with different methanol-ammonia volume ratios. They found that it was possible to control the existence and the position of γ'-nitride in compound layers, and that when an atmosphere composition of 45-60% CH_3OH + 55-40% NH_3 was used the compound layers formed consisted solely of ϵ-nitride.

Dawes and coworkers[42] showed that a carbonitride compound layer forms when using an atmosphere mixture of 50% NH_3, 45% N_2 and 5% CO_2. It was claimed that although tribological properties of the surface layer are not influenced by the presence of carbon, the addition of CO_2 gas has a significant effect on increasing the reaction rate of the ammonia at the steel surface. The CO_2 gas reacts with the H_2 produced by the nitriding reaction at the steel/gas interface ($NH_3 \rightarrow [N]_{Fe} + 3/2\ H_2$).

A further development by Lucas Industries plc. has been aimed at improving the scuffing and corrosion resistance of a range of low carbon steels[43]. The newly patented Nitrotec treatment[44] is based on the three processing requirements, namely; nitrocarburizing, oxidizing and sealing. This process is fundamentally a derivative of earlier gas nitrocarburizing techniques, with the important addition of a pre-quench oxidation sequence. The oxidation results in the formation of a surface oxide film of magnetite (Fe_3O_4) and corrosion studies have indicated that maximum corrosion resistance is developed when the magnetite oxide film layer is approximately 1 μm thick.

2.3.5. Formation and growth of the compound layer

In both nitriding and nitrocarburizing processes, an iron nitride compound layer (white layer) up to 25 μm thick is formed on a steel surface. This layer usually consists of either a face centred cubic γ'-phase (Fe_4N) or a close packed hexagonal ϵ-phase ($Fe_{2-3}N$, $Fe_{2-3}(N,C)$) [45]. In some case both phases are formed. The ϵ-phase has a relatively wide range of nitrogen stoichiometry (7.5 - 11.0 wt%, N, at 500°C), compared with the γ'-phase (Fig.2.2 [17]). In nitrocarburizing both nitrogen and carbon are introduced into a steel so that the ternary Fe-N-C phase diagram (Fig.2.5 [35]) must be considered[32,39]. The presence of carbon stabilizes the ϵ-phase at a much lower nitrogen concentration than in the Fe-N system.

The phases of the compound layer formed are usually determined by x-ray diffraction analysis. Wells[35], however, has found a simple method for the structural analysis of the compound layer, which involves optical microscopy techniques by using a modified nital etch with the addition of 0.1% concentrated hydrochloric acid to the etchant. Moreover, Rozendaal and coworkers[46] have demonstrated that a Murakami etchant (10g $K_3Fe(CN)_6$ in 100ml of a 10% solution of KOH in distilled water) provides a sensitive discrimination between pure nitrides and carbonitrides in nitrocarburized compound layers.

As a nitriding treatment is a diffusion process of nitrogen into a steel surface, the growth of the surface layer is usually described by a parabolic law. Schwerdtfeger and coworkers[47] have shown that during gas nitriding the square of the thickness of γ'-nitride compound layer is proportional to the treatment time, indicating that the growth of the layer is controlled by diffusion. From the parabolic rate constant and thermodynamic data, the self-diffusivity of nitrogen in the γ'-phase was evaluated; $D = 3.2\times10^{-16}$ and $7.9\times10^{-16}\ m^2\cdot s^{-1}$ at 504°C and 554°C, respectively.

In the case of plasma nitriding the rate of compound layer growth has been found to be initially greater than in gas nitriding because of the more rapid saturation of nitrogen concentration at the surface[30]. However, after longer nitriding times the growth rate falls below that predicted by a parabolic law. Marciniak[48] has considered non-equilibrium models of γ'-phase growth during plasma nitriding in order to explain the deviation from the parabolic law. The models taking account of the surface movement due to cathode sputtering agreed with the experimental observations.

On the other hand, Wells and Strydom[49] have found that γ'-Fe_4N compound layer on the flat faces of pure iron showed anomalous growth behaviour during plasma nitriding, in which the compound layer initially increased and then subsequently decreased in thickness. This cannot be explained by the removal of layer material by sputtering. They claimed that the anomalous growth behaviour can be attributed to the formation of the vapour deposited layer of iron oxynitride which inhibits further nitriding of the substrate.

In nitriding practice, an incubation time for compound layer formation has been reported[50]. Rozendaal and coworkers[51] calculated nitrogen concentration profiles based on both the flux through the surface of NH_3-H_2 gas nitrided steel and the diffusion in α-iron. It was found that during nitriding the surface concentration approached relatively slowly the value in equilibrium with the gas atmosphere. This model predicted correctly the incubation time for the formation of the γ'-Fe_4N compound layer at the surface.

A well known phenomenon frequently observed in the nitrided or nitrocarburized compound layers is the occurrence of porosity at the outer part of the layer. Although many reasons for the porosity have been suggested, recent research has suggested that it is related to the metastability with respect to nitrogen gas in the nitride phases, which would lead to the precipitation of molecular nitrogen (N_2)[46,47,52,53]. From thermodynamic data the pressure of nitrogen gas in equilibrium with ε and γ' nitride phases at 565°C is at least 2.5×10^5 atm and 7.5×10^3 atm respectively, indicating a strong tendency for recombination of nitrogen atoms within the compound layer[46]. After growth and coalescence of the pores, channels perpendicular to the surface and in open contact with the outside atmosphere form.

Mittemeijer and coworkers have studied the detailed morphology and composition of compound layers of nitrocarburized iron, and related these to the absorption of carbon[46,53]. They found that in salt-bath nitrocarburizing, carbon enrichment occurs near the bottom of the compound layer. It was shown that carbon absorption in the ϵ-phase occurs predominantly at some distance from the outer surface via the channel walls produced by pores of nitrogen gas. In the case of gas nitrocarburizing, the increasing carbon concentration at these sites eventually produces a cementite phase in the compound layer.

2.3.6. Wear properties of nitrided steels

An outstanding material property of nitrided steel is its high hardness. High hardness is known to be directly related to abrasive wear resistance. In adhesive wear situations, a hardened surface does not only reduce the real area of contact between surfaces at a given load but also improves the plastic deformation resistance of the contact asperities. In the literature, many studies on the wear behaviour of nitrided steels have been reported, which demonstrate their high wear resistance.

2.3.6.1. Comparison between nitriding processes

Williamson[54] investigated the wear resistance of three nitriding treatments (gas nitriding, Sursulf and Tufftride) and a salt-bath carburizing treatment, under conditions of scuffing, abrasion, fretting and corrosion. He found that there was no significant difference in the wear resistance between the three treatments except that Sursulf had a higher wear rate in the early part of the scuffing and abrasion tests. His main conclusions are that the nitriding treatments are most suitable for applications where scuffing and corrosion are the main wear mechanisms and that the resistance to abrasion and fretting is poorer than that of carburizing. Therefore, he has suggested that care should be taken in assessing the wear process in any application in which these treatments are used.

Habig[55] has made a general assessment of the wear performance of salt-bath nitrocarburizing comparing with boronizing, vanadizing and carburizing under conditions of adhesion in vacuum, adhesion in air, abrasion and surface fatigue. They showed that nitrocarburizing was useful only in adhesive wear in vacuum and that otherwise the wear resistance was poorer than that of the other treatments.

Cohen and Rosen[56] investigated the dry sliding wear of gas and plasma nitrided stainless steels at a low sliding speed (0.15 $m \cdot min^{-1}$). Before the wear tests, the nitrided specimens were ground and lapped to a depth of 20 μm to remove the surface compound layer. It was found that the wear resistance of the plasma nitrided specimen was higher than that of the gas nitrided steel. They have suggested that this is due to the finer and more homogeneous nitrides in a plasma nitrided layer than that in a gas nitrided layer.

Peng[57] studied the abrasive wear resistance of hardened hot-work die steel which was achieved by gas nitrocarburizing, plasma nitriding and spark discharge cladding of WC-Co alloy. The results showed that the ranking of the surface treatments in order of decreasing abrasive wear was (1) plasma nitriding, (2) spark discharge cladding, (3) gas nitrocarburizing. However there was no clear explanation for this ranking result in his paper.

2.3.6.2. Effects of removal of the surface layer

During a wear process, a surface material is removed continuously, and thus the effect of the removal of a nitrided surface layer on the wear behaviour is an interesting subject. A nitrided surface layer involves a compound layer and a diffusion layer which varies in hardness from the surface to the core. Another point to be noted is that any benefits of treatment would be lost once the effective surface layer had been worn away.

Bell and Sun[58] investigated the influence of plasma nitrided case depth on the wear behaviour under dry rolling-sliding conditions. It was shown that a specimen with a shallow nitrided case depth exhibited a sharp increase in wear rate at some stage in the wear test. Although particular attention was paid to sub-surface shear behaviour, they did not take account of the amount of wear depth. This sharp increase in wear rate at some stage in the process can be associated with the case layer removal caused by the wear process.

Williamson[54] showed that during wear there was no change in abrasive wear rate at the compound layer-diffusion layer interface. Gleave and Farrow[59], however, found a wear transition to a higher rate when the wear depth exceeded the thickness of the compound layer.

Burakowski and coworkers[60] investigated the lubricated sliding wear of gas nitrided steels which had been ground to various depths (40, 100 and 200 μm) within the diffusion layer prior to wear tests. These wear characteristics were also compared with that of as-nitrided specimens, which had a compound layer of 6 μm thickness. It was found that those specimens that were ground to 40 μm depth showed the lowest wear rate, and that at deeper into the diffusion layer (100 and 200 μm) the wear rate increased. These results can be related to the hardness profile of the nitrided steel, although this was not discussed in the paper.

On the other hand, Roper[61] investigated the effect on scuffing behaviour by grinding away various amounts (8-200 μm) from the surface of salt-bath nitrocarburized steels, and showed that there was no safe depth to which the nitrocarburized steel can be ground without impairing its scuffing performance.

2.3.6.3. Effects of structure and thickness of the compound layer

Evidence in the literature about the effect of the compound layer (white layer) on the wear of nitrided steels is contradictory. Some researchers[e.g. 33,37] suggest that the compound layer, which is formed on nitrided or nitrocarburized steel up to 20-30 μm, improves adhesive wear properties. On the other hand, other researchers[e.g. 21,22] have suggested that the compound layer causes spalling during service due to its brittleness, leading to accelerated wear or seizure.

Bell[13] has shown that when a nitrocarburized compound layer contains a significant proportion of γ'-phase within ϵ-phase, namely a dual-phased structure, then very poor adhesive wear properties were experienced even under lubricated conditions. It has been suggested that for the optimum improvements in wear and anti-scuffing properties the compound layer should be essentially mono phase, preferably an ϵ-carbonitride phase.

Wang and coworkers[62] investigated the sliding wear behaviour of ion-sulpho-nitrocarburized steels, and related this to the porosity of the compound layer (15-30 µm thickness). This surface layer was produced by a plasma process in an atmosphere of mixed ammonia-alcohol and carbon disulphide. The results indicated that in the early stage of the wear tests under dry conditions the ion-sulpho-nitrocarburizing showed a higher wear rate than salt bath or gas nitrocarburizing. They attributed this to the porosity of the outer part of the compound layer. However, under lubricated and abrasive containing lubricated conditions, the ion-sulpho-nitrocarburizing treatment showed the lowest wear rate even in the early stage. They considered that the porous outer layer was able to not only store oil but also hold abrasive particles. Furthermore, in the steady state, a rather lower wear rate was observed because the more compact and firmer nature of the next inner part of the compound layer was responsible for the wear behaviour.

However, Williamson[54] showed that a Sursulf treatment had a higher wear rate in the early part of lubricated sliding tests than Tufftride and gas nitriding treatments, and considered that this was associated with the greater porosity of the outer part of the Sursulf compound layer.

Wells and Shaw[63] studied the wear of different gas nitrocarburized specimens, in which the compound layers consisted of varying distributions of ϵ and γ'-phases.

They found that dry sliding wear behaviour was not significantly affected by the variation in the compound layer, although the failure mechanism during scratch tests is dependent on the layer structure. Those layers that have more porous structures showed a ductile deformation, leading to a higher load to failure in the scratch tests.

Karamis[64] investigated the effects of thickness of the compound layer on dry sliding wear behaviour. The thickness of the compound layers, which were produced by plasma nitriding at 550°C for 4 and 100 hours, were 6 and 17 μm, respectively. He showed that the wear rate of the specimen nitrided for 100 hours was higher than that for 4 hours, owing to the thicker compound layer. It was found that spalling within the layer occurred during the wear process because the thicker compound layer included some pores and was more brittle.

2.3.6.4. Wear transitional behaviour

Cleave and Farrow[59] investigated the dry wear behaviour of nitrided steels using a pin-on-disc machine over a wide range of sliding speed (0.1~10 $m \cdot s^{-1}$). Wear tests on untreated steels showed a mild-severe-mild transition in wear rate, which is broadly similar to that in work published by Welsh[65]. In contrast, the nitriding processes almost eliminated severe wear. It was found that the protection from severe wear by the nitriding treatments was attributed to the presence of an oxidative (mild) wear mechanism. Moreover, they proposed that the increase in hardness by the surface treatments was responsible for the reduction in the wear rate, not directly, but by providing those surface conditions that favour oxidative wear.

On the other hand, Whittle and Scott[66,67] have observed a transition from mild to severe wear in gas nitrided and Tufftrided austenitic alloys by variations of load and sliding speed. The wear tests were carried out under unlubricated conditions using a pin-on-disc machine. The wear transition behaviour was dependent upon both sliding speed and applied load. They described that mild wear was associated with the formation of an oxide film on the wear pin. In the severe wear regime, the wear rates of the nitrided alloys were higher by approximately an order of magnitude than those of the untreated alloys. They suggested that under severe wear conditions the oxide was removed faster than it was formed, and that wear was controlled by the characteristics of the underlying nitride compound layers.

A wear transition caused by a variation of temperature has been reported by Cullen and Cameron[68], who studied the effects of temperature on the lubricated wear properties of salt-bath nitrocarburized steels. They found that the wear rate increased logarithmically with temperature up to 160°C when it dropped by two orders of magnitude. Below 160°C, the wear debris was red ferric oxide Fe_2O_3; above 160°C it changed to magnetite Fe_3O_4. However, no explanation for the transition at 160°C, which was independent of speed and contact pressure, could be found.

2.4. Sliding wear mechanisms

2.4.1. Classification of wear mechanisms

Wear can be defined as the progressive loss of material from the operating surface of a body as a result of relative motion at the surface[69]. The systematic study of a phenomenon as complex as wear can be simplified by first classifying it into its various forms. Burwell[70] proposed four defined classes of wear:

(1) Adhesive wear
(2) Abrasive wear
(3) Corrosive wear
(4) Surface fatigue.

He also includes a fifth classification under the heading 'Minor Types' of wear, which covers erosion and cavitation.

In this classification, surface fatigue wear implies the so-called rolling contact fatigue, which is characterized by local pitting or flaking of surfaces. However, Kragelskii and coworkers[71] have suggested that fatigue wear can occur under sliding situations. On the other hand, Archard and Hirst[72], and Welsh[65] have shown that sliding wear of metals can be classified into two modes of wear which they called "mild" and "severe". Suh[73,74] has studied conditions of dry wear in which metallic debris has been produced with surface smoothing and without transfer, and Quinn[75] has discussed work in which oxidized debris has been produced without transfer. The mechanisms proposed by these groups have become known respectively as delamination and oxidative wear.

Obviously some of these wear mechanisms overlap and these classifications often cause confusion by loose definitions of wear and contradictory terminology. The difficulty with the classification of wear arises from the complexity of wear phenomena in practical situations.

Rigney[76] has proposed an alternate classification in terms of phenomena. He has suggested that simple descriptive terms like sliding, rolling, impact, wet/dry and lubricated/unlubricated wear are based on simple observations about the wear system, and that they are more appropriate whenever the wear mechanisms are not well characterized.

Apart from the difficulty of the classification of wear mechanisms, Eyre[9] has shown that wear encountered in industrial situations can be broken down into the following categories:

(1) abrasive 50%
(2) adhesive 15%
(3) erosion 8%
(4) fretting 5%
(5) chemical 5% .

It should be noted, however, that in practice one type sometimes changes to another, or two or more wear mechanisms operate together. It is well known for example, that the wear debris produced by adhesive wear causes accelerated abrasive wear.

In order to restrict this literature review to sliding wear situations, this survey considers the three main forms of sliding wear; adhesion, abrasion and fatigue. In particular, adhesive wear is discussed in some depth because it is a primary mechanism caused by sliding of materials, and the heading "adhesive wear" in this survey covers mild (oxidative) and severe (metallic) wear mechanisms.

2.4.2. Adhesive wear

When two surfaces are brought together, contact is made at relatively few isolated asperities because the surfaces of materials are rough microscopically[77]. When a normal load is applied, the local pressure at the asperities becomes so high that the asperities deform plastically until the contact area has increased sufficiently to support the applied load. If the surfaces are sufficiently clean and chemically compatible with each other, adhesive junctions are easily formed. The adhesion occurs between a few asperities which increase in size as sliding motion continues[78]. Eventually the junctions rupture at their weakest point, usually resulting in material transfer from one surface to the other.

2.4.2.1. Archard wear equation

In general, the amount of adhesive wear is found to depend linearly on the distance of sliding and on the load but is independent of the apparent area of contact of the rubbing materials[79]. This may be explained by the fact that the true area of contact between two surfaces is extremely small and directly proportional to the load[77].

Archard[80] has proposed a simple model to describe a quantitative law of adhesive wear. He assumed that each contact junction has a radius a, and that a wear particle is a hemisphere of the same radius as the contact area. The hemispherical wear particle, whose volume δV is $2\pi a^3/3$, is supposed to be produced by a probability k due to sliding of the one pair of asperities through a distance $2a$, so the overall wear per unit sliding distance dV/dL is given by

$$dV/dL = \Sigma(k\ \delta V/2a) = k\ \Sigma(\pi a^2/3) \qquad \text{(Eq.2.9)}$$

The normal load W is supported by the plastic deformation of contact asperities, and described by

$$W = \Sigma(P_m\ \pi\ a^2) \qquad \text{(Eq.2.10)}$$

where P_m is the flow stress of the material. Thus

$$dV/dL = k\ W\ /\ (3\ P_m) \qquad \text{(Eq.2.11)}$$

The overall wear volume can be rewritten by putting the hardness $H = 3\ P_m$ as follows:

$$V = k\ W\ L\ /\ H \qquad \text{(Eq.2.12)}$$

where V is the wear volume, W the load, L the sliding distance, and H the hardness of the wearing material. This equation involves the following important points:

(1) The volume of wear is proportional to the load.
(2) The volume of wear is proportional to the sliding distance.
(3) The volume of wear is inversely proportional to the yield stress or the hardness of the material.
(4) The volume of wear does not depend on the apparent area of the surface.

This Archard theory has been widely accepted for adhesive wear, and the constant *k*, usually termed the wear coefficient, is dimensionless and has been shown to be always less than unity. Archard and Hirst[72] have listed the values of *k* for a number of materials, and found that the values of *k* vary over a wide range from 10^{-7} to 10^{-2}.

The constant *k* must represent the properties of the friction couple, which do not involve the hardness of wearing materials. Roach and coworkers[81,82] have studied the scoring (very severe adhesive wear) characteristics of a number of metals sliding against steel in terms of mutual solubility with iron. It was found that those B-subgroup metals in the periodic table that are either insoluble in iron or else form insoluble intermetallic phases with iron have good scoring resistance. Rabinowicz[83] has also expressed the dependence of adhesion of a number of combinations of metals on the metallurgical compatibility (i.e. mutual solubility), and shown that incompatible combinations reduce adhesion friction.

Although the Archard equation (2.12) has been widely used to describe adhesive wear, experiments on wear of materials are not always represented by this equation, k is found to depend not only on the properties of the friction couple, but also the sliding conditions and geometrical factors. It is known, for example, that lubrication reduces the value of k by more than two orders of magnitude[84]. Therefore k only has real meaning if the wear mechanism does not change, and it is inadequate to describe non-linear running-in behaviour[85,86] or wear transitions[65,87]. There is still little understanding of the physical significance of k[88]. The greatest weakness of the Archard theory is that the mechanism by which wear particles are produced is not clear. This problem will be discussed in the following section.

2.4.2.2. Material transfer and wear particle formation

A well known phenomenon frequently observed in sliding wear situations is the occurrence of transfer of materials from one component of a sliding pair to the other[89]. In general, the adhesive bond formed at the interface between the clean surface is stronger than cohesive bonds in the weaker of the two materials[90]. This phenomenon has reinforced the idea that sliding wear involves adhesion, and that suitable surface layers or the presence of a lubricant reduces wear by reducing adhesion. Material transfer makes adhesive wear mechanisms more complex, transfer is not the same as wear; the transferred fragment may be repeatedly transferred back and forth from one surface to the other. Tabor[2] pointed out that the net wear rate should depend crucially on the transfer-back-transfer process and on the final mechanism which detaches the transferred fragment and converts it into a wear debris particle.

A number of studies on transfer of material between sliding surfaces have been reported. Rabinowicz and Tabor[91] have studied metallic transfer under unlubricated and lubricated sliding conditions, by using radioactive methods. They showed that the metallic transfer did not occur as a uniform smear but as a relatively small number of discrete fragments, and that a good boundary lubricant reduced the friction between metal surfaces by a factor of not more than 20, while the amount of transfer was diminished by a factor of 20,000 or more.

Another comprehensive work on metal transfer and formation of wear debris was carried out by Kerridge and Lancaster[92], using a combination of radioactive and inactive brass pins which were rubbed against hard steel rings under unlubricated conditions. They showed that the amount of wear debris steadily increased with the time of sliding but the amount of transferred metal to the ring soon reached an equilibrium value, and that the equilibrium rate of transfer was equal to the wear rate of the pin. The experiments in which the radioactive pin was replaced by an inactive one confirmed that there was no direct wear from the pin and that all the wear particles were formed from the transferred metal.

Furthermore, an auto-radiographic study of the transferred metal on the ring led to the view that the transferred fragments collected preferentially at particular regions on the ring. The transferred fragments gradually increased in size until they became sufficient to detach themselves as loose wear particles. Their results also showed that the increase in wear rate with load was accompanied by an increase in the mean size of the transferred fragments and wear particles rather than an increase in number.

Sasada and coworkers[93] have proposed a model for the process of formation of adhesive wear particles. When a metal-metal junction formed between surfaces is sheared by the friction motion, a small fragment of either surface portion will be adhered onto the mating surface. They called this small fragment "transfer element". This transfer element creates a new asperity on the counter surface and forms a new junction in the course of further sliding. When the next shearing occurs, a "transfer particle" is formed by the accumulation of the two transfer elements, and this particle still adheres to either surface. Through the repetition of this accumulating process, the transfer particle gradually grows to a considerable size until it is removed from the surface suddenly by a mechanical impulse. This final stage is termed the formation of a "wear particle". In the paper, this model was slightly modified to explain a flake-like wear particle observed; i.e. the transfer particle that grows enough to support the total load is flattened between the mating surfaces before its final removal as a wear particle.

Rigney's research group[94-96] has investigated the detailed structure of transferred materials and wear particles, using a number of metallurgical techniques, namely optical microscopy, scanning and transmission electron microcopy, and X-ray analysis. It was shown that the transferred layers that were produced during a wear process were very small crystallites, 3-30 nm in diameter, and that they were derived from both sliding components. In addition, the loose wear particles had the same structure and composition as the transferred layers, which suggested that the loose wear particles were derived from the transferred layers.

The transfer of soft material to a harder material is to be expected, but the transfer of hard material to softer material has also been reported[91,97]. From the work of Cocks[98] and Antler[99], the dominant direction of transfer may depend on the geometry of the sliding system. For a rider-on-disc system, transferred fragments were originated from the disc material, and grew by a process called wedge or prow-formation. On the other hand, it has been reported that back transfer takes place simultaneously in a process of transfer and removal of transferred material[100].

The discussion in this section has been, so far, oriented toward mainly describing the phenomena of the formation of transferred fragments and wear particles. However, the mechanism by which the final loose wear particles are produced is not clear. It is generally agreed that in adhesive wear, fragments of material are transferred from one surface to another and that loose wear particles subsequently form from the transferred material, Rabinowicz[101] has pointed out that an apparent contradiction is involved. The initial production of adherent fragments presupposes a strong bond between the fragments and the surface onto which they are transferred, whereas the final loose wear particle formation, on the other hand, implies a weak bond. Some models have been proposed to explain this contradiction.

Kerridge[102] has suggested that the formation of loose particles is a result of chemical changes of adherent fragments because of the influence of the environment. Transferred fragments tend to oxidize and gradually loose their coherence to the underlying surface. This would arise from dimensional changes and the generation of large, unfavourable stresses at the fragment-substrate interface. Kerridge also demonstrated by experiments in controlled atmospheres that the wear rate-determining process was the rate of oxidation of the transferred layers.

This result coincides with that of Soda and Sasada's work[103], in which the wear volume in vacuum was less than in air for metals while the coefficient of friction in vacuum was higher than that in air. He considered the effects of the surrounding gas atmosphere on the wear process and concluded as follows. In the case of rubbing of clean metals in high vacuum, the freshly sheared surface of transferred fragments has a high surface activity because there are no gas molecules to be absorbed onto the surface. Thus, the transferred fragments tend to adhere to the surface again during further sliding, and can accumulate and grow to be large size particles by repeated shearing and transfer, but they have no chance to be removed out of the system as wear particles. On the other hand, if there are effective surrounding gas molecules around the sliding system, a surface formed freshly through the shearing of the junction absorbs the gas molecules to reduce its high surface activity. Therefore the sheared fragments cannot adhere onto their original surface, and they are removed as loose wear particles.

Rabinowicz[101,104] has considered the formation of loose wear particles in terms of the elastic properties and surface energies of adherent fragments. He assumed that a fragment transferred during sliding detaches when its elastic energy exceeds the surface energy at its point of attachment. It was shown theoretically and experimentally that the size of loose wear particles was proportional to the surface energy/hardness ratio.

On the other hand, Kerridge and Lancaster[92] attribute the formation of wear particles primarily to fatigue of the transferred material. The bond between a transferred fragment and the original surface becomes gradually weakened as a result of the cyclic stresses during each passage of the counter surface. Finally, when the bond is very weak, detachment of the transferred fragment from the surface takes place rather than further transfer.

2.4.2.3. Mild (oxidative) and severe (metallic) wear

Adhesive wear under sliding conditions has been characterized by two types of wear mechanism; mild and severe wear. Archard and Hirst[72] produced their definitive paper on the wear of metals under unlubricated conditions in which they introduced the terms "mild" and "severe" wear into the tribologist's vocabulary, together with their definition in terms of observable characteristics. In mild wear a metal surface often becomes visibly oxidized, and intermetallic junctions between the two surfaces can form only rarely. This type of wear gives a smooth surface and the wear rate is usually low. In this case fine oxidized wear debris is produced. In severe wear, extensive intermetallic contact occurs, the surfaces are rough and deeply torn and the wear debris is predominantly metallic and several orders of magnitude larger.

Hirst and Lancaster[87] have studied the wear rate and electrical contact resistance for a brass pin against a stellite ring, as a function of normal load. They found a sharp wear transition from mild wear at loads below 5 N to severe wear at loads above 10 N, which was associated with a change in contact resistance. It was concluded that in mild wear a protective surface film, namely oxide, was formed, and that at the transition load the breakdown of the oxide film took place, resulting in intermetallic contact. They also suggested that at this transition there is a balance between the rate of formation of a protective surface film and the rate of destruction of the film.

Lancaster[105] has studied the conditions of sliding in which a transition occurs between the regimes of mild and severe wear. Since oxide formation plays a crucial role in the process of mild wear, any factor which changes the rate of oxidation of the sliding surfaces will influence the transition. Temperature is the most obvious variable affecting oxidation rate; the temperature at the sliding interface will depend on both the ambient temperature and the frictional heating, which in turn depends on the sliding speed and load. It was found that at low loads, low speeds and low temperatures, mild wear occurred when sufficient time is available to establish a protective surface film by oxidation. In addition, mild wear also occurred at heavy loads, high speeds and high temperatures because of an increase in the rate of oxidation. Furthermore, the examination of surface damage in the mild wear regime suggested that the probable mechanism of wear was abrasion by oxide particles, and flaking of the oxide layers from the surface.

Quinn[106,107] has proposed an expression for the wear rate under mild wear conditions, based on the Archard equation (2.12). He modified Archard's[80] interpretation of k by assuming that $1/k$ encounters are necessary to produce a critical oxide thickness ξ at the real areas of contact A and obtained the following equation:

$$W = d\ A\ A_p \exp(-Q_p/(R\ T_0))\ /\ (\xi^2\ \rho^2\ f^2\ V) \qquad \text{(Eq.2.13)}$$

where W is the wear rate per unit sliding distance, d the distance of a wearing contact at an asperity, A_p the Arrhenius constant, Q_p the activation energy for parabolic oxidation, R the molar gas constant, ρ the density of the oxide formed at the real areas of contact, f the fraction of oxygen of the oxide, V the sliding speed and T_0 is the temperature of oxidation.

This model proposes that oxide layers grow on contact asperities by a parabolic diffusion process until they reach a critical or maximum thickness when they spall off completely.

One of the problems with Quinn's theory is obviously that his wear equation (2.13) contains many ill-determined parameters. These are d, ξ, T_0, A_p and Q_p. It was shown that analysis of the thermal aspects of sliding gave relationships between d, ξ and T_0, and that by using a computer search technique, the values of these parameters could be deduced[108]. Although the oxidation constants, A_p and Q_p, can be obtained from the values in the conventional static oxidation case, the tribological values of these oxidation constants were derived from best-fit computer searches and could then be employed to predict wear rates for steels[75,109]. In this calculation, the critical oxide thickness was found to be 1 to 3 μm.

Soda and Sasada[103] have described mild wear in dry sliding condition as well lubricated wear by the surrounding gas molecules even if no organic liquid is applied. Their experiments were carried out by using transition metals (Ni, Fe, Pt, Mo and W) and non-transition metals (Cu, Al, Zn, Ag and Sn), and a wear test metal was rubbed against the same metal. They found that in transition metals which are active to gas chemisorption, two types of wear (i.e. mild and severe wear) were observed. On the other hand, non-transition metals, which are non-active to gas chemisorption, showed no mild wear over the whole sliding condition range.

Mishina[110] has studied the effects of atmospheric pressure on adhesive wear of metals in dry air, oxygen and nitrogen. It was shown that the atmospheric characteristics in wear of metals are classified according to the strength of activity in the chemisorption of gas molecules on the metal surfaces. He has suggested that mild wear is not due to the oxidation of wearing surfaces, but due to the chemisorption of surrounding gas molecules.

2.4.3. Abrasive wear

Abrasive wear is caused by the ploughing-out or cutting-out of material by a hard surface. The term 'abrasive wear' covers two situations; two-body and three-body situations[111]. In the former, a rough hard surface slides against a softer surface, or hard particles are transported along a surface. In three-body abrasion, wear is caused by loose hard particles sliding between rubbing surfaces. It should be noted that not only minerals or environmental dust but also wear debris produced by adhesive or corrosive wear mechanisms can cause three-body abrasion.

Rabinowicz[112] has proposed a simple model in which material is removed by a cutting motion caused by a conical hard asperity moving across a surface, and then described the volume of wear as follows:

$$V = K\ W\ L\ \tan\theta\ /\ H \qquad \text{(Eq.2.14)}$$

where V is the volume of wear, K a constant, W the normal load, θ the base angle of the asperity, and H the hardness of the material.

It is obvious from the nature of abrasive wear that hardness is an important material property influencing wear resistance. Kruschov[113] found that the abrasive wear resistance of a large number of pure metals and of annealed metals was directly proportional to the hardness of the metals. He also showed that for several steels heat treated to different hardness levels the slope of wear resistance against hardness was lower than for pure metals, and that the line was displaced to higher wear resistance values as the carbon content of the steels was increased. He finally studied the effect of increasing material hardness by prior mechanical working and showed that prior work hardening of the material through cold deformation did not improve the wear resistance at all.

Larsen Badse[114], who repeated Kruschov's experiments, proposed that the abrasive wear resistance is a function of both the hardness of the metal and of its work hardening exponent. Richardson[115] and Tylczak[116] have demonstrated that abrasive wear resistance of metals correlates better with the hardness of worn or otherwise work-hardened metals rather than with the hardness of unworn, annealed metals. These studies have suggested that since plastic deformation of wearing surfaces takes place during abrasive wear, the change of material hardness caused by the deformation should be taken into account to describe abrasive wear resistance.

Although hardness is one of most useful guides to abrasive wear resistance, it is not the only parameter that determines wear behaviour. Moore[117] investigated the effects of microstructure of steels on abrasive wear resistance. He found that the wear resistance of pearlitic steels is a linear function of the pearlite volume fraction, and that for martensitic steels the wear resistance is a linear function of the square root of the carbon content. Moore[118] has also shown that the abrasive wear resistance of steels generally increases with increasing hardness, but that austenitic and bainitic structures are superior to ferritic, pearlitic and martensitic structures of the same hardness. He attributed this to the higher work hardening capacity and ductility of an austenite structure.

Hutchings[119] has pointed out that in the abrasive wear of a two-phase or hard-phase dispersed material, the relative sizes of the abrasive particles and the hard-phase regions must be considered. He showed that if the size of an abrasive particle is substantially greater than that of the dispersed hard-second particles, the wear resistance generally increases as the volume fraction of the second phase increases. If the hard-phase particles are comparable in size with the scale of the abrasion damage, wear will depend on the strength of the interface between the hard-second phase and the matrix. These investigations have suggested that material microstructure has a significant influence on abrasive wear resistance.

For very high hardness materials, for example, ceramics, other material properties such as fracture toughness should be taken into account because the wear damage can be initiated by crack formation in these materials. Gahr[120] has introduced the fracture toughness of materials, K_{IC}, to describe abrasive wear resistance of materials, and shown that the wear resistance of materials with high hardness and low fracture toughness increases to a maximum as fracture toughness increases. Over this range, wear resistance is very dependent on fracture toughness, and increases as hardness decreases, because generally there is a negative relationship between hardness and fracture toughness. As fracture toughness increases further, wear resistance decreases and wear is dependent on hardness. In these circumstances maximum wear resistance will be achieved in a material with intermediate values of hardness and fracture toughness.

It has been reported that in abrasive wear situations not only the properties of wearing materials but also the nature of abrasive particles such as hardness and shape have significant effects on wear behaviour. Richardson[121] has emphasized the importance of considering the hardness of abrasive particles, and he referred to "soft" and "hard" abrasives. He showed that the wear resistance of materials increases rapidly when the material/abrasive hardness ratio exceeds some critical value which was found to be 0.8.

In practice, the sizes of abrasive particles cover a wide range, and the abrasive particle size is also a factor influencing abrasive wear behaviour. Moore[118] has shown that abrasive wear generally increases as the abrasive size increases, and suggested that for fine abrasives a lower fraction of the load is carried by particle contacts that are able to remove material, because (i) a large number of contacts will make elastic contact only, (ii) loose wear debris tends to hinder the contact of some particles and (iii) in laboratory tests fine abrasives deteriorate much more rapidly than coarse abrasives. However, Misra and Finnie[122] have found that this size effect becomes less efficient when the abrasive size exceeds about 100 μm. They attributed this to the hard surface layers of material produced during abrasive wear.

In addition to the properties of abrasive particles themselves, geometry and orientation of abrasive particle contacts also have a significant influence on the formation of wear debris during abrasive wear. Mulhearn and Samuels[123] have introduced the concept of attack angle of contacting abrasive particles, which is defined as the angle between the contacting face of an abrasive particle and the material surface, and assumed that microchips are produced by a cutting action only when the attack angle exceeds a critical value. The frequency distribution of the attack angle of contacting abrasive particles was determined by the microscopic examination of sections of abrasive paper, and the critical attack angle for cutting was determined by experiments using a single-point indenter, the geometry of which was known. They found that the critical angle was about 90° for all the materials investigated, and then suggested that the fraction of cutting contact points of abrasives can be estimated from the distribution of the attack angle.

In the model used to derive equation (2.14), it was assumed that all the abrasive particles would have the same geometry and remove material from the grooves they form in the same way. In practice, however, abrasive particles deform the material surface in different ways. Murray and coworkers[124] have described two mechanisms of groove formation in materials. The first one is plastic-flow grooving, often referred to as ploughing, in which material is continuously displaced sideways to form ridges adjacent to the developing groove. In the ideal case no material is removed from the surface. The second mechanism of groove formation is chip-formation cutting, in which the material displaced from the groove is fully detached from the surface by a micro-machining mechanism.

The conditions in which these mechanisms of abrasive groove formation occur are obviously influenced by a number of factors such as the attack angle of contacting abrasive particles and the properties of the wear material. Hokkirigawa and coworkers[125] have investigated the transitions between the mechanisms of groove formation in abrasive wear for steels. The wear tests were carried out in an SEM (Scanning electron microscope) using a scratch tester in which a hard spherical indenter slides over a flat steel specimen, and the wear mechanisms were determined by in-situ SEM observations. They identified three mechanism modes; ploughing, wedge-formation and cutting, and showed that the transitions between these mechanism modes take place as the degree of penetration of the indenter changes. They have also proposed an abrasive wear mode diagram based on the degree of penetration and the hardness of material.

2.4.4. Fatigue theories in sliding wear

It has been shown that when sliding surfaces make contact via asperities, wear can take place by adhesion or abrasion. However, it is conceivable that asperities can make contact without adhering or abrading and can pass each other, leaving one or both asperities plastically deformed[111]. As discussed in section 2.4.2., although adhesive wear theory can explain transferred wear fragments, neither adhesive nor oxidative wear mechanisms explain how loose wear particles are formed as a logical consequence. In addition, the occurrence of wear of the harder of two rubbing surfaces is difficult to understand in terms of adhesion or abrasion theory. Recently, the importance of the role of fatigue in sliding wear situations has increased, apart from rolling-contact fatigue wear. Thus the role of fatigue to be considered here is that in sliding wear.

Kimura[126], who pointed out the deficiencies in the adhesive wear theory, has proposed that fatigue mechanisms are responsible for the majority of the remaining wear cases where, neither abrasive, corrosive, nor adhesive wear by their strict definition, are attributable. The repeated nature of the interfacial interaction in sliding wear suggests that fatigue-like processes should play a significant role in mechanisms of material removal by wear. He started the introduction of the fatigue concept by interpreting the probability factor *k* in Archard's theory[80] in terms of fatigue fracture. The factor *k* was interpreted by assuming that a wear particle is produced when an asperity has experienced a sufficient number of contacts and damage to produce a fatigue fracture. Thus one of the shortcomings in the Archard's theory, in which the sliding contacts have no effect on (1-*k*) asperities even after an interaction between the asperities, was eliminated.

Kragelskii and coworkers[71] have interpreted many wear results in terms of fatigue, and also proposed a mathematical expression of wear. They have suggested that wear results from cyclic stresses and deformation of materials depending on surface roughness, nominal pressure, friction coefficient and the material properties. Wear by plastic contact of asperities is associated with low-cycle fatigue, in which the cyclic stresses are above the elastic limit of the materials. The number of cycles to failure, *n*, was related to the actual amplitude value of the deformation on each cycle, *e*, by the following equation:

$$n = (e_0 / e)^{t} \qquad \text{(Eq.2.15)}$$

where e_0 is the value of the relative elongation of the material at break point. The exponential parameter, *t*, was shown to vary over a narrow range of values, i.e. from 2 to 3.

Another wear theory, called delamination wear, has been proposed by Suh[73] in order to explain the formation of thin plate-like sheets of wear debris. This theory is based on the behaviour of dislocations at the surface, sub-surface crack and void formation, and subsequent joining of cracks by shear deformation of the surface. The mechanism of delamination involves the following stages[74]:

(1) When two sliding surfaces come into contact, normal and tangential forces are transmitted through contacting asperities, which deform to smooth the surface. Once the surface becomes smooth, the contact is not just an asperity-to-asperity contact, but rather an asperity-plane contact; each point along the softer surface experiencing cyclic loading as the asperities of the harder surface plough it.

(2) Plastic shear deformation accumulates in the surface layers.

(3) Cracks are nucleated below the surface. Triaxial compressive stresses are present just below the surface and this forces crack nucleation to a lower level.

(4) The cracks grow and join. The cracks tend to propagate parallel to the surface at a depth.

(5) The cracks finally shear to the surface at certain week positions, and then thin wear sheets "delaminate".

This model is obviously based on the behaviour of dislocations by cyclic loading, and the failure feature in which fracture is caused by formation and growth of cracks in subsurface materials is also similar to a fatigue process. There is, however, some danger of classifying all wear processes which produce plate-like debris as part of a single "delamination" process[2]. Other workers[e.g. 75,127], have shown that plate-like wear particles may be generated by entirely different mechanisms.

Observations of wear surfaces, subsurface layers and wear particles have clearly indicated that fatigue mechanisms are operating during wear processes. Heilmann and Rigney[128] have reported direct experimental evidence for a fatigue mechanism in the formation of wear debris during sliding wear. They examined a part of the worn surface of a Ni-Cu alloy rubbed against stainless steel by SEM. The SEM stereo view showed clear striations similar to those commonly associated with fatigue failure. Rigney and Glaeser[129] have found a cell-type microstructure in sliding metal subsurfaces in a TEM (Transmission electron microscope) observation. The cell structure is produced by a high density of dislocations, which are a result of the repeated ploughing of asperity contacts over the mating surfaces. They suggested that the complex dislocation tangles, comprising high energy cell boundaries, are suitable regions for void formation and crack nucleation, and that the subsurface cracks can run parallel to the cell boundaries. It has been concluded therefore that the cellular microstructure presents many suitable pathways for separation of wear debris from the surface without the requirement of adhesion and shear. A close quantitative correlation between the mean size of wear particles and the thickness of the plastically deformed subsurface layer has been also reported[130].

An impressive study of a correlation between wear and fatigue has been reported by Soda and coworkers[131]. They examined the reversed bending fatigue and the pin-on-disc wear of Ni, Cu and Au pure metals as a function of atmospheric pressure. It was found that similar curves were obtained for each metal when the reciprocal of the fatigue life and the number of wear particles were plotted against the atmospheric pressure. They have suggested, therefore, that the changes in the number of wear particles or the amount of wear with atmospheric pressure are governed by the resistance of the metals to fatigue. This correlation is a strong argument for a similarity between wear and fatigue mechanisms. However, Kimura[126], one of the authors of this work, has remarked that positive evidence to show quantitative correlation between wear and fatigue resistance of materials is sparse because of irregular surface geometry, complicated contact mechanics and uncertain environmental effects.

2.4.5. Wear transition diagrams and wear mechanism maps

Although various wear mechanisms have been reviewed so far, most researchers have been content with simplified models based on a favourite mechanism, and the research has tended to focus on the details of a single mechanism, not on the relationship between mechanisms. Therefore the lack of an overall framework or pattern of wear mechanisms has been recognized recently, and Lim and Ashby[132] have pointed out that it is very important to summarize data and models for wear, showing how the mechanisms interface, and allow the dominant mechanism, for any given set of conditions to be identified.

Wear under metal-to-metal sliding conditions is subject to sharp transitions in behaviour. Welsh[65] was the first to examine systematically the concept of mild (oxidative) wear and severe (metallic) wear, by studying the wear of plain carbon steels under unlubricated conditions over wide ranges of sliding speed and applied load. He demonstrated clearly that large changes in wear rate can result from small changes in speed and load, and produced a transition diagram shown in Fig.2.6. The features of this diagram with increasing load are:

(1) A transition from mild to severe occurring at relatively low load, called T_1.

(2) A transition from severe to mild wear at heavier load, called T_2.

Below T_1, wear occurs by the removal of oxide debris from an oxidized surface. T_1 is a transition to severe wear initiated by the break down of the protective surface oxide. Between T_1 and T_2, severe metallic wear occurs. At the T_2 transition, the surface temperature is high enough for phase hardening to produce a hard layer structure which prevents deformation and helps to establish an oxidized surface once more.

Welsh has also showed that these transition loads depend on the sliding speed and the carbon content of steel. For 0.52% carbon steel, an increase in sliding speed displaces both T_1 and T_2 transitions to lower loads. At a constant sliding speed of 1 $m \cdot s^{-1}$, as the carbon content is reduced, T_1 is displaced to lower loads and T_2 to higher loads, and for the lowest carbon content (0.026% C) severe wear occurs over the whole range. Conversely, an increase of carbon content rapidly narrows the range of severe wear, and for carbon content of no less than 0.78% the severe regime is eliminated.

In addition, it has been shown that varying the hardness of steel by heat treatment also changes the general pattern of transition behaviour. For quenched and tempered 0.52% carbon steel at a high hardness (Hv 855) mild wear occurs over the whole load range at a sliding speed of 1 $m \cdot s^{-1}$. The first appreciable deviation occurs after tempering at 500°C when the hardness has reduced to Hv 436. This deviation increases in extent until a hardness level of Hv 348 at which sharp T_1 - T_2 transitional behaviour is produced. Further softening expands the severe wear range by depressing T_1 and elevating T_2.

Recently, Lim and Ashby[132] have compiled much of the published data on the unlubricated wear of steels in a typical pin-on-disc configuration, and produced a sequence of wear mechanism maps. Fig.2.7 is one of their wear mechanism maps, which is based on normalized stresses and velocities. The wear map shows the wear rate and the regime of dominance of each of a number of mechanisms. The dominant mechanisms of wear were determined in two ways; by plotting empirical data from experiments performed under widely differing conditions, and by the use of simple analytical models for wear rates due to the various mechanisms. In constructing this wear map, they have identified the following wear mechanisms:

(1) Seizure at very high contact pressure
(2) Melt wear at high pressure and high sliding speeds
(3) Oxidation-dominated wear at high sliding speeds
(4) Plasticity-dominated wear at low sliding speeds.

In addition, they have related these wear mechanisms to the "mild" and "severe" classification of Archard and Hirst[72], and indicated the ranges of sliding conditions in which a transition between mild and severe wear takes place as shaded regions in the wear map[133]. However, as they have pointed out themselves, the wear map should be regarded only as a first approximation, not as a precise map, because so many mechanisms have been involved in describing wear.

2.5. Summary

The major features of the literature reviewed can be summarized as follows.

Metallurgical characteristics of nitrided steels, including the hardening mechanism related to the interaction with alloying elements, have been well established. The effects of nitriding process parameters on the mechanical properties are fairly well understood.

There is no shortage of information on nitriding processes, which illustrate an improved method to achieve the desired properties for wear, fatigue and corrosion. Furthermore, most of the literature also demonstrates an improvement in the cost performance or the environmental behaviour of the process. Many types of nitriding and nitrocarburizing techniques have been developed, and they have been very widely used for engineering components, for example, in the automobile industry.

Some investigations, in particular on nitrocarburizing, focus on the formation and the growth of a compound layer (white layer), and relate these to thermodynamics and diffusion theory. Although physical and chemical properties of the compound layer have been explained in great depth, there are still questions about the kinetics and mechanisms of the layer growth.

Regarding the wear of nitrided steels, it has been widely recognized that nitrided or nitrocarburized steels have high wear resistances. However, most of the published work ignores the fact that the wear behaviour is strongly affected by tribological parameters, and some wear tests were carried out under specific wear conditions. Moreover, contradictory evidence has been reported about the effects of the compound layer and nitriding methods. This feature of the literature suggests the importance of systematic research on wear of nitrided steels.

Although the understanding of wear mechanisms has been improving, no reliable and general laws of wear have been established owing to its complexity. A number of authenticated wear theories have been proposed, which are based on experimental observations. These are, for example, oxidative wear, delamination and fatigue theories. However, there is a tendency to isolate each mechanism and over-emphasize its role in the overall wear process. Finally, mapping of wear mechanisms provides a new approach to predict a predominant wear mechanism in practical situations.

Because of the considerable interest in surface engineering and the rapid development of new and improved surface treatment techniques, it is clear that the "wear mapping approach" for surface treatments is required. It is reasonable to use nitriding as the base on which to investigate the "wear mapping approach", because there is a considerable volume of work and experience available on nitriding processes and new or improved processes will be compared to nitriding. Therefore a study of wear mapping of nitrided steels is required as the first step to produce wear maps of surface treatments, which will be useful for designers and engineers to make the best use of surface treatments and coatings for wear applications.

Chapter 3: Experimental

3.1. Wear tests

3.1.1. Wear testing machine

A pin-on-disc wear machine was used to evaluate the wear characteristics of materials. This method involves a stationary loaded pin rubbing against a rotating disc. The technique was chosen for the following reasons:

(1) It is capable of testing materials under a wide range of loads and sliding speeds.

(2) It is one of the most frequently used test systems for sliding wear studies in the literature [134,135], and the results obtained can be used and compared by other investigators to produce a data base.

(3) It has been accepted by ASTM (American Society for Testing and Materials) as Standard G-99.

Fig.3.1 shows a schematic diagram of the pin-on-disc wear machine used in this study, and Fig.3.2 is a general view of the wear testing arrangement. A wear disc is fixed on a rotating shaft connected to the output of a 3-phase 0.75 kW electric motor via a reduction V-belt. The motor, which gives a speed of 1410 rpm, is equipped with a speed reduction drive of the infinitely-variable type. This is capable of giving a disc rotational speed in the range 60-1200 rpm. The rotational speed of the disc was measured by using a tachometer prior to wear tests.

A wear pin is held in a pin holder which is connected to a load arm. The weight of the arm is counterbalanced by a counterweight attached to the opposite end. The pin was loaded onto the disc by a dead weight via the load arm.

Two linear variable differential transducers (LVDT) were set to measure the friction force and the linear descent of the pin during a wear test. The output of the transducers was connected to an ultra violet recorder.

3.1.2. Wear specimens

The schematic diagram of the wear pin and the disc used in this study is shown in Fig.3.3.

The wear pin was 39 mm long and 12 mm in diameter, and the wear faces were flat, and 2 mm in diameter. Consequently the apparent contact area of the pin was 3.14 mm^2. The pins were produced by cutting and machining from BS970,905M39 (EN41B) steel bar and BS970,635M15 (EN351) steel bar. The wear faces of the pin were ground to a surface finish of 1.5 to 2.0 µm in Rt (maximum height of roughness profile). After machining and grinding, the BS970,905M39 (EN41B) and BS970,635M15 (EN351) pins were nitrided and carburized, respectively. The detail of the composition of materials and the surface treatment processes are described in section 3.2.. For the purpose of comparison of wear characteristics, untreated (as received) steel pins were also studied.

The wear discs, 12 mm thick and 130 mm in diameter, were manufactured from BS970,535A99 (EN31) steel bar. Two holes

(12 mm and 6 mm in diameter) were made in the disc to fix to the rotating disc holder of the wear machine. After being heat treated, the discs were ground to produce a surface finish of 0.6 to 0.8 µm in CLA(Centre-Line-Average).

3.1.3. Wear test procedure

For each wear test, new surfaces of a pin and a disc were used. Several tests can be carried out with one disc by changing the wear track diameter within the range of 50 to 110 mm. Prior to making a test, the wear pin and disc to be tested were degreased in acetone. The pin was weighed by a balance accurate to 0.1 mg, and then fixed in the wear machine as shown in Fig.3.1.

A linear variable differential transducer (LVDT) for the wear measurement of a pin was set to give the appropriate span, and the calibration on a chart recorder was carried out by gauges. The linear descent of the pin caused by wear was continuously monitored during each test. With the configuration described, the disc wear depth was so small in comparison with pin wear that the disc wear has been ignored in this study. The length of a pin was also measured before and after the wear test by a micrometer accurate to 1 µm, and the change of the pin length was very close to the value obtained from the wear transducer technique. Thus it is reasonable to consider that the linear expansion of a wear pin caused by friction heating during a wear test is negligible. In addition, the wear volume of a pin calculated by the transducer technique agreed well with that obtained by the direct weighing method. Because this LVDT arrangement has the advantage that wear measurement can be made without interrupting the wear process, the amount of the wear of a pin was evaluated mainly by the transducer technique in this study.

Friction measurement was made directly from the chart print-out via a friction LVDT. The calibration of the recorder was carried out with the aid of spring balances.

One of the aims of this work is to investigate the sliding wear characteristics of nitrided steels over a wide range of sliding speed and applied load. Sliding speeds of 0.2, 0.5, 1, 2 and 5 $m \cdot s^{-1}$, and applied loads of 2 to 200 N were used. The wear running time was between 3 seconds and 12 hours, depending on the pin materials and wear test conditions. All wear tests were carried out under unlubricated conditions in a normal laboratory atmosphere at 55-70% relative humidity and a temperature between 15-22°C. Although most engineering mechanisms involve lubrication apart from those operating in outer space or at elevated temperatures, studies of dry (unlubricated) wear rather than lubricated wear are profitable for the following reasons[136]:

(1) The wear of lubricated systems is extremely small and experimental studies would be long, and also irreproducible owing to the complexity of interaction with a lubricant.

(2) The wear of lubricated systems occurs primarily as a result of the breakdown of the lubricant film, and local lubricant breakdown is equivalent to dry contact. To simplify the problem of imperfectly

lubricated surfaces, it is desirable to eliminate the lubricant, so that interaction of lubricant with the surface does not confuse the wear behaviour.

On completion of a test, the pin was removed from the wear machine and weighed. The worn pin and disc were stored carefully for material examination. Wear debris from the test was also collected for later examination.

3.2. Specimen materials

3.2.1. Material composition and microstructure

The material used for nitriding was BS970,905M39 (EN41B) steel and its chemical composition is shown in Table 3.1. This steel contains Cr, Mo and Al which are nitride-forming elements. These have a significant effect on increasing the surface hardness after nitriding[15]. Fig.3.4 (a) shows the optical microstructure of 'as received' BS970,905M39 (EN41B) steel, which is a normalized fine pearlitic structure. The hardness of this steel was Hv 260.

For carburized and hardened wear pins, BS970,635M15 (EN351) Cr-Ni case hardening steel (Table 3.1) was used. Cr and Ni alloying elements play a role in increasing the hardenability of the steel. The microstructure of 'as-received' BS970,635M15 (EN351) steel is shown in Fig.3.4 (b), which represents a mixture of ferrite and pearlite with a hardness of Hv 200.

Wear discs used throughout the series of tests were BS970,535A99 (EN31) high carbon-chromium bearing steel (Table 3.1). The main reason for its selection is that it is widely used for tribological components (rotating shafts, rolling element bearings, cams etc.) in many industries. This steel was quenched and tempered to give a hardness of Hv 700. The microstructure of the disc steel is shown in Fig.3.4 (c), which represents a tempered martensite structure with some finely dispersed carbides.

3.2.2. Surface treatment processes

Three types of nitriding were carried out for BS970,905M39 (EN41B) steel; gas nitriding, plasma nitriding and gas nitrocarburizing. Also, a gas-carburizing and hardening treatment was carried out for BS970,635M15 (EN351) steel only for the purpose of comparison of the wear behaviour between these treatments. Commercial processes were employed for all of these surface treatments, because the main aim of this work is not to study or develop the nitriding process itself, but to assess the wear characteristics of specimens after using available nitriding processes systematically from an engineering point of view. The details of these processes are described in the following sections.

3.2.2.1. Gas nitriding

Gas nitriding was carried out using a vertical batch-type furnace at Senior Heat Treatment Ltd. Fig.3.5 (a) shows a view of the gas nitriding furnace and the nitriding gas flow control units used in this study. The furnace consists of a heating chamber of 800 mm high and 600 mm in diameter, electrical heating elements, a control thermocouple and a circulating fan capable of making the temperature and atmosphere uniform in the furnace.

Wear pin specimens and a test piece to be examined for metallography were placed in a work-holding basket, which was in turn lowered into the heating chamber. The nitriding atmosphere was ammonia gas which was supplied from an anhydrous liquid ammonia tank. 100% ammonia gas was passed into the treatment chamber, and specimens were nitrided by the following reaction[15]:

$$2NH_3 \rightarrow 2[N]_{Fe} + 3H_2 \qquad \text{(Eq.3.1)}$$

The gas nitriding process in this study was carried out at a temperature of 520°C for 80 hours. These conditions of treatment temperature and time are commonly employed for those gas nitrided engineering components that require a relatively deep case depth, for example, gears or crankshafts. After the nitriding treatment, the furnace heating elements were turned off and the specimens were cooled below 100°C in the ammonia atmosphere chamber. On completion of the process, the nitrided specimens were removed from the furnace and provided for metallurgical examination and wear tests.

In gas nitriding, all of the surface areas of parts which are exposed to an ammonia atmosphere are nitrided via introduction of nitrogen, so that not only the flat wear-face of the wear pin but also the cylindrical side-face of the pin is hardened. Thus, during a wear test, the wear behaviour of a nitrided pin will be affected by the case layers of both the wear-face and the side-face. Therefore, in order to study the effect of the hardness variation through a case layer on wear characteristics, it was necessary to prevent nitriding of the side-face areas of a pin. In this study, wear-face limited gas nitriding of a pin was carried out by covering the side-face areas of the pin with a commercial paste-like agent before nitriding. After gas nitriding, the covering agent was removed from the nitrided pin.

In this study, only a few wear pins were "wear-face-limited" gas nitrided for the purpose of studying the effect of the hardness in the case layer, and the majority of wear pins were gas nitrided without preventing nitriding of the side-face areas of the pins. These normally gas nitrided wear pins were mainly used to investigate the effects of loads and sliding speeds on the wear of nitrided steels, and to compare the wear characteristics with other nitriding processes. In this thesis, the term "nitrided pin" refers to the pin that was nitrided all over, and a "wear-face-limited" nitrided pin is a pin that was nitrided by preventing nitriding of the side face of the pin.

During gas nitriding, an iron-nitride compound layer (white layer) is formed at the surface of a part. In order to investigate the effect of the compound layer on the wear behaviour of nitrided steel, some wear tests were carried out using a nitrided pin without the compound layer. The nitrided pin without the compound layer was prepared by removing the compound layer after gas nitriding. The wear-face of a gas nitrided pin was ground with a silicon carbide paper of 400 grit size to the depth of the compound layer.

3.2.2.2. Plasma nitriding

Plasma nitriding was carried out using a commercial 40 kW Klöckner Ionon GMBH unit at Nitriding Services Ltd (Fig.3.5 (b)). This equipment contains a treatment chamber, a power supply unit to provide a d.c. power input to the chamber, and a gas supply and vacuum system capable of evacuating the chamber and supplying the treatment gas. Treatment parameters i.e. time, temperature, pressure etc., are set at a computer-control unit.

Wear pin specimens to be treated were held in a special steel jig of dimensions 400 x 300 x 7 mm, which was in turn placed on a cathode base plate. The jig has holes of an adjusted diameter for the wear pins to be fixed. Otherwise the contact face between a wear pin and the cathode jig is so small that the face will be heated too much because of the local high current. The cathode components were then placed in the vacuum treatment chamber.

The treatment temperature was controlled via an electrically insulated thermocouple inserted into the cathode plate. The temperature of the specimens was also monitored using a remote pyrometer. The specimens were nitrided at 530°C for 60 hours. The injected gas was a mixture of 25% nitrogen and 75% Hydrogen. The gas pressure was maintained at 300 Pa throughout the treatment, and the d.c. voltage of discharge was 450 ± 50 V. At the end of the treatment, the power was switched off automatically and the specimens were cooled below 150°C in the vacuum chamber.

3.2.2.3 Gas Nitrocarburizing

Nitrocarburizing is a ferritic treatment in which both nitrogen and carbon are introduced to a steel surface. Thus nitrocarburizing is usually carried out in an atmosphere of a mixture of nitriding and carburizing gases. In this study a gaseous method was employed, because salt bath nitrocarburizing is not available in U.K. owing to its environmental problems.

Fig.3.6 shows the nitrocarburizing furnace used in this study at Senior Heat Treatment Ltd. The furnace is a horizontal batch-type with a heating chamber of dimensions 700 x 700 x 900 mm and a sealed oil quenching system. The chamber is heated electrically and the treatment temperature is controlled by a thermocouple in the chamber.

Wear pin specimens to be treated were placed in a basket and pushed into the furnace. Endothermic gas was selected for the carburizing part of the process, because this gas not only provides a high degree of flexibility over the control of the carburizing potential, but also is widely available throughout the heat treatment industry. Endothermic gas, which contains methane (CH_4) and carbon monoxide (CO) [20], was generated from natural gas using a nickel catalyst at 1030°C. A mixture of 50 % ammonia gas and 50 % endothermic gas was passed into the treatment furnace. Because the endothermic gas is combustible, the gas coming from the furnace burns in contact with outside air, as can be seen in Fig.3.6. The nitrocarburizing process in this study was performed at 570°C for 2.5 hours. Because the purpose of nitrocarburizing is to obtain a compound layer and only a shallow hardened surface layer at low cost, a high temperature and short treatment time were employed in comparison with gas nitriding. After the treatment, the specimens were cooled in the oil tank in the furnace.

3.2.2.4. Carburizing and hardening

For the purpose of comparison of wear behaviour, some wear pins were gas carburized and hardened. This process was carried out using the same furnace as nitrocarburizing, as shown in Fig.3.6. Specimens were carburized at 920°C for 3 hours in a mixture of endothermic gas and methane gas. By monitoring the concentration of the carbon dioxide (CO_2), the carbon potential was controlled in the range of 0.8-1.0 %. After carburizing, the specimens were cooled to 810°C and then quenched into oil at 40°C in order to obtain a surface-hardened layer. The specimens were also tempered in an air atmosphere at 160°C for 1.5 hours to improve the toughness of the material.

3.2.3. Metallurgical examination of surface treatments

After nitriding, the heat treated test pieces were sectioned and mounted in bakelite for metallographic examination. The microstructure of nitrided steels was examined by optical microscopy in a 90° cross-section. The sectioned samples were ground and polished via 1 µm diamond paste, and etched in 2% nital. By metallographic observation, a nitride compound layer (γ' or ϵ-nitride), which is formed at a steel surface during the nitriding process, is revealed as a white surface layer, so that the thickness of the compound layer formed can be easily determined.

The hardness through a nitrided case layer was measured on the same sectioned and polished sample. The hardness measurement was performed on a Leitz miniload micro Vickers hardness tester employing a load of 3 N at 50 µm intervals. The effective case depth, which is defined by the perpendicular distance between the surface and the layer having a Vickers hardness of Hv 550[19], was determined from the profile of hardness on the cross section normal to the surface.

The hardness of the compound layer formed at a surface was also measured using the same Vickers tester. In this case, much lighter applied loads of 0.1-0.25 N were employed to prevent the formation of cracks in the compound layer. Moreover, in order to avoid the effect of the surface edge of a sample, microhardness indentations were made at those positions where each corner of the indentation shall be at least half the length of a diagonal from the surface edge[137].

The microstructure and microhardness of a carburized and hardened steel was also examined in the way described above.

In order to identify the phases of the compound layer formed at a nitrided surface, the flat surface of an 'as nitrided' test piece was examined by X-ray diffraction.

This X-ray analysis was carried out using Cu Kα radiation (the wave length; λ=0.15418 nm) on a Philips PW1050 vertical diffractometer in conjunction with a wide-range goniometer and stabilized X-ray generator. The angular range scanned was 25-90 degrees in 2θ (step size; 0.021 degrees in 2θ), which covered major reflections of the phases concerned, and the scan speed was 1.2 degrees in 2θ per minute. The generator voltage and the current were 30 kV and 20 mA, respectively. The phase identification analysis was made using JCPDS (Joint Committee on Powder Diffraction Standards) cards.

3.3. Material examination techniques after wear tests

Several techniques were used to examine worn surfaces and wear debris after wear tests for the identification of the wear mechanisms.

3.3.1. Visual examination

After wear testing all physical changes of wear surfaces visible to the eye, such as colour, surface topography, transfer of material and shape change were noted. In addition, visual appearance of the wear debris collected from each wear test was also noted in terms of colour and particle size. For recording, photomacrography of wear pins, discs and debris was carried out.

3.3.2. Optical microscopy

Wear pins and discs were examined using optical microscopy of the subsurfaces to investigate the metallurgical changes as a result of wear. The subsurface observation was carried out on a transverse section which is perpendicular to the sliding direction and a longitudinal section which is parallel to the sliding direction, as indicated in Fig.3.7. For some wear specimens, the damaged sublayer was too thin to show up well in a normal 90° section. In such cases, a taper sectioning technique was used to expand the sublayer in the vertical direction. The taper sectioning was carried out by polishing at a oblique angle, as shown in Fig.3.8. This method makes use of a special dummy plate when mounting the wear specimen (Fig.3.8 (a)). By knowing the thickness of the dummy plate, *x*, and the distance between the specimen corner to be polished out and the dummy plate, *y*, the ratio of the magnification of the subsurface section in the vertical direction and in the horizontal direction is obtained, i.e. $\surd(x^2+y^2)/x$. After polishing, the samples were etched with 2% nital solution for metallographical observation.

In addition to optical microscopy of the taper sections of wear specimens, microhardness measurement was performed on the same taper sections to investigate the hardness change of the sublayer as a result of wear. The taper sectioning method also has the advantage that microhardness indentations can be obtained at much smaller depth intervals than is possible with sections normal to the surface. The hardness measurement was carried out in the normal way by using the same Vickers tester described in the section 3.2.3..

3.3.3. Scanning Electron Microscopy (SEM)

The SEM technique is particularly useful in the examination of surface topography. The high resolution and large depth of field, which produces apparent three dimensional images, provide invaluable information about the surfaces over a wide range of magnifications.

The worn surfaces of both a pin and a disc were examined using a Cambridge S250 Scanning Electron Microscope to investigate the change of the surface topography as a result of wear. Although some specimen preparation was necessary in order to reduce the sample to a size compatible with the SEM mounting stage, no preparation was made on the wear surface to be examined.

The SEM technique is also very useful for the evaluation of particle shape and size, so that the wear debris produced during a wear test was also examined. A small amount of debris particles to be examined were mounted on double-side sellotape, which in turn was placed on an aluminium holder. In the case of fine wear debris, the small particles tended to be agglomerated together into a larger aggregate, thus the wear particles were separated from each other using an acetone ultrasonic bath. The acetone which contained some wear particles was dropped directly to an aluminium holder, and then the sample holder was set aside until the acetone on the holder evaporated. In both cases the sample was coated with gold and palladium by a sputtering technique for about 5 minutes to give good electrical conductivity. The wear debris was then viewed in the SEM in the normal way.

3.3.4. Electron Probe Micro Analysis (EPMA)

Electron Probe Micro Analysis (EPMA), which utilises the characteristic wavelength X-rays generated by the interaction of the electron beam with a sample, is useful in identifying elements present on the sample surface. This technique was used only to ascertain the presence of the oxides formed on the worn surface of a disc. The EPMA was carried out with a JEOL JXA-840A Electron Probe Microanalyzer. Qualitative line scanning analysis was performed across the wear track on the worn surface, and then the intensity profile of the generated oxygen $K\alpha$ X-ray was obtained on the surface.

3.3.5. X-ray diffraction analysis

The X-ray technique described above in the section 3.3.4. allows the determination of elements present but does not supply information about their chemical compositions. If this data is required then X-ray diffraction analysis can be employed. This method is particularly useful in the analysis of wear debris for its phase identification.

The X-ray diffraction analysis of wear debris produced during a wear test was carried out using the same diffractometer described in the section 3.2.3.. The debris particles to be examined were mounted on a polymer holder by using double sided sellotape. In order to obtain sharp peaks of the phases present for the limited amount of wear debris available, a large step size of 0.05 degrees in 2θ was chosen to reduce the noise of the diffraction pattern, and also a slow scan speed of 0.3 degrees in 2θ per minute was employed to obtain higher intensities. Moreover, for the purpose of saving time by concentrating on the identification of iron oxides and/or iron phases, the sample was scanned only from 30 to 50 degrees in 2θ.

Chapter 4: Results

4.1. Metallurgical characteristics of surface treatments

4.1.1. Microstructure and hardness

4.1.1.1. Optical microstructure

Fig.4.1 shows the optical microstructure of the cross-section of a gas nitrided BS970,905M39 (EN41B) specimen. The gas nitriding process was carried out at 520°C for 80 hours by using an ammonia gas atmosphere furnace. A compound layer (white layer), which has a thickness of 30 μm, was formed at the surface. Under this compound layer, a relative thick diffusion layer which can be seem as a dark etching zone of about 0.5 mm (Fig.4.1 (a)), was produced. These characteristics of the surface layers are usually observed in gas nitrided steels[15].

Fig.4.2 shows the optical microstructure of the cross-section of a plasma nitrided BS970,905M39 (EN41B) specimen. The treatment temperature and time of the plasma nitriding were 530°C and 60 hours, respectively. A much thinner compound layer of 2 μm thickness was observed. It has been reported in the literature that in the case of plasma nitriding the growth rate of the compound layer deviates from a parabolic diffusion law, and that after a long nitriding time the plasma nitrided compound layer is thinner than a gas nitrided compound layer, due to the effect of the material removal from the surface by cathode sputtering in plasma nitriding[48] or due to the formation of the vapour deposited layer of iron oxynitride which inhibits further nitriding[49].

Under this plasma nitrided compound layer, a diffusion layer of about 0.3 mm thickness, which has the same microstructure as observed in the gas nitriding (Fig.4.1 (b)), was produced.

The optical microstructure of the cross-section of a nitrocarburized BS970,905M39 (EN41B) specimen is shown in Fig.4.3. The nitrocarburizing was carried out at 570°C for 2.5 hours in a mixture of 50% ammonia gas and 50% endothermic gas. A thin compound layer of 3 µm thickness and a shallow diffusion layer of only 70 µm thickness were formed because of the short treatment time.

For the purpose of comparison of wear behaviour of surface hardened steels, a gas-carburizing and hardening treatment was carried out for BS970,635M15 (EN351). Fig.4.4 shows the optical microstructure of the cross-section of a carburized and hardened specimen. As usually observed in carburized and hardened steels, a martensite surface layer (0.7 mm thickness) was formed.

4.1.1.2. Hardness profile

Fig.4.5 shows the microhardness (applied load; 3 N) curves plotted against the distance from the surface for gas nitrided, plasma nitrided, and nitrocarburized BS970,905M39 (EN41B) sections.

In gas nitriding, the surface layer had a peak hardness of Hv 1100-1200 at 0.05 mm depth from the surface, and the hardness of the diffusion layer gradually decreased with an increase in distance from the surface. The effective case depth defined by the distance between the surface and the layer having a hardness of Hv 550[19] was 0.42 mm. The surface hardened layer depth at which the hardness reaches the value of the core hardness (Hv 260) was 0.7 mm. The low hardness observed near the surface will be described in some detail in section of 4.1.2. and related to the hardness of the compound layer.

In the case of plasma nitriding, the surface layer had a peak hardness of Hv 1200 at the surface, and the hardness decreased with an increase in distance from the surface more rapidly than that of the gas nitriding. The effective case depth for the plasma nitrided specimen was 0.22 mm, and the surface hardened layer depth was 0.5 mm.

On the other hand, the nitrocarburized surface layer had a lower peak hardness of Hv 700 than that produced by the first two nitrided processes, and the effective case depth for the nitrocarburizing was only 0.05 mm. The surface hardened layer depth was only 0.20 mm because of the short treatment time (2.5 hours). The reason for the low hardness of the nitrocarburized layer can be explained by the nitride-precipitate coarsening due to the higher treatment temperature (570°C) than that of the gas nitriding (520°C) or the plasma nitriding (530°C)[15].

Fig.4.6 shows the microhardness curve for the carburized and hardened BS970,905M39 (EN41B) section. The surface layer had a peak hardness of Hv 750 and an effective case depth of 0.65 mm. Because the carburizing was carried out at a much higher temperature (920°C) than the nitriding processes, the carburized case layer was deeper than the nitrided case layers even though it was produced in a much shorter treatment time (3 hours).

Table 4.1 summarizes the characteristics of the surface treated steels in terms of the case depth, hardened layer depth, surface hardness and compound layer thickness.

4.1.2. Characteristics of the compound layer

As shown in Figs.4.1-4.3, compound layers were formed at the surface of all of the nitrided steels, and these were characterized as discussed below.

4.1.2.1. Phase identification

Figs.4.7 (a)-(c) show the x-ray diffraction diagrams of gas nitrided, plasma nitrided and nitrocarburized BS970,905M39 (EN41B) surfaces, respectively. For the gas nitrided specimen, only an ϵ-Fe_3N iron-nitride phase was identified (Fig.4.7 (a)).

On the other hand, in the plasma nitrided specimen, a γ'-Fe_4N nitride phase was observed (Fig.4.7 (b)). Because the plasma nitrided compound layer was thin (2 μm), the substrate α-iron phase was also identified. The reason for the formation of the γ'-Fe_4N compound layer in the plasma nitrided specimen can be explained in terms of the nitrogen activity at the steel surface. Because the plasma nitriding was carried out using a mixture of 25 % nitrogen gas and 75 % hydrogen gas, it is reasonable to consider that the nitrogen activity in the plasma nitriding case was lower than that in the gas nitriding case in which 100 % ammonia gas was used.

Finally, for the nitrocarburized specimen, the compound layer was found to consist of an ϵ-Fe_3N nitride phase. Because in nitrocarburizing both nitrogen and carbon are introduced into the steel surface, the formation of ϵ-nitride was considered to be favoured[32].

4.1.2.2. Microhardness

It is important from a tribological point of view to obtain information about the hardness of the compound layer. Figs.4.8 (a)-(c) show several Vickers microhardness indentations at different applied loads in a gas nitrided compound layer. It was difficult to measure the hardness employing a load of 3 N because the indentor caused cracks in the compound layer (Fig.4.8 (a)) probably due to its brittleness[21,22]. In addition, the applied test load of 3 N might be too high to be supported close to the edge of the sample. Thus, much lighter loads of 0.1-0.25 N were employed in the microhardness test for the compound layer. Moreover the microhardness indentations were made at those positions where each corner of the indentation was at least half the length of a diagonal from the surface edge to avoid the effect of the sample edge[137]. As shown in Figs.4.8 (b) and (c), these indentors caused no cracks.

The result of the microhardness of the compound layer for a gas nitrided BS970,905M39 (EN41B) specimen is shown in Fig.4.9. The compound layer hardness was about Hv 500 at the outer part of the layer, and increased steeply with an increase of the distance from the surface, and had a peak hardness of Hv 1100-1300 near the interface of the compound/diffusion layers. The peak hardness at the inner part of the compound layer is as high as the hardness of the diffusion layer close to the interface of the compound/diffusion layers.

Fig.4.9 also shows the hardness profile of the gas nitrided sample that was ground to a depth of 40 µm from the surface to remove all the compound layer. This sample showed a peak hardness close to the surface edge of the test piece, which corresponds to the outer part of the diffusion layer. This result confirmed that the outer part of the compound layer had a relatively low hardness. If it were assumed that the low hardness of the outer part of the compound layer was due to the effect of the surface edge of the test piece, the ground sample should also have shown a low hardness near the surface. However, as shown in Fig.4.9, the ground sample had a peak hardness near the surface.

In the case of plasma nitrided and nitrocarburized BS970,905M39 (EN41B), the compound layers were so thin (2-3 µm) that it was not possible to measure the hardness of these layers.

As can be seen in Fig.4.1 (b) and Fig.4.8, a porous structure was observed at the outer part of the gas nitrided compound layer. Thus it is reasonable to consider that the relatively low hardness of the outer part of the compound layer is due to its porous microstructure. On the other hand, the inner part of the compound layer was found to be dense and hard. It has been reported in the literature that the porous structure in the compound layer is formed by the precipitation of molecular nitrogen due to the high nitrogen pressure within the compound layer[46,47,52,53].

Fig.4.10 shows an SEM photograph of the surface of an 'as-gas nitrided' BS970,905M39 (EN41B) specimen. The evidence of the porosity at the surface of the compound layer is clear, and a number of pores of 1-3 µm in size were observed. Fig.4.11 is an SEM photograph of an 'as-nitrocarburized' surface, and shows finer porosity than the gas nitrided specimen. It is considered that the coarse pore formation for the gas nitriding is attributed to the long treatment time (80 hours) in comparison with that of the nitrocarburizing (2.5 hours).

4.1.3. Examination of gas nitrided pin before wear test

4.1.3.1. "Wear-face-limited" gas nitrided pin

For the purpose of the investigation of the effect of the hardness variation through a nitrided case layer on wear behaviour, wear-face limited gas nitriding of a pin was carried out by covering the side-face areas of the pin with a masking agent before nitriding. Fig.4.12 shows the optical microstructure of the cross-section of the "wear-face-limited" gas nitrided pin. Microstructural observation and a hardness test on the pin section confirmed that there was no evidence of nitriding at the side-face areas of the pin and that nitriding occurred only on the wear-face of the pin.

The microhardness of the cross-section of the "wear-face-limited" gas nitrided pin is plotted against the distance from the pin wear surface, and shown in Fig.4.13. For the purpose of comparison, the microhardness curve for a normally gas nitrided pin is also shown in this figure. The "wear-face-limited" gas nitrided pin had the same hardness profile from the wear surface to the core as the normally gas nitrided pin, and the effective case depth was 0.42 mm, which was the same value as that of the gas nitrided specimen. Therefore it can be concluded that in the "wear-face-limited" gas nitrided pin the wear-face of the pin was normally nitrided although the nitriding of the side-face of the pin was completely prevented.

4.1.3.2. Compound-layer-removed pin

In order to study the effect of the presence of the compound layer on the wear behaviour of a gas nitrided pin, the compound layer formed at the wear surface of a gas nitrided pin was removed before a wear test. Fig.4.14 shows the microstructure of the cross-section of the gas nitrided and wear-face-ground pin. It can be seen that the surface compound layer at the wear surface was completely removed, and that the diffusion layer remained without any damage. Because all of the surface areas of the pin were exposed to an ammonia atmosphere, the gas nitrided case layers (dark zone) were produced at both the wear-face and the side-face of the pin.

4.2. Wear test results

4.2.1. Effects of load and sliding speed

The study of the effects of load and sliding speed on wear behaviour was carried out for untreated and gas nitrided BS970,905M39 (EN41B) pins under the conditions of sliding speeds of 0.2, 0.5, 1, 2 and 5 $m \cdot s^{-1}$, and applied loads of 2 to 200 N. The gas nitrided pins were nitrided all over the faces, and had a compound layer of 30 μm thickness and an effective case depth of 0.42 mm. The amount of wear was determined by the change of pin length which was monitored during each wear test by using a linear variable differential transducer (LVDT).

4.2.1.1. Wear curve and wear rate

(1) Sliding speed: 0.2 $m \cdot s^{-1}$

Fig.4.15 (a) shows the relationship between the wear length of untreated BS970,905M39 (EN41B) pins and sliding distance at a sliding speed of 0.2 $m \cdot s^{-1}$. The equivalent weight loss of the pin which can be obtained by the following equation is also shown in the right-hand longitudinal axis of this graph:

$$W = \pi r^2 l \rho \qquad \text{(Eq.4.1)}$$

where W is the weight loss of the pin, r the radius of the wear face of the pin (= 1 mm), l the wear length of the pin, and ρ the density of iron (= 7.9×10^3 $kg \cdot m^{-3}$). The gradient of each single trace is a measure of the wear rate (weight loss per sliding distance) for a particular load.

It can be seen from Fig.4.15 (a) that three types of wear curves were observed as follows:

Type-A: The wear rate was very low and constant throughout the duration of the test (20 N).

Type-B: Initially the wear rate was relatively high (running-in wear), but later the slope of the curve decreased and stayed constant (40 N).

Type-C: The wear rate increased as the sliding distance increased (80 N).

Fig.4.15 (b) shows the wear curves for gas nitrided BS970,905M39 (EN41B) pins at the same sliding speed (0.2 $m \cdot s^{-1}$). It is obvious that the amount of wear of the gas nitrided steel was much smaller than that of the untreated steel at the same load. Because the compound layer thickness of the gas nitrided steel was only 30 μm and this layer was worn away quickly, the wear behaviour was controlled mainly by the diffusion layer. Moreover there was no significant wear transition at the wear length of the pin corresponding to the compound layer thickness. Except for the test at 80 N in which initial high wear rate was observed (type-B wear curve), a linear relationship between the wear length of the pin and the sliding distance was observed. This suggests that the wear mechanism governing the wear rate remained constant throughout the duration of the test.

Fig.4.16 shows the wear rates of untreated and gas nitrided BS970,905M39 (EN41B) pins plotted against the test load for a sliding speed of 0.2 $m \cdot s^{-1}$. For those cases where the wear rate changed at some sliding distance (the untreated pin tests at 40 N and 80 N, and gas nitrided pin test at 80 N), the wear rate was calculated from the slope of the straight line after steady state wear was established. It can be seen that there was no wear transition for both the untreated and gas nitrided steels. However, the slope of the wear rate curve against the test load was steeper for the untreated steel than the gas nitrided steel, and at a high load of 80 N the wear rate of the gas nitrided pin ($\approx 10^{-3}$ $mg \cdot m^{-1}$) was two orders of magnitude lower than that of the untreated pin ($\approx 10^{-1}$ $mg \cdot m^{-1}$).

(2) Sliding speed: 0.5 $m \cdot s^{-1}$

The relationship between the wear length of untreated and gas nitrided BS970,905M39 (EN41B) pins and sliding distance at a sliding speed of 0.5 $m \cdot s^{-1}$ is shown in Figs.4.17 (a) and (b), respectively. A type-B wear curve (the wear rate was initially high but later decreased to a low constant) was identified for the untreated pin tests at 4, 10, 80 and 160 N, and for the gas nitrided pin tests at 10 and 20 N. In the case of the untreated pin tests at 80 N and 160 N, the change of the wear rate at the transition was small in comparison with those of the untreated pin tests at 4 and 10 N. In addition to the type-B wear curves, another type of wear curve described as follows was observed in the untreated pin tests at 20, 40 and 60 N and the gas nitrided pin tests at from 40 to 200 N; Type-D: The wear rate was relatively high and constant throughout the duration of the test.

The wear rate obtained from the slope of the straight line at steady state in Fig.4.17 is plotted against the test load, and shown in Fig.4.18. It is clear that the wear behaviour of the gas nitrided steel differed quite markedly from that of the untreated steel. For the untreated steel, a transition from low to high wear rate (at 20 N) and a transition from high to low wear rate (at 80 N) were identified. This behaviour suggests the changes in the wear mechanisms at the transition loads, and the two transitions correspond to the Welsh[65] T_1 (mild to severe) and T_2 (severe back to mild) transitions, respectively. In contrast, no wear transition was observed for the wear rate of the gas nitrided pin, and the gas nitrided steel exhibited mild wear over the whole load range investigated, eliminating severe wear. Moreover, in the mild wear regime below the T_1 load of the untreated steel, the wear rate was reduced by an order of magnitude by the gas nitriding (from 3×10^{-3} to 1.6×10^{-4} $mg \cdot m^{-1}$ at 10 N). The gas nitriding also reduced the wear rate of the steel in the mild regime above the T_2 load by a factor of four (from 2×10^{-2} to 5×10^{-3} $mg \cdot m^{-1}$ at 80 N). The wear rates of the untreated steel in the severe regime ($3 \sim 8 \times 10^{-2}$ $mg \cdot m^{-1}$) were one or two orders of magnitude higher than those of the gas nitrided steel at the same loads ($10^{-4} \sim 10^{-3}$ $mg \cdot m^{-1}$).

(3) Sliding speed: $1\ m \cdot s^{-1}$

The relationship between the wear length of untreated and gas nitrided BS970,905M39 (EN41B) pins and sliding distance at a sliding speed of $1\ m \cdot s^{-1}$ is shown in Figs.4.19 (a) and (b), respectively. In the untreated pin tests, type-B wear curves were identified at 4 and 10 N, and type-D at 20, 40 and 80 N (the wear curve at 40 N can be regarded as a straight line). The untreated pin tests at 120 and 160 N exhibited a type-E wear curve described as follows; Type-E: The wear rate was very high throughout the duration of the test, which was fairly short (~10 seconds). For the gas nitrided pin tests, type-B wear curves were observed at 4 and 10 N, while type-C wear curves were observed at 60, 80 and 160 N.

Fig.4.20 shows the wear rate at the steady state of the untreated and gas nitrided BS970,905M39 (EN41B) pins for a sliding speed of 1 $m \cdot s^{-1}$. In the gas nitrided pin tests, the wear rate for the type-C wear curves was calculated from the gradient of the wear curve point at which the wear length of the pin reached the value of the gas nitrided case depth, i.e. 0.42 mm. The reason for the selection of effective case depth is that it is the most important parameter to describe the surface hardened layer produced by a diffusion process.

It was found at a sliding speed of 1 $m \cdot s^{-1}$ that a transition from mild to severe wear, which corresponds to the Welsh T_1 transition, was identified for both the untreated and gas nitrided steels. In addition, another sharp transition from severe to extremely-severe wear (7×10^{-2} to 4 $mg \cdot m^{-1}$ in wear rate) was observed at 120 N in the case of the untreated steel. The transition from severe to extremely-severe wear will be designated T_s. The gas nitriding increased the T_1 transition load from 20 N to 60 N, leading to a wider region of the mild wear regime for the gas nitrided steel. Furthermore, the gas nitriding reduced the wear rate by an order of magnitude in the mild regime (from $2x10^{-3}$ to $3x10^{-4}$ $mg \cdot m^{-1}$ at 10 N) and by a factor of three in the severe regime (from $7x10^{-2}$ to $2.7x10^{-2}$ $mg \cdot m^{-1}$ at 80 N). No extremely-severe type of wear was observed for the gas nitrided steel over the whole load range investigated.

<u>(4) Sliding speed: 2 $m \cdot s^{-1}$</u>

Figs.4.21 (a) and (b) show the relationship between the wear length of a pin and sliding distance at a sliding speed of 2 $m \cdot s^{-1}$ for untreated and gas nitrided BS970,905M39 (EN41B) steels, respectively. Type-B wear curves (the wear rate was initially high but later decreased to a low constant) were identified for the untreated pin tests at 4 and 10 N and the gas nitrided pin test at 4 N, and type-C (the wear rate increased as the sliding distance increased) for the untreated pin tests at 20 and 30 N and the gas nitrided pin tests at 30, 40 and 80 N. A type-D wear curve (the wear rate was relatively high and constant) was also observed for the gas nitrided pin test at 20 N, and a type-E (the wear rate was very high throughout the duration of the test) for the untreated pin tests at 40 and 80 N.

The wear rates at steady state of the untreated and gas nitrided BS970,905M39 (EN41B) pins for this sliding speed (2 $m \cdot s^{-1}$) are shown in Fig.4.22. The wear rates for the type-C wear curves of the gas nitrided pin tests (at 30, 40 and 80 N) were obtained in the same way as described in the case of 1 $m \cdot s^{-1}$. The transitional behaviour in wear rate at 2 $m \cdot s^{-1}$ sliding speed showed a similar pattern to that of 1 $m \cdot s^{-1}$ sliding speed for both the untreated and gas nitrided steels; i.e. T_l (mild to severe) and T_s (severe to extremely-severe) transitions for the untreated steel, and a T_l (mild to severe) wear transition for the gas nitrided steel. However, the T_s transition load of the untreated steel and the T_l transition load of the gas nitrided steel were reduced from 120 N to 40 N and from 60 N to 30 N, respectively, by increasing the sliding speed from 1 $m \cdot s^{-1}$ to 2 $m \cdot s^{-1}$, while the T_l transition load of the untreated steel remained constant at 20 N. Another point to be noted is that the difference in wear rate between the untreated and gas nitrided pins was small in both the mild and severe regimes. At a high load of 80 N, however, the wear rate was reduced by two orders of magnitude (from 3 $mg \cdot m^{-1}$ to 4×10^{-2} $mg \cdot m^{-1}$) by the gas nitriding.

(5) Sliding speed: 5 $m \cdot s^{-1}$

The wear curves of the untreated and gas nitrided steels for a sliding speed of 5 $m \cdot s^{-1}$ are shown in Figs.4.23 (a) and (b), respectively. In the untreated pin tests, the wear of the pin was proportional to the sliding distance at each load (the curve at 2 N was regarded as a straight line). For the gas nitrided pin tests, on the other hand, a type-C wear curve (the wear rate increased as the sliding distance increased) was identified except for the test at 4 N, in which a type-D wear curve was observed.

Fig.4.24 shows the wear rates of the untreated and gas nitrided BS970,905M39 (EN41B) pins for a sliding speed of 5 $m \cdot s^{-1}$. In the untreated steel, no wear transition was observed, and severe type wear occurred over the whole load range investigated. In contrast, the gas nitrided steel showed a T_1 (mild to severe) transition at 10 N, and reduced the severe wear rate by more than an order of magnitude (from 2 $mg \cdot m^{-1}$ to $7x10^{-2}$ $mg \cdot m^{-1}$ at 40 N).

4.2.1.2. Transition load

Fig.4.25 shows the influence of sliding speed on the T_1 (mild to severe wear) transition load for the untreated and gas nitrided BS970,905M39 (EN41B). Because the gas nitrided pin tests at 0.5 $m \cdot s^{-1}$ showed mild wear over the whole load range, the maximum load of the tests (200 N) is plotted by a dashed triangle and the extrapolation of the transition load curve was drawn by a dashed line. In addition, because the untreated pin tests at 5 $m \cdot s^{-1}$ showed severe wear even at the lowest load of 2 N, the transition load for this case is also shown in the same way. It is clear that the gas nitriding increased the T_1 load over the whole sliding speed, and that this effect for increasing the transition load was remarkable particularly at sliding speeds of lower than 0.5 $m \cdot s^{-1}$ and higher than 5 $m \cdot s^{-1}$.

This graph provides in a convenient fashion the means for predicting the wear behaviour. A combination of load and speed lying above the transition load curve for each material will give severe wear except for the case of the loads above T_2 at 0.5 $m \cdot s^{-1}$ for the untreated steel. Any combination below the transition curve for each material will give mild wear (at steady state). It is apparent that the gas nitriding expanded the mild wear region toward higher loads and sliding speeds.

4.2.2. Wear through surface hardened layer

The wear behaviour of nitrided pins through the surface layers was investigated by continuing the wear tests for a long sliding distance even after the pin wear length corresponding to the surface hardened layer depth was worn away. The tested specimens were untreated, gas nitrided, plasma nitrided and nitrocarburized BS970,905M39 (EN41B) pins. In addition, a "wear-face-limited" gas nitrided pin was also involved to study the influence of the hardness variation through the surface layer, which was capable of eliminating the effect of the hardened layer in the side-face of the pin. These wear tests were carried out under a constant sliding condition; i.e. at 1 $m \cdot s^{-1}$ sliding speed and 40 N load. It should be noted that in this sliding condition, the untreated steel showed a severe wear regime, contrasting with a mild wear regime of the gas nitrided steel (Fig.4.20).

The wear test results are shown in Fig.4.26, in which the wear length of the surface treated pins is plotted against the sliding distance. The wear rates through the surface layer, which were obtained from the gradients of the each wear curve in Fig.4.26, are plotted against the wear length of the pin, and shown in Fig.4.27. In this figure, the wear length of a pin corresponding to the effective case depth is also described for the three nitrided steels.

There are a lot of interesting points to be noted in these figures. The untreated pin showed a high wear rate, which was constant throughout the duration of the test, suggesting that the wear mechanism remained constant and that severe wear occurred during the test. The (normally) gas nitrided pin showed a relatively high wear rate at the start of sliding, and after that a low wear rate in the case layer. The wear rate increased slightly at the gas nitrided case depth (0.42 mm), but it was still much lower than that of the untreated pin, by more than an order of magnitude even after the surface hardened layer (0.7 mm thickness) was completely worn away. On the other hand, the "wear-face-limited" gas nitrided pin started with a low wear rate, but showed a sharp transition to a high wear rate at the gas nitrided case depth. After this transition, the wear curve became almost parallel to that for the untreated pin, which means that the wear rate was as high as that of the untreated steel. The plasma nitrided pin showed a similar wear rate curve to that of the (normally) gas nitrided pin, except that the wear rates were two or three times higher than that of the gas nitrided pin at the start of sliding and after the surface hardened layer (0.5 mm thickness) was worn away. After the wear length of the pin passed the value of the plasma nitrided case depth (0.22 mm), the transition from low to high wear occurred. The wear rate change at this transition (from 3×10^{-4} to 4×10^{-3} $mg \cdot m^{-1}$) was greater than that of the (normally) gas nitrided pin. Lastly, the nitrocarburized pin showed a considerably lower wear rate initially, but soon after the wear rate increased rapidly, and reached the same value as that of the untreated pin when the surface hardened layer (0.2 mm thickness) was worn away.

4.2.3. Influence of surface treatment processes

The study of the comparison of the wear behaviour between surface treatments was carried out under a specific sliding speed condition, i.e. 1 $m \cdot s^{-1}$, and only the applied load was varied. The investigated surface treatments were gas nitriding, plasma nitriding, nitrocarburizing, and carburizing-and-hardening.

4.2.3.1. Gas nitrided steel

The wear curves and the wear rates for gas nitrided BS970,905M39 (EN41B) pins at a sliding speed of 1 $m \cdot s^{-1}$ have been already shown in Fig.4.19 (b) and Fig.4.20, respectively, and the results are not repeated in this section.

4.2.3.2. Plasma nitrided steel

Fig.4.28 shows the relationship between the wear length of a pin and sliding distance for plasma nitrided BS970,905M39 (EN41B). The effective case depth of the plasma nitriding was 0.22 mm. It can be seen that the tests at 10 and 40 N showed type-B wear curves (the wear rate was initially high but later decreased to a low constant), contrasting with type-C wear curves (the wear rate increased as the sliding distance increased) of the tests at 80 and 160 N. The test at 60 N showed a mixture of type-B and type-C wear curves, which is described as follows; Type-F: Initially the wear rate was relatively high, but decreased to a low constant, and then increased again later. Because the further sliding test at 40 N (Fig.4.26) showed the same form as the test at 60 N, the curves for 10 and 40 N shown in Fig.4.28 can be regard as the first part of the type-F wear curve.

The wear rate at each load for the plasma nitrided steel was obtained from the gradient of the wear curve point at which the wear length of the pin reached the value of the plasma nitrided case depth (0.22 mm). For the test load of 10 N, the wear rate was obtained from the slope of the straight line at steady state. It is reasonable to assume that at 10 N the wear rate at the case depth will be close to that of the steady state, because in the case of 40 N the difference of the wear rate between the two stages was small.

Fig.4.29 shows the wear rate of the plasma nitrided BS970,905M39 (EN41B) pin plotted against the test load. For comparison purposes the wear rate of untreated and gas nitrided BS970,905M39 (EN41B) pins (the same data of Fig.4.20) are also plotted in this graph. It was found that the plasma nitrided steel showed a mild to severe wear (T_1) transition at 60 N, which was the same pattern as the gas nitrided steel. The wear rate of the plasma nitrided steel was lower than that of the gas nitrided steel by a factor of two, in both the mild and severe wear regimes.

4.2.3.3. Nitrocarburized steel

Fig.4.30 shows the relationship between the wear length of a nitrocarburized BS970,905M39 (EN41B) pin and sliding distance. A type-C wear curve (the wear rate increased as the sliding distance increased) was identified for all of the tests. The initial wear rate was considerably lower in comparison with that of the gas nitrided and plasma nitrided steels. However, the wear rate quickly increased because the nitrocarburized surface layer was shallow.

Fig.4.31 shows the wear rate of the nitrocarburized BS970,905M39 (EN41B) pin plotted against the test load. The wear rate was obtained from the gradient of the wear curve at the case depth (0.05 mm). It can be seen that the wear rate of the nitrocarburized steel increased markedly as the test load increased, and that the wear rate was higher than that of the gas nitrided steel at 10, 40 and 160 N, but lower at 80 N. The sharp increase in wear rate at 80 N can be regarded as a T_1 transition from mild to severe wear.

4.2.3.4. Carburized and hardened steel

Because a carburizing and hardening process was carried out for BS970,635M15 (EN351) steel, the wear behaviour of an untreated BS970,635M15 (EN351) pin was also studied. Figs.4.32 (a) and (b) show the relationship between the wear length of a pin and sliding distance for untreated, and carburized-and-hardened BS970,635M15 (EN351), respectively. In the untreated pin tests, type-B wear curves were observed at 2 and 4 N, type-D (the wear rate was relatively high and constant) at 10 and 40 N, and type-E (the wear rate was very high throughout the duration of the test) at 80 and 160 N. In the carburized-and-hardened pin tests, on the other hand, a type-B wear curve was identified at 10 N, a type-D at 40 N, a type-C at 80 N, and a type-E at 160 N.

Fig.4.33 shows the wear rate at steady state for the untreated, and carburized-and-hardened BS970,635M15 (EN351) pins. The wear rate of the carburized-and-hardened pin tested at 80 N was obtained from the gradient of the curve at the case depth (0.65 mm). Again, for comparison purposes, the wear rate of the gas nitrided BS970,905M39 (EN41B) is also plotted in this graph. The untreated BS970,635M15 (EN351) showed a T_1 (mild to severe) transition at 10 N and a T_s (severe to extremely-severe) transition at 80 N, which were identified in the untreated BS970,905M39 (EN41B) pin tests at the same sliding speed. However, both the transition loads were somewhat lower for the untreated BS970,635M15 (EN351) steel. On the other hand, the carburized-and-hardened BS970,635M15 (EN351) pin tests showed only a T_1 transition at 60 N, and the wear rates were almost the same values as those of the gas nitrided BS970,905M39 (EN41B), except that the wear rate at 160 N was much higher than that of the gas nitrided steel at the same load.

4.2.3.5. Comparison between surface treatments

In order to compare the wear rates between the surface treatments (gas nitriding, plasma nitriding, nitrocarburizing, and carburizing-and-hardening) separately from the untreated steels, the 4 different types of pin material are all plotted in Fig.4.34. It can be seen that a sharp T_1 (mild to severe wear) transition was observed at the same load (60 N) for each surface treated steel, except for the nitrocarburized steel. Furthermore, the wear rates were of the same order of magnitude between the surface treated steels, except for the carburized-and-hardened steel test at 160 N. It can be concluded, therefore, that there was no significant difference between the surface treatments in terms of wear transitions and wear rates. The wear characteristics of the untreated and surface treated steels at a sliding speed of 1 $m \cdot s^{-1}$ are summarized in Table 4.2.

4.2.5. Effect of the compound layer

In order to study the effect of the presence of the compound layer on the wear of the gas nitrided steel, some tests were carried out by using the pin in which the compound layer was removed prior to the test. The wear tests were carried out only at a sliding speed of 0.5 $m \cdot s^{-1}$, and low applied loads of 10 N and 20 N were employed, because in higher wear sliding conditions the compound layer (30 μm thickness) would be worn away too quickly to evaluate its wear behaviour.

Fig.4.35 shows the relationship between the wear length of the gas nitrided BS970,905M39 (EN41B) pin without the compound layer and sliding distance. For comparison purposes, the wear curves of 'as-gas nitrided' pins are also shown in this graph. Except for the test of the pin without the compound layer at 20 N, type-B wear curves (the wear rate was initially high but later decreased to a lower constant value) were observed. At both loads of 10 N and 20 N, the pin without the compound layer showed a lower wear rate at the start of sliding than the 'as-nitrided' steel pin. However, the wear rate at steady state was almost same between the two types of pin material. Therefore it was concluded that the compound layer increased the wear rate of the gas nitrided steel only at the initial stage of sliding.

In the 'as nitrided' steel pin tests, the wear lengths of the pin at which a transition from running-in wear to steady state occurred were found to be 20 μm for 10 N, and 40 μm for 40 N. These values did not agree with the thickness of the gas nitrided compound layer (30 μm). This suggests that the initial high wear (running-in) behaviour of the 'as-nitrided' pin cannot be directly related to the wear of the compound layer.

4.3. Material examination after wear tests

Wear specimens and wear debris were examined after the wear tests by several techniques (optical microscopy, SEM, EPMA, and x-ray diffraction analysis) to investigate the wear mechanisms. Because there was no significant difference between the different surface treatments in terms of wear rate and transition load apart from the wear behaviour through the surface layers, the material examinations were carried out only for untreated and gas nitrided BS970,905M39 (EN41B) pin tests.

4.3.1. Wear pin

4.3.1.1. SEM of worn surface

(1) Untreated pin test

Fig.4.36 (a) shows the whole area of the worn surface of the untreated BS970,905M39 (EN41B) pin that was tested at 1 $m \cdot s^{-1}$ sliding speed and 4 N load. This wear test showed a mild wear regime below the T_1 load. It can be seen that the worn surface was smooth and that there was little plastic deformation. Fig.4.36 (b) is a high magnification image of the pin surface of Fig.4.36 (a), and shows some pits together with the smooth surface areas. Moreover, some parts of the smooth surface were covered with dark grey areas which were shown up by atomic number contrast, backscattered electrons, in the SEM . This suggests the presence of an oxide on the worn surface.

Figs.4.37 (a) and (b) present the surface of the worn untreated pin that was tested in a severe wear regime (sliding speed: 0.5 $m \cdot s^{-1}$, test load: 40 N). It is clear that there is considerable evidence of plastic deformation (Fig.4.37 (a)) and intensive adhesion on the pin surface (Fig.4.37 (b)).

Figs.4.38 (a) and (b) show the worn surface of the untreated pin that was tested in an extremely-severe regime above the T_s load. The test sliding conditions were 1 $m \cdot s^{-1}$ sliding speed and 160 N load. The pin was heavily damaged, and there was evidence of an intensive plastic flow of the material in the disc sliding direction.

<u>(2) Gas nitrided pin test</u>

Figs.4.39 (a) and (b) show the worn surface of the gas nitrided BS970,905M39 (EN41B) pin that was tested at 1 $m \cdot s^{-1}$ sliding speed and 10 N load. The wear test exhibited a mild wear regime below the T_1 load. It was found that the pin surface was very smooth and featureless apart from some small ploughing scars parallel to the sliding direction of the disc (Fig.4.39 (b)).

Figs.4.40 (a) and (b) represent the worn surface of the gas nitrided pin that was tested in a severe wear regime above the T_1 load (sliding speed: 1 $m \cdot s^{-1}$, test load: 160 N). The surface was relatively rough contrasting with the mild wear test pin (Fig.4.39), and there was evidence of plastic deformation and granular debris production. The surface features at a higher magnification image (Fig.4.40 (b)) were very similar to that of the untreated pin in the extremely-severe wear regime (Fig.4.38 (b)), although the degree of the damage of the pin was much less than that of the untreated pin (Fig.4.38 (a)).

In order to study the wear mechanism of the compound layer which was formed at a gas nitrided surface, a wear test was interrupted before the compound layer (30 µm thickness) was completely worn away. This test was carried out at 0.5 $m \cdot s^{-1}$ sliding speed and 10 N load. The worn surface of the pin is shown in Fig.4.41, in which considerable pitting was observed parallel to the disc sliding direction, with very smooth areas of the remainder of the surface.

4.3.1.2. Optical microscopy of subsurface

4.3.1.2.1. Longitudinal section

(1) Untreated pin test

Figs.4.42 (a)-(d) show optical micrographs of the longitudinal sections normal to the worn surfaces of untreated BS970,905M39 (EN41B) pins. Fig.4.42 (a) is the pin tested in a mild wear regime (sliding speed: 0.5 $m \cdot s^{-1}$, test load: 10 N). There was no significant change caused by the wear in the subsurface microstructure.

Fig.4.42 (b) represents the longitudinal section of the untreated pin tested in severe wear between the T_1 and T_2 loads (sliding speed: 0.5 $m \cdot s^{-1}$, test load : 40 N). It is apparent that plastic deformation in the disc sliding direction occurred within a depth of 25 μm from the surface.

Fig.4.42 (c) is the untreated pin tested in a mild wear regime above the T_2 load. The test conditions were 0.5 $m\cdot s^{-1}$ sliding speed and 160 N load. The degree of subsurface plastic deformation was somewhat greater than that of the severe wear specimen shown in Fig.4.42 (b).

Fig.4.42 (d) shows the longitudinal section of the untreated pin tested in an extremely-severe wear regime above the T_s load (sliding speed: 2 $m\cdot s^{-1}$, test load: 80 N). The subsurface material was strained parallel to the disc sliding direction more extensively than that of the severe wear test pin. In addition, a thin 'white-etched' layer was observed at the worn surface.

(2) Gas nitrided pin test

Figs.4.43 (a)-(d) show the optical micrographs of the longitudinal sections normal to the worn surfaces of gas nitrided BS970,905M39 (EN41B) pins. Fig.4.43 (a) is the gas nitrided pin tested in a mild wear regime (sliding speed: 0.5 $m\cdot s^{-1}$, test load: 40 N), and the wear length of this pin was 250 μm. It can be seen that there were the remains of the gas nitrided diffusion layer without any change in the microstructure.

Fig.4.43 (b) represents the longitudinal section of the gas nitrided pin tested in a mild wear regime again (sliding speed: 2 $m\cdot s^{-1}$, test load: 20 N), but in this case the wear length of the pin was 509 μm, which means that the case layer (0.42 mm depth) had been completely worn away. Even after the case layer was worn away, there was no evidence of the change in the subsurface microstructure as a result of the wear process.

Fig.4.43 (c) is the gas nitrided pin tested in severe wear (sliding speed: 2 $m \cdot s^{-1}$, test load: 80 N). Contrasting with the mild wear specimens, a 'white-etched' layer was observed at the surface. In addition, there was a thin plastically deformed layer under the 'white-etched' layer.

Fig.4.43 (d) shows the longitudinal section of the gas nitrided pin which was obtained from the test that was terminated before the compound layer was completely worn away. This specimen is the same that is shown in Fig.4.41. There was evidence of the remains of the compound layer (white layer) at the surface. This layer had been formed before the wear test, and it is completely different from the 'white-etched' layer shown in Fig.4.43 (c) in terms of the mechanism of formation

4.3.1.2.2. Transverse taper section

<u>(1) Untreated pin test</u>

Figs.4.44 (a)-(d) show optical micrographs of transverse taper sections through the worn surfaces of untreated BS970,905M39 (EN41B) pins. Fig.4.44 (a) is the untreated pin tested in a mild wear regime (sliding speed: 1 $m \cdot s^{-1}$, test load: 4 N). It was found that grey patchy layers were formed at the surface, which suggests that some parts of the worn surface were covered with an oxide. Moreover, there was little evidence of plastic deformation in the subsurface.

In contrast, the microstructure of the severe wear test pin at 1 $m \cdot s^{-1}$ sliding speed and 40 N load (Fig.4.44 (b)) shows considerable evidence of heavy plastic deformation in the sublayer. Moreover a 'white-etched' layer was observed at the surface, while no oxide type layer was identified for this specimen.

Fig.4.44 (c) is the untreated pin tested in a mild wear regime above the T_2 load (sliding speed: 0.5 $m \cdot s^{-1}$, test load: 80 N). In spite of the relatively high load, the degree of plastic deformation was considerably reduced in comparison with the severe wear specimen, and thin grey patchy layers were again formed at the surface. A microhardness test, which was carried out on this taper section, showed that the hardness of the sublayer close to the surface increased slightly (from Hv 252 to Hv 362) probably due to work-hardening as a result of the wear process.

On the other hand, in the extremely-severe wear test pin at 1 $m \cdot s^{-1}$ sliding speed and 120 N load (Fig.4.44 (d)), a fragment of material was found to have adhered to the worn surface. The adhered fragment showed a 'white-etched' microstructure, and very high hardness values (Hv 666 to 739). The subsurface microstructure showed evidence of plastic deformation, and the hardness of the section through the worn surface increased (from Hv 310 to Hv 418) with a decrease in the depth from the surface.

(2) Gas nitrided pin test

Figs.4.45 (a) and (b) show optical micrographs of the transverse taper sections through the worn surfaces of gas nitrided BS970,905M39 (EN41B) pins. Fig.4.45 (a) is the mild wear pin tested at 1 $m \cdot s^{-1}$ sliding speed and 10 N load. In this specimen, there was still the remains of the diffusion layer, and no metallurgical change caused by wear was observed.

Fig.4.45 (b) is the taper section of the gas nitrided pin tested in a severe wear regime (sliding speed: 1 $m \cdot s^{-1}$, test load: 160 N). Contrasting with the mild wear specimen, a 'white-etched' layer of 10 µm thickness was clearly observed at the surface. The 'white-etched' layer had a high hardness of Hv 909. The subsurface microstructure showed evidence of thermal changes probably due to the frictional heating.

4.3.2. Wear disc

4.3.2.1. Visual observation of wear track

The wear tracks on the discs produced by the wear tests varied markedly in appearance according to whether mild or severe wear was operative. The colour macrographs of the wear tracks on the discs rubbed against gas nitrided BS970,905M39 (EN41B) pins are shown in Figs.4.46 (a)-(c).

For mild wear, the tracks were reddish in the tests at relatively low loads and sliding speeds (Fig.4.46 (a)), and black in the tests at relatively high loads and sliding speeds (Fig.4.46 (b)). These appearances suggest that the surfaces of the disc tracks were covered with oxides; Fe_2O_3 for the reddish tracks, and Fe_3O_4 or FeO for the black tracks. On the other hand, in the case of severe wear, the disc tracks were bright and shiny in appearance, and material transfer to the disc surface was also observed (Fig.4.46 (c)).

4.3.2.2. SEM of worn surface

(1) Untreated pin test

Figs.4.47-4.49 show worn surfaces of the discs rubbed against untreated BS970,905M39 (EN41B) pins. Figs.4.47 (a) and (b) are the disc tested in a mild wear regime below the T_l load (sliding speed: 1 $m \cdot s^{-1}$, test load: 4 N). The worn surface was relatively smooth, and there was some evidence of adhesion between asperity contacts (Fig.4.47 (b)).

Figs.4.48 (a) and (b) represent the worn surfaces of the disc tested in a severe wear regime between the T_l and T_s load (sliding speed: 1 $m \cdot s^{-1}$, test load: 40 N). There was no significant difference in the topography of the disc worn surfaces between mild and severe wear, because disc wear is much less than pin wear, with the pin-on-disc configuration, and the hardness of a disc was much higher than that of an untreated pin. The degree of the adhesion and damage of the worn surface for the severe wear disc was somewhat greater than that of the mild wear specimen.

Figs.4.49 (a) and (b) are the worn surfaces of the disc tested in an extremely-severe regime above the T_s load (sliding speed: 1 $m \cdot s^{-1}$, test load: 160 N). It is clear that considerable metal transfer occurred from the pin to the disc surface, and that the size of the transferred metal particles was almost 1 mm in length.

(2) Gas nitrided pin test

Figs.4.50 and 4.51 show the worn surfaces of the discs tested against gas nitrided BS970,905M39 (EN41B) pins in a mild wear regime (sliding speed: 1 $m \cdot s^{-1}$, test load: 10 N) and in a severe wear regime (1 $m \cdot s^{-1}$, 160 N), respectively. For the mild wear specimen, the worn surface was very smooth and flat (Figs.4.50 (a) and (b)).

On the other hand, in severe wear, considerable metal transfer was observed. The length of the transferred metal particles in the sliding direction was much greater than that of the untreated-pin-test specimen(Fig.4.49), suggesting that more intensive junction growth of the contact asperities occurred[78]. However, the thickness of the transferred particles was smaller in comparison with that of the untreated-pin-test specimen.

4.3.2.3. EPMA of worn surface

Figs.4.52 and 4.53 are the EPMA results of the worn surfaces of the discs tested against gas nitrided BS970,905M39 (EN41B) pins in a mild wear regime (sliding speed: 1 $m \cdot s^{-1}$, test load: 10 N) and in a severe regime (1 $m \cdot s^{-1}$, 160 N), respectively. Fig.4.52 (a) shows the secondary electron image of the worn surface of the mild wear specimen, together with the oxygen x-ray analysis result which was obtained by scanning on the horizontal line shown in Fig.4.52 (b). It was confirmed that the dark areas which were shown up by an atomic number contrast were oxidized, and that the worn surface was covered with patchy oxides.

For the severe wear disc (Figs.4.53 (a) and (b)), on the other hand, there was no evidence of surface oxidation, contrasting with the mild wear specimen.

4.3.2.4. Optical microscopy of subsurface

4.3.2.4.1. Transverse taper section

(1) Untreated pin test

Figs.4.54 (a)-(c) show the optical micrographs of the transverse taper sections through worn surfaces of the discs rubbed against untreated BS970,905M39 (EN41B) pins. Fig.4.54 (a) is the disc tested in a mild wear regime (sliding speed: 1 $m\cdot s^{-1}$, test load: 4 N). Once again patchy oxides (dark grey areas) were clearly observed on the worn surface. The subsurface microstructure was the same as the disc before the wear test as shown in Fig.3.4 (c), suggesting that there was no metallurgical change in the sublayer as a result of wear.

Fig.4.54 (b) represents the optical microstructure of the transverse taper section of a severe wear disc (sliding speed: 1 $m\cdot s^{-1}$, test load: 40 N). There was no evidence of oxidation at the surface, and a dark etched sublayer of 10 µm thickness was observed below the worn surface. This layer suggests that the wear process had a thermal effect on the sublayer, resulting in a tempered martensite structure.

Fig.4.54 (c) is the disc tested in an extremely-severe wear regime (sliding speed: 1 $m\cdot s^{-1}$, test load: 160 N). A transferred layer, which had a 'white-etched' microstructure, was formed at the surface. The thickness of this layer was 20 µm. A microhardness test showed that the transferred layer had a high hardness of Hv 782. Below this layer, a tempered martensite layer, which was somewhat softer than the matrix martensite (Hv 572 against Hv 612), was observed. The tempered martensite layer extended to a depth of 25 µm, which was greater than that of the severe wear specimen.

(2) Gas nitrided pin test

Figs.4.55 (a) and (b) show the optical micrographs of the transverse taper sections through the worn surface of the discs rubbed against gas nitrided BS970,905M39 (EN41B) pins in a mild wear regime (sliding speed: 1 $m \cdot s^{-1}$, test load: 10 N) and in a severe wear regime (1 $m \cdot s^{-1}$, 160 N), respectively. In the mild wear specimen, a tempered martensite sublayer was observed (Fig.4.55 (a)).

On the other hand, the severe wear specimen clearly showed the formation of a transferred layer of 10 μm thickness on the surface. This layer also exhibited a 'white etched' microstructure and a high hardness of Hv 743. Another interesting point to note here is that a tempered martensite was observed only under the transferred layer, suggesting that the applied load was supported by only a few contacts between the surfaces and that the supporting region was tempered to a high temperature due to the frictional heating. The hardness of the tempered layer was Hv 542 contrasting with the relatively high hardness of the matrix martensite (Hv 847).

4.3.2.4.2. Longitudinal section

Fig.4.56 shows the optical microstructure of the longitudinal section normal to the worn surface of the disc rubbed against an untreated BS970,905M39 (EN41B) pin. The wear test was carried out in an extremely-severe wear regime at 1 $m \cdot s^{-1}$ sliding speed and 160 N load. It is clear that a wedge or prow-type profile transferred particle, which had a thickness of 20 μm, was formed on the worn surface. Once again a tempered martensite was observed in the subsurface only below the transferred particle.

Fig.4.57 is the optical micrograph of the longitudinal taper section through the worn surface of the disc rubbed against a gas nitrided BS970,905M39 (EN41B) pin in a severe wear regime (sliding speed: 1 $m \cdot s^{-1}$, test load: 160 N). Once again a 'white-etched' layer of high hardness (Hv 720), and a tempered martensite layer of relatively soft hardness (Hv 627 against Hv 786 in the matrix) were identified. However, the 'white-etched' layer extended in the sliding direction longer than that of the untreated-pin-test specimen (Fig.4.56), suggesting that this layer can be related to the transferred metal shown in Fig.4.51. The thickness of the 'white etched' layer was 10 μm, which was the same as that shown in Fig.4.55 (b), and thinner than that of the transferred layer of the untreated-pin-test disc (Fig.4.56).

4.3.3. Wear debris

4.3.3.1. Visual observation

(1) Untreated pin test

The wear debris produced by the wear tests also varied very markedly in appearance according to which wear type was operative. Figs.4.58 (a)-(d) show the colour macrographs of the wear debris collected from untreated BS970,905M39 (EN41B) pin tests. It was found that four types of wear debris differing in appearance were produced as follows:

(1) red and fine-powdery particles, which were generated from mild wear tests (Fig.4.58 (a));
(2) black and fine-powdery particles, which were generated from severe wear tests at relatively low loads (Fig.4.58 (b));
(3) a mixture of black powdery particles and relatively-large, shiny and bright particles, which were generated from severe wear tests at relatively high loads (Fig.4.58 (c));
(4) very large, shiny and bright particles, which were generated from extremely-severe wear tests (Fig.4.58(d)).

(2) Gas nitrided pin test

The colour macrographs of the wear debris produced from gas nitrided pin tests are also shown in Figs.4.59 (a)-(c). For gas nitrided pin tests, the characteristics of the wear debris differing in appearance are described as follows:

(1) red and fine-powdery particles, which were generated from mild wear tests at relatively low sliding speeds and loads (Fig.4.59 (a));
(2) black and fine-powdery particles, which were generated from mild wear tests at relatively high sliding speed and loads (Fig.4.59 (b));
(3) a mixture of black powdery particles and relatively-large, shiny and bright particles, which was generated from severe wear tests (Fig.4.59 (c)).

In gas nitrided pin tests, no very-large, shiny wear debris such as shown in Fig.4.58 (d) was observed. The red and black colour appearances of the wear debris suggest that the debris was oxidized, while the shiny and bright wear debris appear to be metallic (Fe).

It has been widely recognized that in the case of the type-B wear curve described in section 4.2.1.1. (the wear rate is high at the initial stage of sliding, but decreases to a lower constant value), a shiny and metallic type of wear debris is produced during the initial severe wear stage, and that the debris becomes fine and dark when the equilibrium mild wear is established[87,138]. In the present study, the wear debris produced during the initial stage of sliding was not collected because the amount of the running-in wear was too small to produce sufficient debris for examination.

4.3.3.2. SEM of wear debris

(1) Untreated pin test

Figs.4.60 (a)-(d) show wear debris produced from untreated BS970,905M39 (EN41B) pin tests. The debris shown in Figs.4.60 (a)-(d) are from the same samples that are shown in Figs 4.58 (a)-(d), respectively; i.e. Fig.4.60 (a) is the red powdery debris from a mild wear test, Fig.4.60 (b) is the black powdery debris from a severe wear test at a relatively low load and sliding speed, Fig.4.60 (c) is debris consisting of a mixture of black particles and shiny particles, which was produced from a severe wear test at a relatively high load and sliding speed, and Fig.4.60 (d) is the shiny debris from an extremely-severe wear test.

In mild wear, very fine spherical particles of up to 1 µm in size were produced as shown in Fig.4.60 (a). In the severe wear test at a relatively low load and sliding speed, fine spherical particles of up to 2 µm in size and some plate-like particles of 4~6 µm in size were observed (Fig.4.60 (b)).

Contrasting with these fine particles, Fig.4.60 (c), which is the severe wear test debris at a relatively high load, show a large plate-like particle of 50 µm in size, and fine spherical particles clinging to the plate-like particle. Thus it is reasonable to consider that the black powdery debris shown in Fig.4.58 (c) consists of fine spherical particles, and that the relatively large shiny debris consists of plate-like metal particles.

On the other hand, in extremely-severe wear tests, very large wear particles of up to 1 mm in size were observed as shown in Fig.4.60 (d). Some particles were plastically deformed into long and slender shapes, and the surfaces of the wear particles were striped probably due to the result of the junction growth of asperities during the wear process[78].

(2) Gas nitrided pin test

Figs.4.61 (a)-(d) show the wear debris produced from gas nitrided BS970,905M39 (EN41B) pin tests. Again the debris shown in Figs.4.61 (a)-(c) are from the same samples that are shown in Figs 4.59 (a)-(c), respectively.

Fig.4.61 (a) is the red powdery debris generated from a mild wear test at a relatively low load and sliding speed, and shows very fine spherical particles of 0.5 µm in size. The

SEM of the black powdery debris generated from a mild wear test at a relatively high load is shown in Fig.4.61 (b). It can be seen that fine spherical particles of up to 1 µm in size and some plate-like particles of up to 4 µm in size were produced in this test.

In severe wear, on the other hand, very large wear particles of irregular shape were produced as shown in Fig.4.61 (c). The sizes of these particles were up to 200 µm, and much smaller than that of the untreated-pin-test debris of an extremely-severe wear regime shown in Fig.4.60 (d).

Fig.4.61 (d) shows wear debris generated from the test that was terminated before the gas nitrided compound layer was completely worn away. Consequently, these particles were mainly produced from the compound layer of the gas nitrided pin, apart from the small amount of the wear debris from the disc. It is clear that a number of plate-like particles of 1 µm thickness were produced together with some fine spherical particles.

4.3.3.3. X-ray diffraction analysis

<u>(1) Untreated pin test</u>

Figs.4.62 (a)-(d) show the X-ray diffraction analysis results for the wear debris produced from untreated BS970,905M39 (EN41B) pin tests. It was found that in mild wear below the T_1 load the wear debris consisted of Fe_2O_3 (and Fe_3O_4) as shown in Fig.4.62 (a), contrasting with the metallic (Fe) wear debris in severe wear (Fig.4.62 (b)). It was

difficult in this analysis to examine which oxide(s) (Fe_2O_3 or/and Fe_3O_4) was produced in mild wear, because the diffraction angles for the peaks of the two oxides are very close. In mild wear above the T_2 load, both metallic (Fe) debris and oxidized (Fe_2O_3, Fe_3O_4) debris were observed as shown in Fig.4.62 (c), suggesting that the running-in wear during the initial stage of sliding produced metallic debris. In extremely-severe wear above the T_s load, only Fe was identified (Fig.4.62 (d)).

(2) Gas nitrided pin test

Figs.4.63 (a)-(c) represent the X-ray diffraction diagrams of the wear debris produced from gas nitrided pin tests. Fig.4.63 (a) is the result for the red powdery debris generated from a mild wear test at a relatively low load and sliding speed. It was confirmed that the debris was oxidized to Fe_2O_3 (and Fe_3O_4). For the black powdery debris generated from a mild wear test at a relatively high load, only Fe_3O_4 was identified as shown in Fig.4.63 (b). It can be concluded, therefore, that in the mild wear of the gas nitrided steel, Fe_2O_3 was dominant in the red debris of the low load tests, and that Fe_3O_4 became dominant at higher loads.

On the other hand, in severe wear, which produced a mixture of black particles and shiny particles, FeO and Fe were identified as shown in Fig.4.63 (c). Thus the black particles shown in Fig.4.59 (c) were oxidized to FeO, suggesting that a considerably higher temperature above 500°C was generated during the wear test[106,107].

Chapter 5: Discussion

5.1. Wear mapping

5.1.1. Wear behaviour of untreated and gas nitrided steels

Two of the main aims of the present work are to compare the wear behaviour of untreated and gas nitrided BS970,905M39 (EN41B) over a wide range of sliding speed and applied load, and to identify the wear mechanisms by material examination after the wear tests in order to construct wear maps. The wear behaviour and the characteristics of the worn specimens and wear debris are summarized in Table 5.1 in terms of the wear regimes.

(1) Untreated steel

For the untreated steel, three basic wear regimes were observed, i.e. mild, severe and extremely-severe wear. In mild wear, type-A (the wear rate is very low and constant throughout the duration of the test) and type-B (the wear rate is initially high, but later decreased to a lower constant value) wear curves were identified, and the wear rates (at steady state) were very low ($10^{-4} \sim 10^{-2}$ $mg{\cdot}m^{-1}$). The worn surfaces of the pins and discs were smooth and covered with patchy oxides. The mild wear debris was characterized by very fine red particles, which were oxidized to Fe_2O_3 (and Fe_3O_4).

In contrast, severe wear exhibited type-C (the wear rate increased as the sliding distance increased) and type-D (the wear rate is relatively high and constant throughout the duration of the test) wear curves, and the wear rates (10^{-2} ~ 10^{-1} $mg \cdot m^{-1}$) were one or two orders of magnitude higher than those of mild wear. The worn specimens were characterized by a rough surface, plastic deformation and 'white-etched' layer formation, and relatively-large metallic wear debris was produced.

In the third regime, extremely-severe wear, type-E wear curves (the wear rate is very high throughout the duration of the test, which is fairly short (~ 10 seconds)) were observed, and the wear rates were 1 ~ 10 $mg \cdot m^{-1}$. The wear mechanism was characterized by strong adhesion between the pin and disc, plastic deformation, adhesion and fracture of metallic particles from the pin surface, which resulted in transfer to the disc counterface and the production of very large, metallic wear debris.

These observations are in general agreement with the work that has been previously reported[65,72]. It has been widely recognized that sliding wear of metals exhibits two forms of behaviour; mild (oxidative) and severe (metallic) wear. In mild wear a metal surface is covered with a protective oxide film which prevents intermetallic contact, resulting in a low wear rate and the production of oxidized debris[87]. It can be concluded, therefore, that the low wear rates obtained in the mild wear regime are attributed to an oxidative wear mechanism.

At higher loads, however, a severe metallic type of wear was observed. This is associated with the breakdown of oxide surface films and intensive adhesion between metal surfaces[87], which results in a higher wear rate and the production of metallic debris.

On the other hand, the present study is the first to show a wear rate transition within a metallic wear regime. At higher loads and sliding speeds, extremely-severe wear, which was characterized by a very high wear rate and the production of very large metallic wear particles, was observed. The wear rate of the extremely-severe regime was two orders of magnitude higher than that of the severe wear regime. Thus the "severe wear" regime identified in the present study can be regard as 'low-wear-rate' metallic wear. The difference in the wear mechanisms between the two metallic wear regimes will be discussed in some detail in section 5.2.2.

The type-B wear curve which was observed in mild wear can be interpreted in terms of running-in and steady-state wear behaviour[65,138]. During the initial high wear stage, which is referred as running-in, a severe metallic type of wear occurs prior to the establishment of steady-state oxidative wear.

Welsh[65] carried out a comprehensive study into the wear of plain carbon steels under unlubricated conditions over a wide range of load and sliding speed, and found sharp transitions in wear rate between mild and severe wear. These are a T_1 transition from mild to severe wear at a low load, and a T_2 transition from severe back to mild wear at a high load. Therefore the mild to severe wear transitions observed in the present work (Figs. 4.18, 4.20 and 4.22) correspond to the Welsh T_1, and the severe to mild wear transition observed at 0.5 $m \cdot s^{-1}$ sliding speed (Fig.4.18) is the T_2 transition.

Welsh[65] has attributed the mild wear above T_2 loads primarily to phase hardening which is induced by frictional heating. However, he has also shown that at loads immediately above T_2 the hardness was initially high, but decreased if the wear test was prolonged, and that a combination of work-hardening and oxidation became responsible for preserving the mild wear state. He found that the high hardness caused by the phase hardening was not persistent until a higher load which coincided with a T_3 transition (a minor transition in wear rate above the T_2). This explains the microstructures of the worn pin tested in a mild wear regime above the T_2 (Figs.4.42 (c) and 4.44 (c)). There is no evidence of phase changes, but patchy oxides were observed at the surface and the hardness of the sublayer increased slightly. The wear debris generated from this test consisted of oxides and iron (Fig.4.62 (c)). The iron wear debris is considered to have been produced in the running-in wear stage. Thus it is reasonable to consider that oxidative mild wear occurred at the steady state in this regime, and this mild wear was probably initiated at the end of the running-in wear by phase hardening, which was not sustained in further sliding.

(2) Gas nitrided steel

The wear behaviour of BS970,905M39 (EN41B) steel was altered dramatically by gas nitriding. The effects of the gas nitriding can be summarized as follows:

(1) The wear rate of the steel was reduced for all sliding conditions. The degree of the reduction in wear rate was from a factor of four to two orders of magnitude, depending on the sliding speed and test load.

(2) The T_1 transition loads were increased by the gas nitriding. This means that the gas nitrided steel showed mild wear at higher loads than the untreated steel.

(3) The gas nitriding changed the wear mechanisms of the steel. For instance, at a sliding speed of 0.5 $m \cdot s^{-1}$, the gas nitrided steel exhibited mild wear over the whole load range, eliminating severe wear of the untreated steel. At higher loads than the T_s (severe to extremely-severe wear transition), the gas nitriding inhibited the extremely-severe type of wear, and changed it to 'low-wear-rate' severe wear.

A significant material property of the gas nitrided steel is its high hardness at the surface layer. Welsh[65] has also studied the influence of hardness on the wear transitional behaviour of steel. He showed that as the hardness increased, the T_1 (mild to severe wear) transition was displaced to higher loads and the T_2 (severe to mild wear) transition to lower loads, and that with the hardest sample (Hv 855) mild wear occurred over the whole load range. This wear transitional behaviour is very similar to the wear rate pattern at 0.5 $m \cdot s^{-1}$ sliding speed shown in Fig.4.18.

The gas nitrided steel had sufficient hardness (Hv 1100-1200) to inhibit severe wear, and also reduced the wear rate in the mild wear regime. Welsh has shown that the wear rate did not depend on the hardness if the wear regime remained the same. Thus the improvement in wear resistance by gas nitriding in mild wear can be explained by the harder gas nitrided steel and the difference in the microstructure. The microstructure of the nitrided surface layer is ferrite with finely precipitated alloy-nitrides, which has a higher resistance to tempering in comparison to Welsh's quenched-martensite specimens.

On the other hand, at higher sliding speeds of 1, 2 and 5 $m \cdot s^{-1}$, a mild to severe wear transition was clearly identified for the gas nitrided steel. The change in wear rate at the T_1 transition was approximately two orders of magnitude. The characteristics of the worn specimens and wear debris for both the regimes are summarized in Table 5.1 (b). As has been reported in the literature[65,72] and also mentioned in the wear behaviour of the untreated steel, the mild wear of the gas nitrided steel was characterized by dark smooth worn surfaces and the production of very fine, oxidized debris; contrasting with the rough surfaces, and the transfer and production of large metallic particles in the severe wear regime.

This is the first work to show clearly the wear transitional behaviour for a nitrided steel. Whittle and Scott[66,67] have identified a transition from mild to severe wear in nitrided austenitic alloys by increasing the test load at 1.5 $m \cdot s^{-1}$ sliding speed. They have also shown that the mild wear of the nitrided specimens is due to the formation of an oxide film, which was favoured by the hard nitrided layer underneath the film. However, their wear rate transitional behaviour was slightly different to that of Welsh's, because they plotted the wear rate against the load on a double linear scale rather than plotting on a double logarithmic scale.

5.1.2. Transition load

(1) Effect of sliding speed

Fig.4.25 shows the variation of the T_1 (mild to severe) transition load with sliding speed for untreated and gas nitrided steels. It can be seen that there is a trend for the T_1 load to decrease with an increase of sliding speed for both materials. This trend is very similar to Welsh's[65] work, in which an increase of sliding speed lowered both the T_1 and T_2 transition loads.

As mentioned previously, in mild wear below the T_1 load, a protective oxide film is formed at the surface, resulting in a low wear rate and the production of oxidized debris. As the applied load increases, the breakdown of the surface oxide film occurs at a critical load, and severe metallic wear takes place. Thus it is reasonable to consider that at the transition there is a balance between the rate of formation of a oxide film and the rate of destruction of that film[87]. When the rate of the oxide formation is faster than that of the removal of the oxide, mild wear will occur. In contrast, if the wear rate exceeds the oxidation rate, the oxide film has no chance to develop at the surface [139].

As the applied load increases, the asperities between the rubbing surfaces are encountered more frequently, because the number of asperity contacts between the surfaces increases[136]. This causes the higher rate of removal of surface oxide films, resulting in a metallic wear mechanism. The same story can be applied to the effect of increasing sliding speed. An increase of sliding speed also increases the frequency of encounters of asperities between the surfaces per unit time (not per unit sliding distance). Therefore, it is likely that at high sliding speeds, the rate of material removal from the surface exceeds the rate of oxide formation. This is the reason why the T_1 load decreased with an increase of sliding speed.

This view is supported by Soda and Sasada's work[103], which showed that as atmospheric pressure decreased, a mild to severe wear transition was displaced to a lower sliding speed, because the oxidation rate was reduced at a lower atmospheric pressure. They have introduced a new parameter connected with contact asperities to explain this result, and this parameter was defined by a time over which an asperity of a rubbing surface is being exposed freely to the surrounding atmosphere without any contact. It was suggested that the transition between mild and severe wear corresponds to the condition where the free time of an asperity is just enough for the asperity surface to be covered with sufficient oxygen molecules. Lancaster[105] has also suggested that mild wear occurs when sufficient time is available to establish a protective surface film by oxidation.

However, this concept is insufficient to explain the transition load curve for the untreated steel shown in Fig.4.25. The T_1 loads at sliding speeds of 0.5, 1 and 2 $m \cdot s^{-1}$ were the same (20 N), suggesting that another factor which had an influence on the T_1 load needs to be taken into account. Because oxide formation plays a crucial role in the process of mild wear, any factor which changes the oxidation rate of the sliding surface will influence this transition[105]. Temperature is the most obvious variable affecting oxidation rate, and the temperature at the sliding interface will depend on frictional heating, which in turn depends on the sliding speed and load. Thus the reason why the T_1 load of the untreated steel at 2 $m \cdot s^{-1}$ was relatively high in spite of the high sliding speed is probably due to the high temperature generated by frictional heating because of the relatively high sliding speed, resulting in a higher oxidation rate.

(2) Effect of gas nitriding

It is clear from Fig.4.25 that the gas nitrided steel exhibits higher T_1 loads than the untreated steel over the whole sliding speed range, which means that gas nitriding expanded the mild wear regime toward higher loads. This suggests that the breakdown of an oxide film at the gas nitrided surface occurred at higher loads. Two explanations for this result can be put forward.

The first explanation is that the hard gas nitrided surface is better able to support an oxide film than the untreated steel, and that the oxide breakdown does not occur until appreciable deformation of the surface has occurred; that is, until the load is appreciable[140]. In contrast, for the soft untreated steel, the thin oxide film suffers from more deformation and more consequent fragmentation because of the plastic deformation of the substrate.

The second explanation is associated with the rate of oxide formation. Because the gas nitrided steel has greater resistance against plastic deformation and material removal, the frictional energy input is more likely to be diverted to heat evolution in the form of a temperature rise[141]. Fig.4.55 (a) shows a tempered martensite sublayer of the disc rubbed against a gas nitrided pin in mild wear, contrasting with no metallurgical change in the sublayer of the untreated-pin-test disc in mild wear (Fig.4.54 (a)). This suggests that a higher temperature was generated in the gas nitrided pin test than the untreated pin test. Therefore, the increase in the T_1 load by the gas nitriding is partly due to the increase of the oxidation rate as a result of the high temperature at the surfaces in the tests of gas nitrided pins.

5.1.3. Wear mechanism maps

It has been shown, for the first time, that a gas nitrided steel exhibits transitional wear behaviour in terms of mild (oxidative) and severe (metallic) regimes. Fig.4.25, which shows the T_1 transition loads between mild and severe wear regimes, is a type of wear map, and is very useful for understanding the wear behaviour over a wide range of sliding speed and load. Furthermore, as has been recently proposed by Lim and Ashby[132], a wear mechanism map which indicates the regimes of dominant mechanisms in more detail, will be more valuable to predict the overall wear behaviour of a particular material. Thus an attempt was made to construct wear mechanisms maps for the untreated and gas nitrided steels as described below.

The wear mechanism maps for untreated and gas nitrided BS970,905M39 (EN41B) are shown in Figs.5.1 (a) and (b), respectively. The axes are sliding speed and load. Both the wear rates and the material characteristics after the wear tests were taken into account in determining the regions of the dominant wear mechanisms. In particular, these wear maps are based on the characteristics of the wear debris produced from the wear tests, because wear debris characteristics are directly related to the mechanisms of its formation, namely the wear mechanisms[142,143], and debris analysis is very useful in diagnosing the wear state of tribological components[144,145].

Four types of wear debris were identified as shown in Figs.5.1 (a) and (b). In these diagrams, the wear rates are not indicated, because the effect of both load and sliding speed on the wear mechanisms is more important than a knowledge of actual wear rates from a design point of view[9]. Actual wear rates will not be of direct value to a design engineer because it is not possible to translate these values into meaningful wear rates for specific engineering applications. As far as the present study is concerned, the wear rates of the pins were considerably affected by the types of wear regimes (see Tables 5.1 (a) and (b)), and it is possible to predict the order of magnitude of the wear rate by knowing the operating wear mechanism.

For the untreated steel, as discussed previously, three wear regimes were identified; oxidative (mild), metallic ('low-wear-rate' severe) and very severe adhesive (extremely-severe) wear. The wear map (Fig.5.1 (a)) shows the boundaries separating the regions of dominance of the wear mechanisms by solid lines. These boundaries are the T_1 transition from oxidative to metallic wear at a low load, the T_2 transition from metallic to oxidative wear at a high load and the T_s transition from metallic to very severe adhesive wear. It can be seen that oxidative mild wear occurs only at very low loads and sliding speeds, and that at high sliding speeds very severe adhesive wear is dominant. When the load is relatively high and the sliding speed is relatively low, metallic wear becomes dominant apart from oxidative wear above the T_2 load.

For the gas nitrided steel (Fig.5.1 (b)), only oxidative (mild) and metallic (severe) wear mechanisms were identified. The solid line is the T_1 transition between oxidative and metallic wear. In the oxidative wear regime, Fe_2O_3 was dominant as a red powdery debris, contrasting with the Fe_3O_4 of black powdery debris (Figs.4.59 and 4.63). These observations are in general agreement with those of previous work[59,108,109], in which Fe_2O_3 was formed at relatively low loads or sliding speeds, while at higher loads or sliding speeds Fe_3O_4 was detected. Thus the boundary between the two regimes divided according to which oxide was produced is also shown by a dashed line. It should be noted that this boundary is not a transition in wear rate. It can be seen that the wear map pattern is markedly different from that of the untreated steel. The oxidative mild wear is dominant even at relatively high loads and sliding speeds, and metallic wear occurs only under conditions of very high loads and sliding speeds.

The present work is the first to show a wear mechanism map for a surface treated steel, and is very useful in predicting the type and severity of wear. The metallic wear region can be regarded as a dangerous region of sliding speed and load which should be avoided when considering component design, because wear in these conditions will be very high and unacceptable for most engineering applications. Therefore, the wear maps of untreated and gas nitrided steels can be used to make the best use of gas nitriding for wear applications. In addition, these maps will also enable comparisons to be made with other processes and materials, including surface treatments and coatings.

5.2. Sliding wear mechanisms of untreated and gas nitrided steels

5.2.1. Oxidative wear

One of the main characteristics of mild wear is the production of oxide. Figs.4.44. (a) and (c) are microstructures of transverse taper sections of the untreated pins tested in mild wear regimes below the T_1 load and above the T_2 load, respectively, and show that patchy grey oxide layers were produced at the worn surfaces of both pins. The oxide layers were 1 ~ 3 μm in thickness and 5 ~ 10 μm in width. Figs.4.46 (a) and (b) represent the wear tracks of the discs rubbed against gas nitrided pins in mild wear regimes, and these tracks were found to be discoloured to red or black. An EPMA study confirmed that the worn surface of the disc was covered with a patchy oxide layer (Fig.4.52). The thickness and the width of the oxide layer were estimated to be 1 ~ 2 μm and about 80 μm, respectively. In both the untreated and gas nitrided pin tests, very fine oxidized wear debris was produced (Figs.4.58 (a), 4.59 (a) and (b), 4.62 (a) and (c), 4.63 (a) and (b)). The wear debris consisted of mainly spherical particles of 0.2 ~ 1 μm in diameter (Figs.4 60 (a) and 4.61 (a)), and partly plate-like particles of 0.5 μm in thickness (Fig.4.61 (b)). There was no significant difference in the characteristics of worn specimens and wear debris between the untreated and gas nitrided pin tests in mild wear.

Although these observations confirm that oxidative wear operated in the mild wear regime, the mechanisms of the formation of the patchy oxide surface layer and fine oxidized wear debris have not been described so far. In particular, the size of the patchy oxide layer (up to 3 μm in thickness and 80 μm in width) was much larger than that of the spherical wear particles (up to 1 μm in diameter). Accordingly, the oxidative wear mechanism will be discussed now in some detail.

(1) Quinn's model

The work of Quinn's group is dedicated to the study of mild oxidative wear to produce a quantitative wear equation[75,106-109]. This model is based on the formation and removal of plate-like oxide layers at the real areas of contact. Oxidation is caused by a relatively high frictional temperature, which is the "hot-spot" temperature at the surfaces of contacting asperities, and the oxidation rate is controlled by the diffusion rates of oxygen and iron. When each oxide layer reaches a critical thickness, the oxide breaks down through a fatigue mechanism at the layer-metal interface[146], and eventually appears as wear debris.

Quinn has found that the critical thickness obtained from the model is 1 ~ 3 μm, depending on the sliding conditions[75], and that these values agree with the experimental observations[147]. However, as Batchelor and coworkers[148] have pointed out, one of the doubts on this model is the assumed limiting layer thickness, because there is no reason why layer thickness should be the controlling parameter in practice. Although Quinn showed by electron microscopy that a large, flat and extremely smooth plateau of 1 μm in thickness was formed on a worn surface[147], the greatest weakness of Quinn's studies is that there are no observations on the wear debris generated. According to his model, the wear particles should have the same thickness, which corresponds to the critical thickness of the oxide layer. Moreover, the large flat plateau which Quinn observed does not coincide with his oxidation model at the contacting asperity surface, in terms of the size of the oxide area.

(2) The model of Scott and coworkers

Scott and coworkers[149,150] have proposed an alternative model by studying the development of oxides on sliding metal surfaces. They have found that oxide "islands", which consisted of compacted fine wear particles (10-50 nm in diameter) of oxides and oxide-covered metals, are formed on a worn surface. In their model, a very thin oxide film grows on a clean metal surface rapidly, and the oxide is removed by shear, either at the oxide/metal interface or within the oxide itself. This process is repeated by each sliding pass, and the removed oxides are fragmented together with oxide-covered metal wear particles. They are then compacted on the surface to form an oxide "island". The thickness of the oxide "island" remains constant (less than 1 μm) while the number and the area of the "island" increases during further sliding. It was shown that the reduction of friction and wear rate was associated with the build up of the compacted oxide "islands". They assumed that frictional heating during sliding was negligible.

This view of the model by Scott is consistent with work on the wear behaviour of metals in a magnetic field[151,152]. It has been reported that magnetization accelerates the transition from severe (running-in) to mild wear, partly because oxygen chemisorption is promoted by a magnetic effect, and partly because fine wear particles tend to be accumulated on the worn surface in the magnetic field. Kumagai and coworkers[152] have suggested that oxidized fine wear particles which exist between the rubbing surfaces act as a lubricant and reduce the wear rate, because they prevent metal-metal contact.

(3) Oxidative wear in the present study

The present study shows clearly that patchy oxide layers are formed at worn surfaces (Figs.4.52. and 4.54. (a)), and that very fine oxidized wear particles are produced in mild wear. The thickness of the patchy oxide layer (1 ~ 3 μm) is in very good agreement with the critical oxide thickness of Quinn's model[75]. However, the wear debris observed in the present study consisted of mainly spherical particles of 0.2 ~ 1 μm in diameter, not of plate-like particles of 1 ~ 3 μm in thickness. Thus it is unlikely that the wear debris was produced directly from the patchy oxide layer in the way proposed by Quinn. Because there is no reason why the "*patchy*" oxide layers were formed without the fine wear particles, the observations can be explained by the model of Scott and coworkers[149,150]; i.e. the patchy oxides layers at the worn surfaces are the "islands" which consist of fine compacted oxide wear debris.

It is not clear whether mild oxidative wear is associated with the formation of a thin surface oxide film or a relatively thick and large patchy oxide layer. Buckley[153] has suggested that any amount of oxygen on a steel surface, as an oxide film or as an adsorbed monolayer, will greatly reduce the adhesion of the rubbing surfaces. Soda and Sasada[103] calculated the number of "sufficient oxygen molecules" per unit atom in a nickel surface for mild wear, and found it to be about three. On the other hand, Pethica and Tabor[154] found that a monolayer of oxygen had little effect on the adhesion of a nickel surface, but that it was considerably reduced by a few layers of oxide (5 nm in thickness). It seems from these studies that a very thin oxide film, of only the order of nm in thickness, has a significant effect on preventing the adhesion of metal-metal contact[77]. However, the patchy oxide layer, which is considered to be aggregates of fine oxide debris, may also have an important role in reducing the adhesion and wear rate[149,152].

On the other hand, it is also a question of how the fine spherical oxide wear debris was produced. The oxide debris observed in the present study (0.2 ~ 1 μm in diameter) was much larger than the thin oxide film described above. A possible hypothesis on the processes of the debris formation can be made as follows[119,150]:

(1) Extremely-fine wear particles are produced by asperity contact from very thin surface oxide films (of the order of nm), which cover the clean metal surface rapidly. In addition, in some cases, fine metallic particles are oxidized after their detachment from the surface.

(2) These oxide particles agglomerate together and roll-up between the rubbing surfaces, into a final loose spherical particle.

(3) Some of the spherical wear particles remain on the surface together with the extremely-fine oxide

particles, and these are aggregated and compacted to a patchy oxide layer. As the area of the patchy oxide layer increases during further sliding, some wear particles may be detached from the oxide layer, resulting in plate-like wear debris (Fig.4.61. (b)).

However, there is not sufficient experimental evidence which directly supports this hypothesis at this stage. The extremely-fine wear particles, which are considered to be produced from very thin oxide films, are so small that it was difficult to collect and identify this wear debris. In addition, it is not clear whether the formation of the extremely-fine particles from the oxide film is due to the adhesion or abrasion of contacting asperities, or a fatigue mechanism. Thus oxidative wear is still open to study in terms of the formation mechanisms of wear particles and oxide surface layers.

(4) Effect of gas nitriding

Because there was no significant difference in the characteristics of worn specimens and wear debris between the untreated and gas nitrided pin tests in mild oxidative wear, it is reasonable to consider that the wear mechanism is also similar between the pin materials. However, as mentioned previously, gas nitriding reduced the wear rates of mild wear by up to one order of magnitude at the same loads, depending on the sliding conditions (Figs.4.18 and 4.20). This suggests that oxidative wear rates are strongly dependent on the material hardness. It can be concluded that the rate of formation of extremely-fine wear particles from thin surface oxide films was considerably reduced, partly because the real contact area of the surfaces was reduced by the high hardness of the gas nitrided steel, and partly because the thin oxide film was better supported by the hard substrate nitrided layer[140].

5.2.2. Metallic wear

Metallic (severe) wear is characterized by plastic deformation, metal transfer and the production of large metallic wear debris. The most remarkable metallurgical change observed in the present study as a result of the metallic wear was the formation of 'white-etched' layers at the worn surfaces. This section will therefore start with a brief review of 'white-etched' layers, and then discuss the metallic wear mechanism in some detail.

5.2.2.1. Formation of 'white-etched' layer

The phenomena of so-called "white layer" during wear processes have been reported in many studies[e.g. 155-158], and useful reviews of the literature have been given by Eyre and Baxter[159], and Scott and coworkers[160]. The term "white-layer" refers to a hard surface layer formed in a variety of ferrous materials under a variety of conditions which appear white under the microscope[155]. This layer has two common features; firstly, a high hardness in comparison to the bulk hardness, and secondly an apparently featureless structure when viewed under optical microscopes.

Although "white layer" seems to have become the usual way of referring to such layers, other terms are used such as "phase transformed materials", "white phase", "nonetching layers", "white etching" and others have been used. In order to avoid confusion between this layer and the compound layer (white layer) produced by a nitriding process, the term 'white-etched' layer is used throughout this thesis to describe the "white layer" formed as a result of wear.

Three main or general mechanisms have been proposed which are associated with 'white-etched' layer formation. These are:

(1) the mechanism of intensive plastic deformation which produces a homogeneous structure or one with a very fine grain structure[158,159];

(2) the mechanism of frictional flash temperature heating and rapid cooling which results in a phase hardening transformation[65,157,160];

(3) the mechanism of chemical reaction with, for example, carbon or nitrogen in the environment or the bulk material[156,157].

It is likely that a combination of these mechanisms is responsible for the formation of 'white-etched' layers. Although there is argument that 'white-etched' layers are martensite-based structures, Eyre and Baxter[159] have claimed that the high hardness cannot be explained in terms of simple conventional martensite of a carbon steel. They have concluded that there is general agreement that 'white-etched' layers are produced by a combination of surface flash temperatures and extensive cyclic deformation, and that their properties are due to a fine dispersion of second phase particles pinning an extremely fine crystallite structure.

A recent extensive study by Bulpett and coworkers[158] has confirmed that there is no chemical change in terms of carbon, nitrogen and oxygen compositions in a 'white-etched' layer formed on digger teeth, and demonstrated that this layer is a structurally and chemically homogeneous phase which consists of an extremely fine-grained martensite, produced by a thermomechanical mechanism incorporating transformation at high strain rates. It has been also suggested that the "white" appearance in a standard metallographic section is entirely due to its structural and chemical homogeneity, and that the high hardness, which exceeds the attainable value for a particular steel composition, is attributed to the extremely fine grain size of this layer.

In the present study, 'white-etched' layers were identified in metallic wear at the worn surfaces of both the pins and discs, in both untreated and gas nitrided pin tests. Fig.4.42 (d) shows a thin 'white-etched' layer formed at the worn surface of an untreated pin tested in an extremely-severe wear regime. Another 'white-etched' layer was observed in a taper section of an untreated pin tested in 'low-wear-rate' severe wear (Fig.4.44 (b)), and shows evidence of considerable plastic deformation. Fig.4.44 (d) demonstrates a 'white-etched' particle (not layer) adhered to the worn surface of an extremely-sever wear specimen. The adhered particle has high hardness (Hv 666-739) in comparison with the matrix hardness. In gas nitrided pin tests, relatively thick 'white-etched' layers (5-10 μm) were produced at the pin surfaces (Figs.4.43. (c) and 4.45 (b)).

For the discs in metallic wear, 'white-etched' layers were also observed on worn surfaces except for the untreated pin test in a 'low-wear-rate' severe wear regime (Fig.4.54 (b)). Figs.4.54 (c) and 4.56 show 'white-etched' layers of 20 μm in thickness, which were formed on the disc rubbed against untreated pins in extremely-severe wear. The gas nitrided pin tests in severe wear also produced 'white-etched' layers of 10 μm in thickness on the worn disc surfaces (Figs.4.55 (b) and 4.57). Because the 'white-etched' layers of the discs are observed "*above*" the worn surfaces, it is reasonable to consider that these layers are transferred particles from the pin materials. This view is supported by the fact that intensive metal transfer to the disc surfaces occurred in metallic wear (Figs.4.49 and 4.51).

The adhered fragment of material to an untreated pin in extremely-severe wear (Fig.4.44 (d)) exhibits a similar 'white-etched' microstructure to that of the transferred particle on the disc (Fig.4.54 (c)). Therefore the adhered fragment is considered to be either a back-transferred particle from the disc surface or a trapped particle of wear debris.

All the observed 'white-etched' layers show very high hardness values in comparison with the matrix materials. Below the 'white-etched' layer of the disc surface, a tempered martensite layer was produced, which suggests that the 'white-etched' layer had been heated to a high temperature during its formation. In addition, FeO was identified together with Fe in the wear debris generated from a gas nitrided pin test in severe wear (Fig.4.63), suggesting that a high temperature of at least 500 °C was generated during the wear test[106,107].

There is also evidence of considerable plastic deformation of the 'white-etched' layer (Fig.4.44 (b)). Moreover, it is most likely that the transferred layers and metallic wear debris were plastically deformed intensively at high strain rates. Rigney and coworkers[94,95] have demonstrated by TEM (Transmission Electron Microscopy) that a transferred layer produced during a wear process has a very fine crystallite size, 3 - 30 nm in diameter, and that the loose wear particles have the same structure and composition as the transferred layer. They did not mention 'white-etched' layers, but these materials would have probably shown 'white-etched' structures in optical microscopy.

Therefore it can be concluded that both the 'white-etched' layers formed on the pins and the 'white-etched' transferred particles on the discs and the untreated pin shown in Fig.4.44 (d) were produced by the same thermomechanical mechanism as has been reported in the literature[158,159].

Some investigators[159,161] have drawn attention to the tribological advantage of a 'white-etched' layer because of its high hardness. Welsh[65] has suggested that the formation of a hard transformed ('white-etched') layer is responsible for a severe-to-mild wear transition and the establishment of the consequent oxidative wear. However, those wear experiments where the 'white-etched' layers were formed in the present study had to be terminated at relatively short times because of the high wear rates, and there was no beneficial aspect of this layer. Thus the 'white-etched' layers can be associated with catastrophic wear or "scuffing" behaviour in rubbing situations[159,160].

5.2.2.2. Metal transfer and wear debris formation

Intensive metal transfer from pin to the disc surface and also back transfer to the pin were identified in metallic wear. Many phenomena of metal transfer in sliding wear situations have been reported in the literature, and metal transfer is inevitable in metallic (adhesive) wear. Bowden and Tabor[77] have suggested that most metal surfaces are covered with a thin oxide layer and other contaminating films, but that during sliding these oxide and surface films will be broken up resulting in some metallic contact. The metallic junction caused by adhesion is usually stronger than the metal of one component of a sliding pair, and shearing occurs within the weaker metal, which results in metal transfer to the other component.

<u>(1) Untreated pin test</u>

In untreated pin tests, two types of metallic wear were observed; 'low-wear-rate' metallic wear and extremely-severe wear. For the 'low-wear-rate' metallic wear, there was considerable evidence of plastic deformation of the pins (Figs.4.37 (a), 4.42 (b) and 4.44 (b)) and intensive adhesion on a pin surface (Fig.4.37 (b)). Metallic (Fe) wear debris

(Fig.4.62 (b)) was produced from this wear regime. However, the sizes of the transferred fragments to the disc (Fig.4.48) and the wear debris generated (Fig.4.60 (b) and (c)) were very much smaller than those from extremely-severe wear tests (Fig.4.49 and 4.60 (d)). Thus the most marked difference in the mechanisms between the 'low-wear-rate' and extremely-severe metallic wear regimes is the degree of the metal transfer, which can be directly related to the wear rate of the pin.

In extremely-severe wear, a prow-type profile transferred particle was produced on the worn surface of a disc (Fig.4.56). This type of metal transfer has been reported by Antler[99], who studied the processes of metal transfer and wear through a stereomicroscope in a rider-flat apparatus. He has shown that so-called "prow formation" is characterized by build up of work-hardened transfer metal which grows by continuous plastic shearing of the sliding metals in a direction slightly inclined to the surface. It has been suggested that the necessary conditions for prow formation are:

(1) prow formation occurs only under severe sliding conditions, and oxidation or lubrication of the surface will give a mild regime without prow-formation.

(2) there must be welding (strong adhesion) in order for particles to adhere to the rider.

(3) the metals must not be excessively hard.

(4) the metals which form prows must show a marked

work-hardening capability.

(5) the transfer metal must be harder than the flat.

Although he showed that the metal transfer in the prow formation occurred from a flat to the rider, contrasting with the transfer from a pin to the disc in the present study, it is considered that the prow-type transferred particle on the disc surface was produced by the same mechanism as reported by Antler. This view of particle growth can be supported by two pieces of evidence; that the transferred particle showed a 'white-etched' structure (i.e. high hardness), and that the final loose wear particles had striped surfaces (Fig.4.60 (d)).

It is clear from the prow formation and the intensive metal transfer to the disc that the junction growth of contact asperities was operative during the wear process[78]. This junction growth is based on a plasticity theory which takes account of a combination of normal and tangential stresses. Patchy transferred layers shown in Figs.4.49, 4.54 (c) and 4.56 suggest that the applied load was supported by only a few growing contact points between the surfaces. This view is very similar to that suggested in previous work[93,98], which showed that most of the time during severe sliding wear the surfaces of the sliding components were held apart by a particle of displaced metal.

It is reasonable to consider that in the 'low-wear-rate' severe wear, the sliding conditions were not sufficient for prow-formation or junction growth in terms of plastic deformation. This could be the reason why microscopic metallic wear was favoured in this wear regime.

Large metallic wear debris (up to 50 μm in size) and extremely large metallic particles (up to 1 mm in size) were produced from the 'low-wear-rate' severe wear and extremely-severe wear, respectively (Figs.4.60 (b), (c) and (d)). Although metal transfer presupposes a strong bond between transferred fragments and the surface onto which they are transferred, final loose wear particles are eventually removed out of the sliding system[101]. The mechanism of the formation of the loose wear debris can be explained in terms of chemical reactions of the transferred particles with the environment[102,103], or increasing strain energy of the transferred fragments[101,104], or fatigue of the transferred metals[92].

<u>(2) Gas nitrided pin test</u>

Intensive metal transfer to a disc surface (Fig.4.51) and relatively large metallic wear debris of up to 200 μm in size (Fig.4.61 (c)) were also observed for gas nitrided pin tests in severe wear. Because these features are similar to those of the untreated pin tests in extremely-severe wear, it can be concluded that the metallic wear mechanism is basically the same for the two pin materials. However, some differences to be noted were observed as follows.

(1) A gas nitrided steel inhibited intensive plastic deformation of the pin (Fig.4.40) and prow-type metal transfer to the disc (Fig.4.51). This

results in the production of smaller wear debris (Fig.4.61 (c)) and a much lower wear rate than those of an untreated pin test exhibiting extremely-severe wear.

(2) In gas nitrided pin tests, thicker 'white-etched' layers at the worn surfaces of the pins (Figs.4.43 (c) and 4.45 (b)), and deeper tempered martensite sublayers in the discs (Figs.4.55 (b) and 4.57) were formed in comparison with untreated pin tests showing extremely-severe wear. This suggests that a considerably higher temperature was generated during the gas nitrided pin tests.

The second result described above can be related to the first one, i.e. because the gas nitrided steel reduced the degree of plastic deformation, metal transfer and the production of wear debris owing to its hard surface layer, more of the frictional energy was turned into heat, resulting in a high temperature and the formation of the thicker "white-etched' layers[141].

5.3. Wear through nitrided surface layer

5.3.1. Wear of the compound layer

The wear tests of an 'as-gas nitrided' pin and a gas nitrided pin without the compound layer showed that the amount of the wear of the pin without the compound layer was lower than that of the 'as-nitrided' pin at the initial stage of sliding, and that the wear rate at steady state was almost the same between the two types of pin material (Fig.4.35). However, there was no significant change in wear rate at the wear length of the pin corresponding to the thickness of the compound layer (30 μm), and the initial high wear (running-in) behaviour of the 'as-nitrided' pin cannot be directly related to the wear of the compound layer. Thus it was concluded that the compound layer increased the wear rate of the gas nitrided steel only at the start of sliding.

Fig.4.41 shows a worn surface of an 'as-gas nitrided' pin in which the compound layer was not completely worn away, and pitting was observed parallel to the disc sliding direction in the surface. A number of plate-like wear particles were produced from the compound layer of the gas nitrided pin (Fig.4.61 (d)). The size of the plate-like particles (5~10 μm in length) also agrees well with that of the pits in the worn surface. Thus these observations suggest that a pitting fracture is responsible for the wear of the compound layer. Suh[73,74] has proposed a delamination wear theory which is based on crack formation in the sublayer and crack propagation parallel to the worn surface in order to explain the production of plate-like wear debris. Therefore it is considered that the wear of the compound layer is due to crack formation and growth within this layer rather than adhesion or abrasion.

This view can be supported by the structure and mechanical properties of the compound layer. As shown in Fig.4.8 (a), a microhardness indentor caused a crack in the compound layer due to its brittleness[21,22]. Moreover, the outer part of the compound layer showed a porous structure and lower hardness in comparison with the diffusion layer (Fig.4.9). Therefore it can be concluded that the compound layer increased the initial wear rate of the gas nitrided steel owing to its porous and brittle structure and low hardness.

In addition, the "wear-face-limited" gas nitrided pin, in which the side-faces of the pin were covered by a masking agent during the nitriding, also showed a lower wear rate than the 'as-gas nitrided' pin at the initial stage of sliding (Figs.4.26 and 4.27). Fig.4.12 shows the microstructure of the cross-section of the "wear-face-limited" gas nitrided pin, and it can be seen that no compound layer was formed on the wear surface of the pin, while a normal diffusion layer was produced at the wear-face of the pin. Thus this observation confirms that the gas nitrided steel without the compound layer reduces the initial wear rate in comparison with the 'as-nitrided' steel with the compound layer.

It should be emphasized that when wear of a gas nitrided steel became governed by the diffusion layer, the wear rate did not depend on the presence of the compound layer. This suggests that the compound layer influences only the initial wear behaviour of a nitrided steel.

A nitrocarburized steel showed a considerably lower wear rate at the initial stage of sliding in comparison with gas nitrided and plasma nitrided steels (Fig.4.30). This can be explained by the characteristics of the nitrocarburized compound layer, which was only 3 μm thickness (Fig.4.3), and had finer porosity than a gas nitrided specimen (Fig.4.11). Thus it is reasonable to consider that the nitrocarburized compound layer is less brittle than the gas nitrided compound layer, resulting in the initial low wear rate of the nitrocarburized steel. Gregory[33] has also suggested that the compound layer prevents adhesive wear because of the chemical incompatibility between steel surfaces.

On the other hand, a plasma nitrided steel showed a relatively high wear rate at the initial stage of sliding in spite of its thin compound layer (2 μm). These conflicting results can be explained by the difference in the structure of the compound layer. The plasma nitrided compound layer consisted of only a γ'-Fe_4N nitride phase (Fig.4.7 (b)), which appears to be inferior to an ϵ-Fe_3N nitride from a tribological point of view[35].

Contradictory results have been reported in the literature about the effects of the compound layer on the wear behaviour, depending on the sliding conditions. Karamis[64,162] investigated the effect of thickness of the compound layers produced by plasma nitriding for varied treatment times. It was shown that under dry sliding conditions a thicker compound layer increased the wear rate because of the porous and brittle structure of this layer. This result is consistent with the wear behaviour in the present work. However, he has also mentioned that the presence of the compound layer at a nitrided surface can improve the resistance to scuffing and seizure, especially under lubricated conditions where the porous compound layer is able to store oil.

Wang and coworkers[62] studied the wear behaviour of plasma sulpho-nitrocarburized steels under three different conditions; unlubricated, lubricated and lubricated with abrasives. In the case of an unlubricated condition, the sulpho-nitrocarburized steel showed a higher wear rate at the early stage of sliding than salt-bath and gas nitrocarburized steels. This result was explained by greater porosity of the outer part of the sulpho-nitrocarburized compound layer. On the other hand, he showed that under lubricated and abrasive-containing lubricated conditions, the porous outer layer was beneficial, probably because it was able to store oil or abrasive particles.

However, more contradictory results have been reported even under lubricated conditions. Williamson[54] found that in lubricated wear tests, a salt-bath nitrocarburized steel which had a very porous compound layer showed a higher wear rate than the other thermochemical treatments. Burakowski and coworkers[60] have reported that those gas nitrided specimens that were ground to 40 μm depth showed lower wear rates than 'as-nitrided' specimens under lubricated sliding conditions.

Although there is still a question whether a compound layer improves the wear resistance under lubricated conditions, it was confirmed by the present study that under dry sliding conditions the porous and thick ϵ-Fe_3N compound layer formed on a gas nitrided steel has poor wear properties, as has been reported previously[62,64]. However, a thinner and less porous ϵ-Fe_3N compound layer produced by the nitrocarburizing was beneficial to improve dry sliding wear performance. Further investigations are obviously necessary at this stage in order to establish optimum conditions of the compound layer in terms of thickness, structure and composition.

5.3.2. Effect of hardness variation in the diffusion layer

The hardness of the diffusion layers in the nitrided steels decreased gradually with an increase of distance from the surface (Fig.4.5). Accordingly, it was expected that the wear rate would increase as the surface layer was worn away. However, the wear tests of gas nitrided and plasma nitrided pins through the surface hardened layer showed that the wear rates were much lower than that of an untreated pin even after the wear length of the pin reached the value of the surface hardened layer depth (Figs.4.26 and 4.27). On the other hand, a "wear-face-limited" gas nitrided pin, in which nitriding occurred only on the wear-face of the pin, exhibited a catastrophic change to a very high wear rate when the wear length of the pin reached the value of the case depth (0.42 mm). These wear results suggest that hardness plays an important role in the wear behaviour and that the hardened layers of the side-faces of normally nitrided pins (see Figs.4.12 and 4.14) should be taken into account to explain the wear behaviour through the surface layers. Thus the apparent mean hardness at the sections parallel to the wear faces of the normally nitrided pins was calculated as a function of distance from the wear face in order to discuss the effect of hardness variation of the pins on the wear rate quantitatively.

The mean value of the pin hardness at each cross-section that is parallel to the wear-face, H_{pin}, is obtained by dividing the integral value of the hardness at the cross-section by the section area, i.e.;

$$H_{pin} = (\int H \Delta A) / A \qquad \text{(Eq. 5.1)}$$

where H is the hardness at each point of the pin, and A is the area of the pin section parallel to the wear-face. H is obtained by assuming that nitriding occurred uniformly from both the wear-face and side-face of the pin, and that the relationship between the hardness at each point and the distance from the pin faces is the same as that shown in Fig.4.5. The calculated H_{pin} is plotted against the distance from the wear-face of the pin, and shown in Fig.5.2 for gas nitrided, plasma nitrided and nitrocarburized pins. In this graph, the hardness variation of a "wear-face-limited" gas nitrided pin, which is the same data shown in Fig.4.13, is also presented. The hardness of an untreated pin is obviously constant (Hv 260) throughout the pin.

It was found from Fig.5.2 that the apparent hardness of the normally gas nitrided pin was very high (Hv 770) even after the distance from the wear face reached the value of the surface hardened layer depth (0.7 mm) because the hardened layer of the side face of the pin has a considerable effect on the apparent hardness of the pin. In the plasma nitrided pin, the effect becomes less because the hardened layer is shallower (0.5 mm) than the gas-nitrided hardened layer, but the apparent mean hardness of the pin at the core distance from the wear face is still high (Hv 590). On the other hand, for the nitrocarburized specimen, in which the hardened layer is very shallow (0.2 mm), the apparent mean hardness at the core distance is nearly equal (Hv 340) to the untreated specimen.

These hardness variations of the nitrided pins explain very well the wear behaviour of the normally nitrided pins through the surface layers (see Figs.4.26 and 4.27). The relatively low wear rates of the gas nitrided and plasma nitrided pins at the core depth is due to the effect of the hardened layers at the side-faces of the pins. This was confirmed by the wear tests of nitrocarburized and "wear-face-limited" gas nitrided pins, in which the effect of the hardened layers at the side-face of the pins was eliminated. These specimens showed catastrophic wear behaviour when the surface case layers were worn away. Therefore it can be concluded that in practice the benefits of nitrided steels will be lost once the effective surface layers have been removed. Furthermore, the discussion given so far suggests that the wear rates in the diffusion layers were determined by the material hardness, apart from the running-in wear behaviour.

Some investigators[59,141] have reported that even after a surface layer had been completely worn away, surface treated steels exhibit a lower wear rate than would be predicted from the properties of the substrate steel. Eyre[163] has suggested that the subsequent low wear of the substrate is due to the presence of a black (oxide) layer which builds up on the counterface during the mild low wear stage when protected by the surface layer. However, he has also shown that once this black layer was removed a higher wear rate was then obtained. The wear test of a "wear-face-limited" gas nitrided pin showed that the wear rate increased sharply at the case depth and that the wear rate was the same as that of an untreated pin after the surface hardened layer was completely worn away. Because the wear test was carried out under the conditions of 1 $m \cdot s^{-1}$ and 40 N, in which the untreated steel showed metallic severe wear, contrasting with the mild wear of the gas nitrided steel, it is considered that the oxidation rate was no longer able to outweigh the increasing wear rate, and that the breakdown of the oxide layer occurred quickly when the soft substrate steel became responsible for the wear process.

There can be little doubt that the hardness and state of oxidation of the surfaces are the principal factors controlling the wear rate pattern,and that oxidation can only inhibit severe wear if the hardness exceeds a critical value under a given sliding condition[65]. The critical value is the hardness required to maintain mild wear when the surface are oxidized and run-in. Because the "wear-face-limited" gas nitrided pin showed a transition from mild to severe wear at a case depth of 0.42 mm, the critical hardness for mild wear in the sliding condition of 1 $m \cdot s^{-1}$ and 40 N can be estimated to be Hv 550, which is defined as the specific hardness required for the case depth of a surface hardened layer[19].

It is interesting to note that the wear rate of the "wear-face-limited" gas nitrided pin was almost constant up to 0.3 mm of the wear length of the pin, although the hardness of the pin fell from Hv 1100 to Hv 700. This suggests that an oxidative wear rate does not depend on the material hardness if the hardness is sufficient to stabilize the oxidative mild wear.

In Fig.5.2, attention should be paid to the apparent mean values of the hardness of the normally nitrided pins at the case depths, because the wear tests for the investigations of the effects of load and sliding speed and the influence of surface treatment processes were carried out using normally nitrided pins, and the wear rates were obtained from the gradients of the wear curve points at the case depths. These values for gas nitrided, plasma nitrided and nitrocarburized pins are Hv 830, 820 and 630, respectively. The values of apparent mean hardness of the gas nitrided and plasma nitrided pins at each case depth are almost the same and very high. However, the value for the nitrocarburized pin is lower than the first two materials, because the maximum hardness of the nitrocarburized specimen (Hv 800) was lower than that of gas nitrided and plasma nitrided specimens (Hv 1200). If all wear tests are carried out using "wear-face-limited" nitrided pins and the wear rates are obtained from the gradients of the wear curve points at the depths having the same hardness values mentioned above, the wear rates and the transitional behaviour will be the same as shown in the present study. For the gas nitrided specimen, for example, the depth at which the layer has a hardness of Hv 830 is 0.22 mm (Fig.4.5), which is nearly equal to half the value of the gas nitrided case depth.

5.4. Comparison between surface treatments

5.4.1. Effect of surface treatment processes on wear behaviour

The main differences in metallurgical characteristics of the three nitriding surface treatments are the compound layer microstructure and the surface layer depth. As shown in the previous sections, these factors considerably affected the wear behaviour through the nitrided layers. Because the effect of the compound layers produced by the different nitriding processes has been already described in section 5.3.1., the discussion in this section will be concerned mainly with the wear behaviour of the diffusion layers.

5.4.1.1. Wear curve

A remarkable difference in the wear behaviour between the nitriding treatments is the change in the sliding distance at which the surface layer was completely worn away. It has been shown that a sharp increase in wear rate was observed when the wear length of the pin reached the value of the case depth (Fig.4.27 and 4.28). Therefore the transition to a higher wear rate occurred at a very long sliding distance for the gas nitrided pin because of the deep case depth (0.42 mm). In contrast, the nitrocarburized pin, which had a shallow case depth (0.05 mm), showed a sharp increase in wear rate at a considerably shorter sliding distance. These results are clearly explained by the hardness profiles of the nitrided pins as discussed in section 5.3.2..

5.4.1.2. Wear rate and transition load

It was not possible to compare the wear rates between surface treatments simply, because the hardness profile was different according to the process. In order to make meaningful comparisons in wear rate between the surface treatments, the wear rate was obtained from the gradient of the wear curve point at the effective case depth for each. The reason for the selection of effective case depth is that it is the most important parameter which describes a surface hardened layer.

The variations of the wear rates with load at a sliding speed of 1 $m \cdot s^{-1}$ are shown in Fig.4.34 for the gas nitrided, plasma nitrided, nitrocarburized, and carburized-and-hardened steels. It has been concluded that there was no significant difference between the surface treatments in terms of wear rates and transition loads, because the wear rates were of the same order of magnitude except for the carburized-and-hardened steel test at 160 N, and a mild to severe wear (T_1) transition was observed at the same load (60 N) for each surface treated steel. This conclusion is broadly valid, but more detailed observation and discussion will now be made on the comparison of the wear behaviour between the surface treated steels.

When making comparisons between only the gas nitrided and plasma nitrided steels, the wear rate of the plasma nitrided steel was lower than that of the gas nitrided steel by a factor of two at all the test loads. The same result has been reported by Cohen and Rosen[56], who studied the dry wear resistance of gas nitrided and plasma nitrided stainless steels in which the surface compound layers had been removed prior to the wear tests. They did not show the microstructure nor the hardness profile, but did mention that the hardness of both the nitrided layers was Hv 960. It was suggested that the low wear rate of the plasma nitrided specimen was due to the finer and more homogeneous nitrides distributed in the plasma nitrided layer than those of the gas nitrided layer. They have described that in plasma nitriding, nitrogen penetrates into the steel surface with a high energy and propagates rapidly through the bulk and grain boundaries, resulting in the formation of fine and homogenous nitrides. In contrast, the nitrides produced by a gaseous process are coarse because precipitation occurs only in high energy regions such as grain boundaries owing to the relatively low energy reaction with nitrogen at the steel surface. However, there was no evidence of the fine microstructure of the plasma nitrided specimen, and the fine precipitation should have increased the hardness of the nitrided layer. The differences in the mechanisms of nitrogen-diffusion and nitride-precipitation between gas and plasma processes have not been clarified. Therefore it would be dangerous to conclude that the lower wear rate of the plasma nitrided steel was due to the fine microstructure.

A possible explanation for the higher wear rate of the gas nitrided steel than that of the plasma nitrided steel in the present study is that the wear rate of the gas nitrided steel was obtained at a longer sliding distance than that of the plasma nitrided steel. Because the gas nitrided case layer was thicker than the plasma nitrided case layer, the sliding distance at which the wear length of the pin reached the value of the gas nitrided case depth was longer than that of the plasma nitrided steel. It should be noted that the apparent mean hardness of the gas nitrided and plasma nitrided pins was almost the same (Hv 830 and 820, respectively) at each case depth (Fig.5.2). However, the wear test with a longer sliding distance (= longer test time) generates a higher temperature at the surface and a larger amount of wear debris. These factors can be responsible for the higher wear rate at the case depth of the gas nitrided steel.

In comparison with the gas nitrided and plasma nitrided steels, the carburized-and-hardened specimen showed higher wear rates at all the test loads. Particularly at 160 N, the wear rate of the carburized-and-hardened pin was more than an order of magnitude higher than those of the two nitrided pins. This behaviour can be directly related to the hardness of the pin, because both the maximum hardness of the carburized-and-hardened pin (Hv 750) and the apparent mean hardness of the pin at the case depth (Hv 650) were lower than those of the gas nitrided and plasma nitrided pins.

Moreover it is well known that a nitrided microstructure is able to maintain the high hardness up to higher temperatures than the martensite structure which is produced by carburizing and quenching[8,15]. It can be considered that at the highest load of 160 N, the worn surface of the carburized-and-hardened pin was considerably softened because of the high frictional heating, resulting in the very high wear rate. Indeed the wear debris produced from this test was very large metallic particles, which was similar to that of the untreated pin test in an extremely-severe wear regime. In contrast, the nitrided steels inhibited the extremely-severe wear even at the highest load. Therefore it can be concluded that the wear rate of the diffusion layer produced by gas or plasma nitriding is lower than that of the carburized-and-hardened surface layer, because of the higher hardness and higher resistance to tempering of the nitrided surface layers.

Because the nitrocarburized surface layer was much thinner than those of the other surface treatments, the wear rate pattern was slightly different from the others. The nitrocarburized steel did not show a sharp T_1 transition in wear rate as observed in the other surface treatments, but did exhibit a considerable increase in wear rate with an increase in load. The wear rates were of the same order of magnitude as those of the gas nitrided and plasma nitrided steels. Thus it can be said that the wear rate pattern of the nitrocarburized steel was similar to the T_1 transitional behaviour of the other two nitrided steels.

However, the significant characteristics of the wear behaviour of the nitrocarburized steel were the low wear rate at the initial stage of sliding and the catastrophic failure at a relatively short sliding distance (Fig.4.30). Because the main purpose of nitrocarburizing is to produce a thin ϵ-Fe_3N compound layer at the surface, not to form a deep and hard diffusion layer[16,34], it is not meaningful to compare the wear rate of the nitrocarburized diffusion layer with the other surface treated steels.

5.4.2. Endurance of nitrided surface layers

It has been shown that the nitrided steels exhibited an increase in wear rate at their respective case depth. This result is of considerable practical importance for industry, particularly when considering the wear life of surface treated components, because the benefit of the surface treatment will be lost once the effective surface layer is worn away.

Fig.5.3 shows the relationship between the applied load and the wear life of the surface layer for gas nitrided, plasma nitrided and nitrocarburized steels. The life of the surface layer, which was obtained from the wear curve of a normally nitrided pin at a sliding speed of 1 $m \cdot s^{-1}$ (in Figs.4.19 (b), 4.26, 4.28 and 4.30), is the sliding distance at which the wear length of the pin reached the value of the effective case depth. In the case of the tests at 10 N for the gas nitrided and plasma nitrided pins, the lives of the surface layers were estimated by the extrapolation from the wear curves at steady state.

It can be seen from Fig.5.3 that the gas nitrided case layer has the longest life because the effective case layer is the deepest of all the nitriding treatments. In contrast, the nitrocarburized case layer has the shortest life because the case layer is very shallow and worn away quickly. In particular, the life of the nitrocarburized layer is an order of magnitude shorter than those of the plasma nitrided and gas nitrided layers at loads of 10 and 40 N. Another point to be emphasized here is that for the gas nitrided and plasma nitrided steels, the lives of the surface case layers were reduced by two orders of magnitude as the load increased from the mild wear regime (10, 40 N) to the severe wear regime (80, 160 N). This suggests that in severe wear the endurance of the surface layer is very poor, and that the severe wear should be avoided in engineering component design.

5.4.3. Suggestions for the selection of surface treatments

Some suggestions can be made from the results obtained in the present study on the selection of nitriding processes for wear applications as follows:

(1) Prior to the selection of nitriding processes, the operating conditions of the severe (metallic) wear regime should be avoided, because severe wear is very high and unacceptable, and the life of the effective surface layer is very short as shown in Fig.5.3. Moreover, it should be noted that in severe wear, nitrided steels always exhibit a type-C wear curve (the wear rate increases as the sliding distance (= time) increases). The wear map (Fig.5.1 (b)) indicates the dangerous region in which metallic (severe) wear occurs in terms of sliding speed and load.

(2) The required thickness of the surface layer should be primarily taken into account at the design stage. In nitriding, a suitable case depth can be obtained by optimizing the treatment time, temperature, and steel composition[15,16,20].

(3) Under conditions where a relatively large amount of wear is expected or high stresses are applied, gas nitriding or plasma nitriding, in which a relatively deep hardened surface layer is produced, is more suitable and reliable than nitrocarburizing in which a shallow surface layer is formed. On the other hand, in situations of relatively low wear, for example lubricated conditions or low stress applications, nitrocarburizing is superior to the other two treatments, because a nitrocarburized steel does not only show a considerably lower wear rate at the initial stage of the wear process (Fig.4.30), but also nitrocarburizing is a cheaper process due to the short process time. However, it should be emphasized that the life of a nitrocarburized surface layer is much shorter than those of gas nitrided and plasma nitrided layers (Fig.5.3), and that a catastrophic failure occurs once the shallow surface layer is worn away.

(4) A thin nitrocarburized ϵ-Fe_3N compound layer appears to be beneficial to prevent adhesive wear. On the other hand, a thick and porous gas nitrided ϵ-Fe_3N compound layer causes a problem under dry

sliding conditions because it increases the initial wear due to its brittleness. When a relatively deep diffusion layer without a thick compound layer is required, for example, under rolling-sliding situations, plasma nitriding may be superior to gas nitriding because the compound layer produced by plasma nitriding is much thinner than that of gas nitriding[48,49].

(5) If the specific wear process is governed by the hardness in a nitrided diffusion layer and the hardness profiles (peak hardness, case depth etc.) obtained by different processes are the same, the wear behaviour seems to be independent of the nitriding processes, because the microstructures of nitrided diffusion layers are essentially the same whatever nitriding process is employed. In this situation the cost performance of nitriding processes should be considered. In some cases conventional ammonia gas nitriding may still have an economic advantage against more expensive plasma nitriding. However, the cleanliness and environmental harmlessness of a plasma nitriding process should be also considered[31].

(6) Gas nitrided and plasma nitrided diffusion layers show lower wear rates than a carburized-and-hardened surface layer, because of their higher hardness and higher resistance to tempering. However, in a carburizing-and-hardening process, the same case depth can be obtained in a much

shorter treatment time than a nitriding process, which will yield a considerable economic benefit. Therefore, in this case, both the wear characteristics and the cost performance should be taken into account. Other factors such as the ease of manufacturing (e.g. the degree of distortion by the processes, the selection of the substrate steel grade) must be considered from a manufacturing engineering point of view.

One final comment can be made concerning the selection procedure for an optimum surface treatment to meet the required wear properties; this has been the subject of much discussion in the literature[e.g. 7,164,165]. Although surface treatments and coatings are now being increasingly considered at the design stage, it is very difficult to select treatment techniques properly, partly because many surface treatments and coatings are now available, and partly because a large number of factors should be considered from mechanical, tribological and economical points of view.
As has been pointed out by Syan and coworkers[165], there is unfortunately no widely accepted procedure to aid in the selection of an optimum surface treatment. The selection has often been based on experience, and design engineers have to rely largely on producers' guides and internally produced company data which normally does not allow meaningful comparison between different techniques. Therefore, it is clear that a more systematic program in the area of wear of surface treatments is required; for example investigations of

the "wear mapping approach" of surface treatments, and the developments of suitable database and computer expert systems[165] will be very useful for the selection of the most appropriate surface treatment.

However, a warning must be also made. Although these systematic approaches yield useful guides for the selection, these are not perfect tools. In some cases, empirical knowledge or case studies[166] may still be of more direct use in practical engineering than the systematic database, which needs so much data and experience on tribology and surface engineering that there is no hope of constructing a universal database which describes all aspects of all surface treatments. One of the most important things is to produce "well-organized" data, for example, which describes clearly a relationship between wear properties and the characteristics of surface treatments.

Chapter 6: Conclusions

1. An ϵ-Fe_3N compound layer (white layer) of 30 µm thickness and a relatively thick diffusion layer of 0.42 mm case depth were observed at the surface of a gas nitrided BS970,905M39 (EN41B). In a plasma nitrided steel, a very thin γ'-Fe_4N compound layer (2 µm) and a diffusion layer of 0.22 mm case depth were produced. Both these nitriding processes increased the surface hardness to Hv 1100-1200, and the hardness decreased gradually with an increase in distance from the surface. Gas nitrocarburizing produced a thin ϵ-Fe_3N compound layer of 3 µm thickness and a very shallow diffusion layer of only 50 µm case depth at the steel surface.

2. Wear experiments over a wide range of sliding speed and applied load using a pin-on-disc machine showed that gas nitriding considerably improved the wear properties of BS970,905M39 (EN41B). The wear rates were reduced by gas nitriding by up to two orders of magnitude, depending on the sliding condition. In addition, gas nitriding increased the T_1 (mild to severe wear) transition loads over the whole sliding speed.

3. Sharp transitions in wear rate with variation of load were observed for both untreated and gas nitrided steels. In the untreated steel, three basic wear regimes, i.e. mild, severe and extremely-severe wear were identified. On the other hand, the gas

nitrided steel exhibited only mild and severe wear regimes. Mild wear was associated with the formation of patchy oxide layers at the worn surfaces, and the production of very fine oxidized (Fe_2O_3, Fe_3O_4) wear debris. In contrast, severe wear was characterized by plastic deformation, metal transfer to the disc surface, 'white-etched' layer formation, and the production of large metallic (Fe) wear debris.

4. A wear test on a gas nitrided pin without the compound layer confirmed that a thick and porous surface compound layer increased the dry sliding wear rate only at the initial stage of sliding, because of its brittleness and lower hardness than the diffusion layer. A plasma nitrided specimen, in which a thin γ'-Fe_4N compound layer was formed, also showed a relatively high initial wear rate. However, a nitrocarburized steel, which had a thin and dense ϵ-Fe_3N compound layer, exhibited a much lower initial wear rate than the other two nitrided specimens.

5. A "wear-face-limited" gas nitrided pin test, which eliminated the effect of the hardened layer in the side-face of the pin, showed a sharp increase in wear rate once the effective case layer was worn away. The wear behaviour through the nitrided diffusion layers was determined by the hardness variations of nitrided pins.

6. The wear rate at each specific case depth from the wear-

face of the pins was of the same order of magnitude for gas nitrided, plasma nitrided and nitrocarburized steels. Furthermore, a mild-to-severe wear transition was observed at the same load for each surface treated steel. Thus it was concluded that there was no significant difference between the surface treatments, apart from the wear behaviour through the surface layers. However, gas nitrided and plasma nitrided steels exhibited lower wear rates than a carburized-and-hardened steel because of the higher hardness and resistance to tempering.

7. The wear lives of gas nitrided and plasma nitrided surface layers were reduced by two orders of magnitude by increasing the applied load to cause a transition from the mild to severe wear regime. The life of a nitrocarburized surface layer was considerably shorter than those of gas nitrided and plasma nitrided layers owing to its shallow case depth.

Chapter 7: Suggestions for Further Work

It is clear from the work described in this thesis that further investigations can be made on the following specific topics.

1. It is well known that the characteristics of a nitrided steel are considerably influenced by the treatment time, temperature, process atmosphere and steel composition. In particular, these factors influence the hardness profile of the surface layer (i.e. peak hardness and case depth), which in turn has a significant effect on the wear behaviour. Although the relationships between process parameters and metallurgical properties of nitrided steels have been well established [8,15,16,20], only a few studies have been reported about the effect of process parameters on wear[58,63,162]. Thus the relationships between process parameters and wear behaviour are not completely understood. The present study suggests that the hardness of a surface layer will play the most important role in the wear process. Therefore it would be very interesting to study the wear behaviour of nitrided steels with different hardness profiles, which could be produced by varying the process parameters and steel compositions.

2. A surface compound layer is strongly affected by the nitriding method, process parameters and steel

composition, in terms of its thickness, porosity and composition. Although the present study has confirmed that a thick and porous ϵ-Fe_3N layer has poor dry sliding wear performance, a thin nitrocarburized ϵ-Fe_3N appears to prevent adhesive wear at the initial stage of sliding. Thus it is clear that a further study is required to establish the optimum process condition for compound layer formation in order to improve the wear properties of this layer.

3. A wear mechanism map for a gas nitrided steel has been produced for the first time, and a wear mapping approach is very useful to understand and predict the wear behaviour over a wide range of operating conditions. Therefore, this approach should be extended to establish wear maps for plasma nitrided and nitrocarburized steels, and also other surface treated materials. The comparison of these wear maps will be very helpful for designers and engineers to make the best use of surface treatments in wear applications

4. Although the present work has focused on dry sliding wear only, engineering components encounter many types of wear; e.g. abrasive and fatigue wear. For instance, gears, in which a nitriding process is often used to improve the surface mechanical properties, operate in a high pressure rolling-sliding situation. Thus rolling wear of nitrided steels should be also investigated. In addition, most tribological

components, for example, engine parts, are operated in a lubricated system. Accordingly, studies of the lubricated wear behaviour of nitrided steels are also important. It would be of particular interest to investigate the interaction of a lubricant with a nitrided compound layer, because this layer has some porosity at the surface.

Acknowledgements

I would like to thank Dr.T.Eyre and Prof.B.Ralph for the valuable discussions and supervision of this work.

I would also like to acknowledge the help and cooperation of Mr.K.Dutta and the technical staff in Materials Technology and Experimental Techniques Centre at Brunel University.

I would like to express my appreciation to Senior Heat Treatment Ltd and Nitriding Services Ltd for providing the surface treated specimens used in this investigation.

I also gratefully acknowledge the provision of the financial support by Komatsu Ltd in Japan throughout the period of this work.

Finally I would like to thank Mrs.Tomoko Kato for her encouragement and typing of the thesis.

References

1. T.S.Eyre, Friction and wear control in industry, Met.Mater., 7, 1991, 143-148

2. D.Tabor, Wear - a critical synoptic view, Trans.ASME, J.Lubr.Tech., 99, 1977, 387-395

3. H.Czichos, Failure criteria in thin film lubrication - the concept of a failure surface, Tribology Int., 8, 1974, 14-20

4. C.Lipson, "Wear consideration in design", Prentice-Hall, 1967

5. A.R.Lansdown and A.L.Price, "Materials to resist wear, a guide to their selection and use", Pergamon Press, 1986

6. M.Donovan and J.L.Sanders, Surface coatings, 1- Introduction, Tribology Int., 5, 1972, 205-206

7. R.F.Smart, Selection of surfacing treatments, Tribology Int., 11, 1978, 97-104

8. International Research Development, "Wear resistant surfaces in engineering", HMSO, 1986

9. T.S.Eyre, The mechanisms of wear, Tribology Int., 11, 1978, 91-96

10. D.H.James, R.G.Smart and J.A.Reynolds, Surface treatments in engine component technology, Wear, 34, 1975, 373-382

11. T.Bell, Surface engineering: past, present and future, Surf.Eng., 6, 1990, 31-40

12. R.W.Wilson, Surface treatments to combat wear, Proc.1st. Euro.Tribol.Conf., Inst.Mech.Eng., London, 1973

13. T.Bell, Surface heat-treatment of steel to combat wear, Metallurgia, 49, 1982, 103-111

14. A.Fry, The theory and practice of nitrogen case-hardening, J.Iron and Steel Inst., 125, 1932, 191-212

15. K.E.Thelning, "Steel and its heat treatment", Butterworths, 1984

16. H.C.Child, "Surface hardening of steel, Engineering design Guides No.37", Oxford Univ. Press., 1980

17. M.Hansen, "Constitution of binary alloys", McGraw-Hill, 1958

18. K.H.Jack, Nitriding, Heat Treatment '73, 39-50, The Metals Society, 1973

19. BS 6479, "Determination and verification of the effective depth of carburized and hardened cases in steels", 1984

20. ASM, "Metal Handbook Vol.2, Heat treatment, Cleaning and Finishing", Metals Park, 1964

21. T.Bell, B.J.Birch, V.Korotchenko, and S.P.Evans, Controlled nitriding in ammonia-hydrogen mixtures, Heat Treatment '73, 51-57 The Metals Society, 1973

22. D.B.Clayton and K.Sachs, Reduction of 'white layer' on the surface of nitrided components, Heat Treatment '76, 1-6, The Metals Society, 1976

23. C.K.Jones, S.W.Martin, D.J.Sturges and M.Hudis, Ion nitriding, Heat Treatment '73, 71-77, The Metals Society, 1973

24. A.Roelandt, J.Elwart, and W.Rembges, Plasma nitriding of gear wheels in mass production, Surf.Eng., 1, 1985, 187-191

25. W.Rembges, Ion nitriding application grow for automotive components, Heat Treating, (3), 1990

26. B.Edenhofer and T.J.Bewley, Low-temperature ion nitriding: nitriding at temperatures below 500°C for tools and precision machine parts, Heat Treatment '76, 7-13, The Metals Society

27. Z.L.Zhang and T.Bell, Structure and corrosion resistance of plasma nitrided stainless steel, Surf.Eng., 1, 1985, 131-136

28. E.Rolinski, Effect of plasma nitriding temperature on surface properties of austenitic stainless steel, Surf.Eng., 3, 1987, 35-40

29. W.Rembges, Plasma nitriding of PM parts, Metal Powder report, Vol.43, No.11, 1988

30. A.M.Staines and T.Bell, Technological importance of plasma-induced nitrided and carburized layers on steel, Thin Solid films, 86, 1981, 201-211

31. F.Hombeck and T.Bell, Environmentally harmless plasma thermochemical process, Surf.Eng., 7, 1991, 45-52

32. J.Slycke and L.Sproge, Kinetics of the gaseous nitrocarburizing process, Surf.Eng., 5, 1989, 125-140

33. J.C.Gregory, Chemical conversion coating of metals to resist scuffing and wear, Tribology Int., 11, 1978, 105-112

34. T.Bell, Ferritic nitrocarburizing, Heat Treat.Met., 1975, (2), 39-49

35. A.Wells, Metallographic analysis of compound layers on ferritic nitrocarburized plain low carbon steel, J.Mater.Sci.,20, 1985, 2439-2445

36. P.Astley, Liquid nitriding: development and present applications, Heat Treatment '73, 93-97, The Metals Society, 1973

37. F.D.Waterfall, Reducing scuffing and wear of ferrous metals, Engineering, 187, 1959, 116-120

38. A.Gaucher, G.Guilhot and C.Amsallem, Surface treatment for iron and steel: Improving the resistance to scuffing, wear and fatigue by treatment in a non-polluting salt bath, Tribology Int., 9, 1976, 131-137

39. T.Bell and S.Y.Lee, Gaseous atmospheric nitrocarburizing, Heat Treatment '73, 99-107, The Metals Society, 1973

40. C.Dawes, D.F.Tranter, and R.W.Reynoldson, Sub-atmospheric oxynitrocarburizing, Heat Treatment '73, 109-120, The Metals society, 1973

41. A.Wells and T.Bell, Structure control of the compound layers formed during ferritic nitrocarburizing in methanol/ammonia atmospheres, Heat Treat.Met., 1983, (2), 39-44

42. C.Dawes, D.F.Tranter, and C.G.Smith, Reappraisal of nitrocarburizing and nitriding when applied to design and manufacture on non-alloy steel automobile components, Heat Treatment '79, 60-68, The Metals Society, 1979

43. S.E.Vanes, The Nitrotec surface treatment process, Met.Mater., 1985, 238-243

44. C.Dawes and D.F.Tranter, Nitrotec surface treatment technology, Heat Treat.Met., 1985, (3), 70-76

45. D.H.Jack and K.H.Jack, Invited review; Carbides and nitrides in steel, Mater.Sci.Eng., 11, 1973, 1-27

46. H.C.F.Rozendaal, P.F.Colijin and E.J.Millemeijer, Morphology, composition and residual stresses of compound layers of nitrocarburized iron and steels, Surf.Eng., 1, 1985, 30-42

47. K.Schwerdtfeger, P.Grieveson and E.T.Turkdogan, Growth rate of Fe_4N on alpha iron in NH_3-H_2 gas mixtures: Self-diffusivity of nitrogen, Trans.Met.Soc.AIME, 245, 1969, 2461-2466

48. A.Marciniak, Equilibrium and non-equilibrium models of layer formation during plasma and gas nitriding, Surf.Eng., 1, 1985, 283-288

49. A.Wells and I.le R.Strydom, Influence of sputtering and deposition on compound layer growth during plasma nitriding, Surf.Eng., 4, 1988, 55-59

50. B.J.Lightfoot and D.H.Jack, Kinetics of nitriding with and without white-layer formation, Heat Treatment '73, 59-65, The Metals Society, 1973

51. H.C.F.Rozendaal, E.J.Mittemeijer, R.F.Colijin and P.J.Van Der Schaaf, The development of nitrogen concentration profiles on nitriding iron, Metall.Trans., 14A, 1983, 395-399

52. P.M.Hekker, H.C.F.Rozendaal and E.J.Mittemeijer, Excess nitrogen and discontinuous precipitation in nitrided iron-chromium alloys, J.Mater.Sci., 20, 1985, 718-729

53. M.A.J.Somers and E.J.Mittemeijer, Formation and growth of compound layer on nitrocarburizing iron: kinetics and microstructural evolution, Surf.Eng., 5, 1989, 125-140

54. P.K.Williamson, Wear of low temperature nitrided steels under different wear process, Tribology Int., 13, 1980, 51-59

55. K.H.Habig, Wear protection of steels by boriding, vanadizing, nitriding, carburising and hardening, Mater.in Eng., 2, 1980, 83-92

56. A.Cohen and A.Rosen, The influence of the process on the dry wear resistance of 15-5 PH stainless steel, Wear, 108, 1986, 157-168

57. Q.F.Peng, Improving abrasion wear by surface treatment, Wear, 129, 1989, 195-203

58. T.Bell and Y.Sun, Load bearing capacity of plasma nitrided steel under rolling-sliding contact, Surf.Eng., 6, 1990, 133-139

59. C.Gleave and M.Farrow, Tribological investigation of compound layers formed by ferritic thermochemical diffusion treatment, Heat Treatment '81, 123-129, The Metals Society, 1981

60. T.Burakowski, J.Senatorski, and J.Tacikowski, Comparison of sliding wear resistance of carburized and nitrided layer on 18 HGT steel, Surf.Eng., 3, 1987, 239-245

61. G.W.Roper, Scuffing behaviour of salt-bath nitrided steel in loaded lubricated sliding/rolling contacts, Tribology Int., 15, 1982, 145-151

62. B.Wang, T.Ma and F.Zhang, Friction and wear behaviour of ion-sulpho-carbonitrided layers on low alloy steels, Wear, 125, 1988, 193-204

63. A.Wells and M.P.Shaw, An investigation into dry sliding wear behaviour of the ferritic nitrocarburized surface of a plain low carbon steel, Wear, 103, 1985, 29-42

64. M.B.Karamis, An investigation of the properties and wear behaviour of plasma-nitriding hot-working steel (H13), Wear, 150, 1991, 331-342

65. N.C.Welsh, The dry wear of steels, Phil.Trans.R.Soc. Lond., A, 257, 1965, 31-70

66. R.D.T.Whittle and V.D.Scott, Sliding-wear evaluation of nitrided austenitic alloys, Metals Tech., 11, 1984, 231-234

67. R.D.T.Whittle and V.D.Scott, Sliding-wear evaluation of Tufftrided austenitic alloys, Metals Tech., 11, 1984, 392-398

68. J.M.Cullen and A.Cameron, Wear properties of salt-bath carbonitrided steels, ASLE Trans., 25, 1982, 64-70

69. Research Group on Wear of Engineering Materials, "Terms and definitions in the field on lubrication, friction and wear-tribology", OECD Publication, 1969

70. J.T.Burwell, Survey of possible wear mechanisms, Wear, 1, 1957/58, 119-141

71. I.V.Kragelskii, M.N.Dobychin and V.S.Kombalov, "Friction and wear, calculation methods", Pergamon Press, 1982

72. J.F.Archard and W.Hirst, The wear of metals under unlubricated conditions, Proc.Roy.Soc.Lond., A, 236, 1956, 397-410

73. N.P.Suh, The delamination theory of wear, Wear, 25, 1973, 111-124

74. N.P.Suh, An overview of the delamination theory of wear, Wear, 44, 1977, 1-16

75. T.F.J.Quinn, Review of oxidational wear, Part 1: The origins of oxidational wear, Tribology Int., 16, 1983, 257-271

76. D.A.Rigney, "Fundamentals of friction and wear of materials", ASM, 1980

77. F.P.Bowden and D.Tabor, "The friction and lubrication of solids", Oxford Univ.Press., 1954

78. F.P.Bowden and D.Tabor, "The friction and lubrication of solids, Part 2", Oxford Univ.Press., 1964

79. J.T.Burwell and C.D.Strang, On the empirical law of adhesive wear, J.Appl.Phys., 23, 1952, 18-28

80. J.F.Archard, Contact and rubbing of flats surfaces, J.Appl.Phys., 24, 1953, 981-988

81. A.E.Roach, C.L.Goodzeit and R.P.Hunnicutt, Scoring characteristics of thirty-eight different elemental metals in high - speed sliding contact with steel, Trans.ASME, 78, 1956, 1659-1667

82. C.L.Goodzeit, R.P.Hunnicutt and A.E.Roach, Frictional characteristics and surface damage of thirty-nine different elemental metals in sliding contact with steel, Trans.ASME, 78, 1956, 1669-1676

83. E.Rabinowicz, The determination of the compatibility of metals through static friction tests, ASLE Trans., 14, 1971, 198-205

84. T.H.C.Childs, The sliding wear mechanisms of metals, mainly steels, Tribology Int., 13, 1980, 285-293

85. T.S.Eyre and D.Maynard, Running-in characteristics of graphitic cast iron, "Tribology Convention 1972", The Inst.Mech.Eng., 1972, 84-90

86. A.D.Sarkar, "Wear of metals", Pargamon Press, 1976

87. W.Hirst and J.K.Lancaster, Surface film formation and metallic wear, J.Appl.Phys., 27, 1956, 1057-1065

88. E.Rabinowicz, Wear, Mater.Sci.Eng., 25, 1976, 23-28

89. D.A.Rigney, Sliding wear of metals, Ann.Rev.Mater.Sci., 18, 1988, 141-163

90. D.H.Buckley, Adhesion of metals to a clean iron surface studied with LEED and Auger emission spectroscopy, Wear, 20, 1972, 89-103

91. E.Rabinowicz and D.Tabor, Metallic transfer between sliding metals; an autoradiographic study, Proc.Roy.Soc., A, 208, 1951, 455-475

92. M.Kerridge and J.K.Lancaster, The stages in a process of severe metallic wear, Proc.Roy.Soc., A, 236, 1956, 250-264

93. T.Sasada, S.Norose and H.Mishina, The behaviour of adhered fragments interposed between sliding surfaces and the formation process of wear particles, Trans.ASME, J.Lubr.Tech., 103, 1981, 195-202

94. P.Heilmann, J.Don, T.C.Sun and D.A.Rigney, Sliding wear and transfer, Wear, 91, 1983, 171-190

95. D.A.Rigney, L.H.Chen and M.G.S.Naylor, Wear processes in sliding systems, Wear, 100, 1984, 195-219

96. L.H.Chen and D.A.Rigney, Transfer during unlubricated sliding wear of selected metals systems, Wear, 105, 1985, 47-61

97. A.J.W.Moore, Deformation of metals in static and in sliding contact, Proc.Roy.Soc., A, 195, 1948, 231-244

98. M.Cocks, Interaction of sliding metals surfaces, J.Appl.Phys., 33, 1962, 2152-2161

99. M.Antler, Processes of metal transfer and wear, Wear, 7, 1964, 181-203

100. R.P.Steijn, Sliding wear and metal transfer under unlubricated conditions, Trans.ASME, J.Basic Eng., 81, 1959, 67-78

101. E.Rabinowicz, The effect of size on the looseness of wear fragments, Wear, 2, 1958, 4-8

102. M.Kerridge, Metal transfer and the wear process, Proc.Phys.Soc., B, 68, 1955, 400-407

103. N.Soda and T.Sasada, Mechanism of lubrication by surrounding gas molecules in adhesive wear, Trans.ASME, J.Lubr.Tech., 100, 1978, 492-500

104. E.Rabinowicz, Influence of surface energy on friction and wear phenomena, J.Appl.Phys., 32, 1961, 1440-1444

105. J.K.Lancaster, The formation of surface films at the transition between mild and severe metallic wear, Proc.Roy.Soc., A, 273, 1963, 466-483

106. T.F.J.Quinn, The effect of "Hot-Spot" temperatures on the unlubricated wear of steel, ASLE,Trans., 10, 1967, 158-168

107. T.F.J.Quinn, Oxidational wear, Wear, 18, 1971, 413-419

108. T.F.J.Quinn, D.M.Rowson and J.L.Sullivan, Application of the oxidation theory of mild wear to the sliding wear of low alloy steel, Wear, 65, 1980, 1-20

109. T.F.J.Quinn, J.L.Sullivan and D.M.Rowson, Origins and development of oxidational wear at low ambient temperatures, Wear, 94, 1984, 175-191

110. H.Mishina, Atmospheric characteristics in friction and wear of metals, Wear, 152, 1992, 99-110

111. J.Halling, "Principles of tribology", Macmillan Press., 1975

112. E.Rabinowicz, "Friction and wear of materials", J.Wiley, 1966

113. M.M.Khruschov, Resistance of metals to wear by abrasion as related to hardness, Proc.Conf.Lubr.Wear, 1957, Inst.Mech.Eng., 655-659

114. J.Larsen Badse, The abrasion resistance of some hardened and tempered Carbon steels, Trans.Met.Soc.AIME, 236, 1966, 1461-1466

115. R.C.D.Richardson, The maximum hardness of strained surfaces and the abrasive wear of metals and alloys, Wear, 10, 1967, 353-382

116. J.H.Tylczak, A study of the abrasive wear of pure metals using a pin-on drum apparatus, Wear, 135, 1990, 305-318

117. M.A.Moore, The relationship between the abrasive wear resistance, hardness and microstructure of ferritic materials, Wear, 28, 1974, 59-68

118. M.A.Moore, Abrasive wear, in "Fundamentals of friction and wear of materials", D.A.Rigney(ed), ASM, 1980, 73-118

119. I.M.Hutchings, "Tribology; Friction and wear of engineering materials", Edward Arnold, London, 1992

120. K.H.Z.Gahr, Relation between abrasive wear rate and the microstructure of metals, Wear of materials, 1979, 266-274

121. R.C.D.Richardson, The wear of metals by relatively soft abrasives, Wear, 11, 1968, 245-275

122. A.Misra and I.Finnie, On the size effect in abrasive and erosive wear, Wear, 65, 1981, 359-373

123. T.O.Hulhearn and L.E.Samuels, The abrasion of metals; A model of the process, Wear, 5, 1962, 478-498

124. M.J.Murray, P.J.Mutton and J.D.Watson, Abrasive wear mechanisms in steels, Wear of materials, 1979, 257-265

125. K.Hokkirigawa, K.Kato and Z.Z.Li, The effect of hardness on the transition of the abrasive wear mechanism of steels, Wear, 123, 1988, 241-251

126. Y.Kimura, The role of fatigue in sliding wear, in "Fundamentals of friction and wear of materials", D.A.Rigney(ed), ASM, 1980, 187-219

127. T.Kayaba and K.Kato, The analysis of adhesive wear mechanism by successive observations of the wear process in SEM, Wear of materials, 1979, 45-56

128. P.Heilmann and D.A.Rigney, Experimental evidence for fatigue during sliding wear, Metall.Trans., 12A, 1981, 686-688

129. D.A.Rigney and W.A.Glaeser, The significance of wear surface microstructure in the wear process, Wear, 46, 1978, 241-250

130. N.Soda, Y.Kimura and A.Tanaka, Wear of some fcc metals during unlubricated sliding, Part III; A mechanical aspect of wear, Wear, 40, 1976, 23-35

131. N.Soda, Y.Kimura and A.Tanaka, Wear of some fcc metals during unlubricated sliding, Part IV; Effects of atmospheric pressure on wear, Wear, 43, 1977, 165-174

132. S.C.Lim and M.F.Ashby, Wear mechanism maps, Acta Metall., 35, 1987, 1-24

133. S.C.Lim, M.F.Ashby and J.H.Brunton, Wear-rate transitions and their relationship to wear mechanisms, Acta Metall., 35, 1987, 1343-1348

134. E.A.Almond and M.G.Gee, Results from a U.K. interlaboratory project on dry sliding wear, Wear, 120, 1987, 101-116

135. A.W.Ruff, Comparison of standard test methods for non-lubricated sliding wear, Wear, 134, 1989, 49-57

136. D.Tabor, Friction and wear - developments over the last fifty years, Tribol.Frict.Lubr.Wear 50 years, 1987, Inst.Mech.Eng., 157-172

137. BS 5411, Part 6, "Methods of test for metallic and related coatings, Part 6, Vickers and Knoop microhardness tests", 1981

138. R.M.Farrell and T.S.Eyre, The relationship between load and sliding distance in the initiation of mild wear in steels, Wear, 15, 1970, 359-372

139. B.J.Taylar, Wear properties of plasma carburized steel, Surf.Eng., 1, 1985, 255-261

140. R.Wilson, Influence of oxide films on metallic friction, Proc.Roy.Soc., A, 212, 1952, 450-452

141. J.Morri, The physical metallurgy and wear properties of boronized iron-carbon alloys, Ph.D. thesis, Brunel University, 1982

142. R.Bowen, D.Scott, W.Seifert and V.C.Westcott, Ferrography, Tribology Int., 10, 1976, 109-115

143. T.Akagaki and K.Kato, Effects of additives on wear mode and morphology of wear debris generated in lubricated sliding of steels, Wear, 143, 1991, 119-135

144. D.Scott, Debris examination - a prognostic approach to failure prevention, Wear, 34, 1975, 15-22

145. A.D.Sarkar, The role of wear debris in the study of wear, Wear, 90, 1983, 39-47

146. V.Aronov, Kinetic characteristics of the transformation and failure of surface layers of metals under dry friction, Wear, 41, 1977, 205-212

147. T.F.J.Quinn, Dry wear of steel as revealed by electron microscopy and X-ray diffraction, Proc.Int.Mech.Eng., 182, 1967-1968, 201-213

148. A.W.Batchelor, G.W.Stachowiak and A.Cameron, The relationship between oxide films and the wear of steels, Wear, 113, 1986, 203-223

149. F.H.Scott and G.C.Wood, The influence of oxides on the friction and wear of alloys, Tribology Int., 11, 1978, 211-218

150. J.E.Wilson, F.H.Scott and G.C.Wood, The development of wear-protective oxides and their influence on sliding friction, Proc.Roy.Soc., A, 369, 1980, 557-574

151. K.Hiratuka and T.Sasada, Wear of metals in a magnetic field, Wear, 160, 1993, 119-123

152. K.Kumagai, K.Suzuki and O.Kamiya, Study on reduction in wear due to magnetization, Wear, 162-164, 1993, 196-201

153. D.H.Buckley, "Surface effects in adhesion, friction, wear and lubrication", Tribology Series 5, Elsevier, 1981

154. J.B.Pethica and D.Tabor, Contact of characterized metal surfaces at very low loads: deformation and adhesion, Surf.Sci., 89, 1979, 182-190

155. B.J.Griffiths, White layer formations at machined surfaces and their relationship to white layer formations at worn surfaces, Trans.ASME, J.Tribology, 107, 1985, 165-171

156. N.C.Welsh, Frictional heating and its influence on the wear of steel, J.Appl.Phys., 28, 1957, 960-968

157. J.F.Archard and R.A.Rowntree, Metallurgical phase transformation in rubbing of steels, Proc.Roy.Soc., A, 418, 1988, 405-425

158. R.Bulpett, T.S.Eyre and B.Ralph, The characterization of white layers formed on digger teeth, Wear, 162-164, 1993, 1059-1065

159. T.S.Eyre and A.Baxter, The formation of white layer at rubbing surfaces, Met.Mater., 6, 1972, 435-439

160. D.Scott, A.I.Smith, J.Tait and G.R.Tremain, Materials and metallurgical aspects of piston ring scuffing - a literature survey, Wear, 33, 1975, 293-315

161. B.J.Griffiths and D.C.Furze, Tribological advantages of white layers produced by machining, Trans.ASME, J.Tribology, 109, 1987, 338-342

162. M.B.Karamis, Tribological behaviour of plasma nitrided 722M24 material under dry sliding conditions, Wear, 147, 1990, 385-399

163. T.S.Eyre, Effect of boronizing on friction and wear of ferrous metals, Wear, 34, 1975, 383-397

164. T.S.Eyre, Selecting the optimum surface technique for wear resistance, Proc.2nd Int.Conf.Surf.Eng., 11-24, The Welding Inst., 1987

165. C.S.Syan, A.Matthews and K.G.Swift, Coating and treatment selection, Surf.Eng., 2, 1986, 249-255

166. T.Bell, Selected case studies in surface engineering - 1988, Conf.New Mat.Process Mech.Design, 1988, 37-51

Table 3.1 Chemical composition of steels (wt%)

steel	C	Si	Mn	Cr	Mo	Ni	Al
BS970, 905M39 (EN41B)	0.35-0.43	0.10-0.45	0.40-0.65	1.40-1.80	0.15-0.25	—	0.90-1.30
BS970, 635M15 (EN351)	0.12-0.18	0.10-0.45	0.60-0.90	0.40-0.80	—	0.70-1.10	—
BS970, 535A99 (EN31)	0.95-1.10	0.10-0.35	0.40-0.70	1.20-1.60	—	—	—

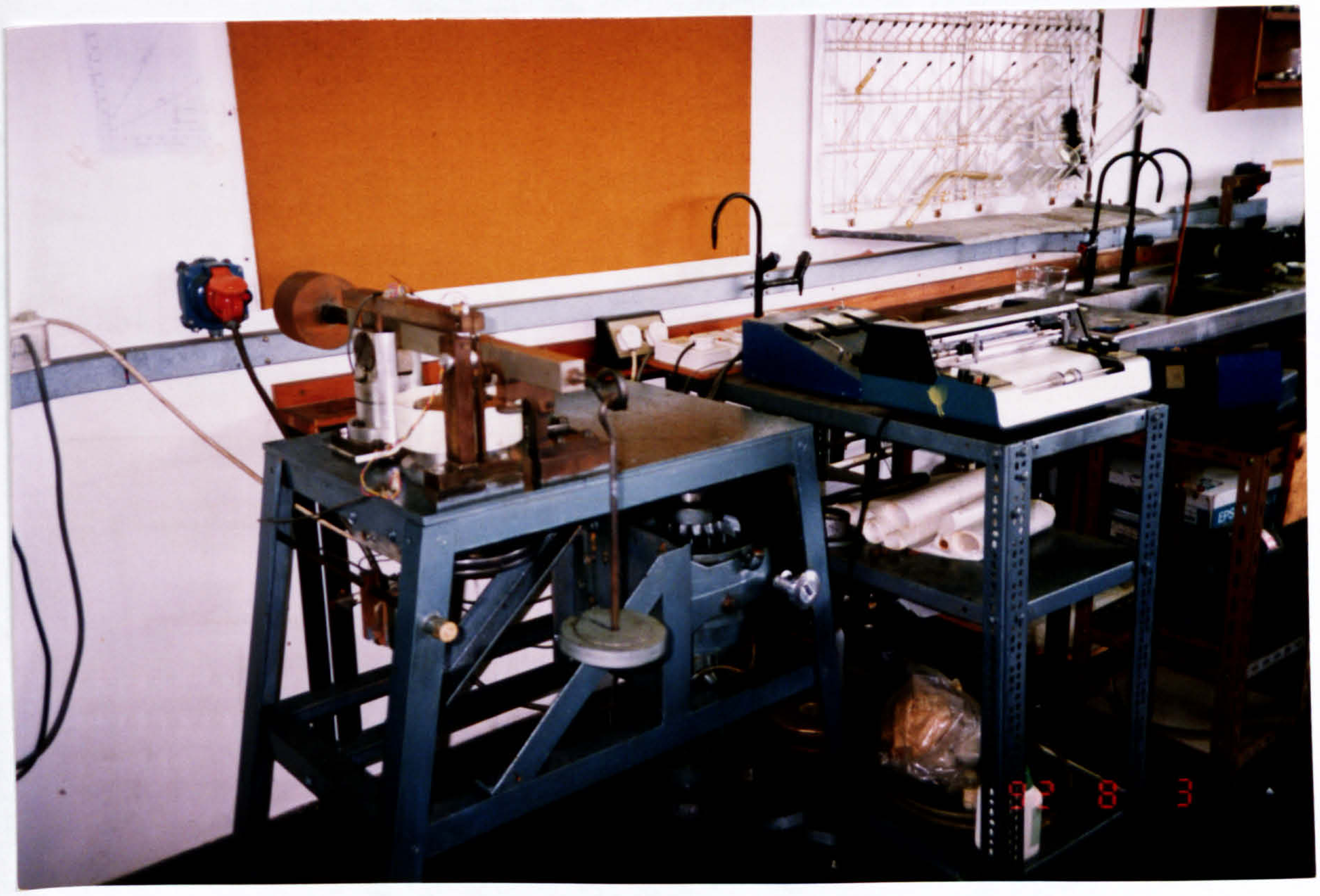

Fig.3.2 View of pin-on-disc wear testing arrangement

(a)Pin

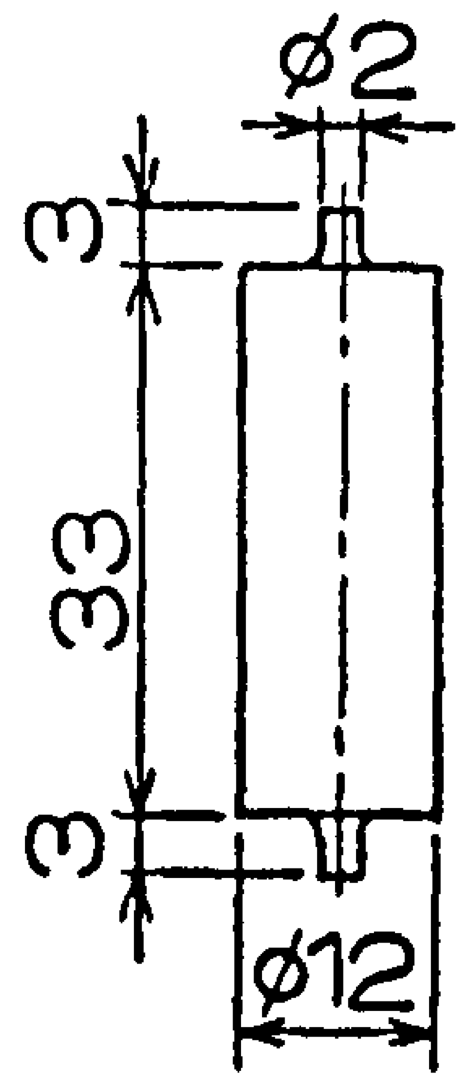

(b)Disc

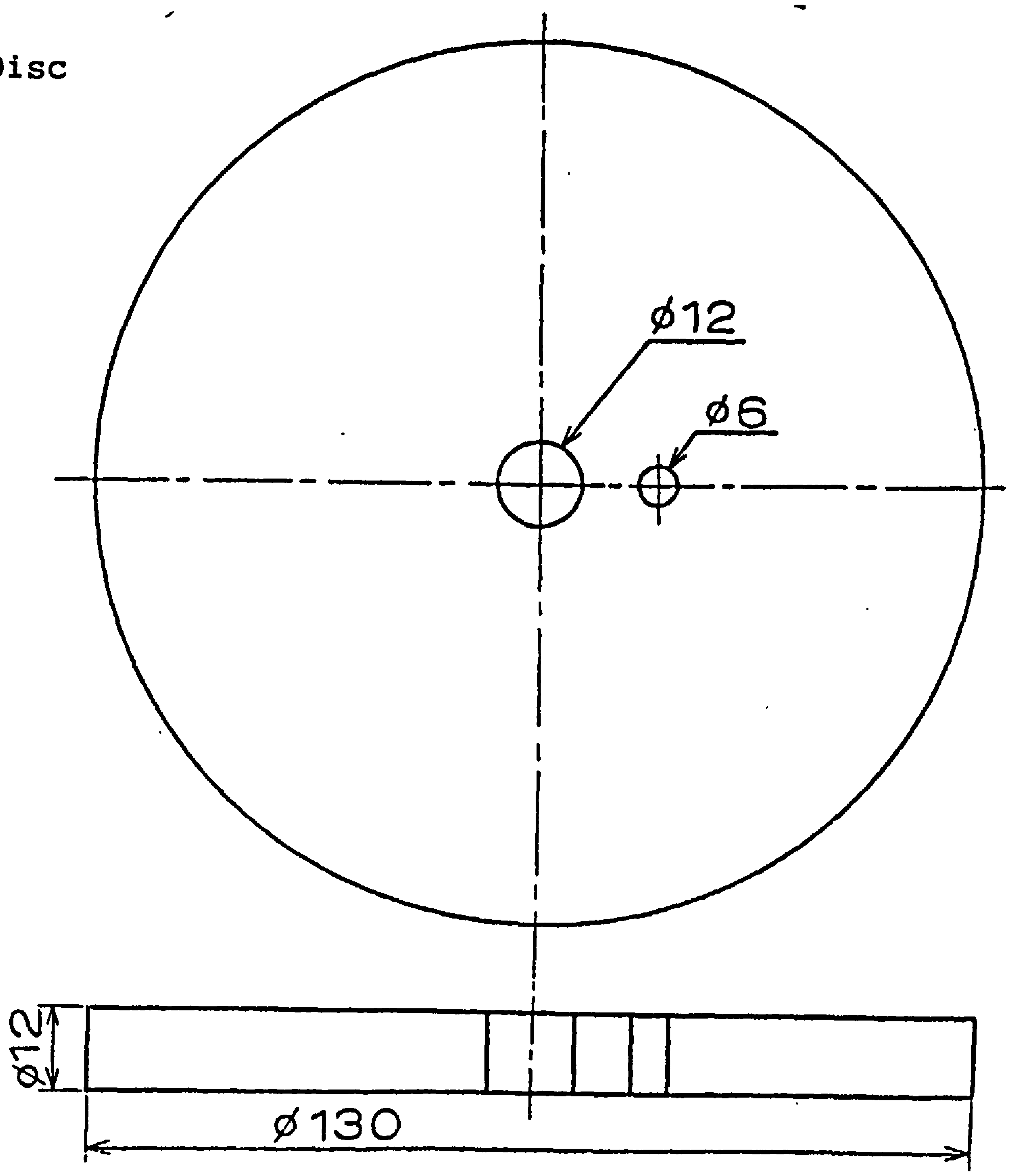

Fig.3.3 Schematic diagram of wear pin and disc

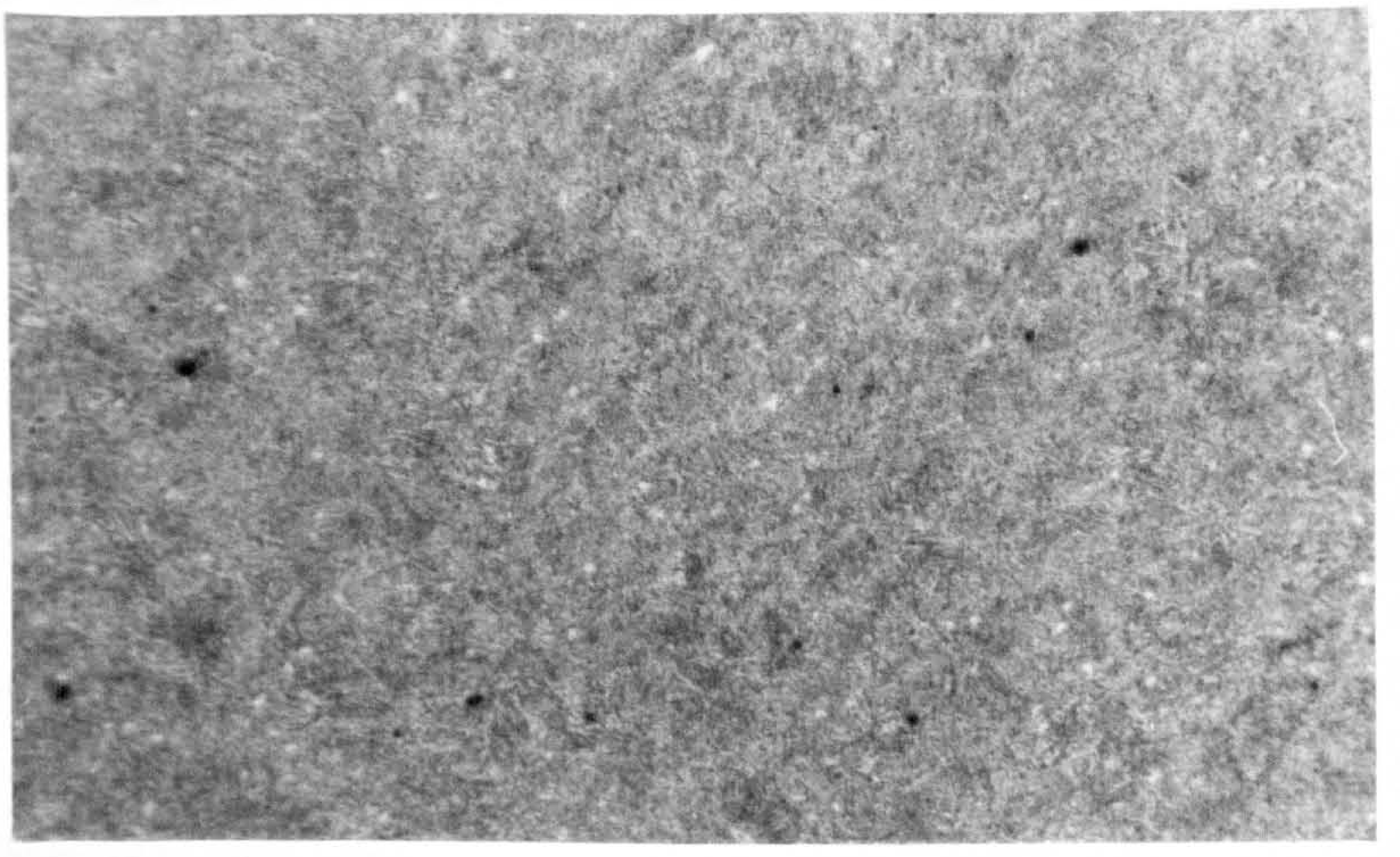

(a) 100µm

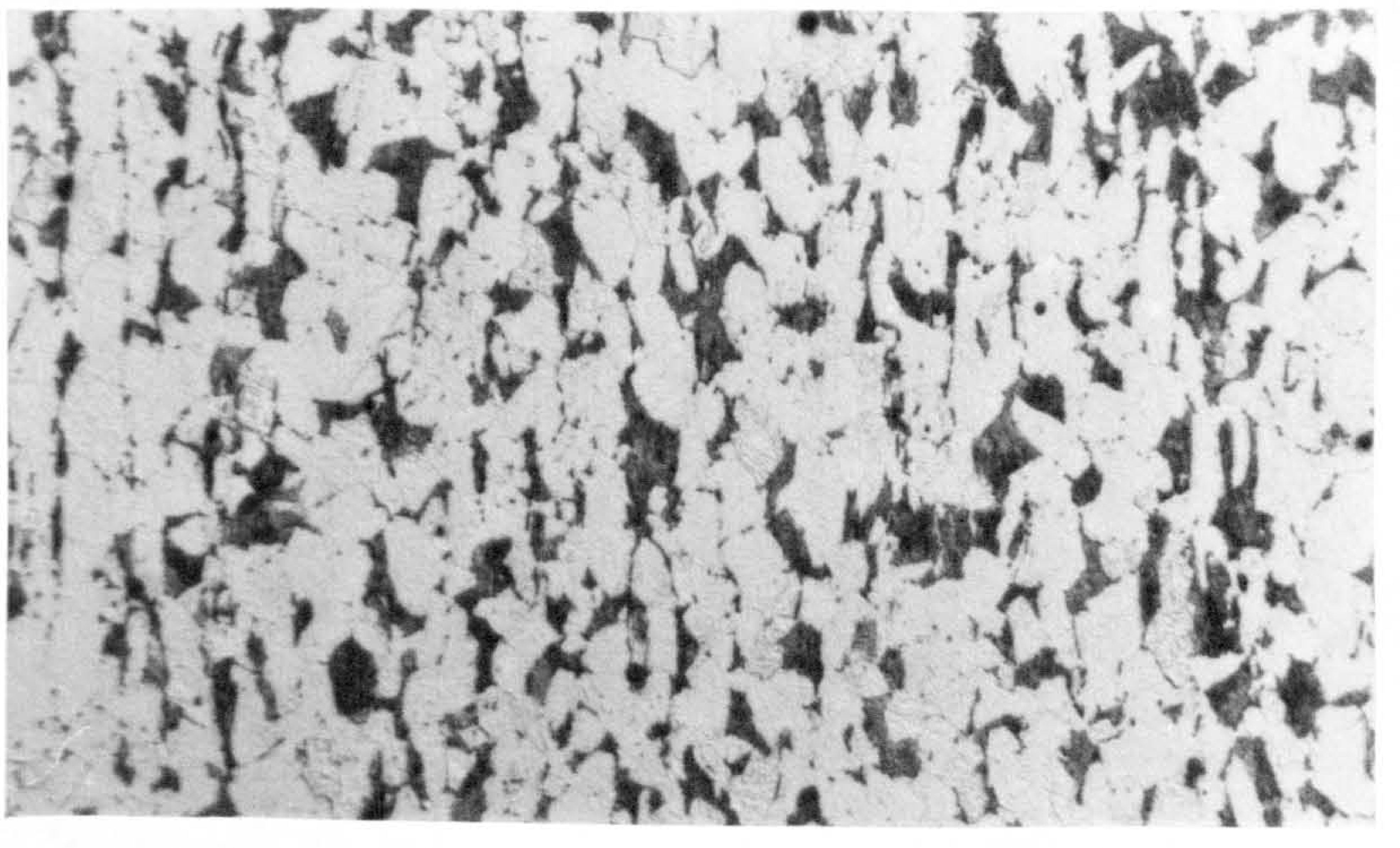

(b) 100µm

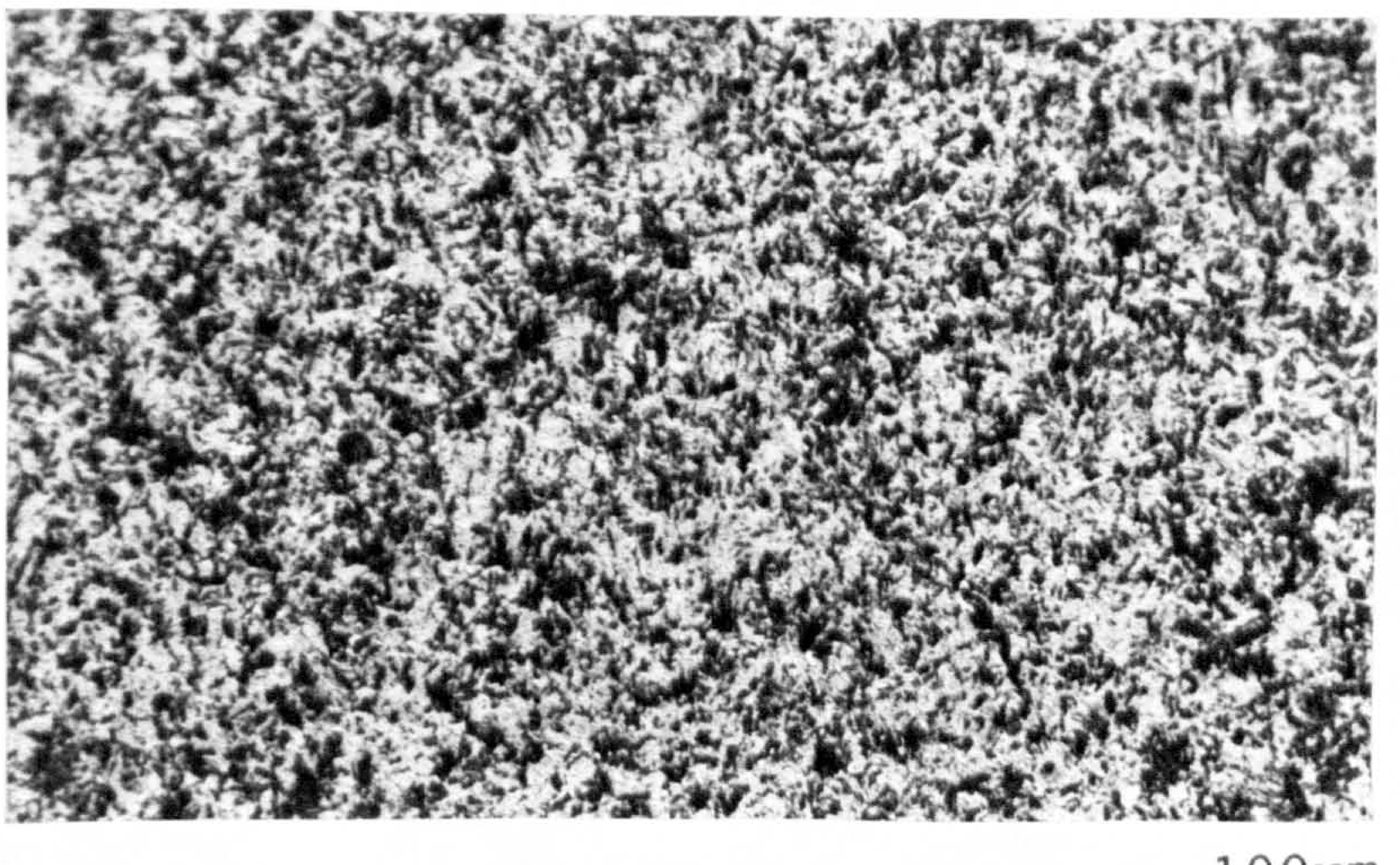

(c) 100µm

Fig.3.4 Microstructure of steels used in the present investigation

(a) as received BS970,905M39 (EN41B)

(b) as received BS970,635M15 (EN351)

(c) heat treated BS970,535A99 (EN31) used for wear disc

(a) Gas nitriding furnace

(b) Plasma nitriding furnace

Fig.3.5 View of nitriding furnace

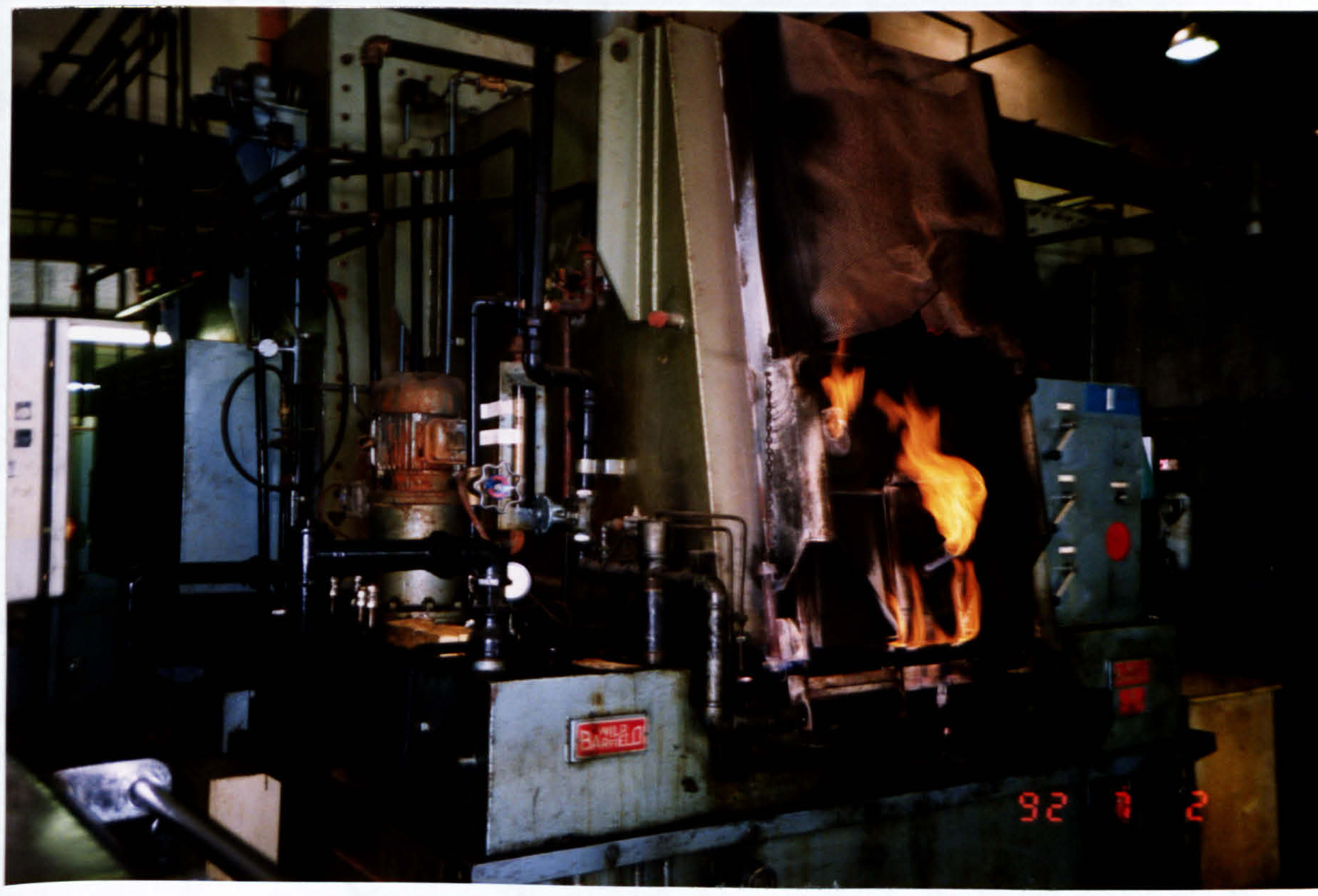

Fig.3.6 View of gas nitrocarburizing furnace

Table 4.1 Comparison of metallurgical characteristics of surface treated steels

	Gas nitrided steel<1>	Plasma nitrided steel<1>	Nitro-carburized steel<1>	Carburized and hardened steel<2>
Case depth (Hv 550)	0.42 mm	0.22 mm	0.05 mm	0.65 mm
Hardened layer depth	0.70 mm	0.50 mm	0.20 mm	1.40 mm
Hardness at 0.05 mm depth	Hv 1107	Hv 1171	Hv 540	Hv 746
Compound layer thickness	30 μm	2 μm	3 μm	____
Process temperature and time	520°C x 80H	530°C x 60H	570°C x 2.5H	920°C x 3H

<1> steel: BS970,905M39 (EN41B)
<2> steel: BS970,635M15 (EN351)

Table 4.2 Wear behaviour of untreated and surface treated steels at a sliding speed of 1 $m \cdot s^{-1}$

	T_1 transition load (N)	Wear rate ($mg \cdot m^{-1}$)	
		mild regime (10 N)	severe regime (80 N)
Untreated steel<1>	20	3.1×10^{-3}	6.6×10^{-2}
Gas nitrided steel<1>	60	3.9×10^{-4}	2.7×10^{-2}
Plasma nitrided steel<1>	60	2.1×10^{-4}	1.6×10^{-2}
Nitro-carburized steel<1>	—	6.8×10^{-4}	7.1×10^{-3}
Carburized and hardened steel<2>	60	3.9×10^{-4}	3.3×10^{-2}

<1> steel: BS970,905M39 (EN41B)
<2> steel: BS970,635M15 (EN351)

Table 5.1 Summary of wear characteristics of untreated and gas nitrided BS970,905M39 (EN41B)

(a) untreated steel

	Mild	Severe	Extremely-severe
Wear curve*	type-A and B	type-C and D	type-E
Wear rate ($mg \cdot m^{-1}$)	$10^{-4} \sim 10^{-2}$	$10^{-2} \sim 10^{-1}$	$1 \sim 10$
Pin	•smooth surface •no plastic deformation •patchy oxides	•plastic deformation •'white-etched' layer	•heavy plastic deformation •'white-etched' particles
Disc	•smooth surface •patchy oxides	•rough surface •tempered martensite	•transferred particles (white-etched)
Wear debris	•very fine (~ 1 μm) •oxidized (Fe_2O_3, Fe_3O_4)	•relatively-large (~ 50 μm) •metallic (Fe)	•very large (~ 1 mm) •metallic (Fe)

(b) gas nitrided steel

	Mild	Severe
Wear curve*	type-A and B	type-C
Wear rate ($mg \cdot m^{-1}$)	$10^{-4} \sim 10^{-2}$	$10^{-2} \sim 10^{-1}$
Pin	•smooth surface •no plastic deformation	•rough surface •'white-etched' layer
Disc	•smooth surface •patchy oxides •tempered martensite	•transferred particles •tempered martensite
Wear debris	•very fine (~ 0.5 μm) •oxidized (Fe_2O_3, Fe_3O_4)	•large (~ 200 μm) •metallic (Fe) and oxidized (FeO)

* Type-A: The wear rate is very low and constant throughout the duration of the test.
-B: Initially the wear rate is relatively high, but later decreased to a lower constant.
-C: The wear rate increased as the sliding distance increased.
-D: The wear rate is relatively high and constant throughout the duration of the test.
-E: The wear rate is very high throughout the duration of the test, which is fairly short.

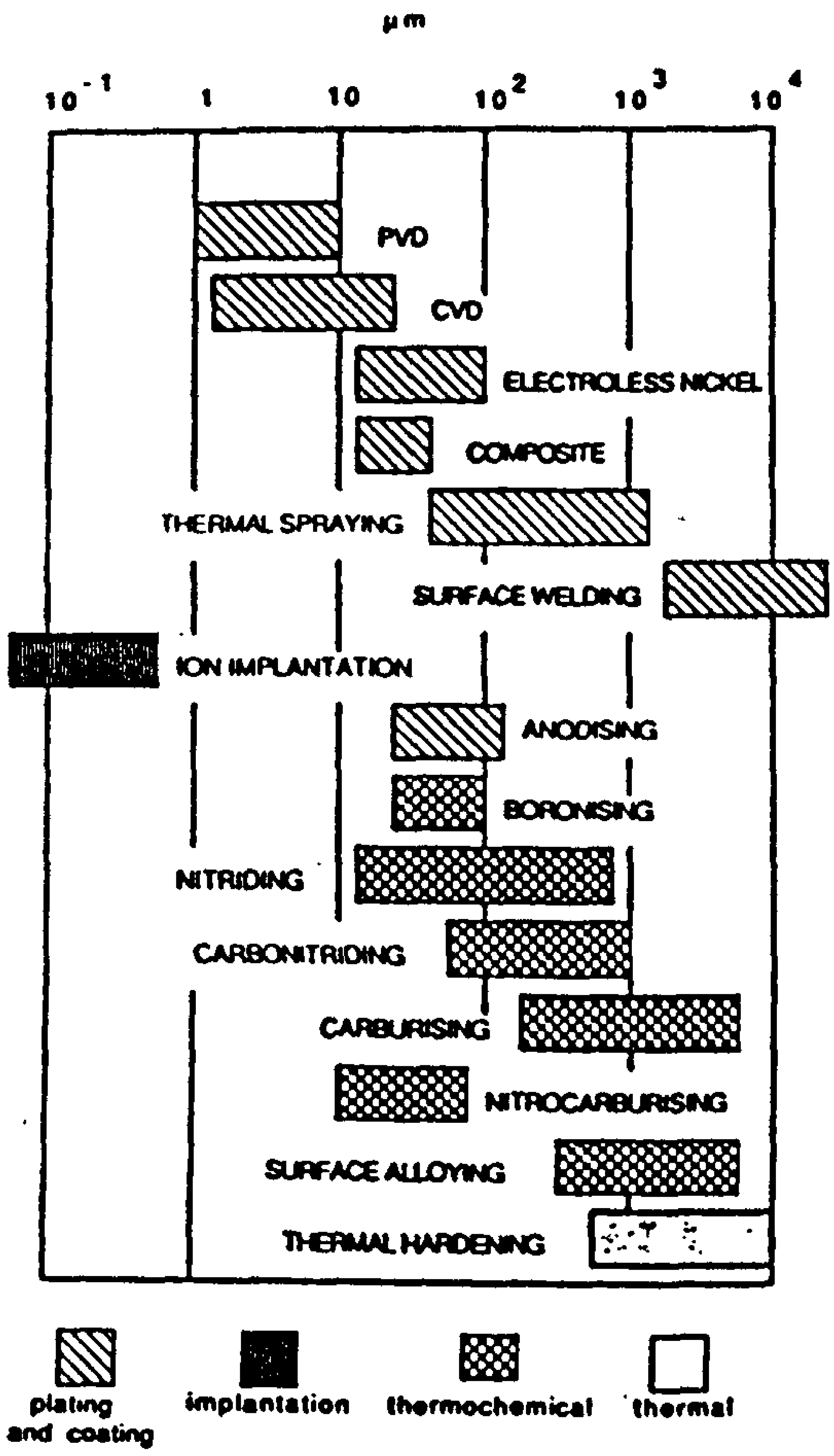

Fig.2.1 Classification of surface treatments and typical thicknesses of the surface layers [11].

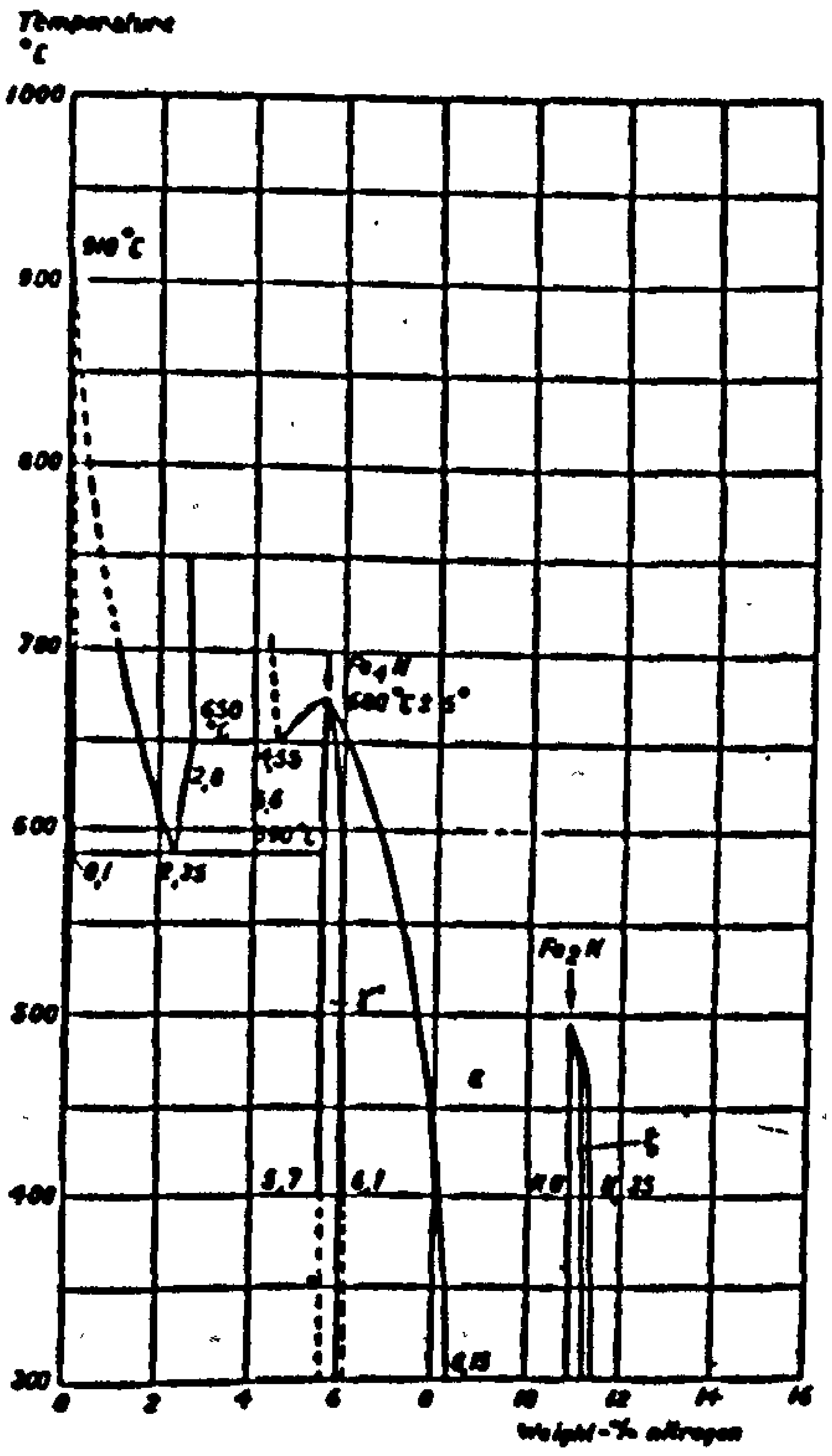

Fig.2.2 Equilibrium diagram for iron-nitrogen [17].

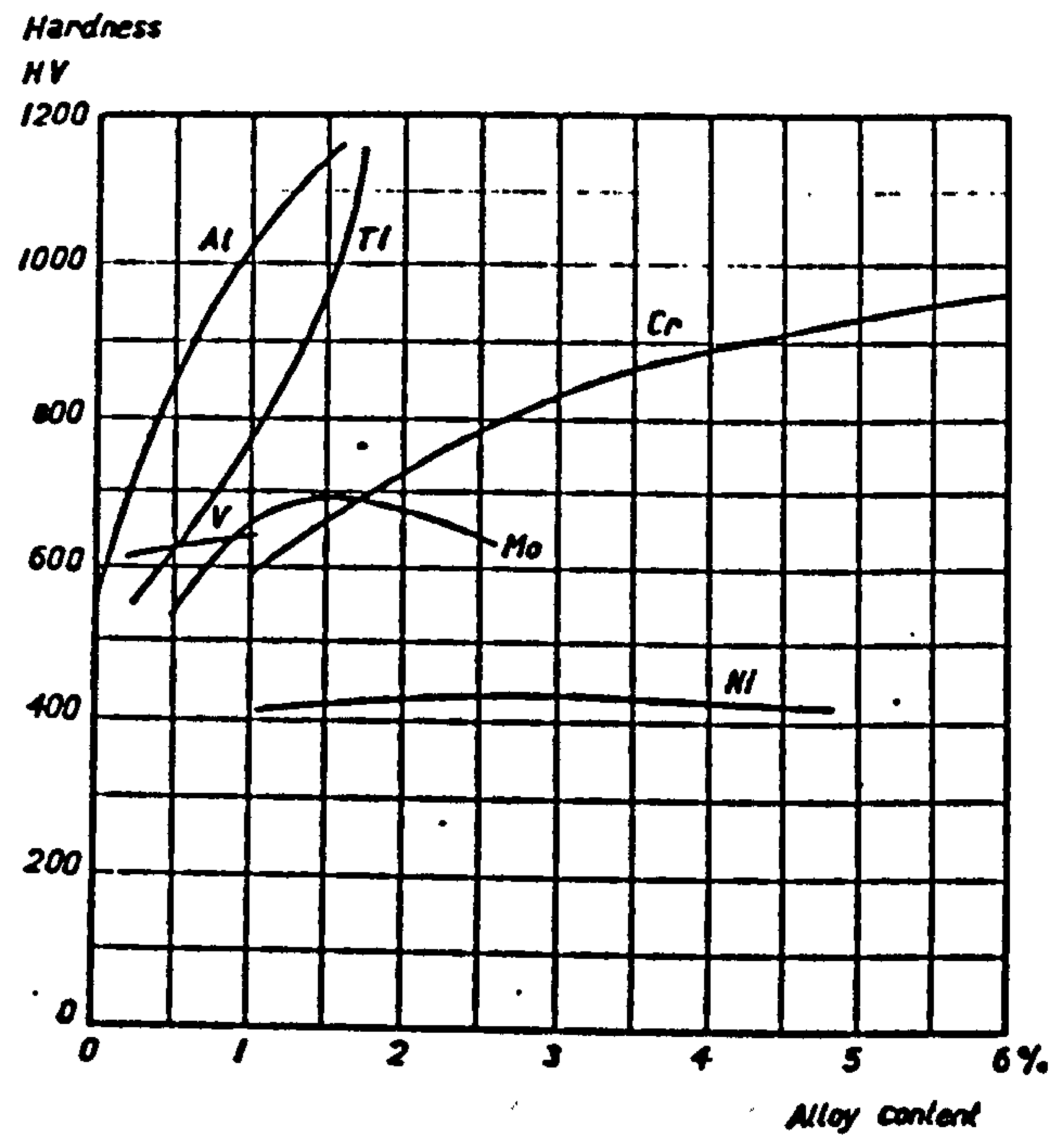

Fig.2.3 Influence of alloying elements on hardness after nitriding. Base alloy 0.35%C, 0.30%Si, 0.70%Mn [15].

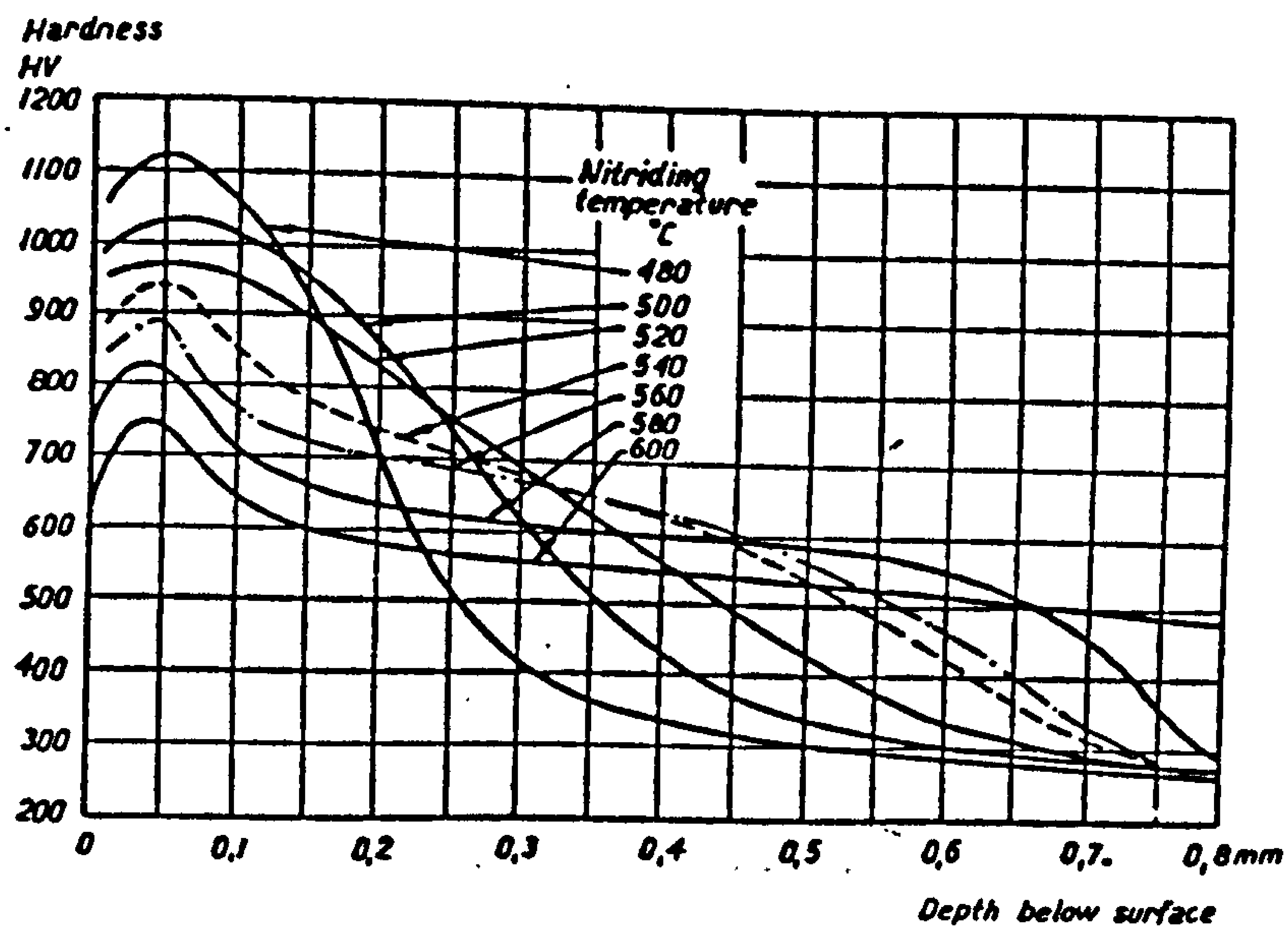

Fig.2.4 Influence of nitriding temperature on hardness and depth of nitriding of BS970.905M39 (EN41B) steel. Nitriding period 60h [15].

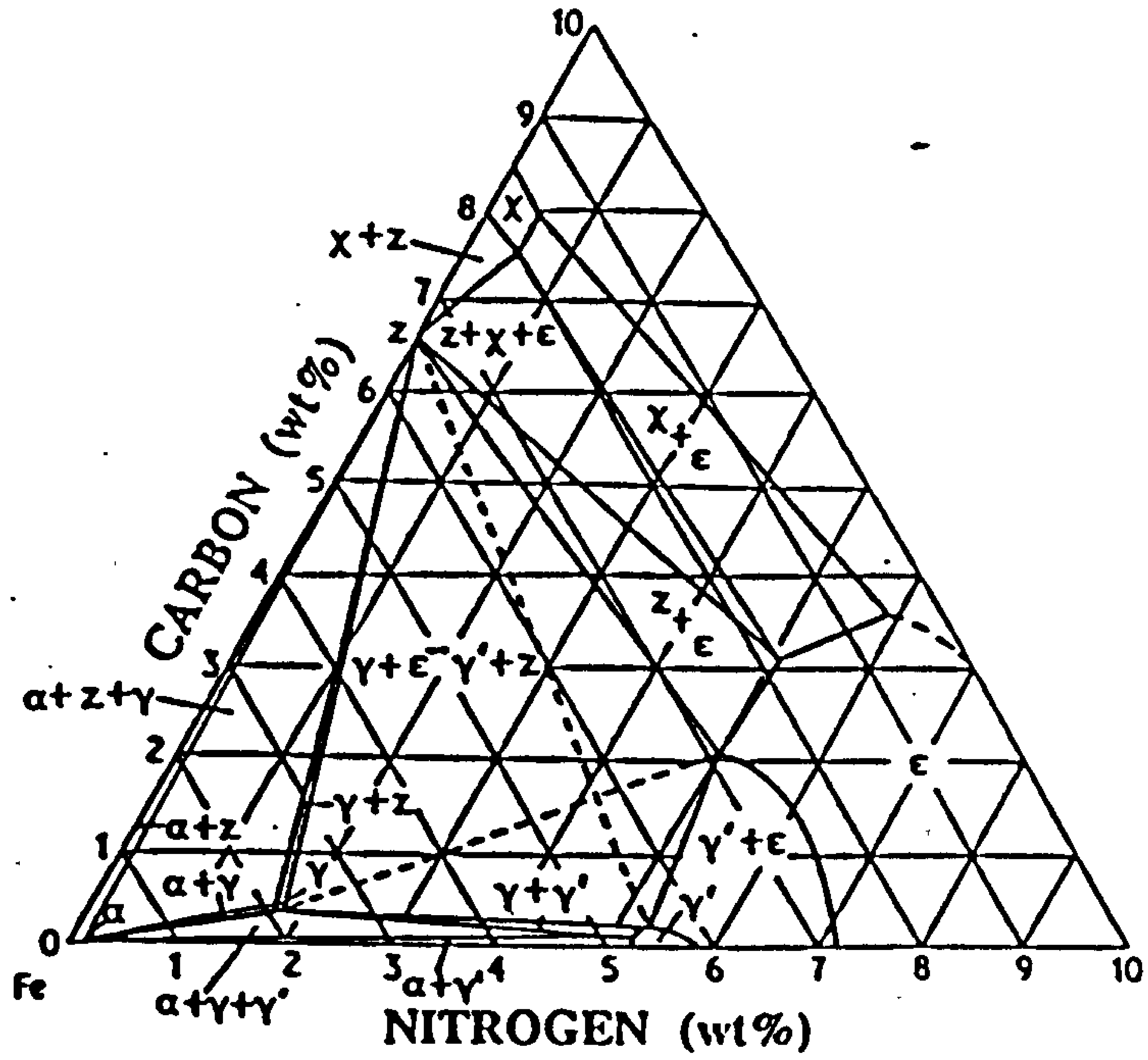

Fig.2.5 Isothermal section of iron-carbon-nitrogen system at 575°C [35].

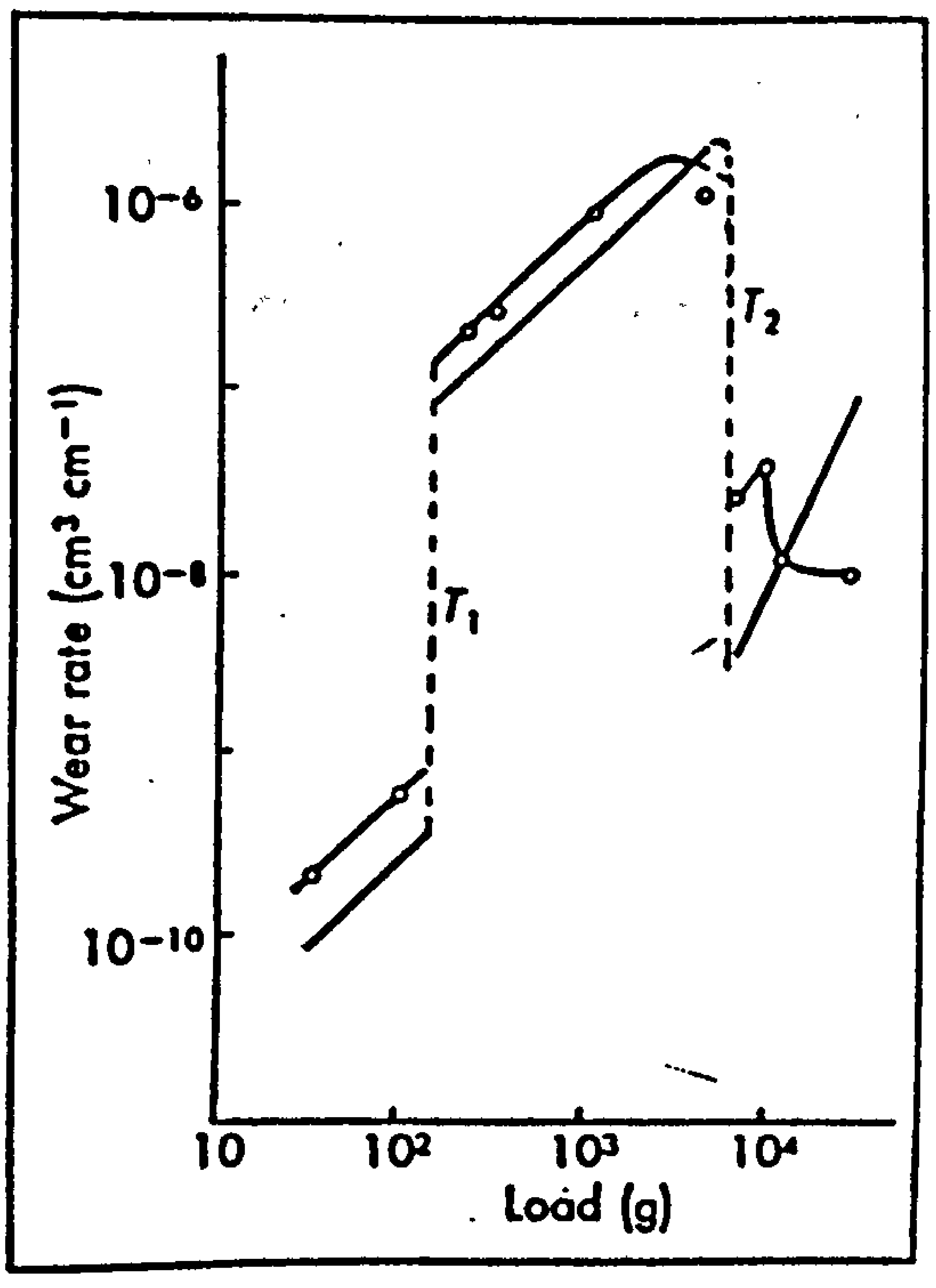

Fig.2.6 Transitional wear behaviour for a 0.52% carbon steel. Sliding speed 1 $m \cdot s^{-1}$ [65].

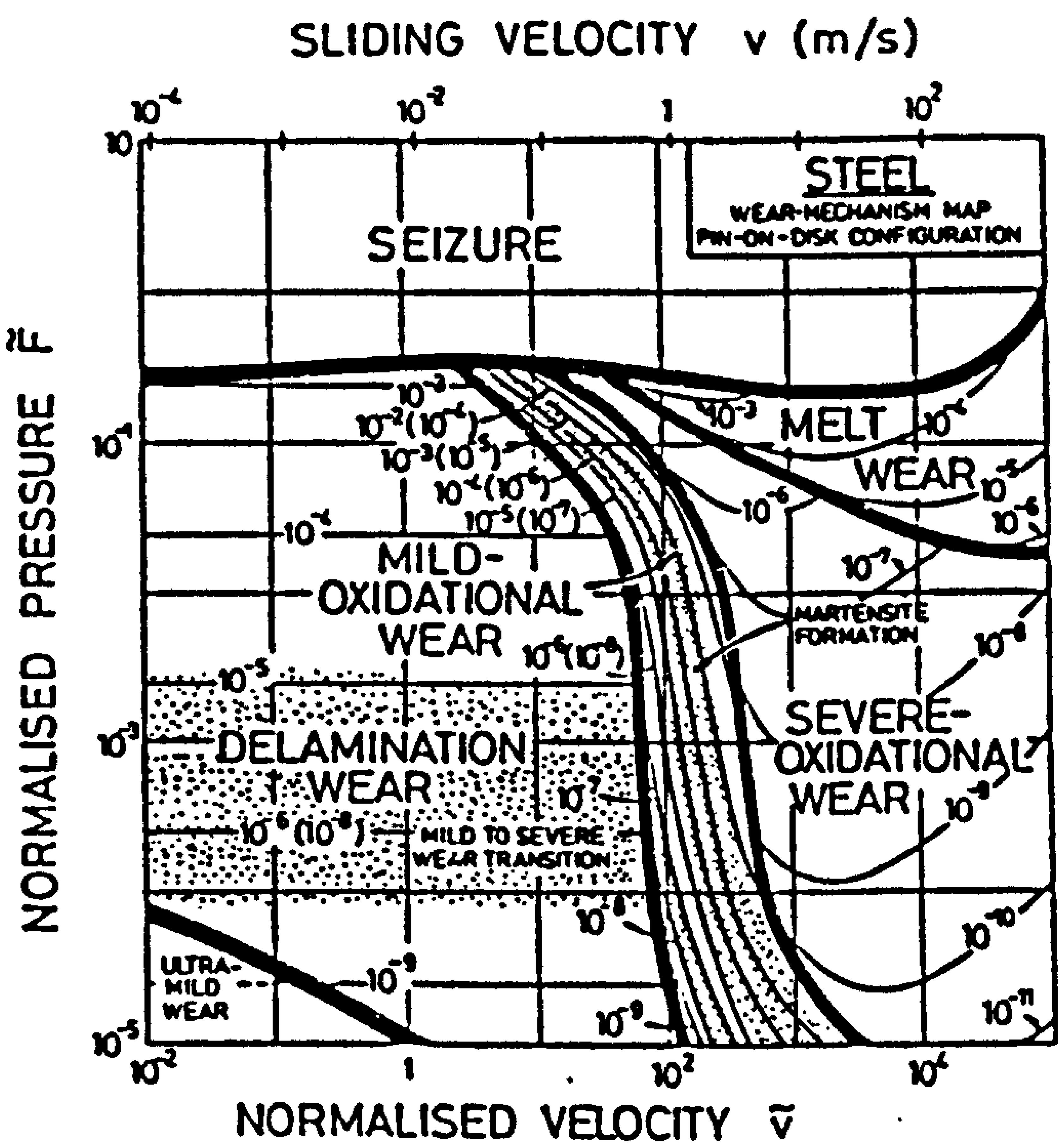

Fig.2.7 Wear mechanism map for a steel under unlubricated sliding conditions [132].

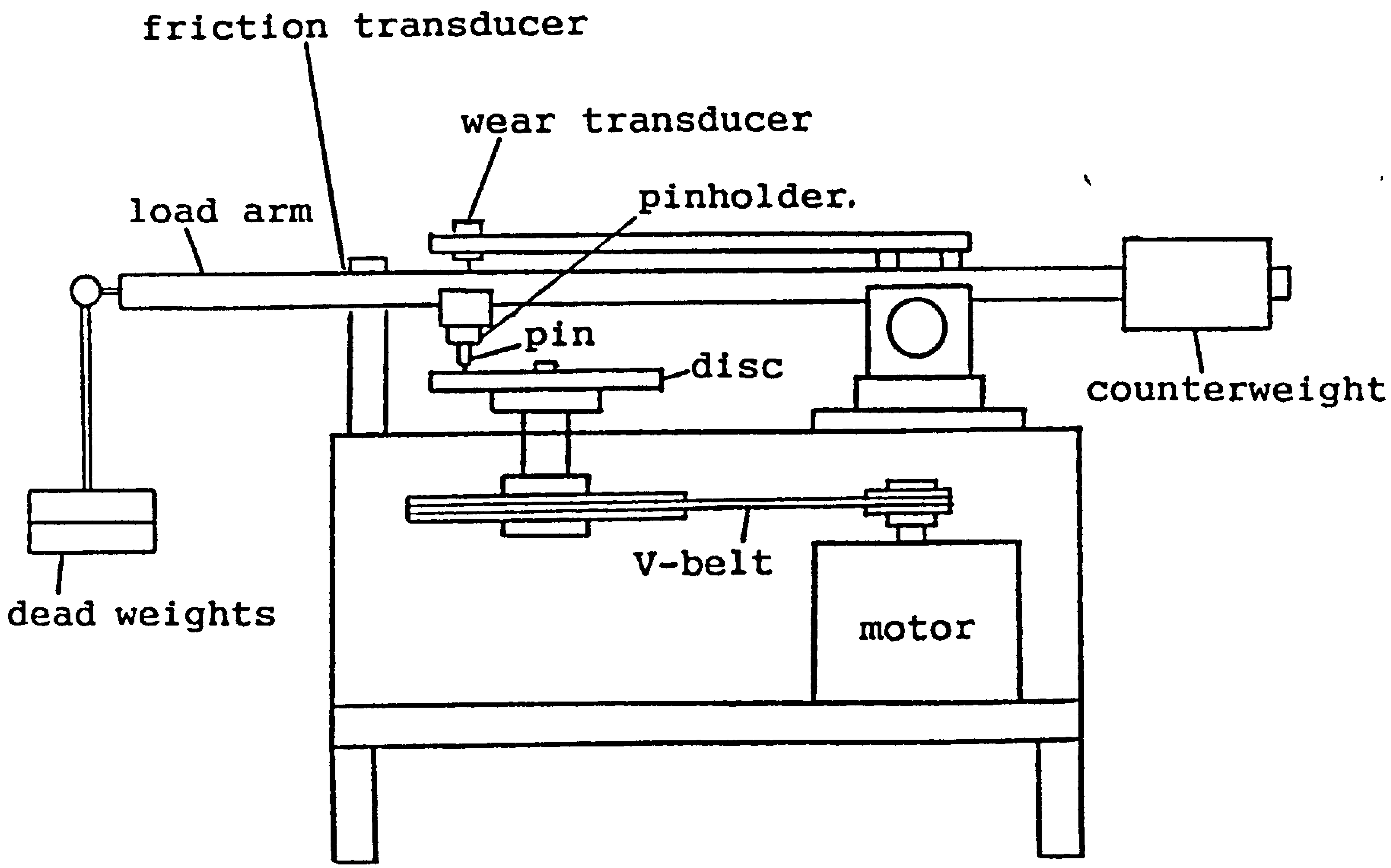

Fig.3.1 Schematic diagram of pin-on-disc wear machine

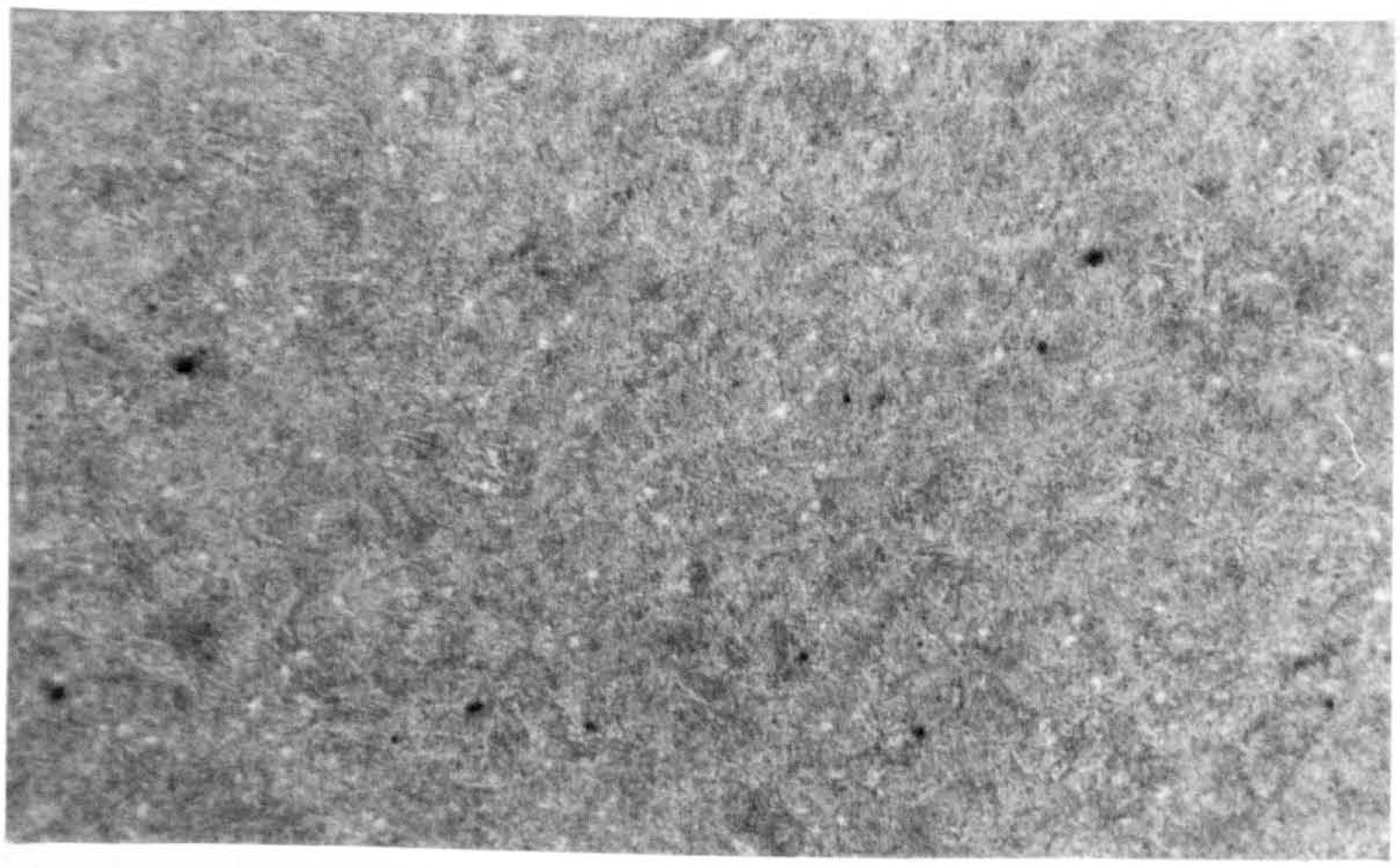

(a) 100μm

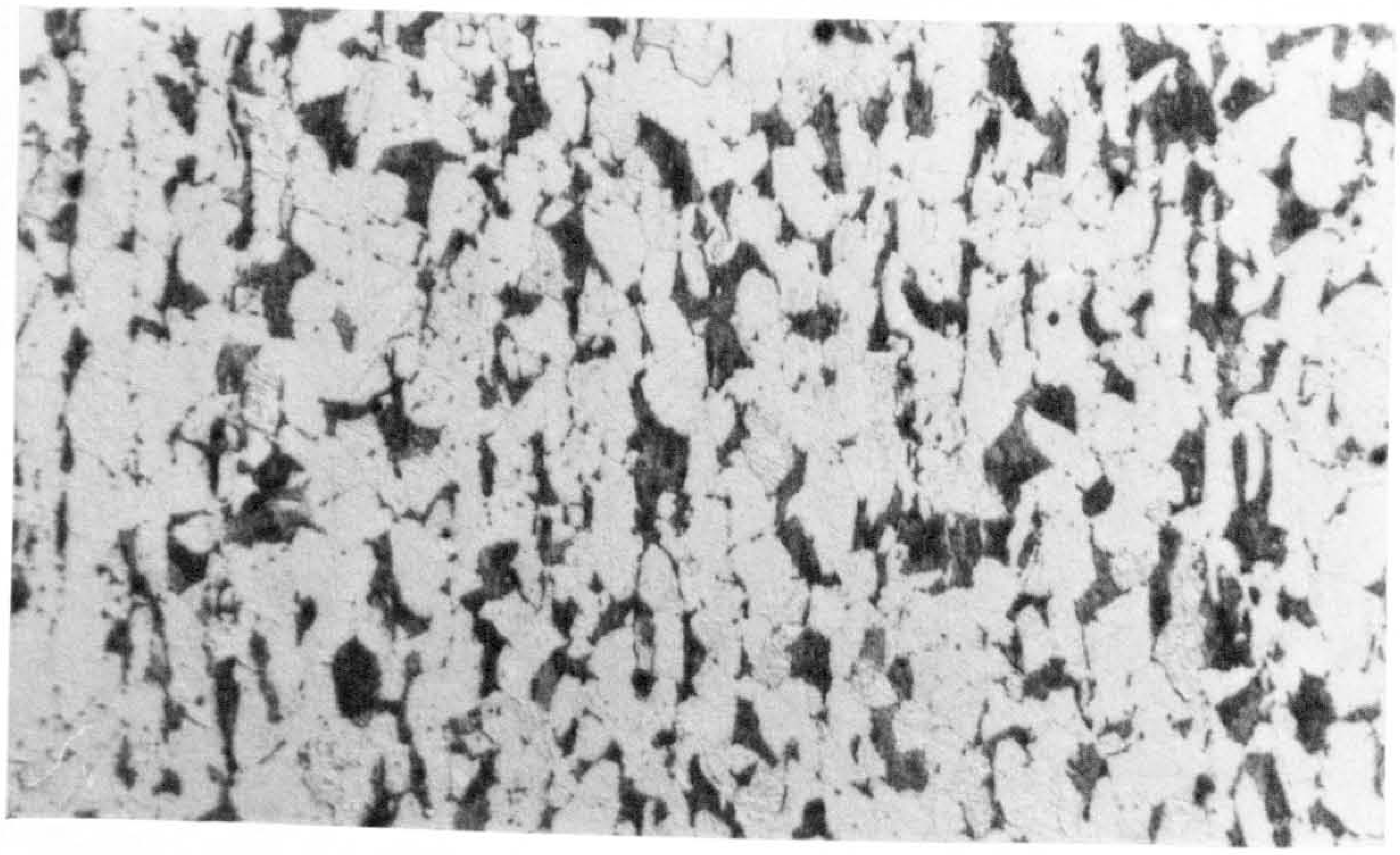

(b) 100μm

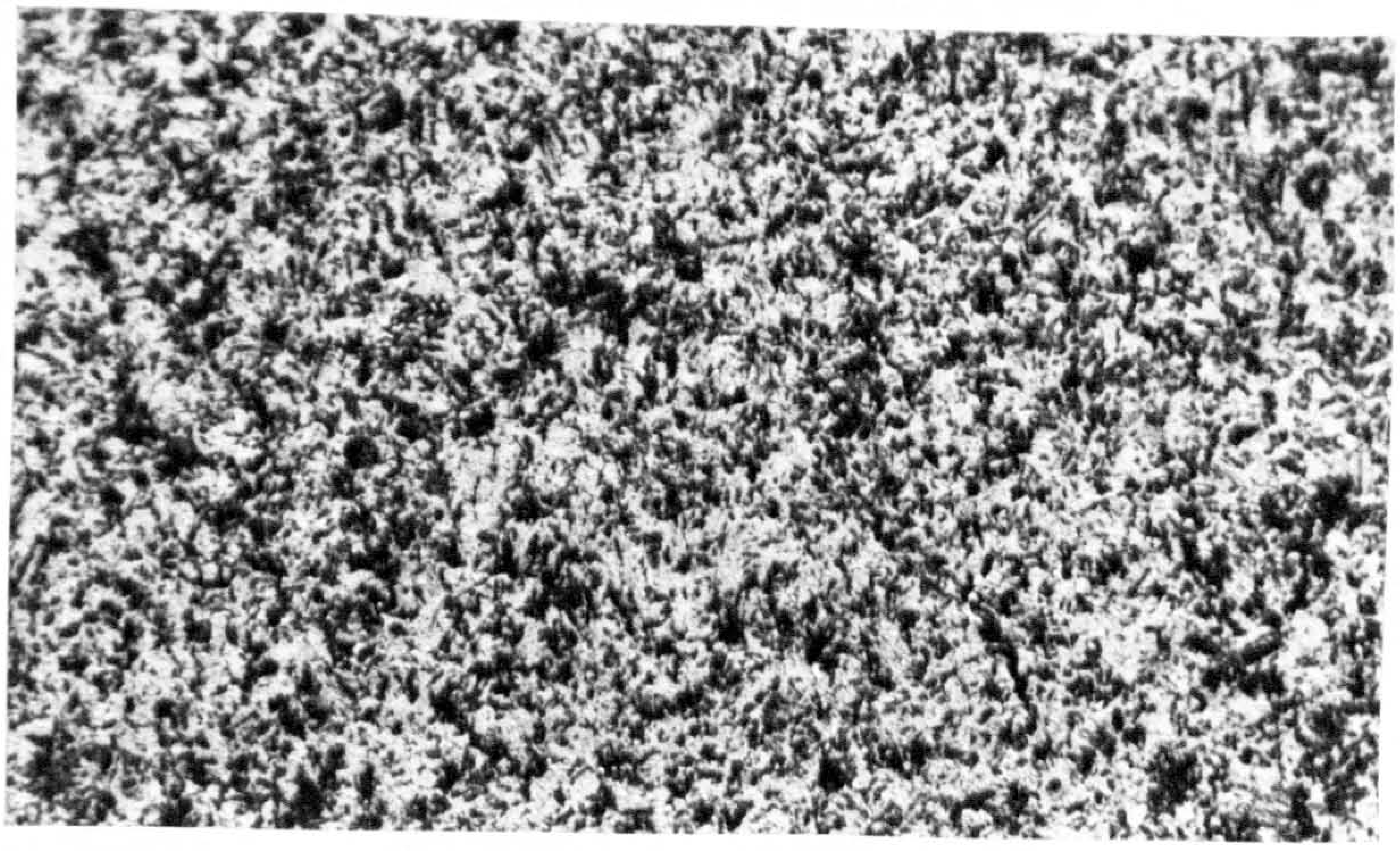

(c) 100μm

Fig.3.4 Microstructure of steels used in the present investigation
(a) as received BS970,905M39 (EN41B)
(b) as received BS970,635M15 (EN351)
(c) heat treated BS970,535A99 (EN31) used for wear disc

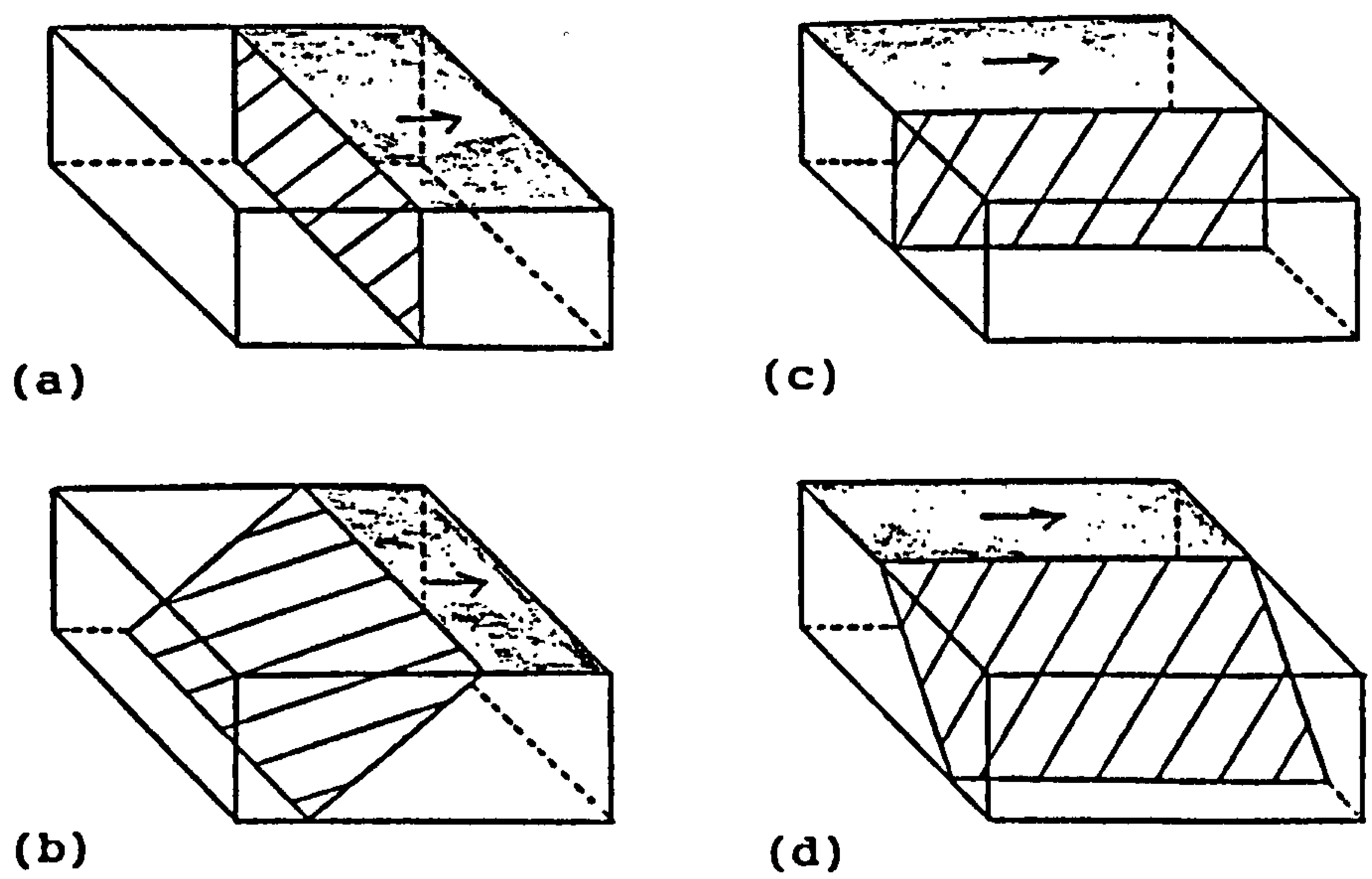

Fig.3.7 Schematic diagrams to describe cross-sections of wear specimens. The arrows show the relative sliding direction of the counterface.
(a) Transverse section normal to the wear surface
(b) Transverse taper section
(c) Longitudinal section normal to the wear surface
(d) Longitudinal taper section

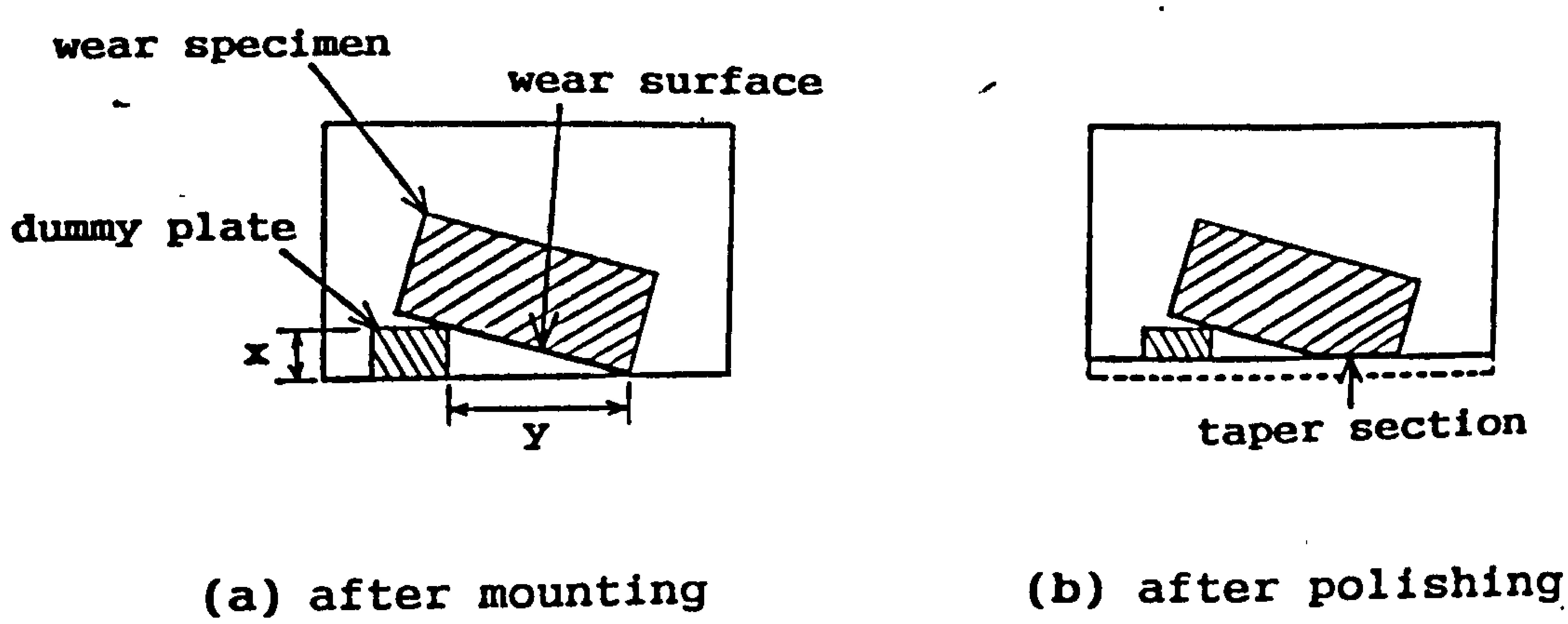

Fig.3.8 Preparation of a taper section of a wear specimen

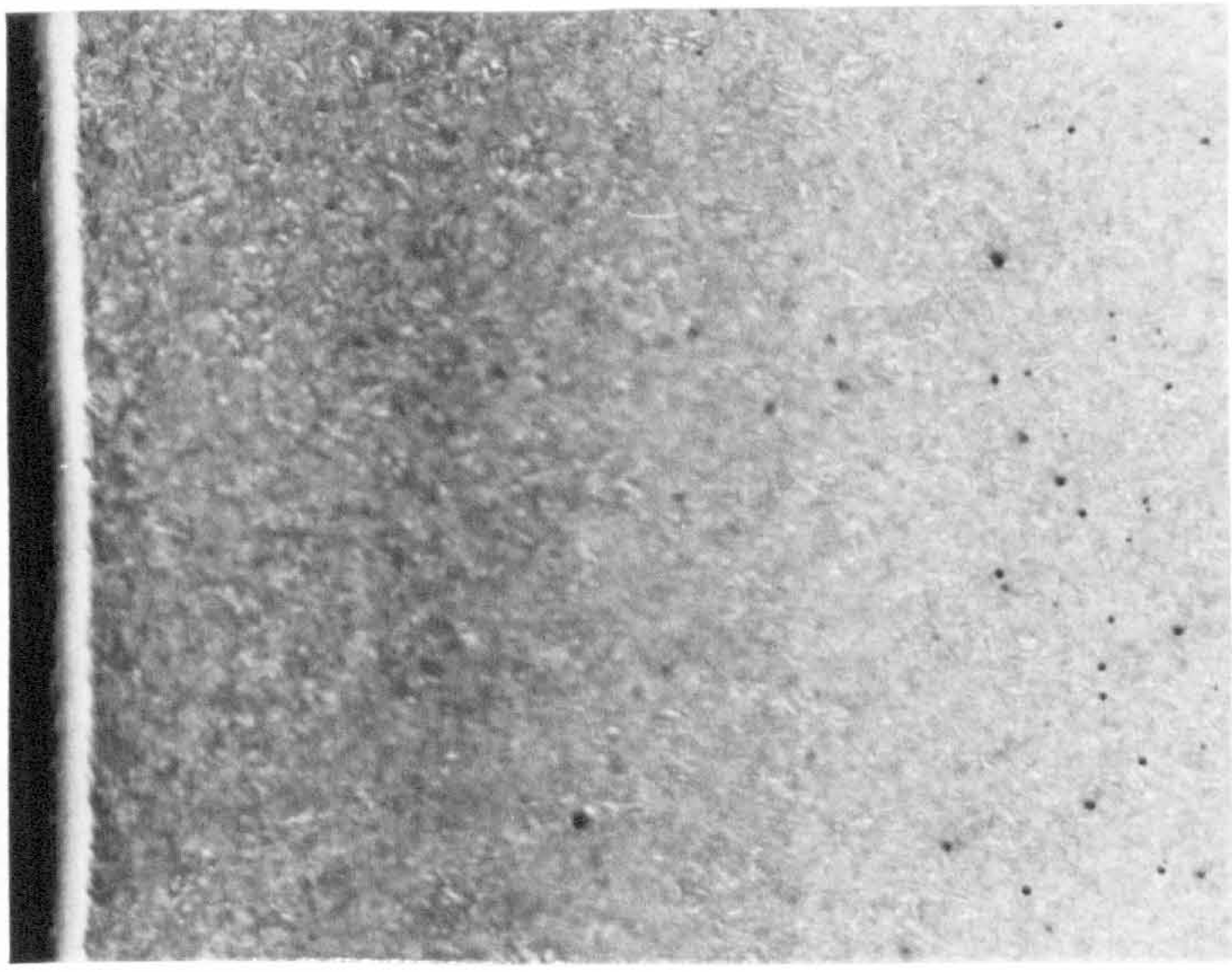

(a) 200μm

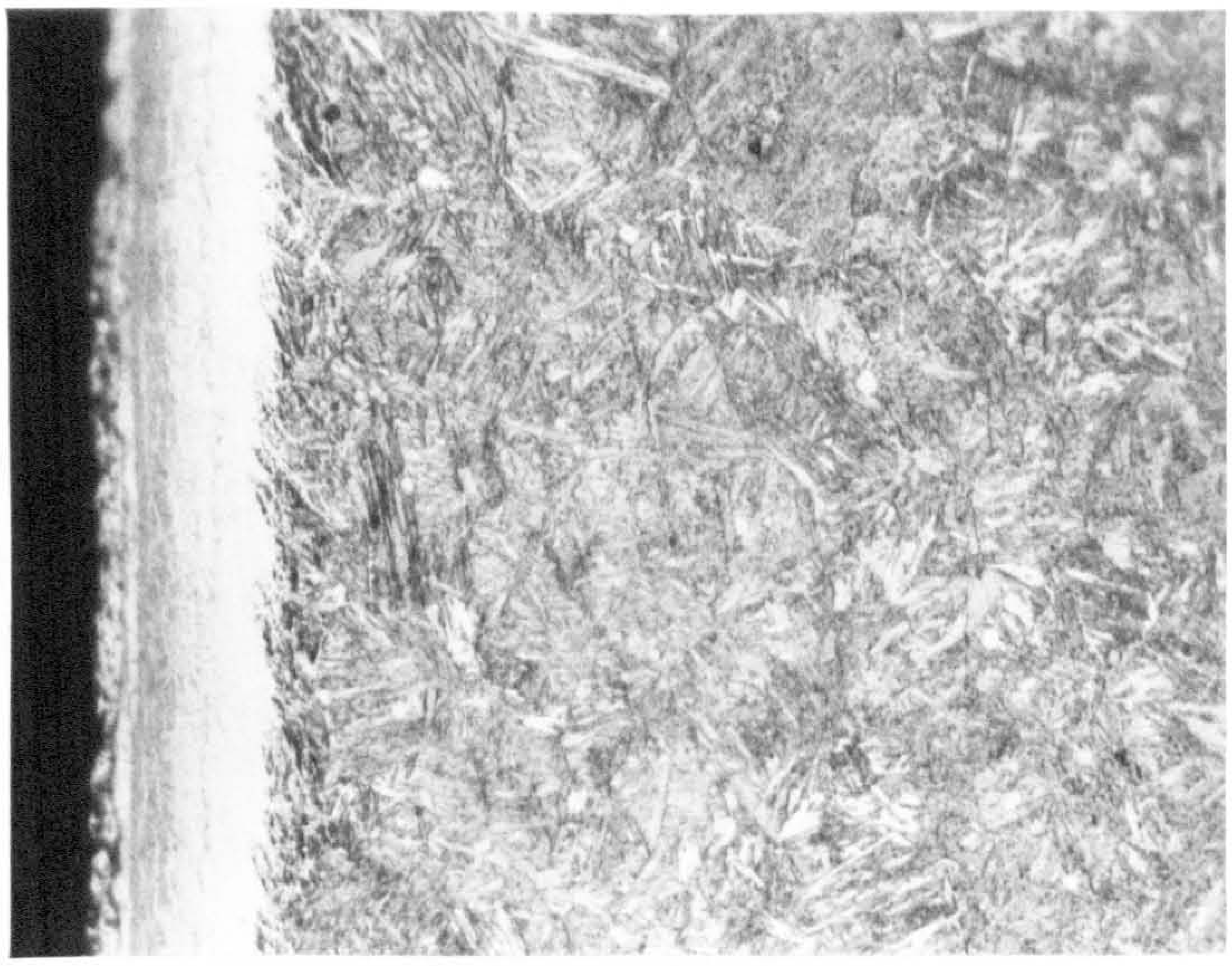

(b) 50μm

Fig.4.1 Optical microstructure of surface layer of gas nitrided BS970,905M39 (EN41B)
(a) x110 **(b)** x440

50μm

Fig.4.2 Optical microstructure of surface layer of plasma nitrided BS970,905M39 (EN41B)

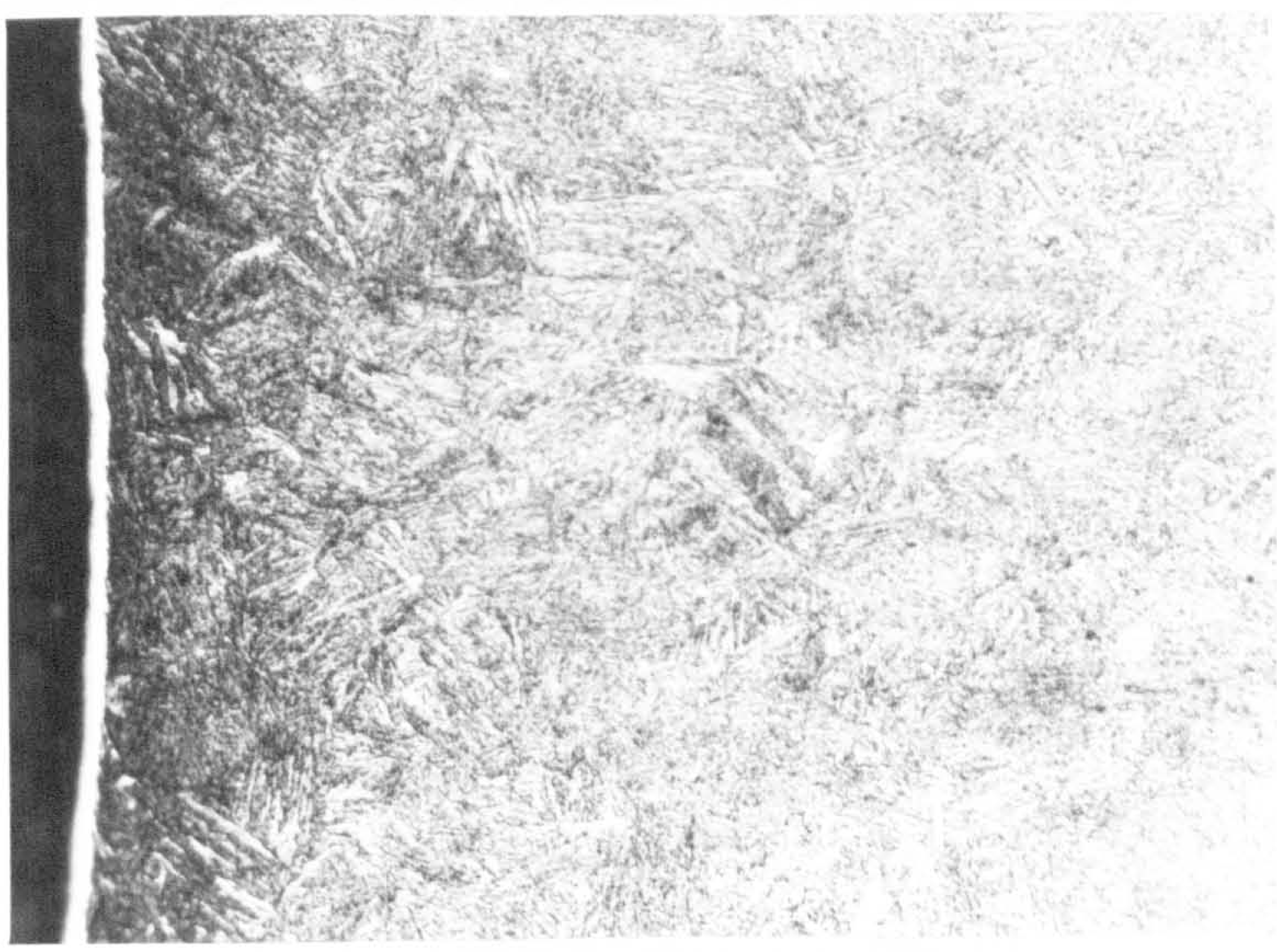

50μm

Fig.4.3 Optical microstructure of surface layer of gas nitrocarburized BS970,905M39 (EN41B)

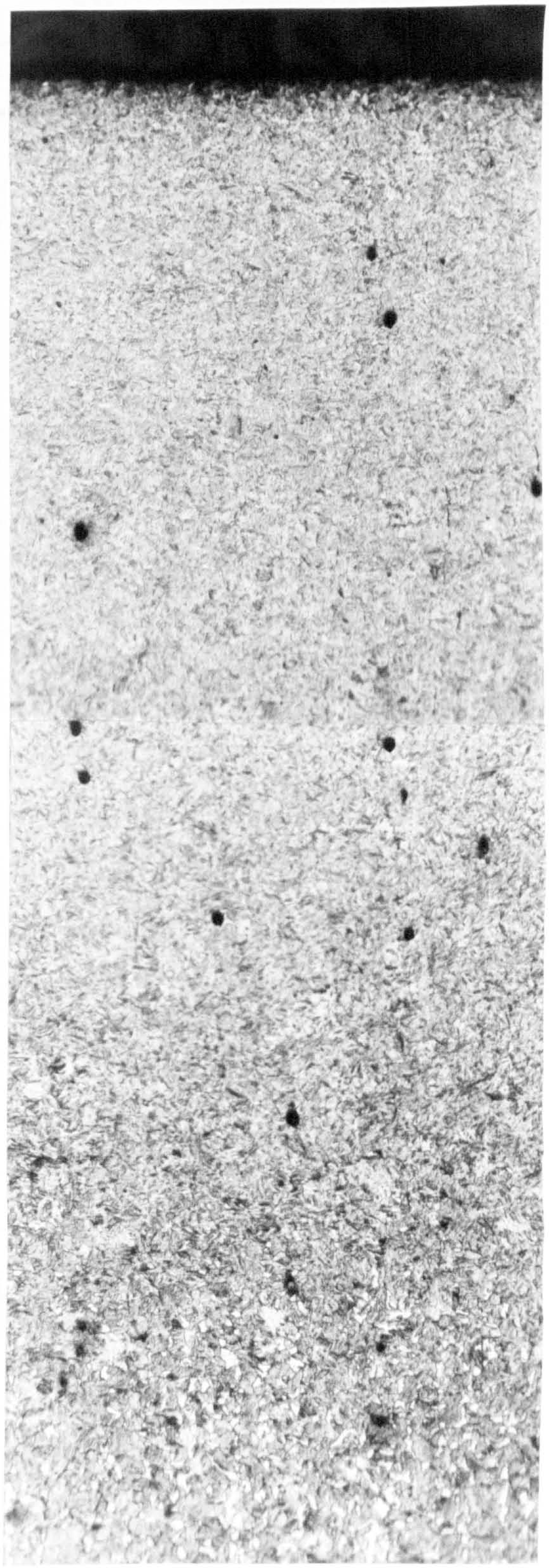

100μm

Fig.4.4 Optical microstructure of surface layer of gas-carburized and hardened BS970,635M15 (EN351)

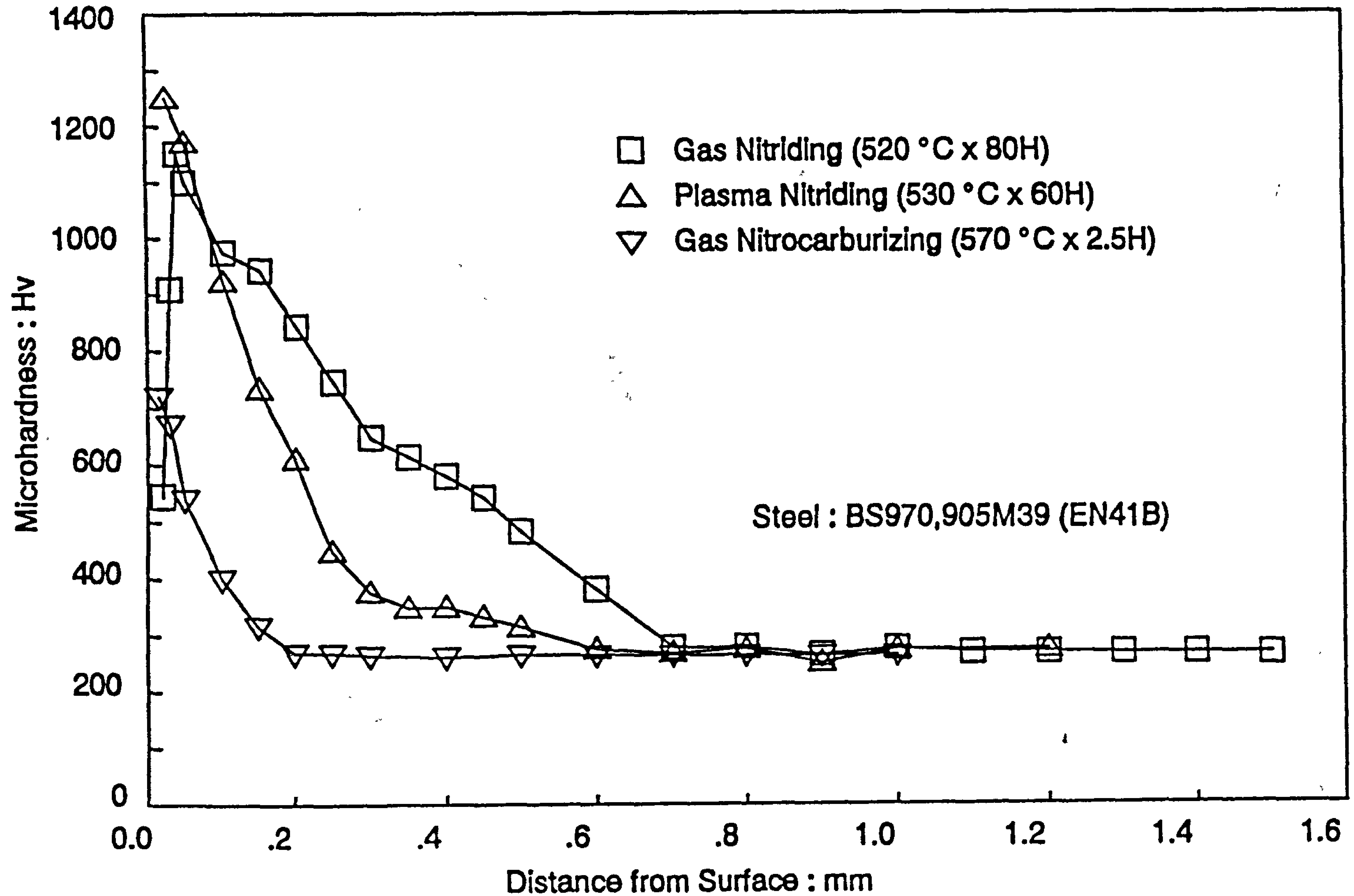

Fig.4.5 Microhardness profile of gas nitrided, plasma nitrided and nitrocarburized BS970,905M39 (EN41B) sections

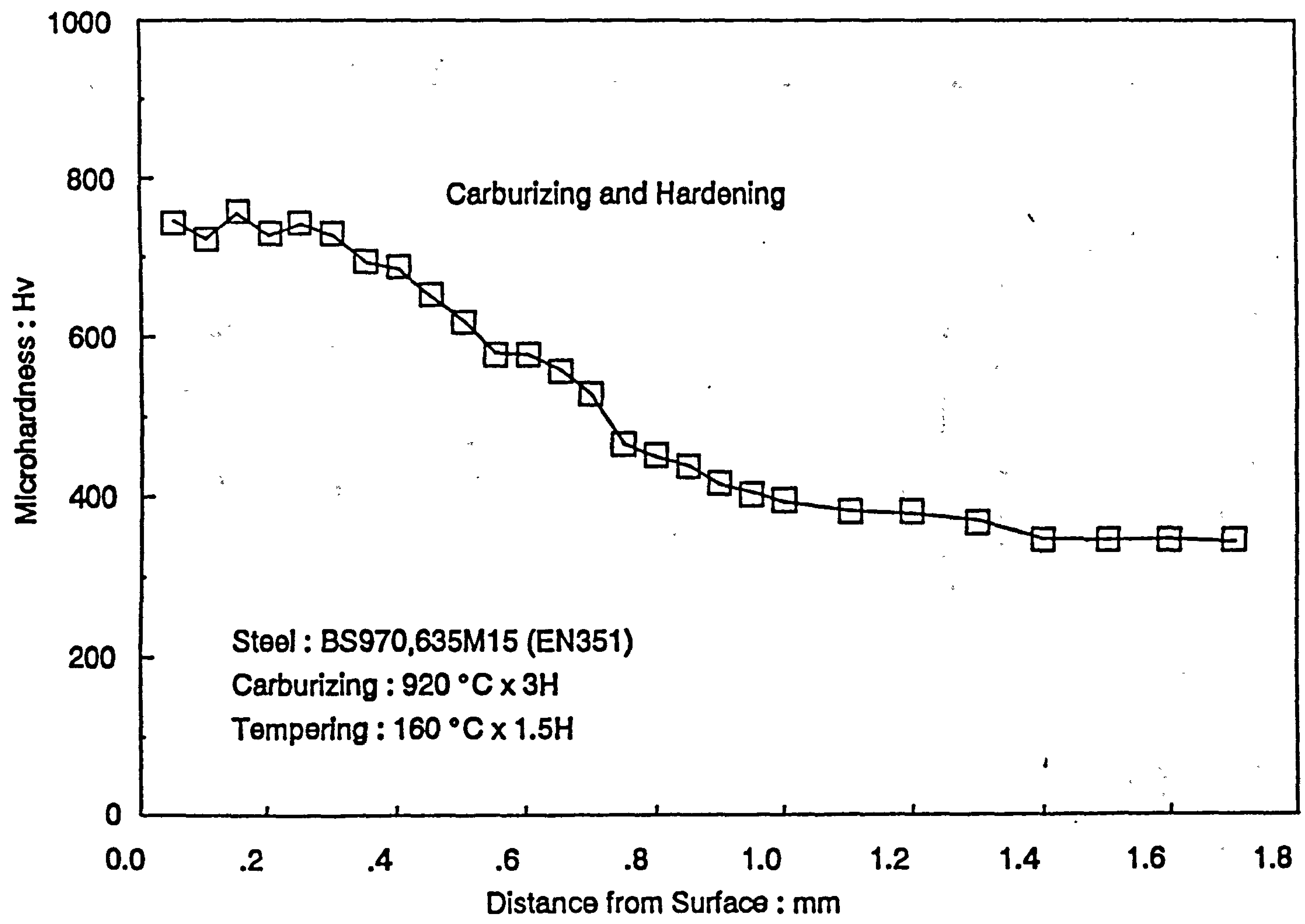

Fig.4.6 Microhardness profile of gas-carburized and hardened BS970,635M15 (EN351) section

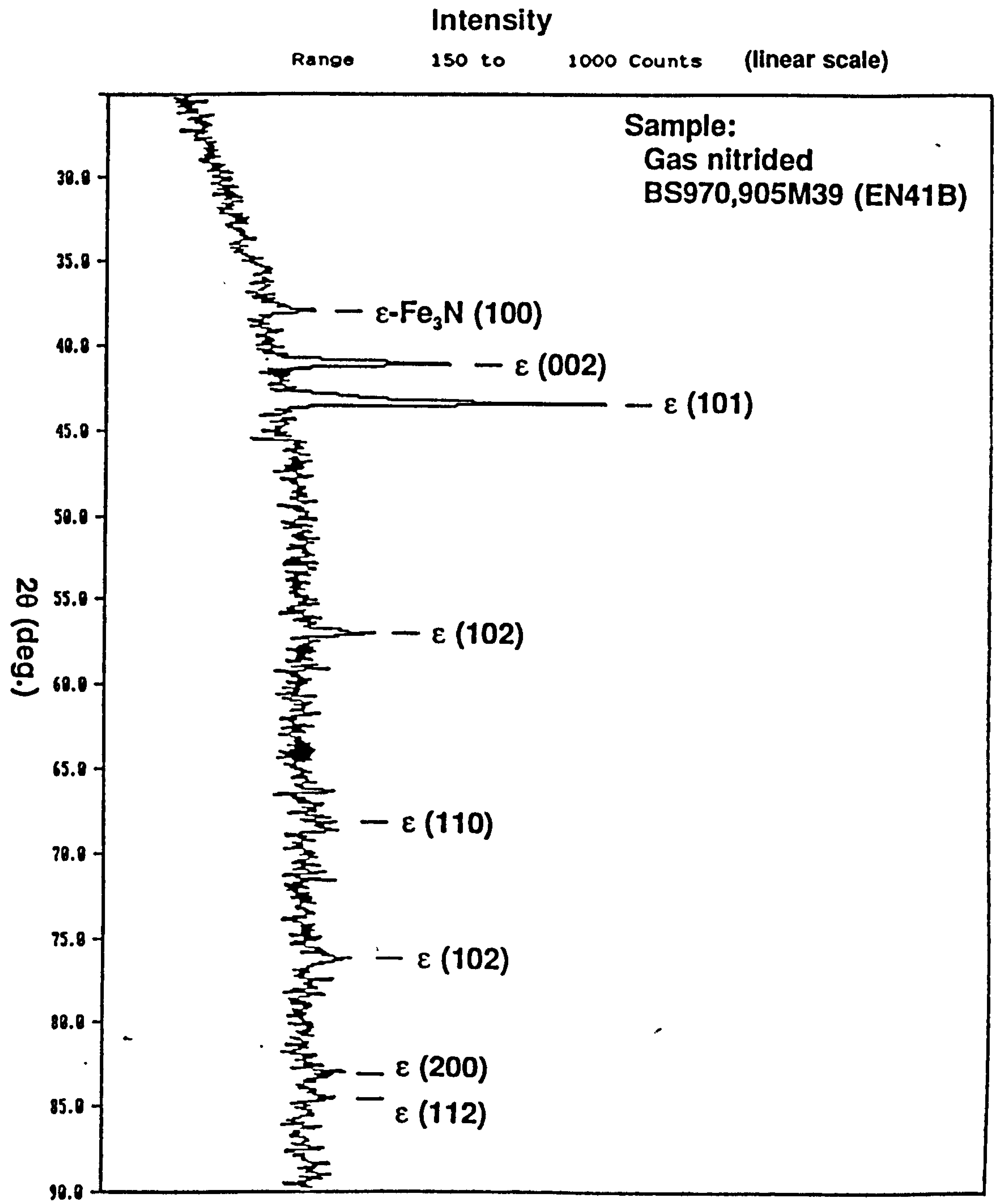

Fig.4.7 (a) X-ray diffraction diagram of gas nitrided BS970,905M39 (EN41B) surface

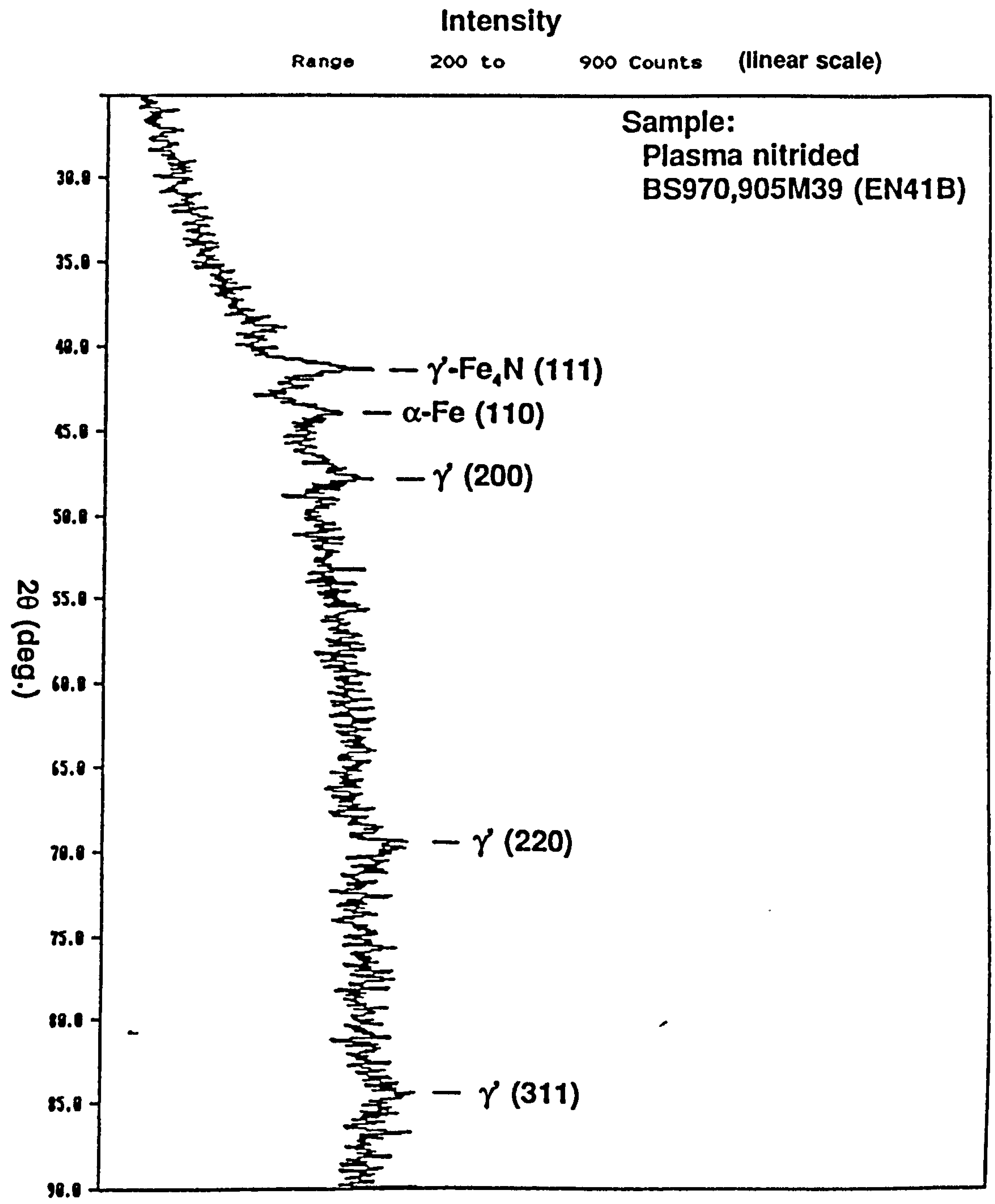

Fig.4.7 (b) X-ray diffraction diagram of plasma nitrided BS970,905M39 (EN41B) surface

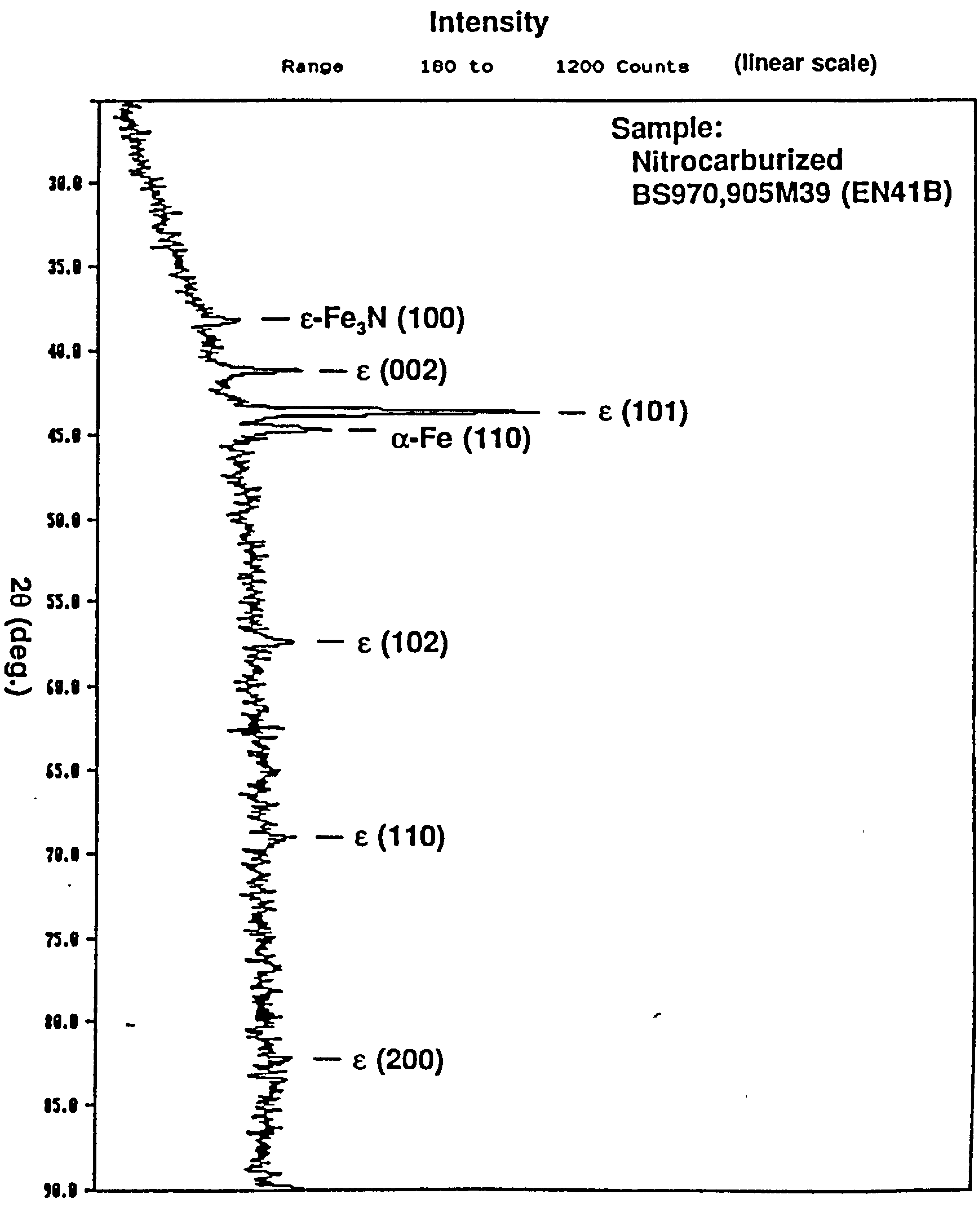

Fig.4.7 (c) X-ray diffraction diagram of gas nitrocarburized BS970,905M39 (EN41B) surface

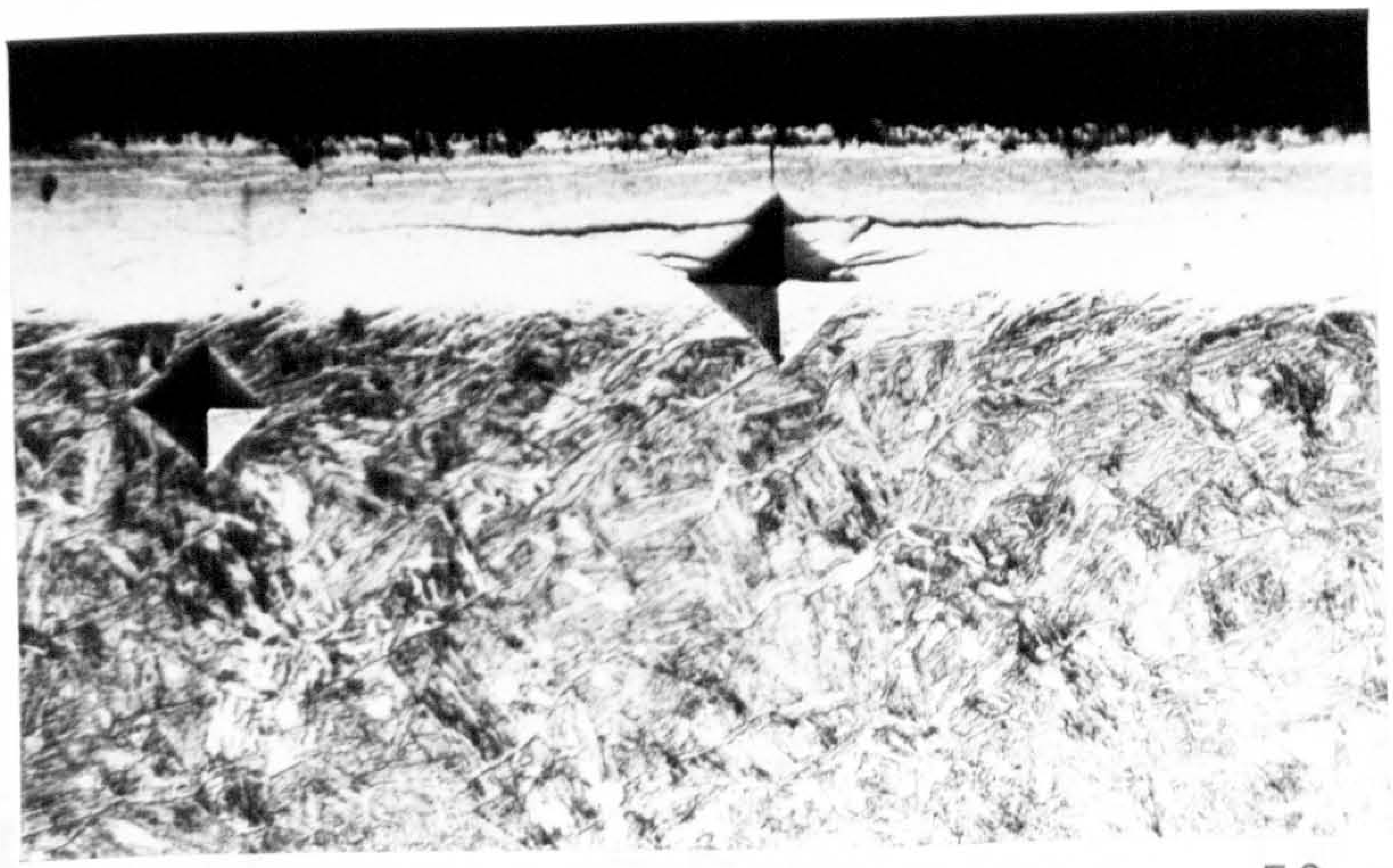

(a) 50μm

(b) 50μm

(c) 50μm

Fig.4.8 Vickers indentations at different applied loads in gas nitrided compound layer
(a) Load: 3 N **(b)** Load: 0.25 N **(c)** Load: 0.1 N

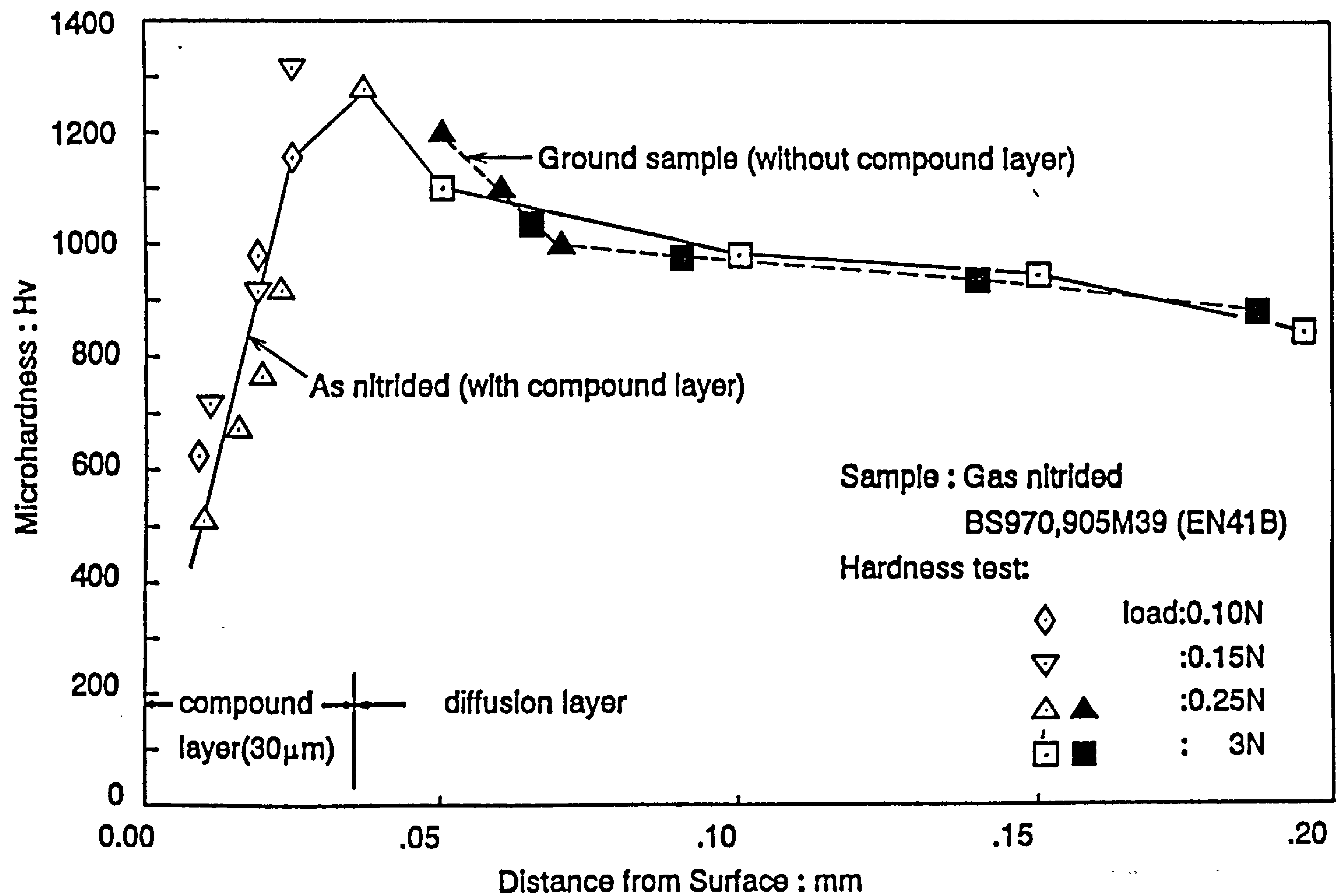

Fig.4.9 Microhardness of compound layer section of gas nitrided BS970,905M39 (EN41B)

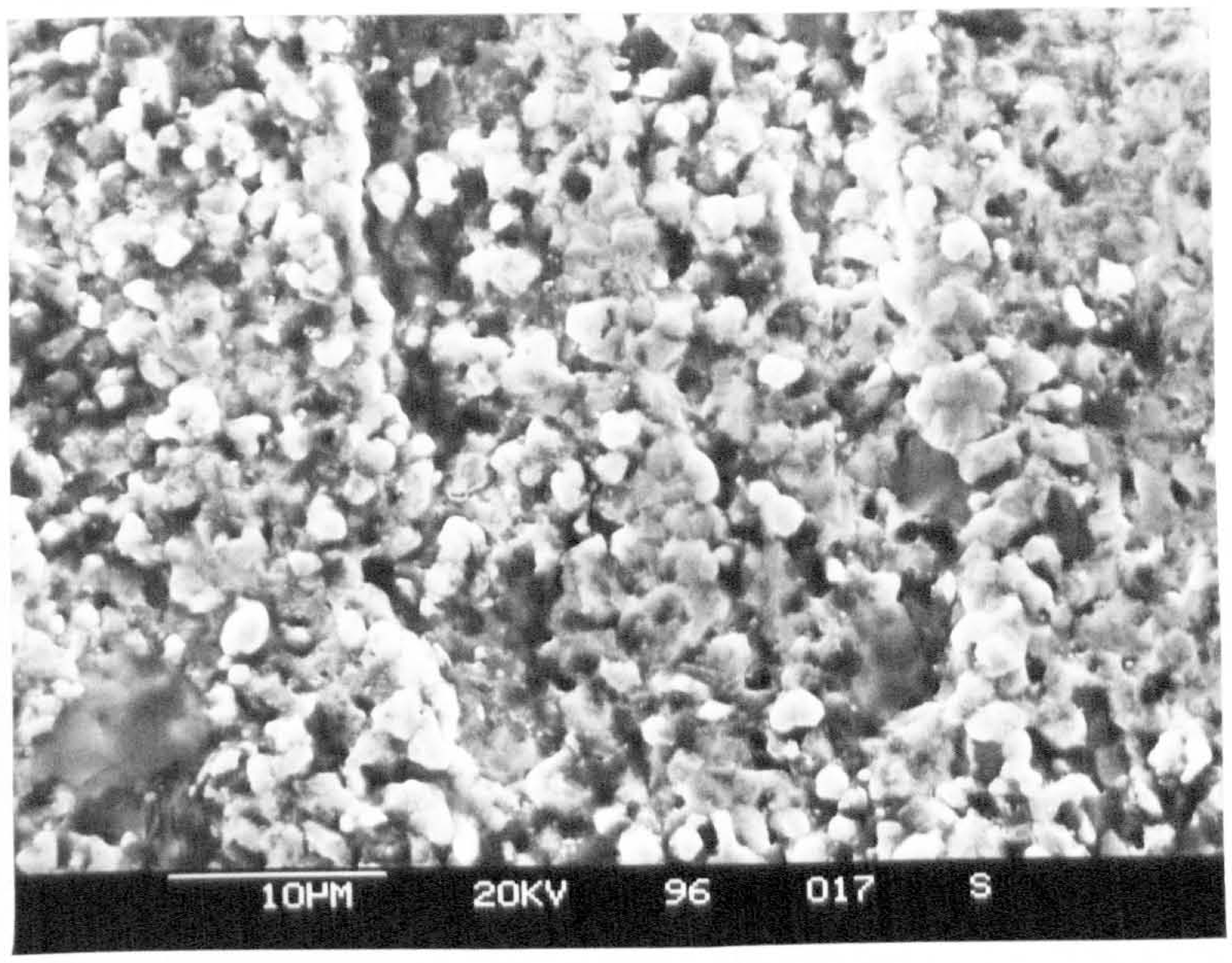

Fig.4.10 SEM of 'as-nitrided' surface for gas nitrided BS970,905M39 (EN41B)

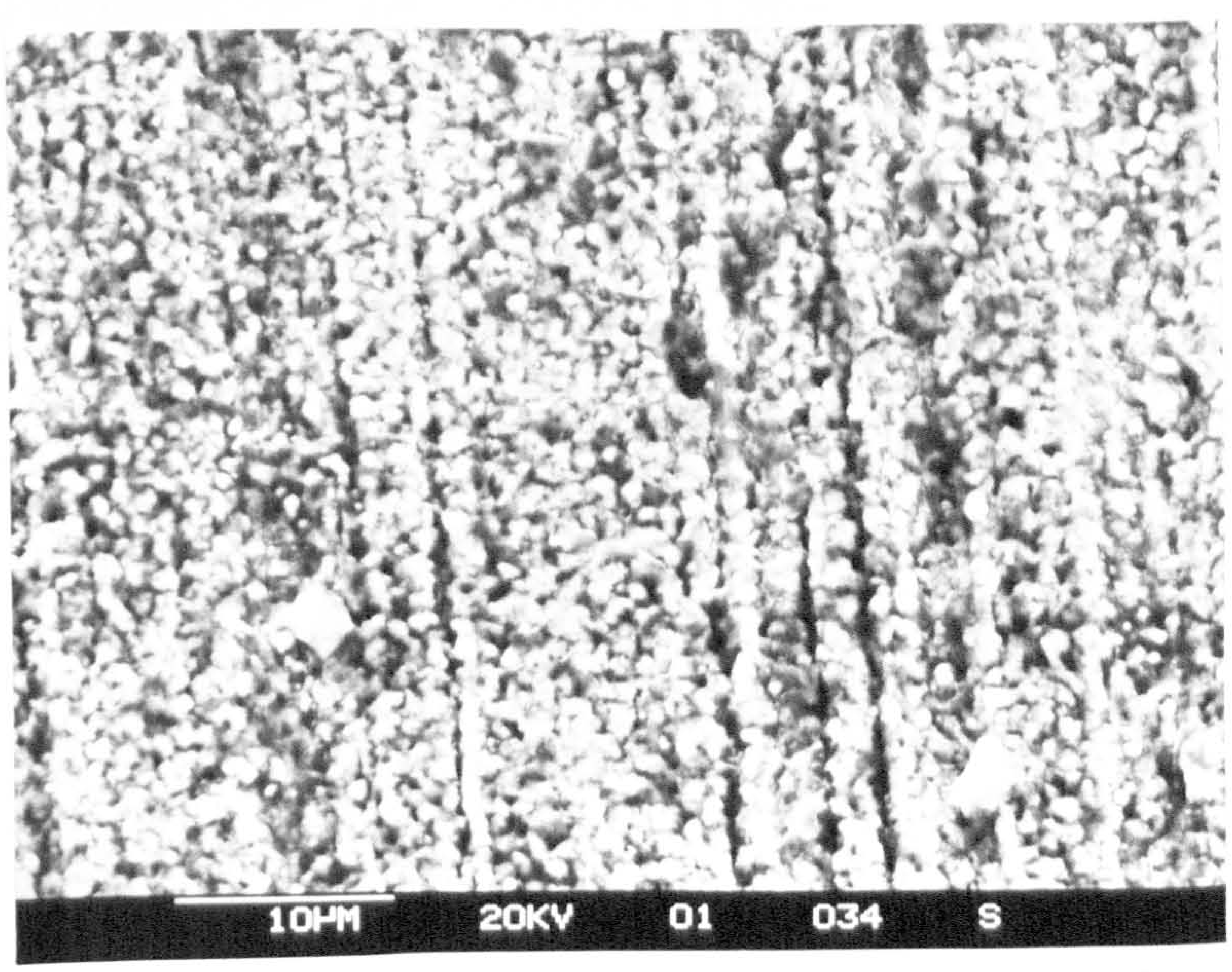

Fig.4.11 SEM of 'as-nitrided' surface for nitro-carburized BS970,905M39 (EN41B)

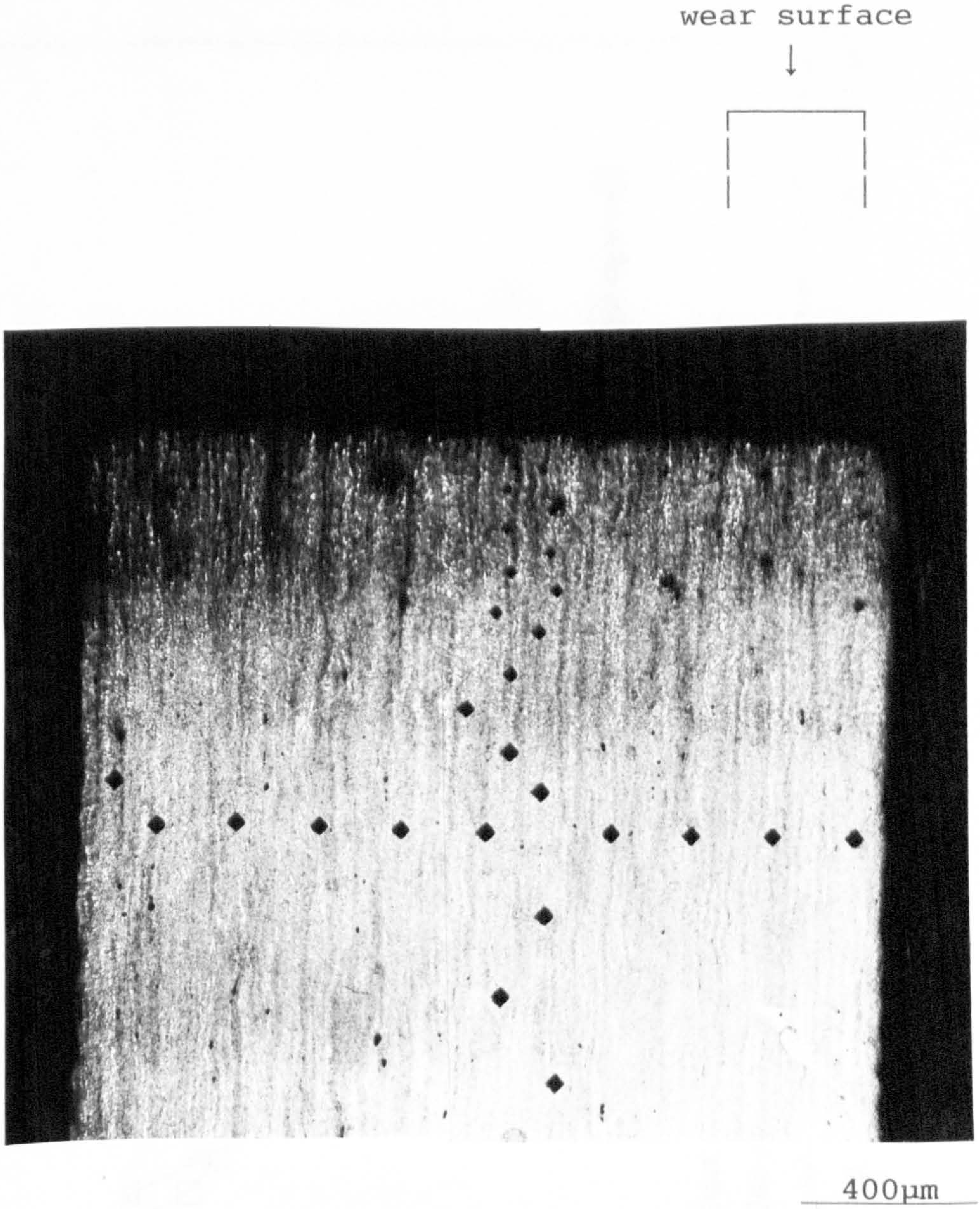

Fig.4.12 Optical microstructure of "wear-face-limited" gas nitrided pin section

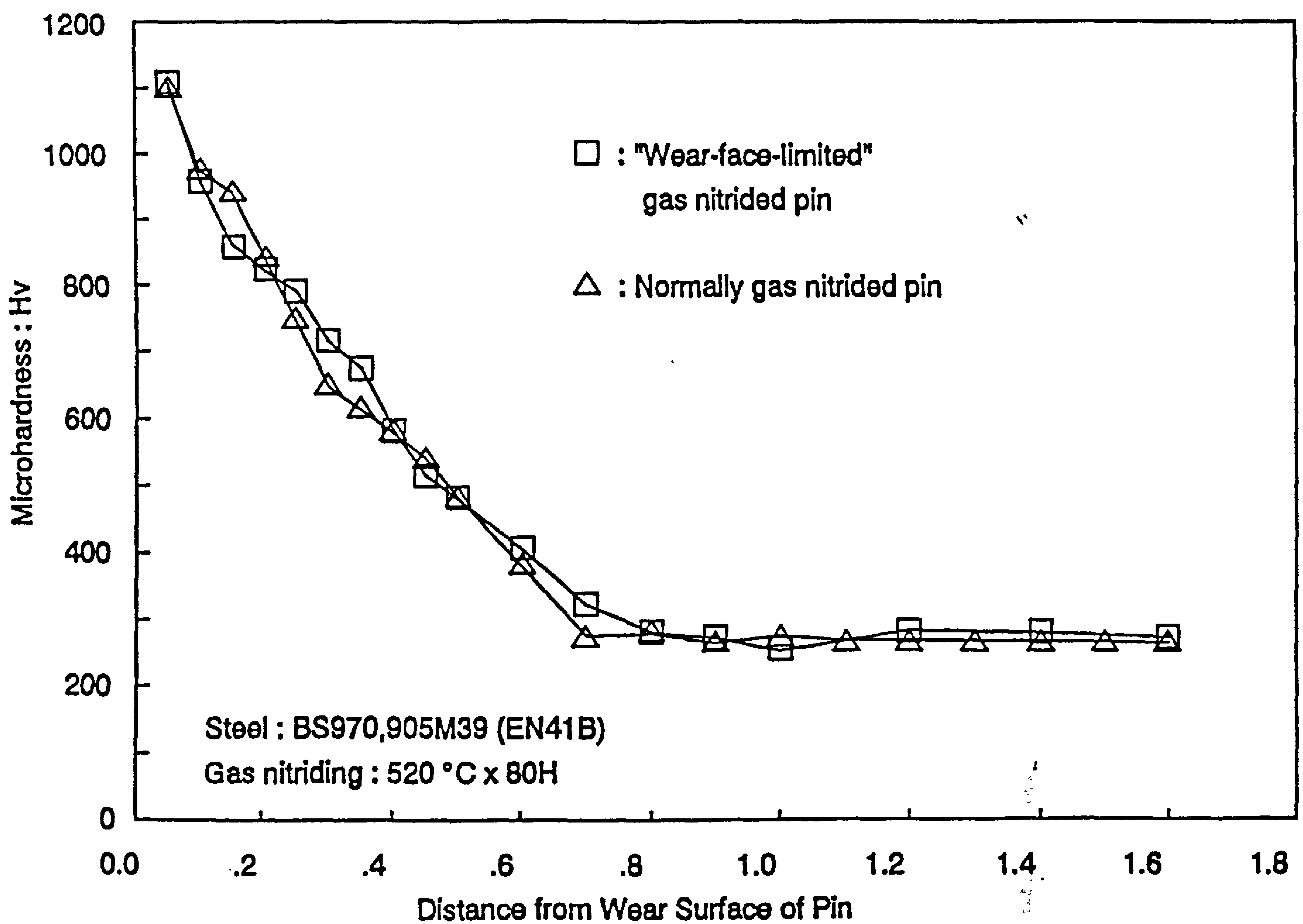

Fig.4.13 Microhardness profile of gas nitrided pin section

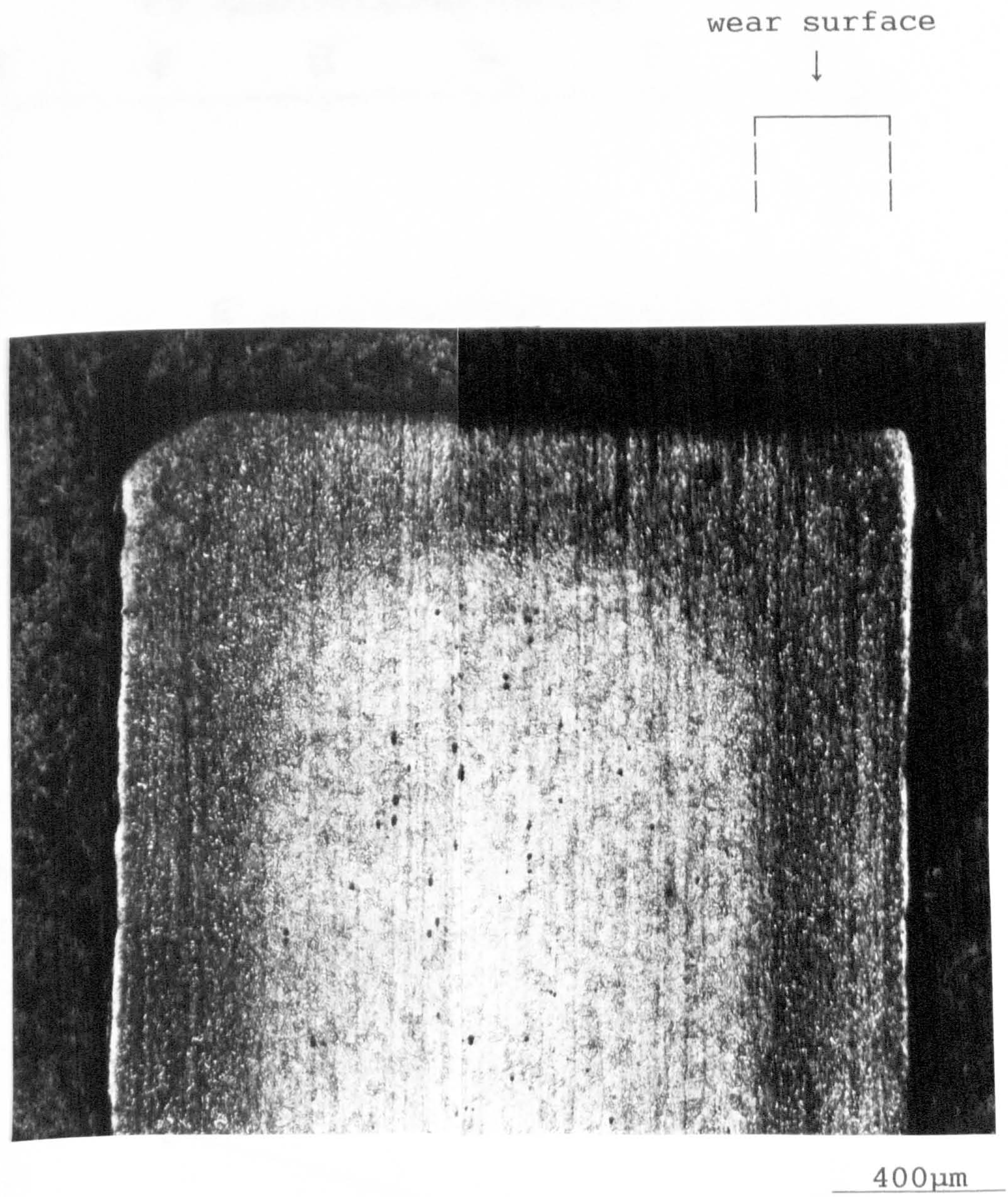

Fig.4.14 Optical microstructure of gas nitrided and wear-face-ground pin section (without compound layer)

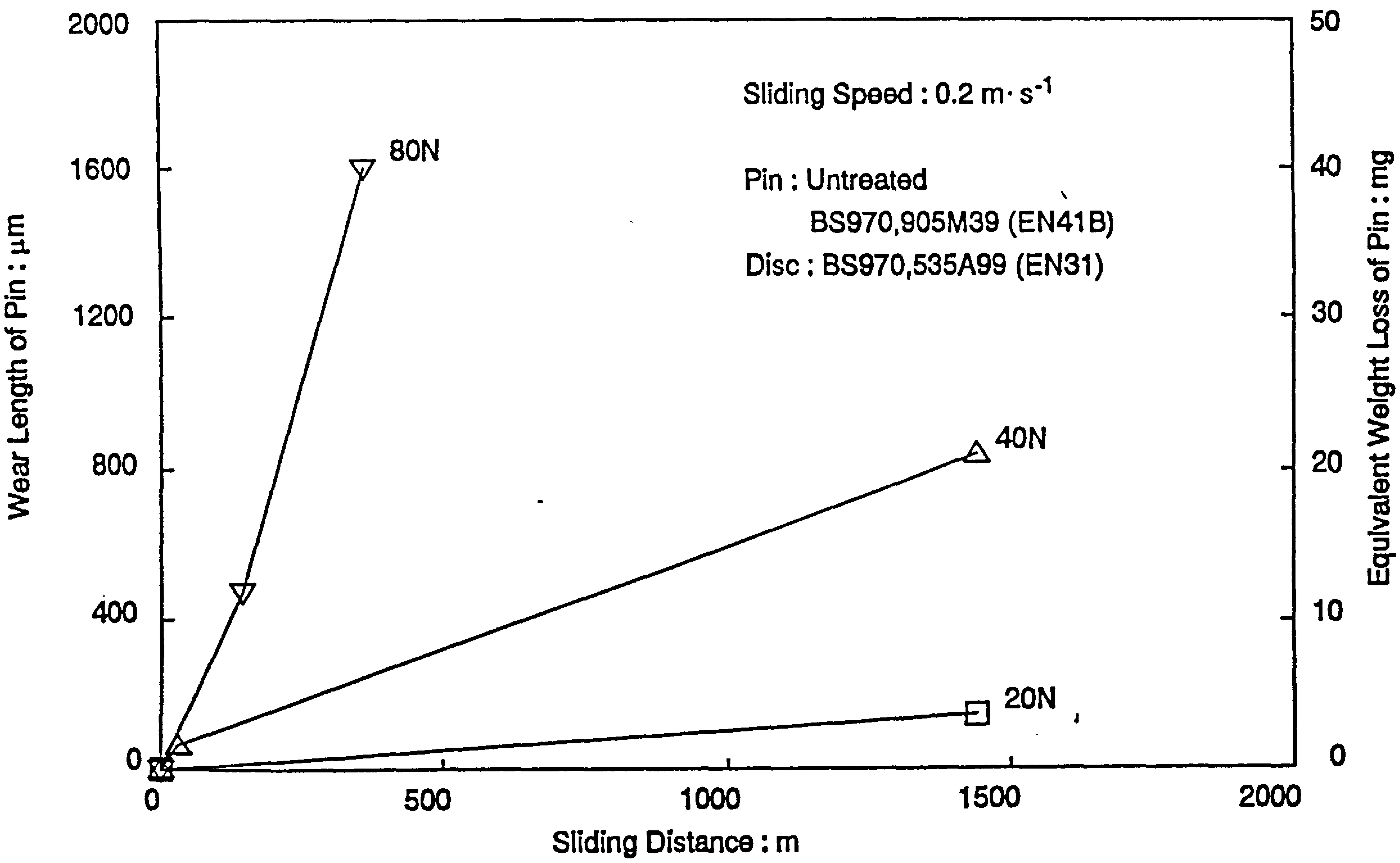

Fig.4.15 (a) Relationship between wear length of untreated BS970,905M39 (EN41B) pin and sliding distance at a sliding speed of 0.2 $m \cdot s^{-1}$

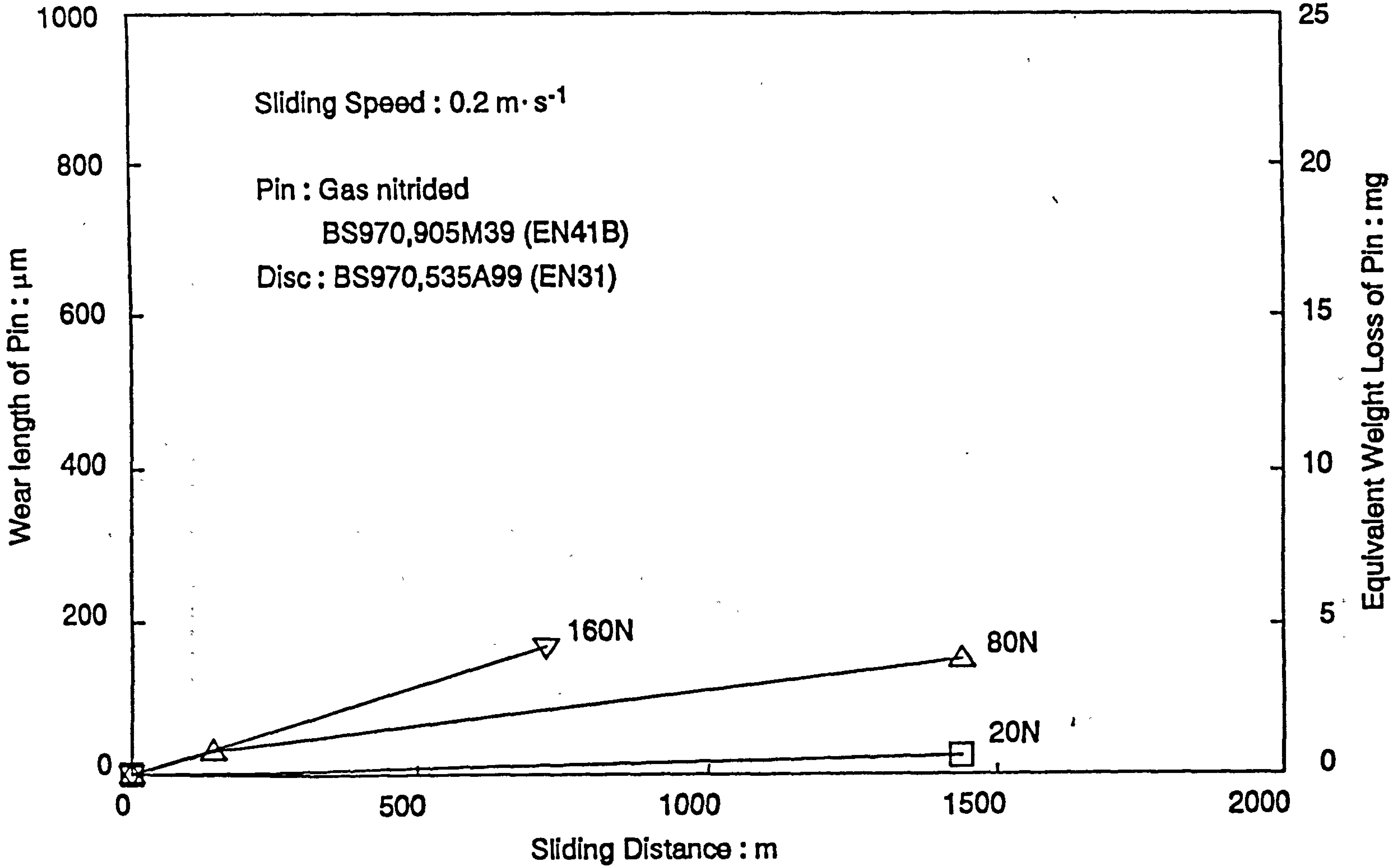

Fig.4.15 (b) Relationship between wear length of gas nitrided BS970,905M39 (EN41B) pin and sliding distance at a sliding speed of 0.2 $m \cdot s^{-1}$

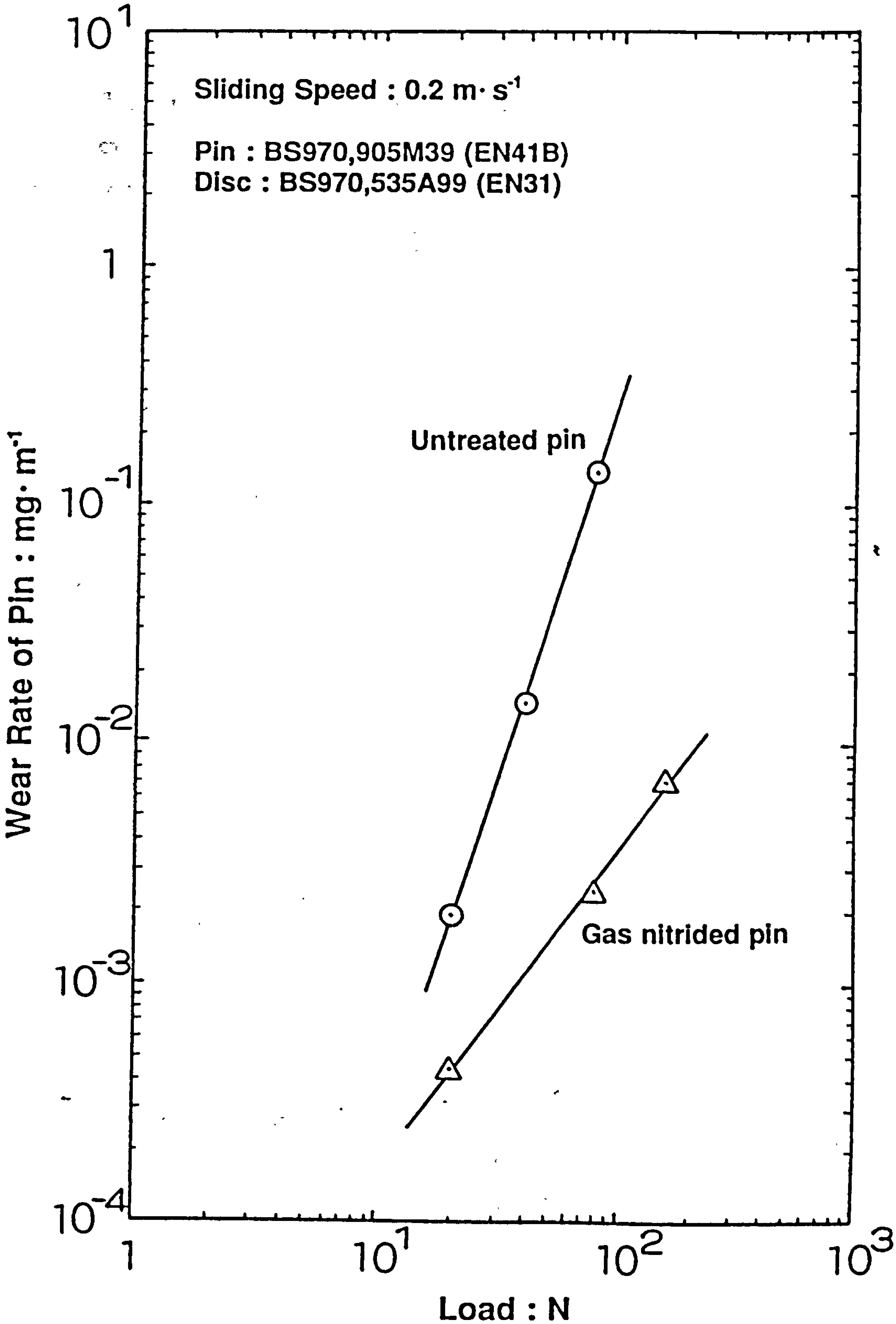

Fig.4.16 Wear rate of untreated and gas nitrided BS970,905M39 (EN41B) pins plotted against test load for a sliding speed of 0.2 $m \cdot s^{-1}$

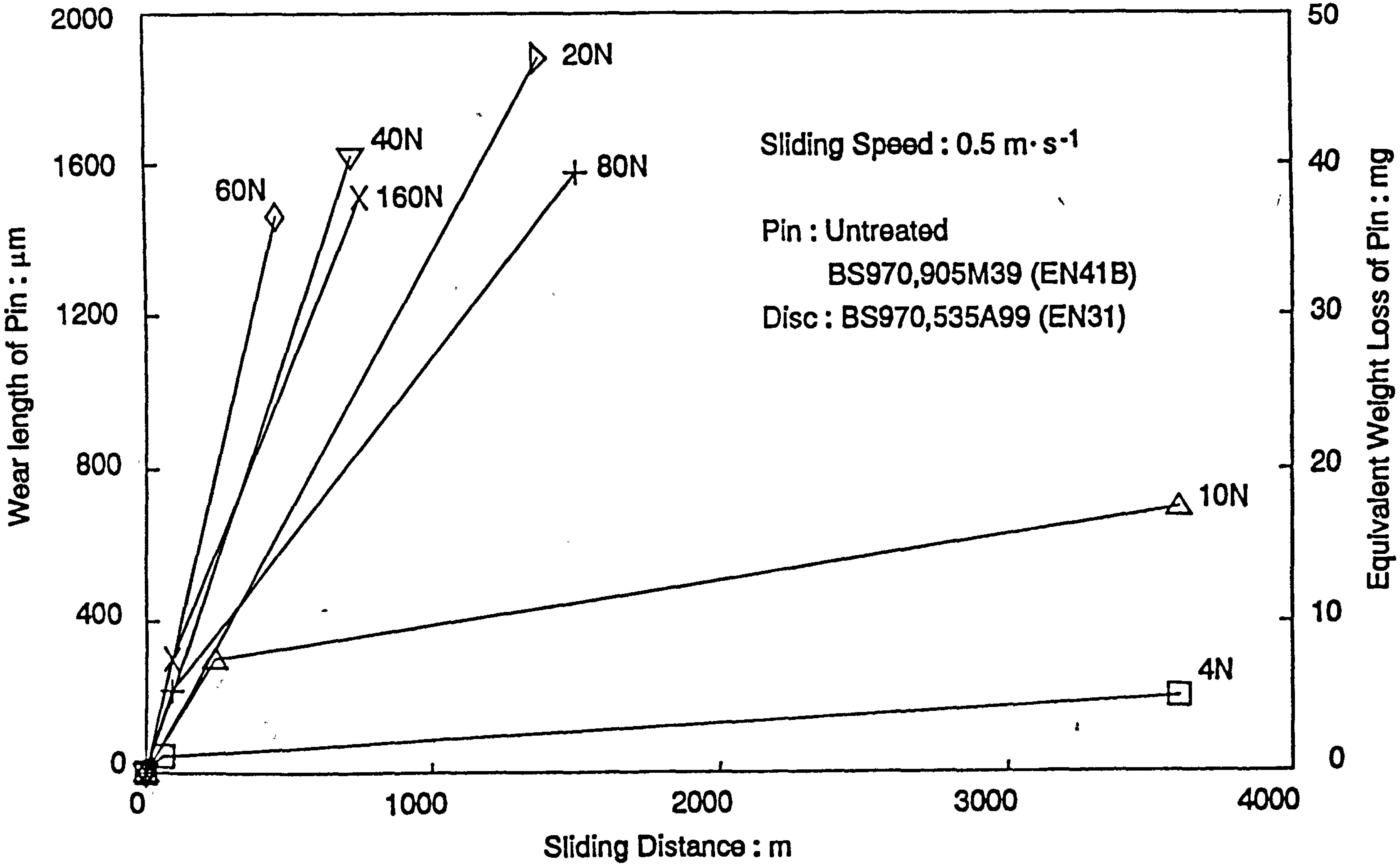

Fig.4.17 (a) Relationship between wear length of untreated BS970,905M39 (EN41B) pin and sliding distance at a sliding speed of 0.5 $m \cdot s^{-1}$

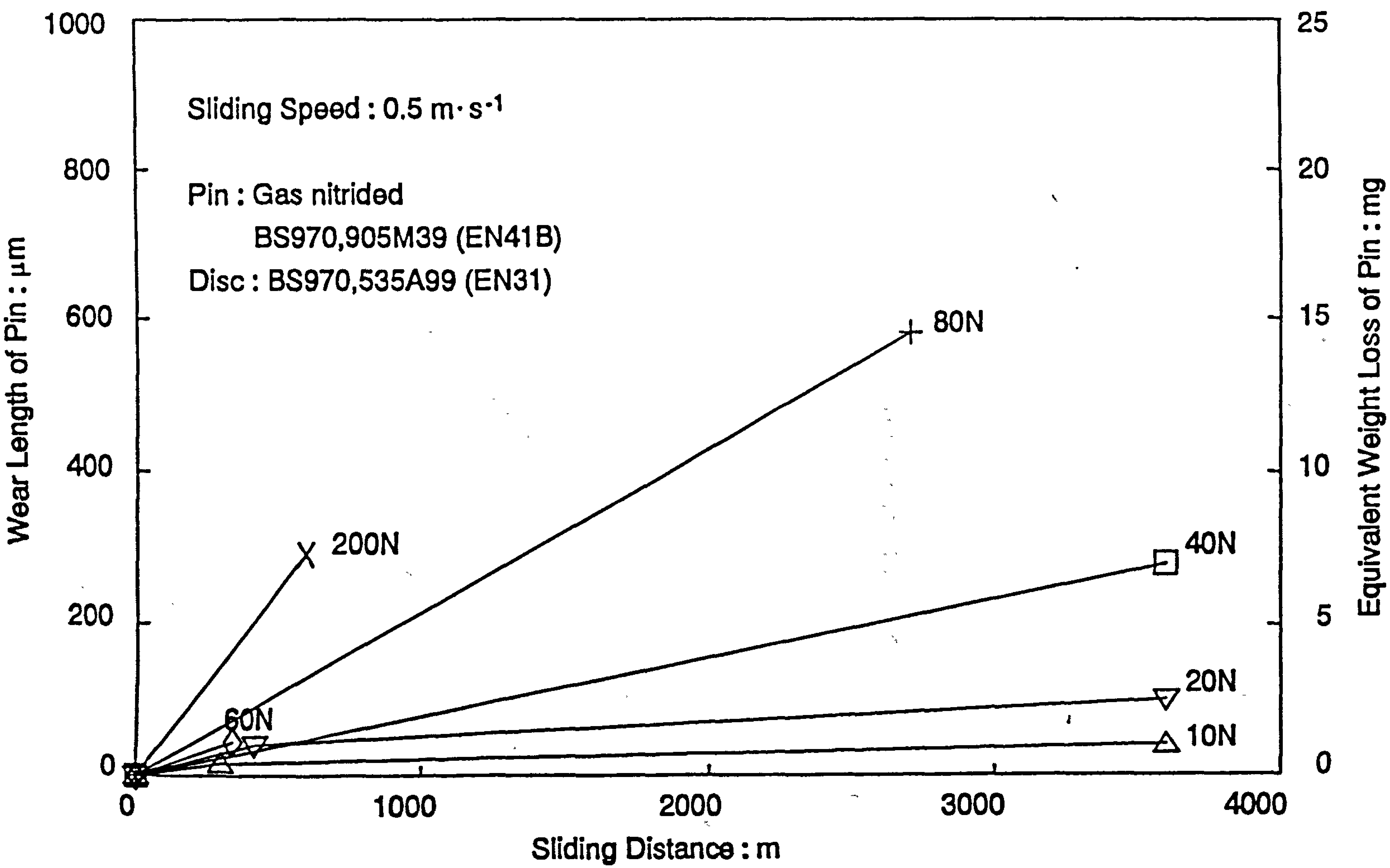

Fig.4.17 (b) Relationship between wear length of gas nitrided BS970,905M39 (EN41B) pin and sliding distance at a sliding speed of 0.5 $m \cdot s^{-1}$

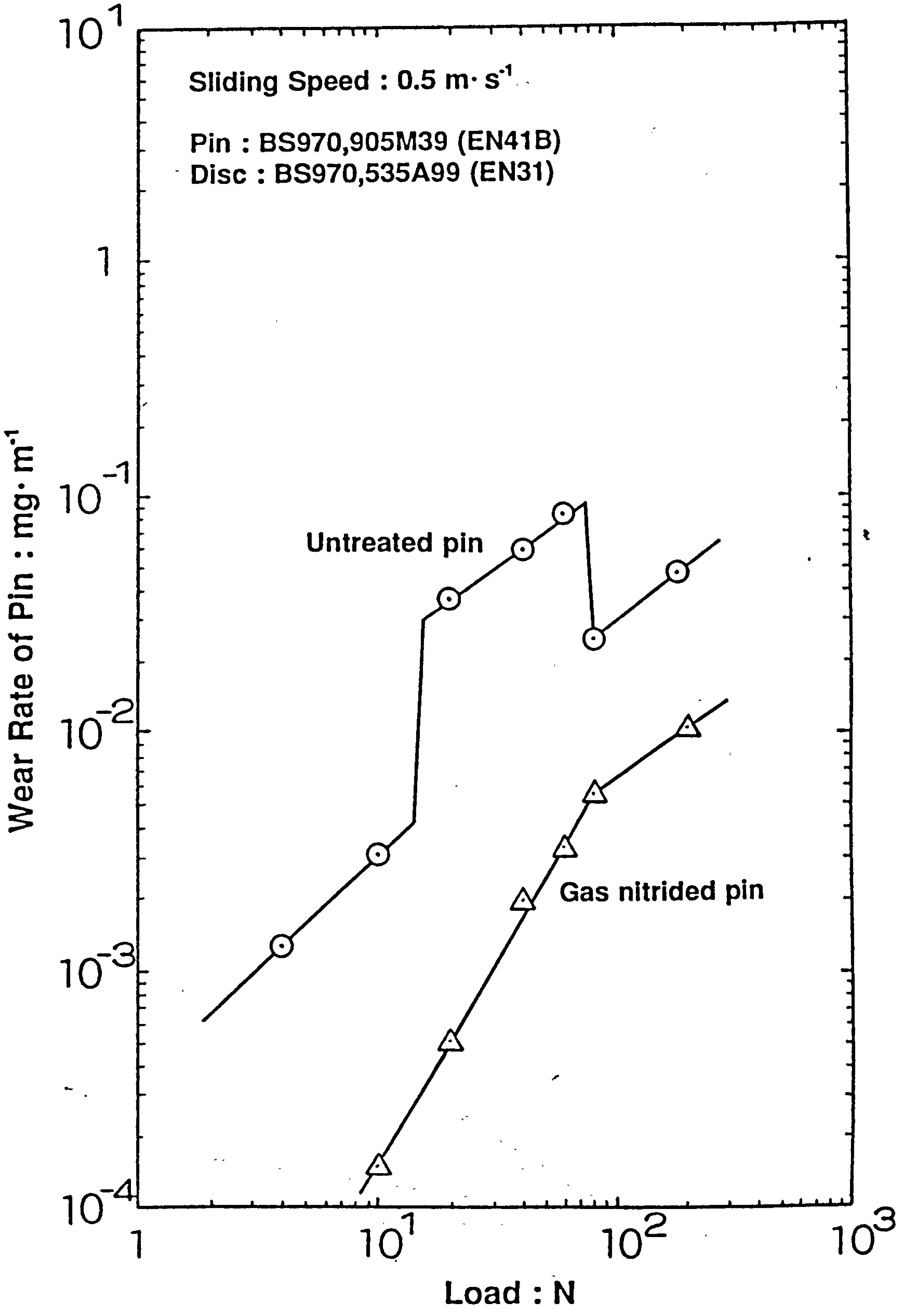

Fig.4.18 Wear rate of untreated and gas nitrided BS970,905M39 (EN41B) pins plotted against test load for a sliding speed of 0.5 $m{\cdot}s^{-1}$

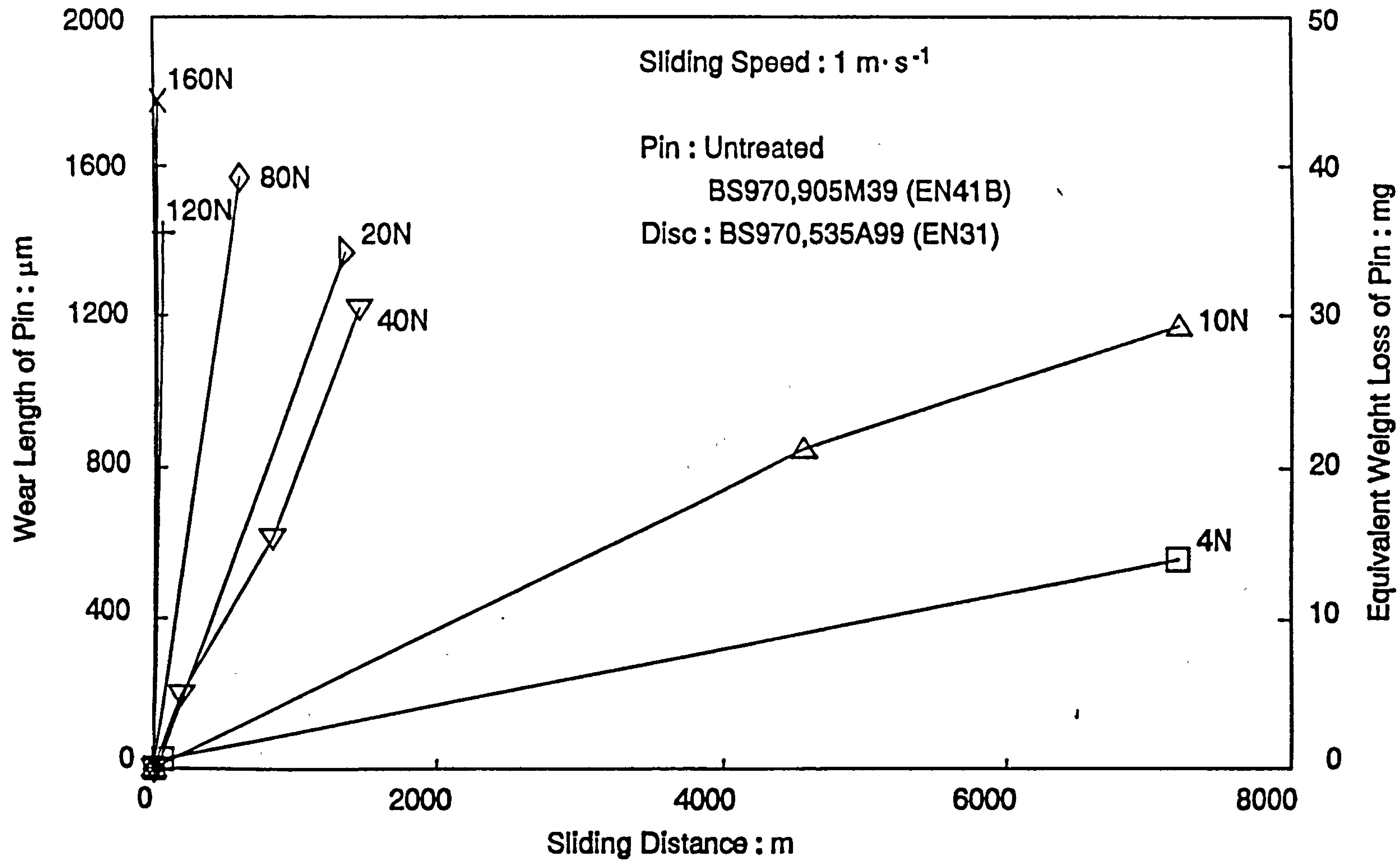

Fig.4.19 (a) Relationship between wear length of untreated BS970,905M39 (EN41B) pin and sliding distance at a sliding speed of 1 $m \cdot s^{-1}$

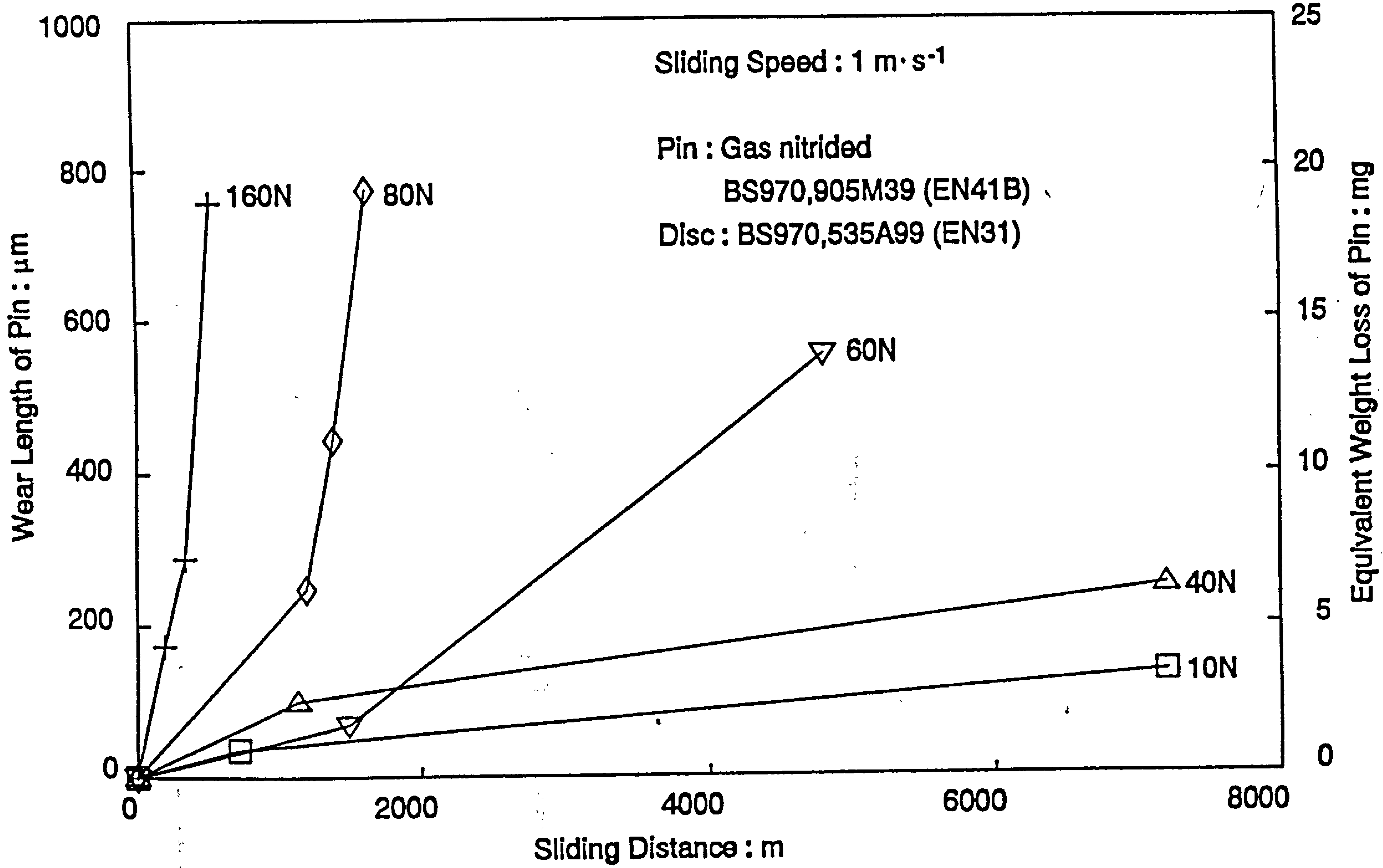

Fig.4.19 (b) Relationship between wear length of gas nitrided BS970,905M39 (EN41B) pin and sliding distance at a sliding speed of 1 $m \cdot s^{-1}$

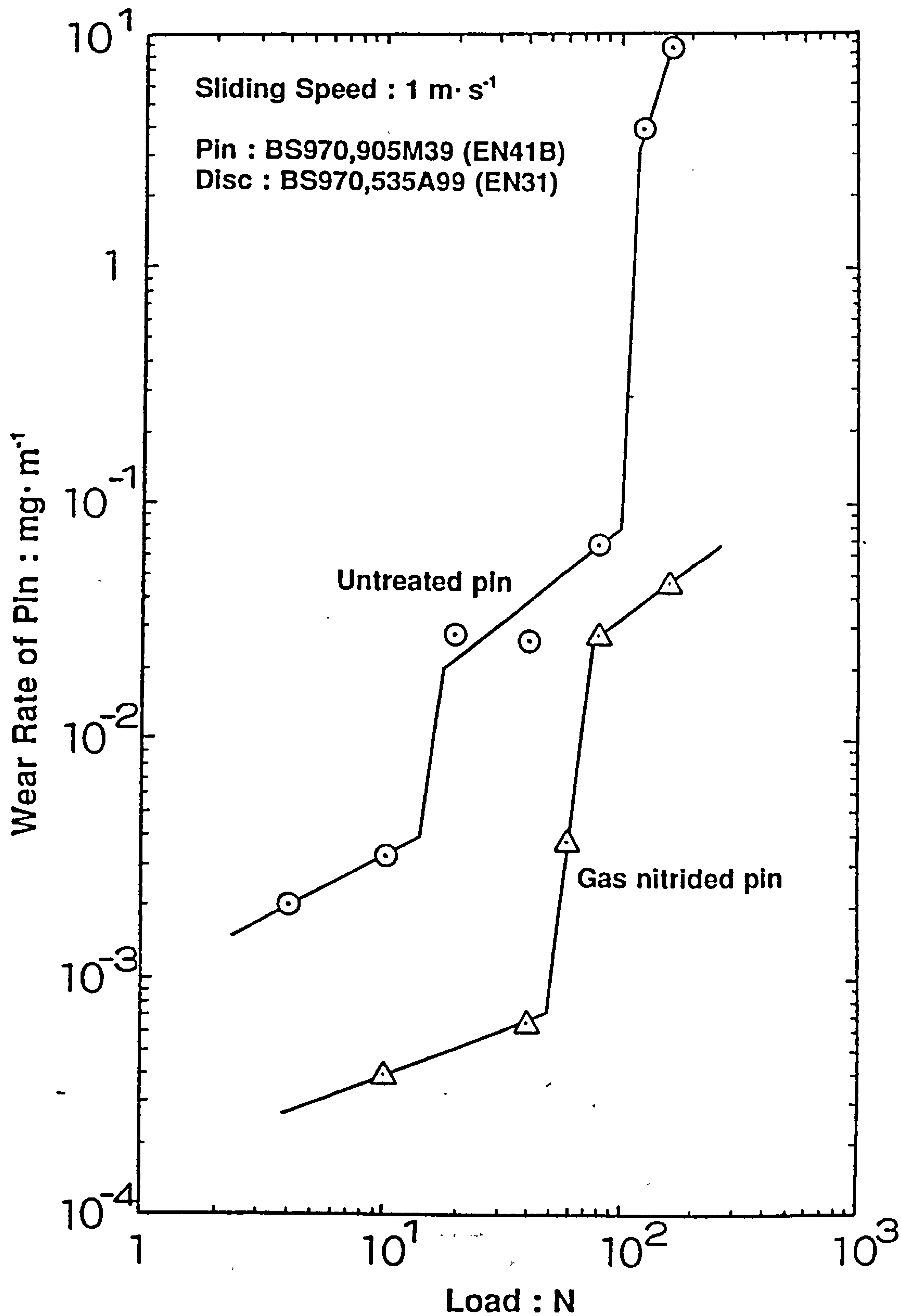

Fig.4.20 Wear rate of untreated and gas nitrided BS970,905M39 (EN41B) pins plotted against test load for a sliding speed of 1 $m \cdot s^{-1}$

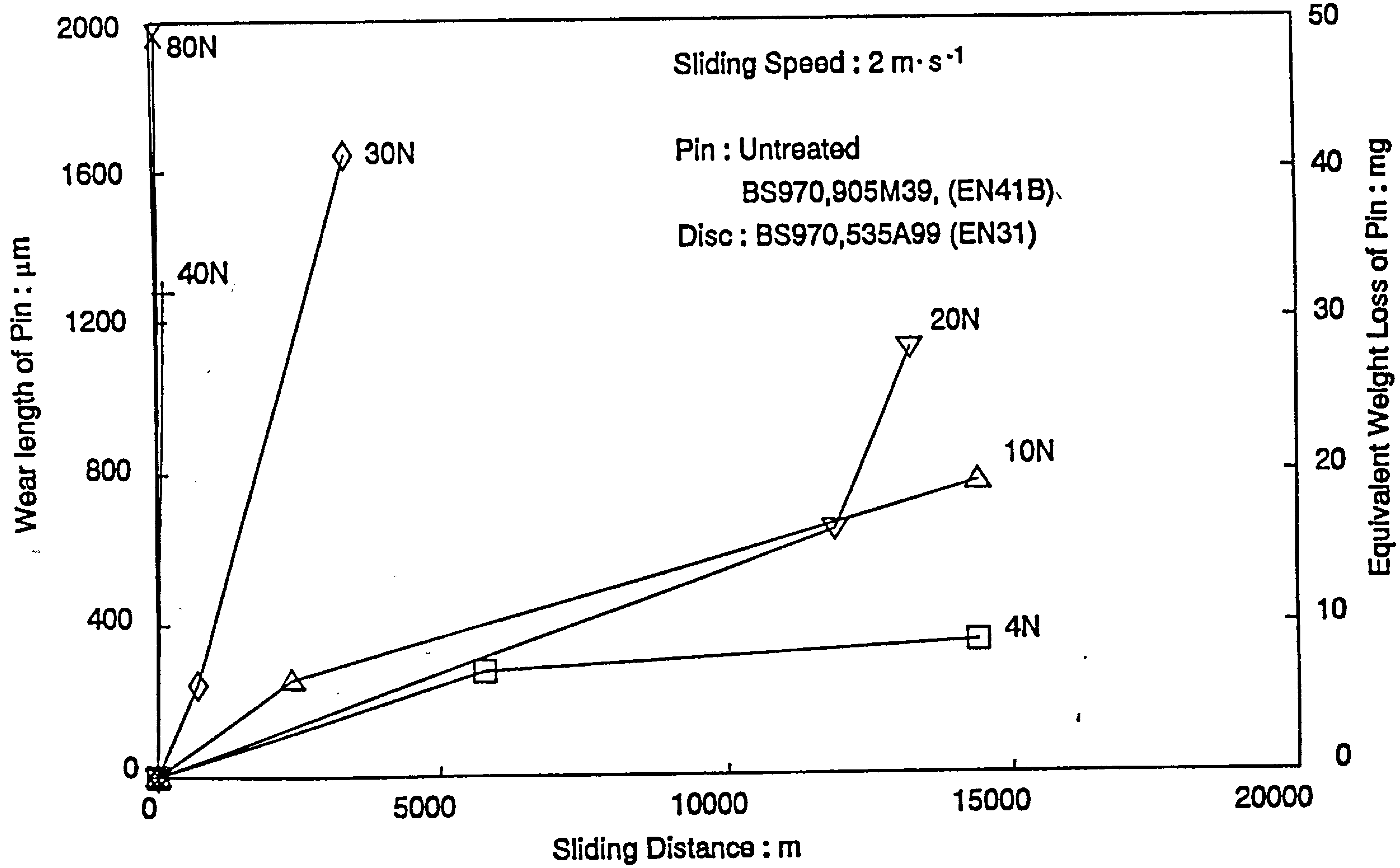

Fig.4.21 (a) Relationship between wear length of untreated BS970,905M39 (EN41B) pin and sliding distance at a sliding speed of 2 $m \cdot s^{-1}$

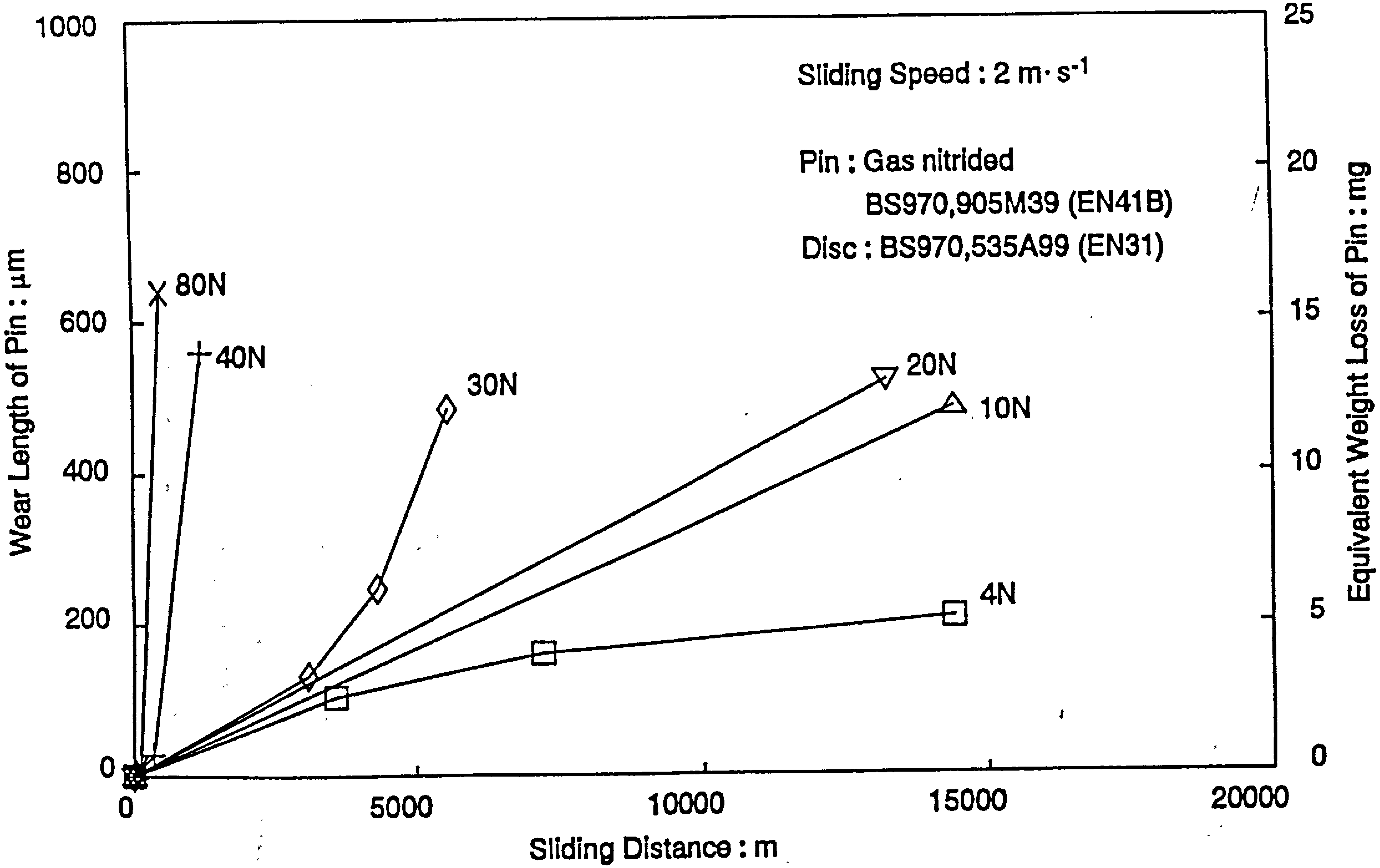

Fig.4.21 (b) Relationship between wear length of gas nitrided BS970,905M39 (EN41B) pin and sliding distance at a sliding speed of 2 $m \cdot s^{-1}$

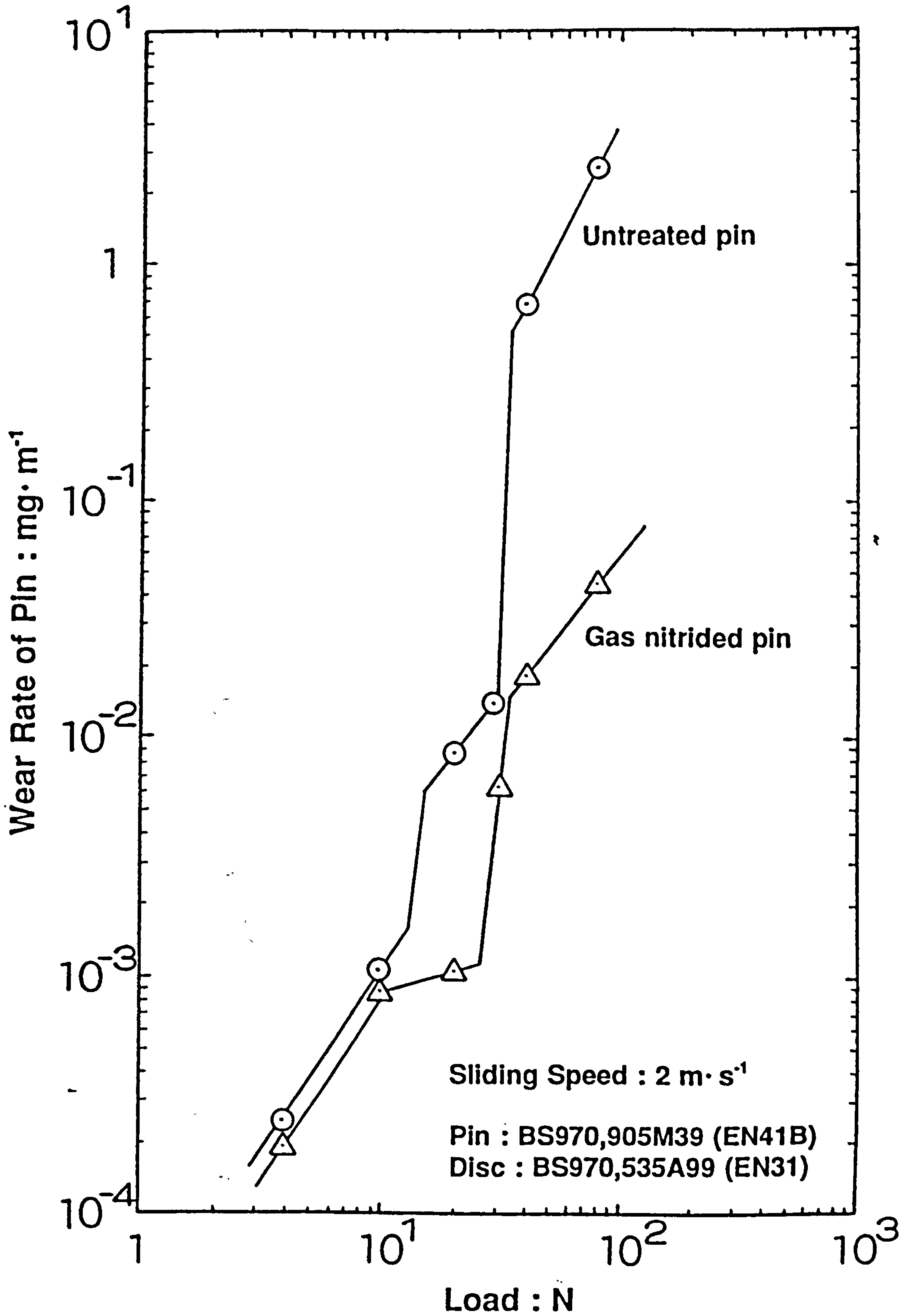

Fig.4.22 Wear rate of untreated and gas nitrided BS970,905M39 (EN41B) pins plotted against test load for a sliding speed of 2 $m \cdot s^{-1}$

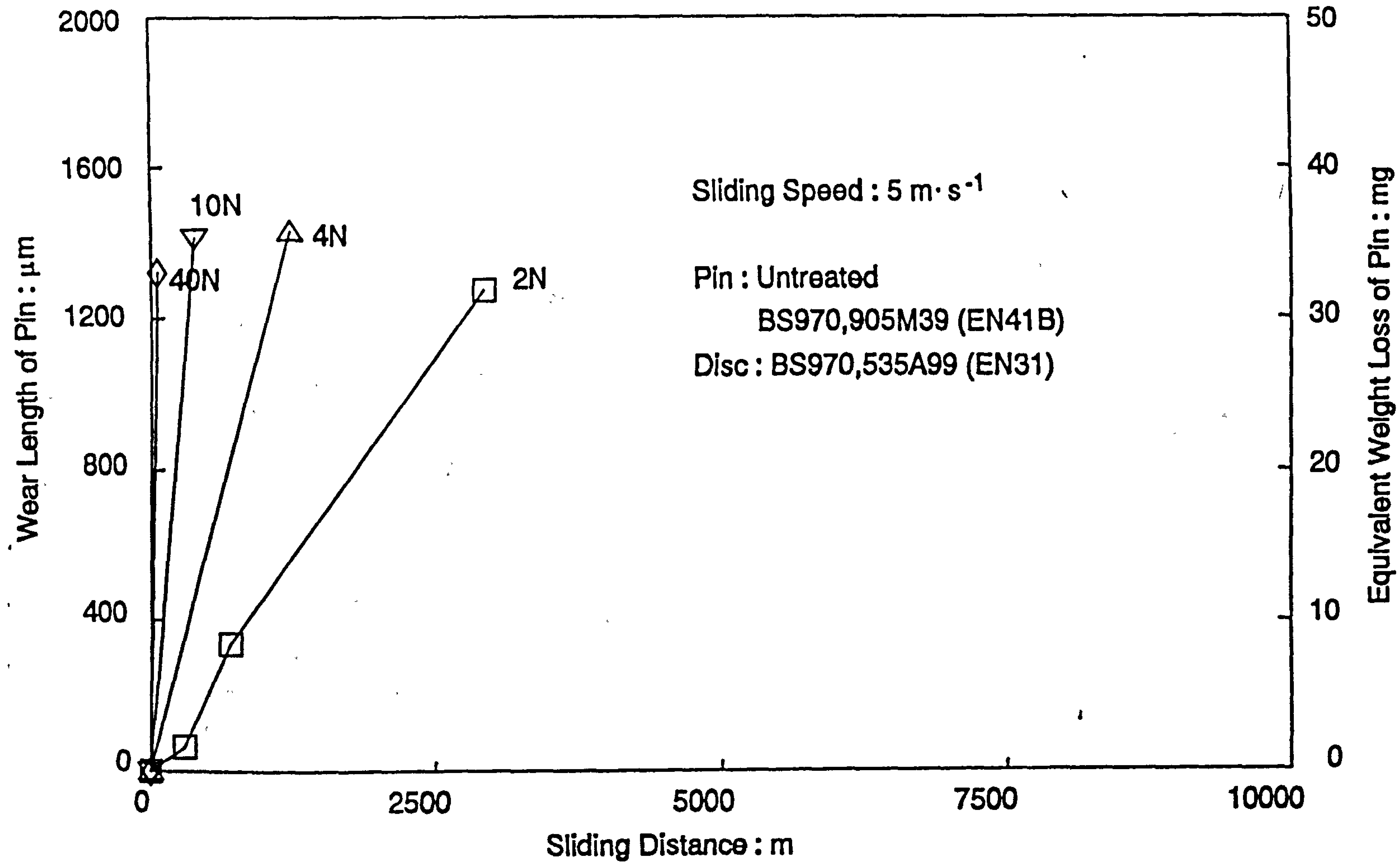

Fig.4.23 (a) Relationship between wear length of untreated BS970,905M39 (EN41B) pin and sliding distance at a sliding speed of 5 $m \cdot s^{-1}$

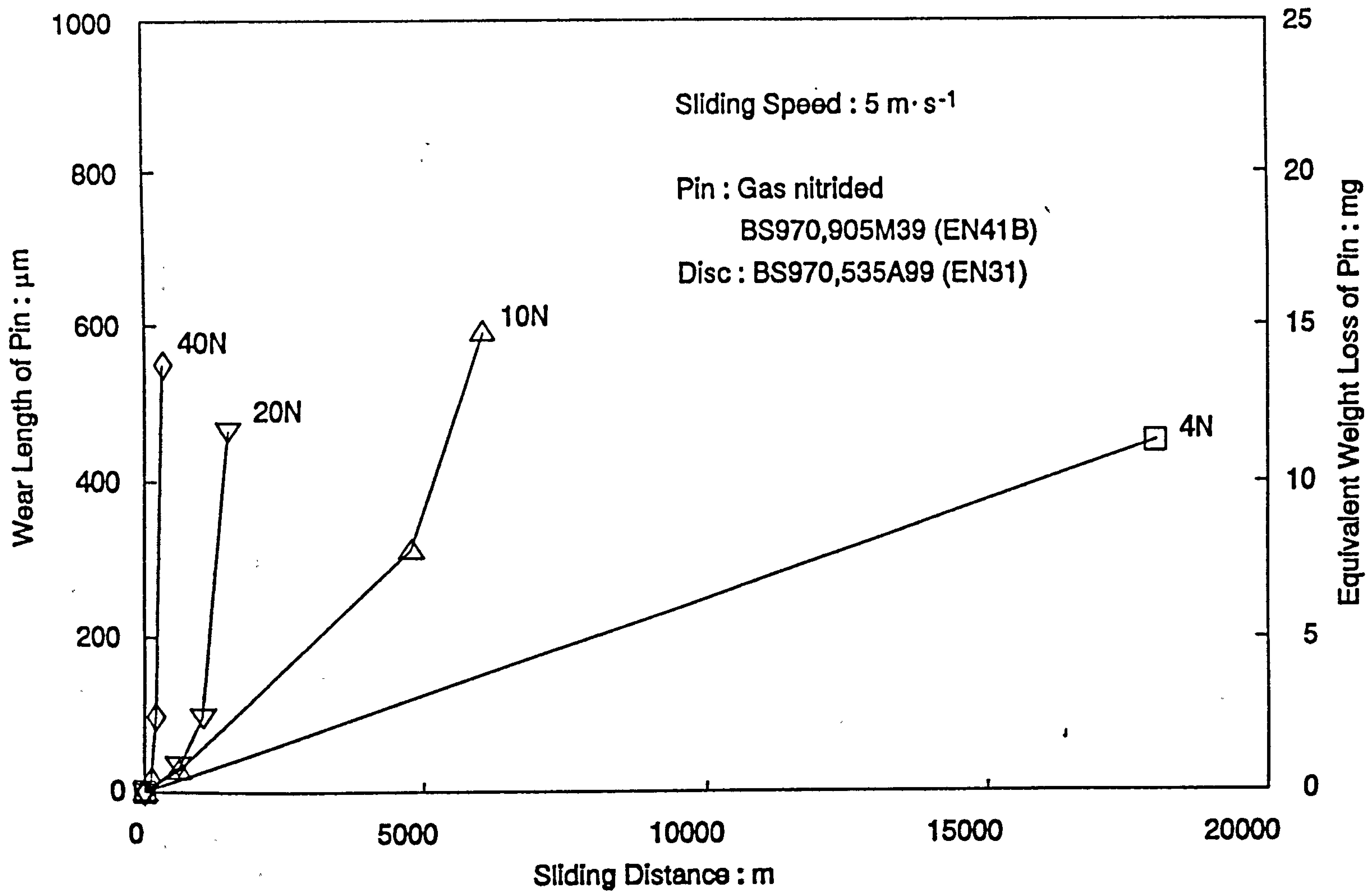

Fig.4.23 (b) Relationship between wear length of gas nitrided BS970,905M39 (EN41B) pin and sliding distance at a sliding speed of 5 $m \cdot s^{-1}$

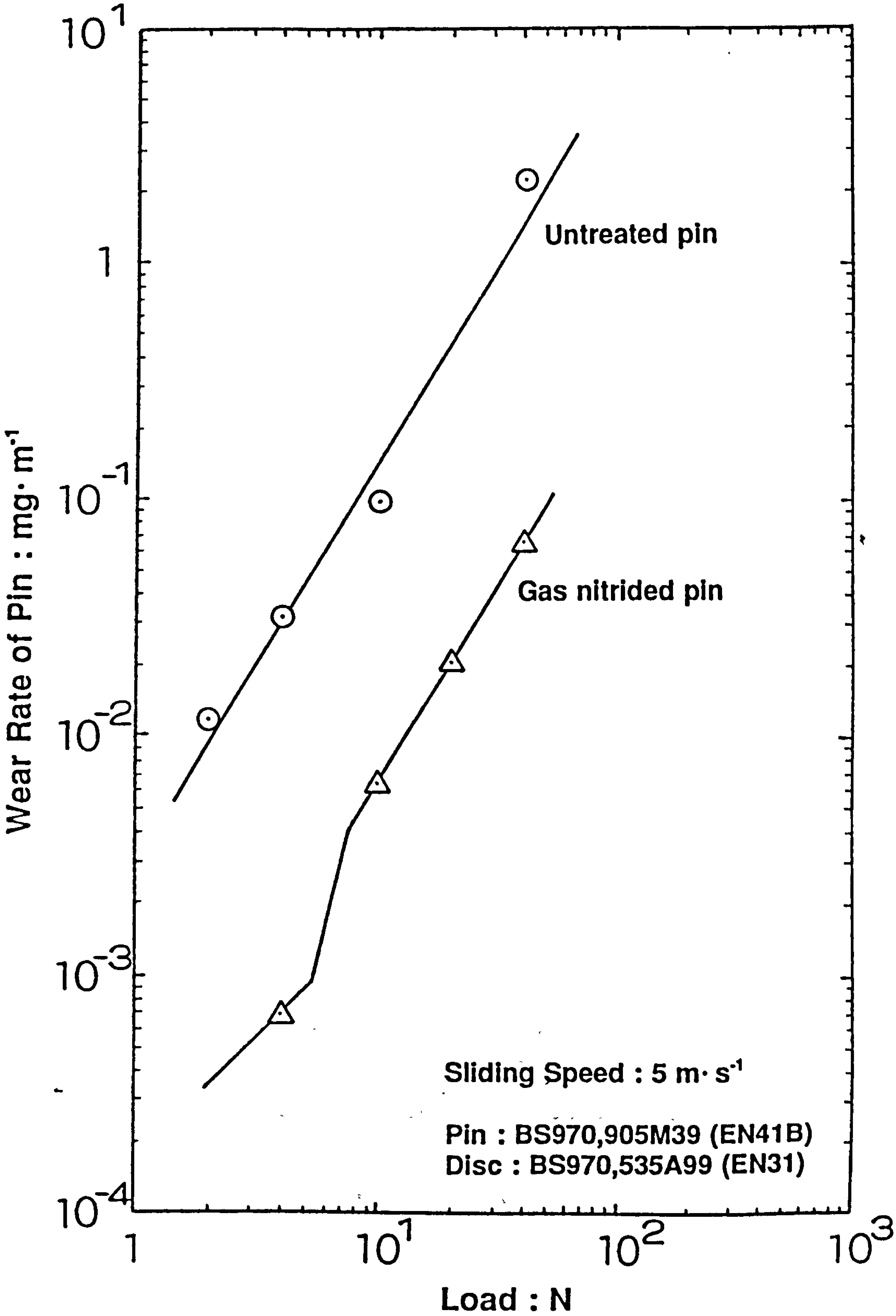

Fig.4.24 Wear rate of untreated and gas nitrided BS970,905M39 (EN41B) pins plotted against test load for a sliding speed of 5 $m \cdot s^{-1}$

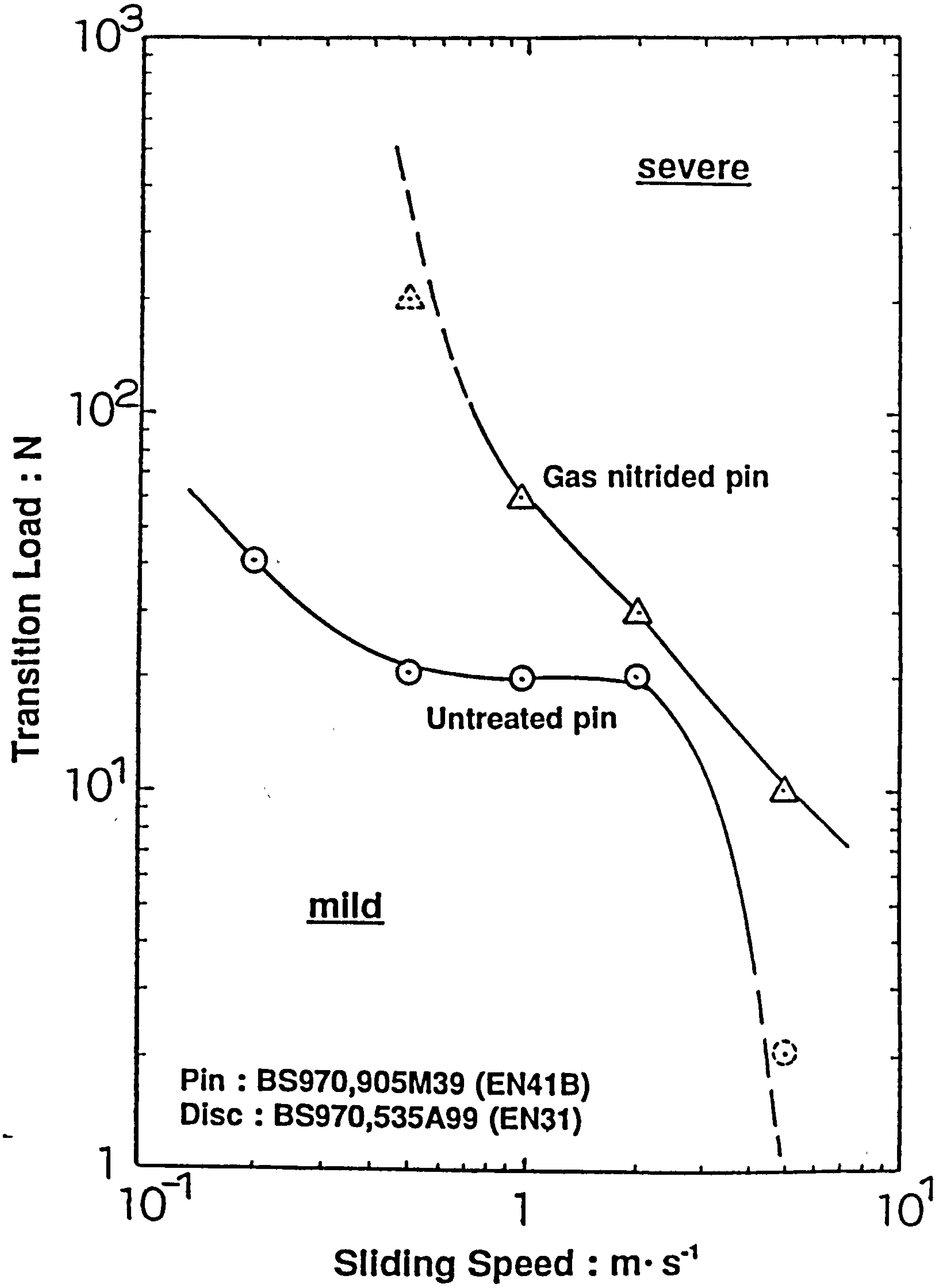

Fig.4.25 T_1 transition load plotted against sliding speed for untreated and gas nitrided BS970,905M39 (EN41B) pins

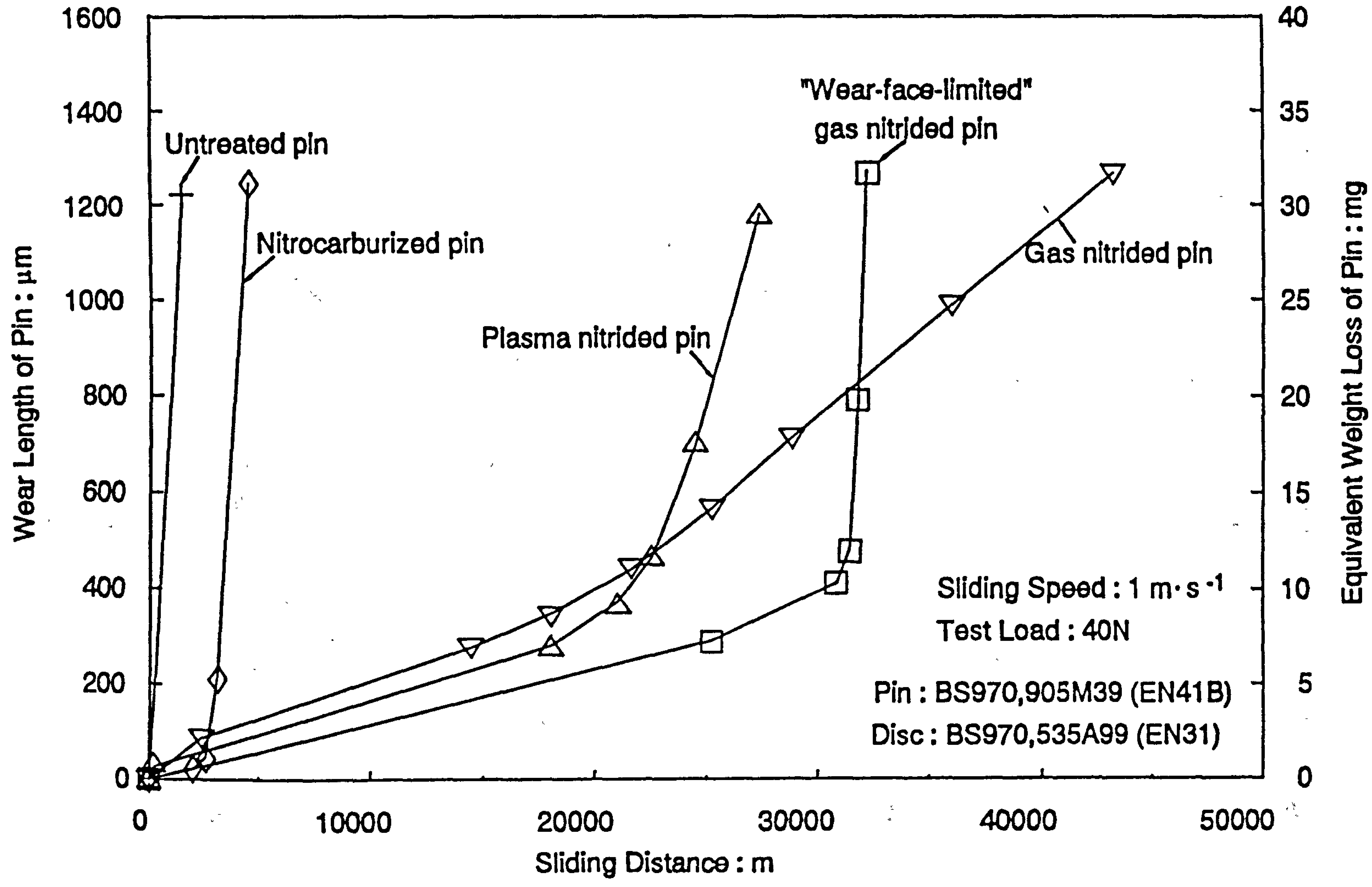

Fig.4.26 Wear through surface hardened layer for variously surface treated BS970,905M39 (EN41B) pins (sliding speed: 1 $m \cdot s^{-1}$, test load: 40 N)

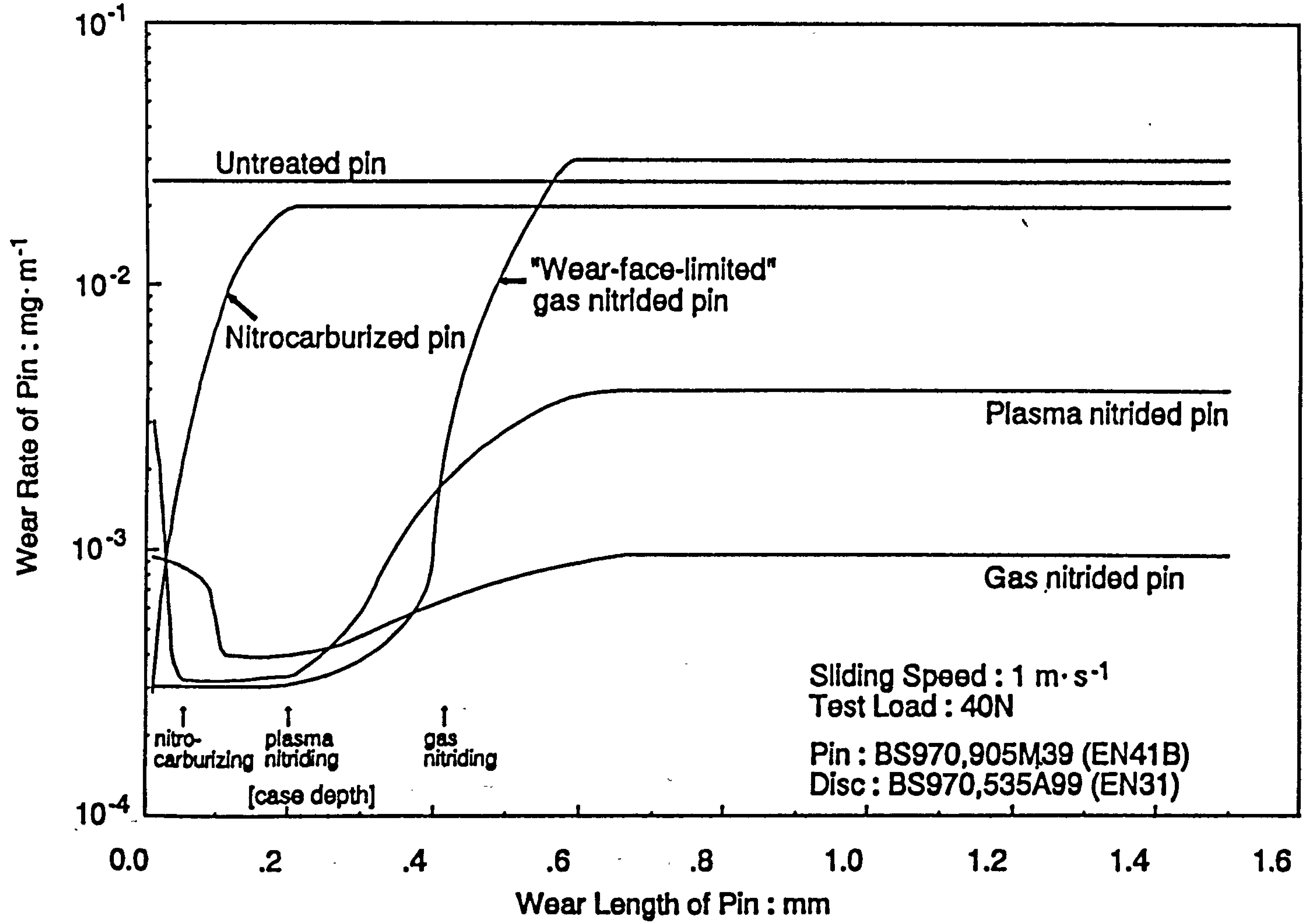

Fig.4.27 Variation of wear rate of pin through surface hardened layer for variously surface treated BS970,905M39 (EN41B) pins (sliding speed: 1 $m \cdot s^{-1}$, test load: 40 N)

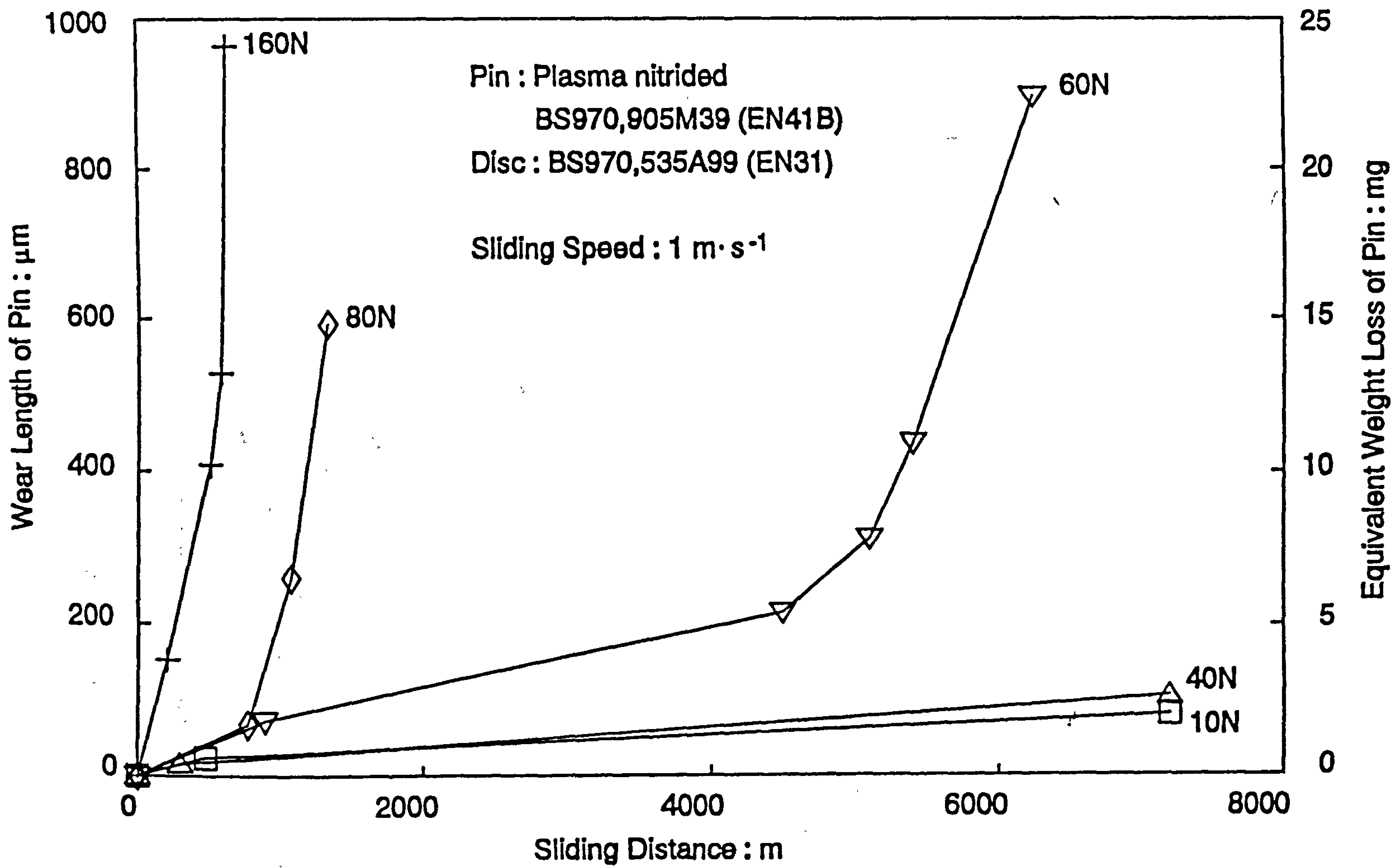

Fig.4.28 Relationship between wear length of plasma nitrided BS970,905M39 (EN41B) pin and sliding distance (sliding speed: 1 $m \cdot s^{-1}$)

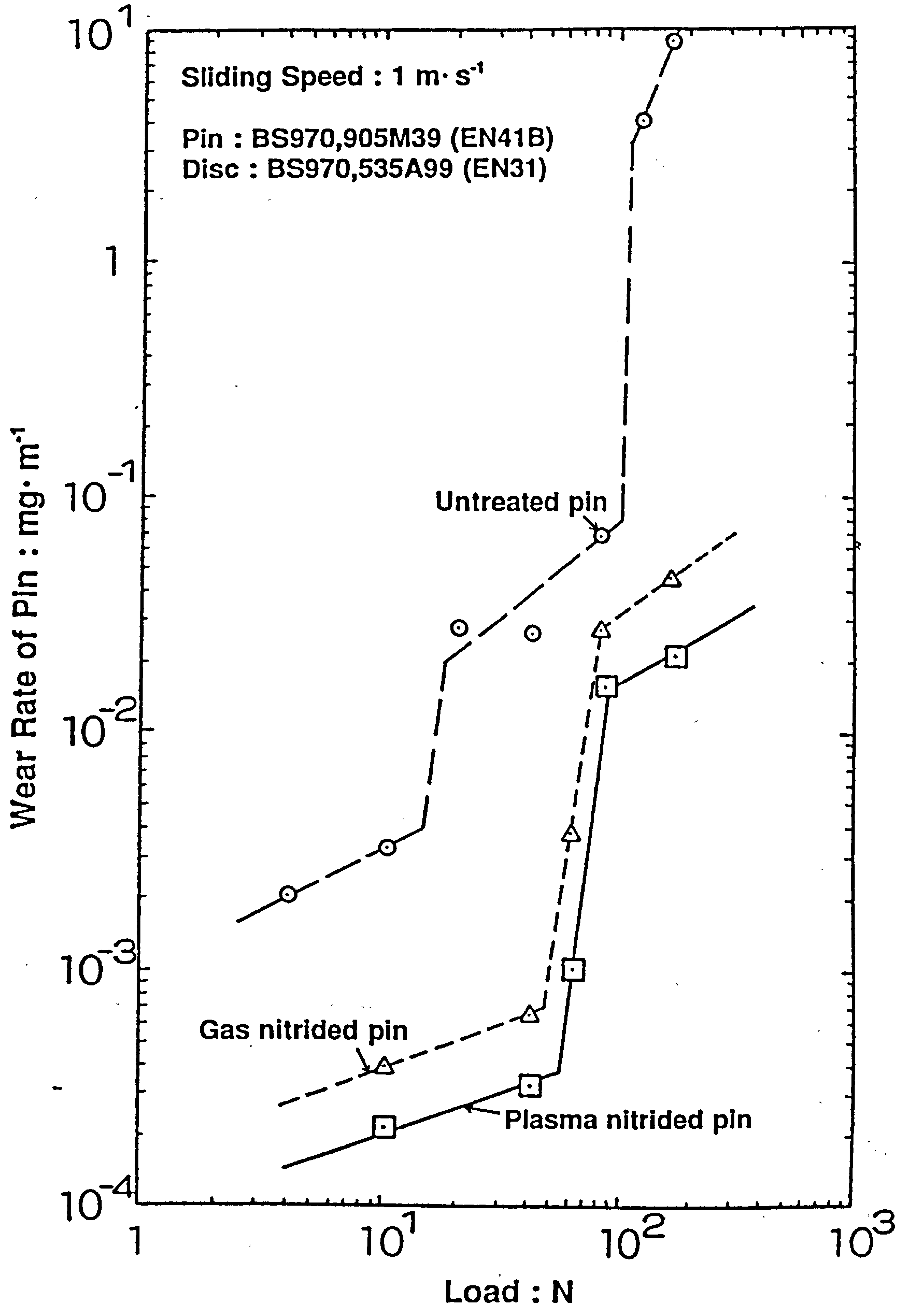

Fig.4.29 Wear rate of plasma nitrided BS970,905M39 (EN41B) pin plotted against test load (sliding speed: 1 $m \cdot s^{-1}$)

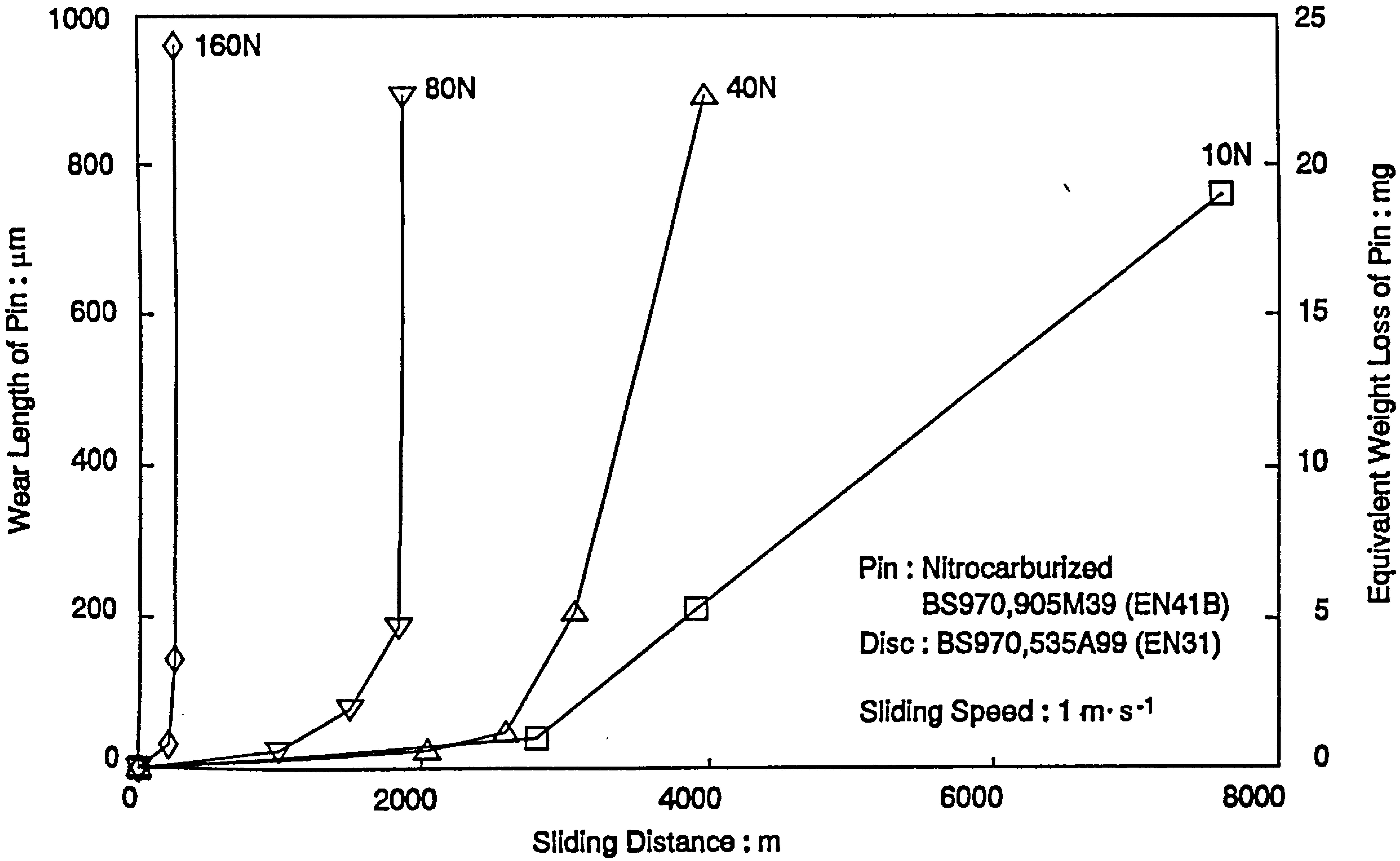

Fig.4.30 Relationship between wear length of nitrocarburized BS970,905M39 (EN41B) pin and sliding distance (sliding speed: $1\ m\cdot s^{-1}$)

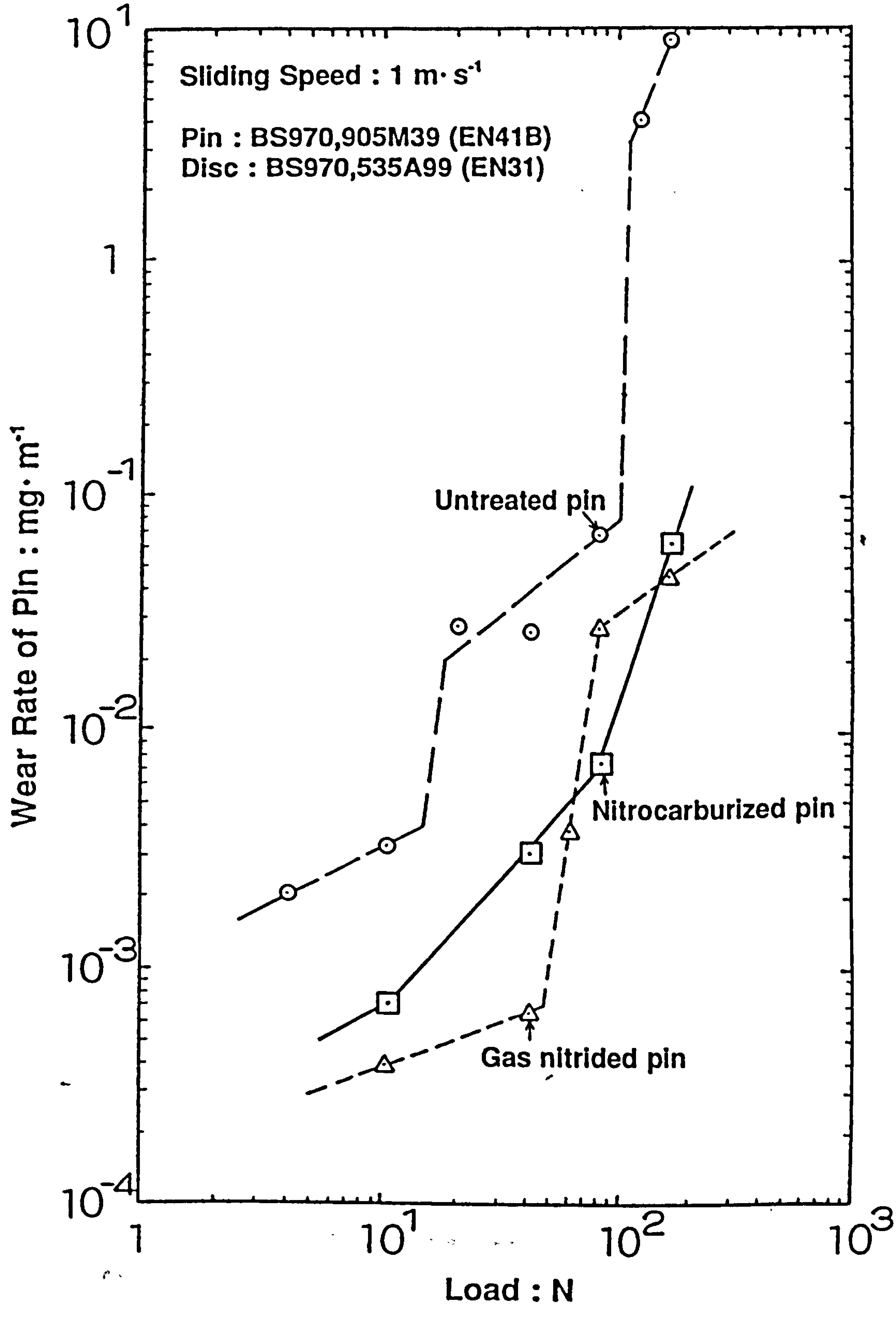

Fig.4.31 Wear rate of nitrocarburized BS970,905M39 (EN41B) pin plotted against test load (sliding speed: 1 m·s^{-1})

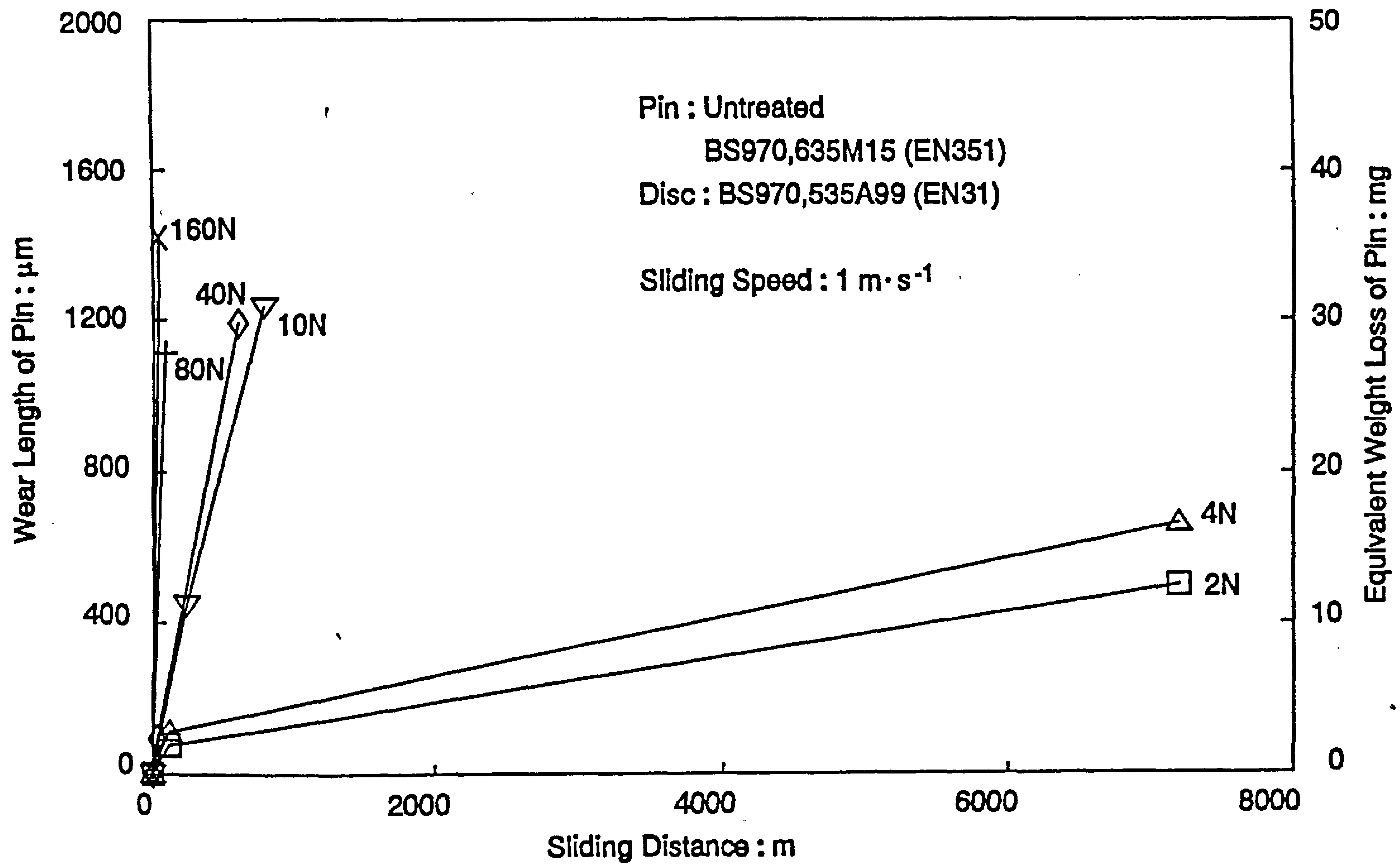

Fig.4.32 (a) Relationship between wear length of untreated BS970,635M15 (EN351) pin and sliding distance (sliding speed: 1 $m \cdot s^{-1}$)

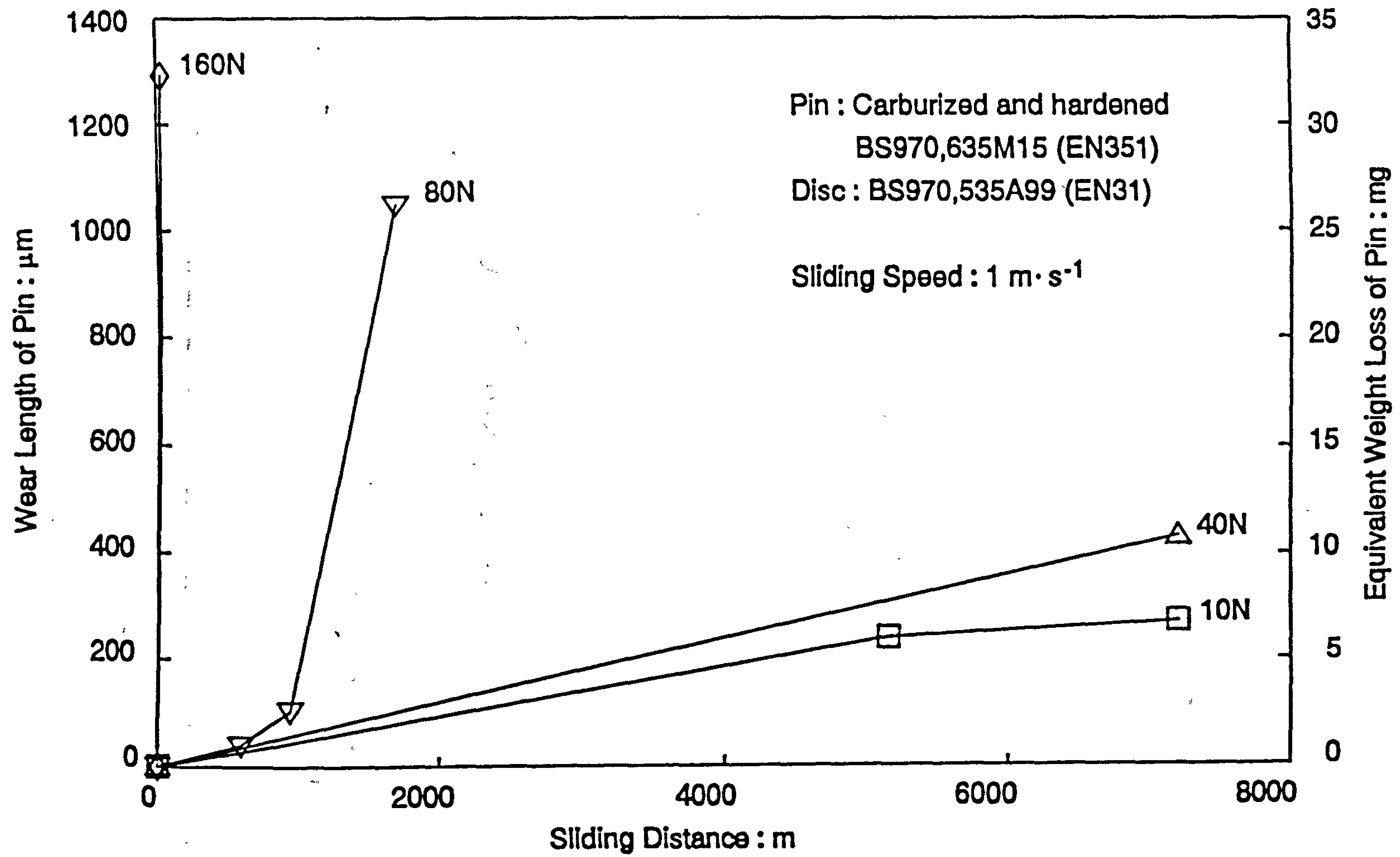

Fig.4.32 (b) Relationship between wear length of carburized and hardened BS970,635M15 (EN351) pin and sliding distance (sliding speed: 1 $m \cdot s^{-1}$)

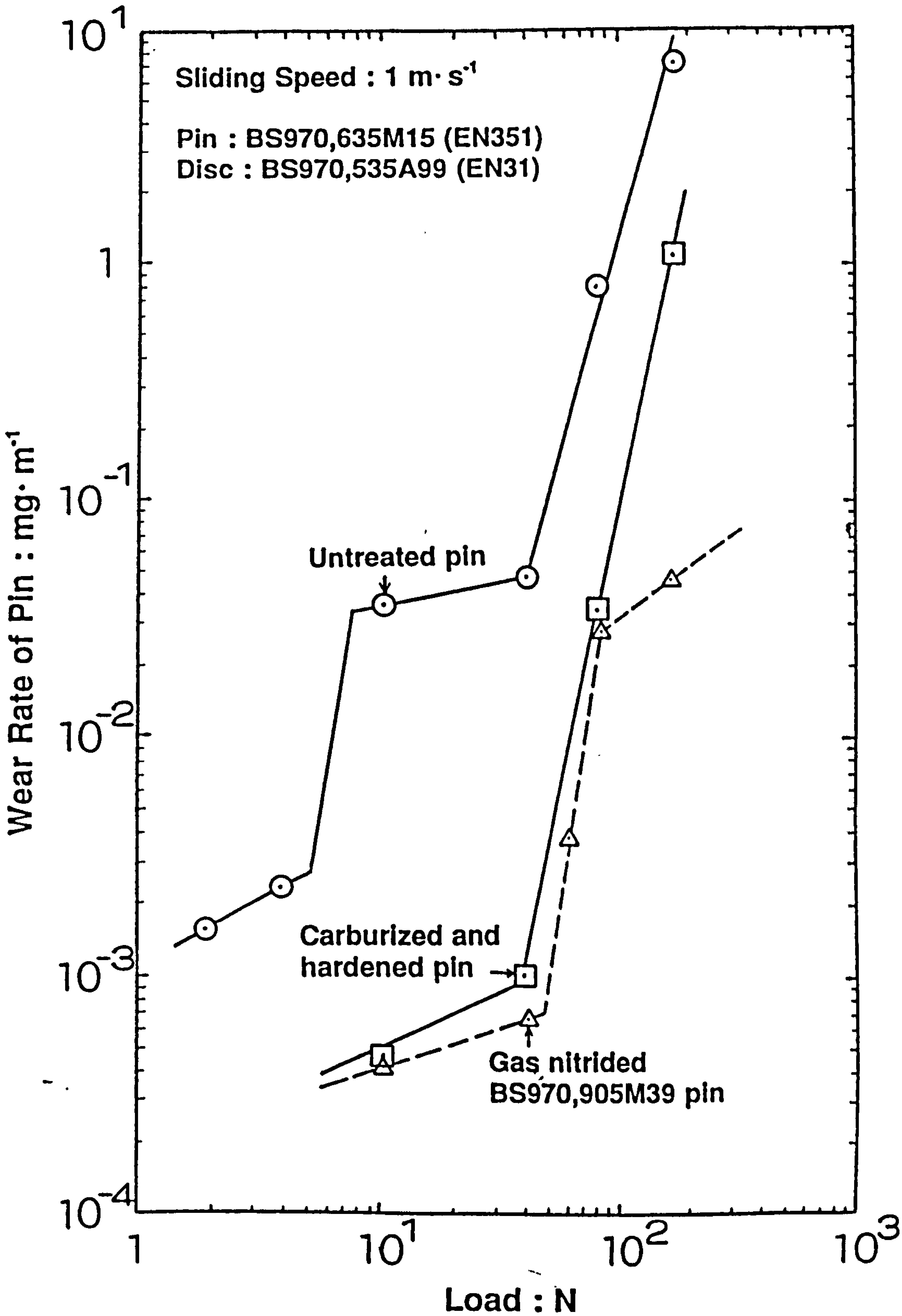

Fig.4.33 Wear rate of untreated, and carburized-and-hardened BS970,635M15 (EN351) pins plotted against test load (sliding speed: 1 $m \cdot s^{-1}$)

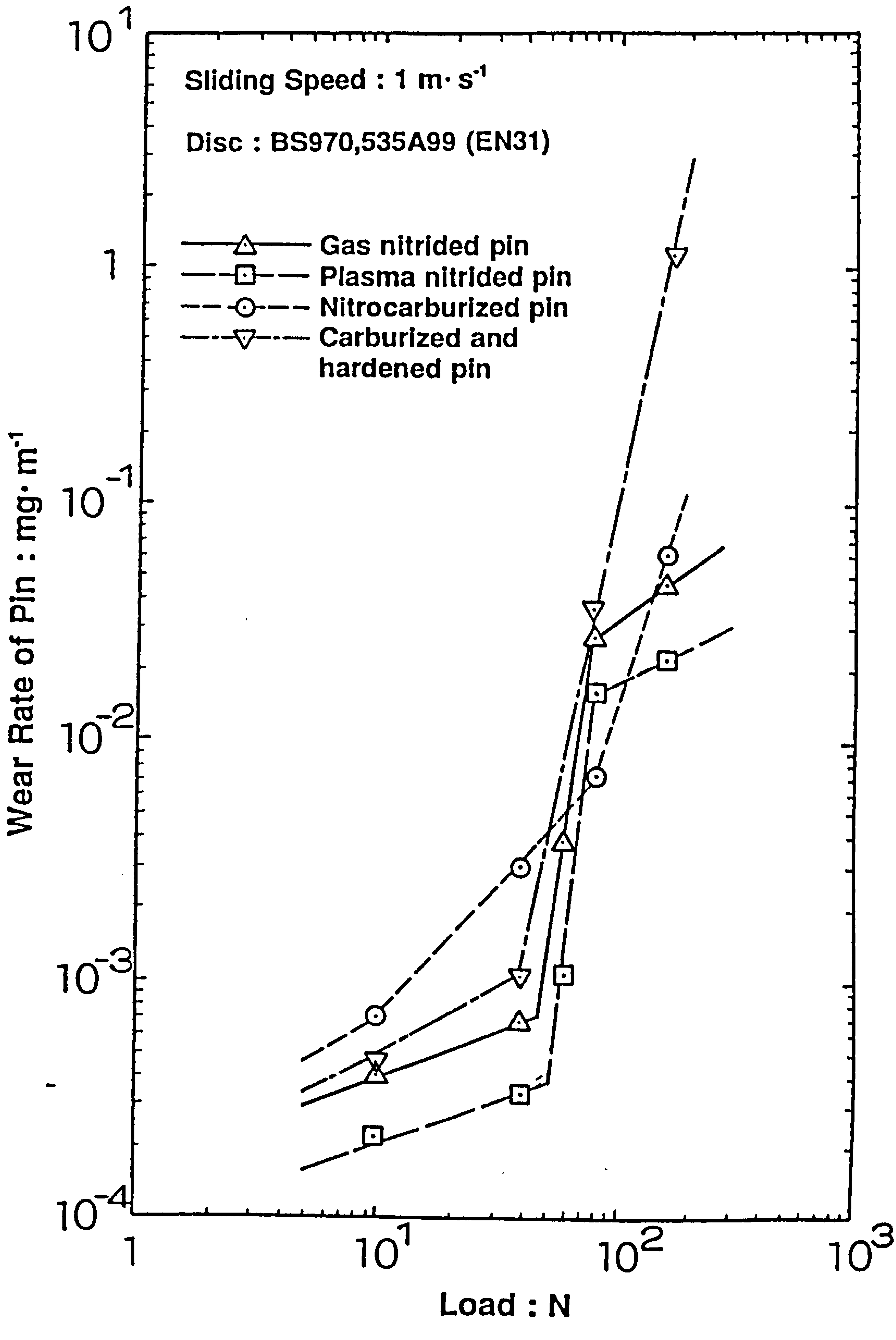

Fig.4.34 Comparison of wear rate of pin between surface treatments

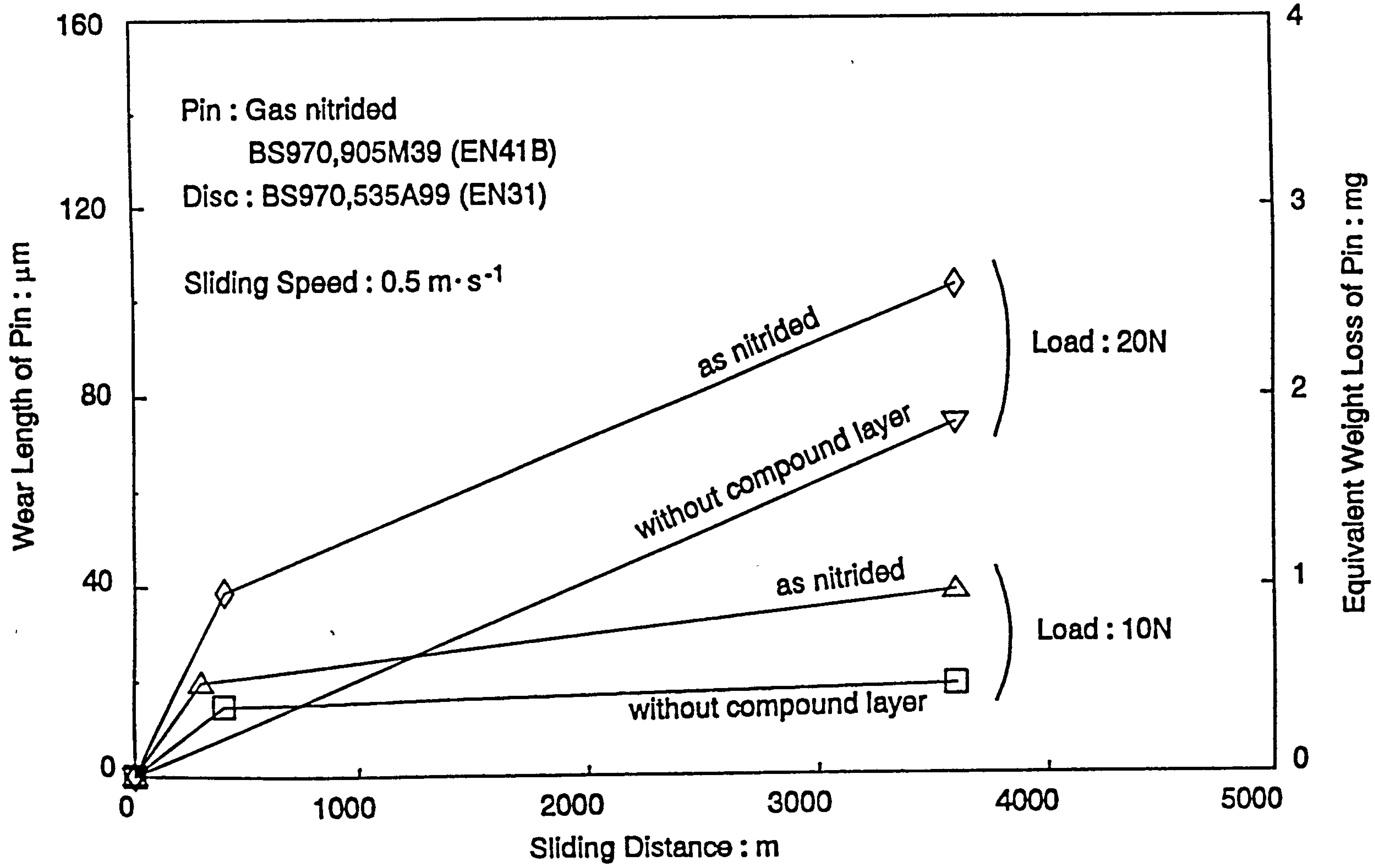

Fig.4.35 Effect of presence of compound layer on wear behaviour of gas nitrided BS970,905M39 (EN41B) pin

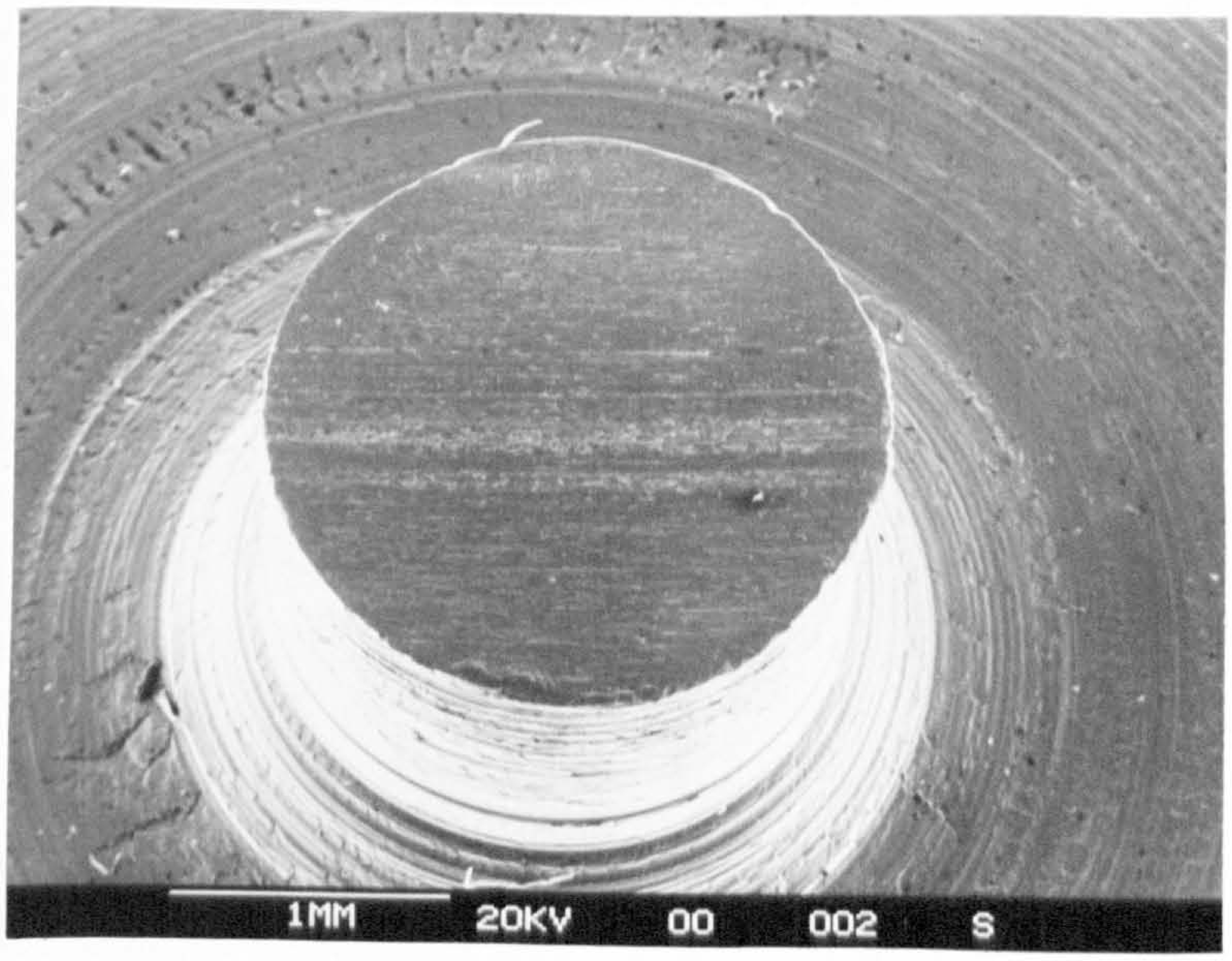

(a)

sliding direction of disc →

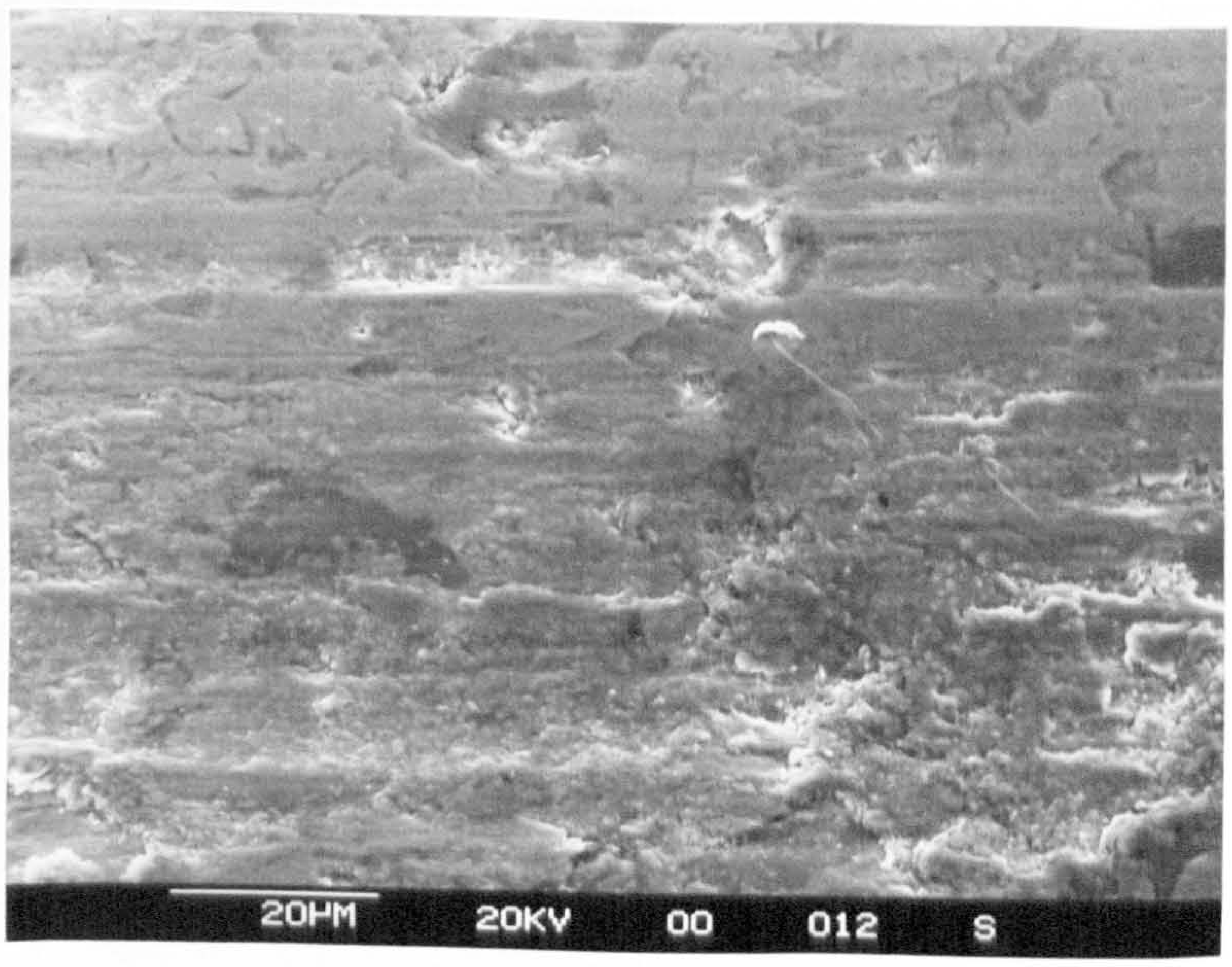

(b)

Fig.4.36 SEM of worn surface of untreated BS970,905M39 (EN41B) pin, tested in mild wear regime (sliding speed: 1 $m \cdot s^{-1}$, test load: 4 N)
(a) x22 **(b)** x800

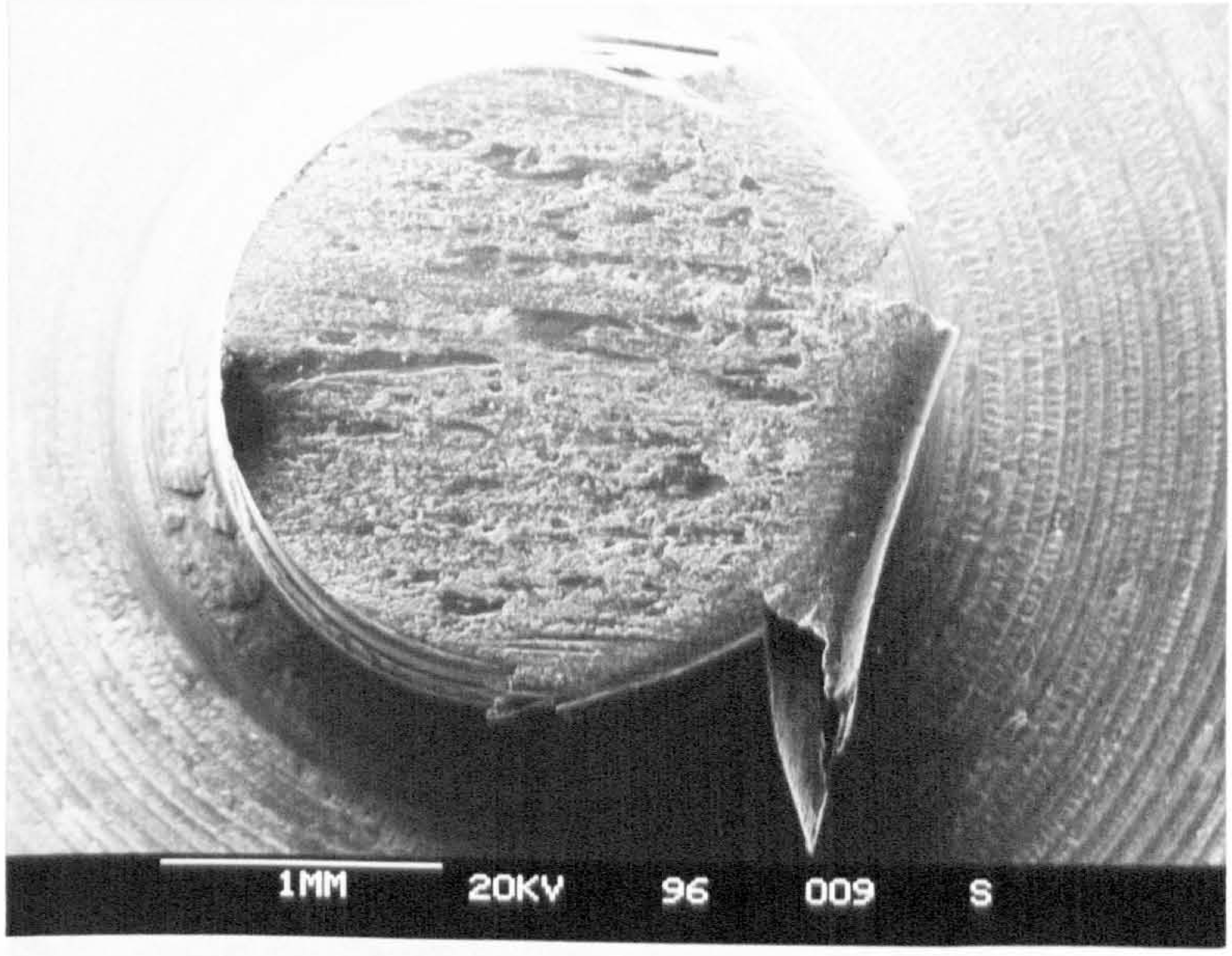

sliding direction of disc →

(a)

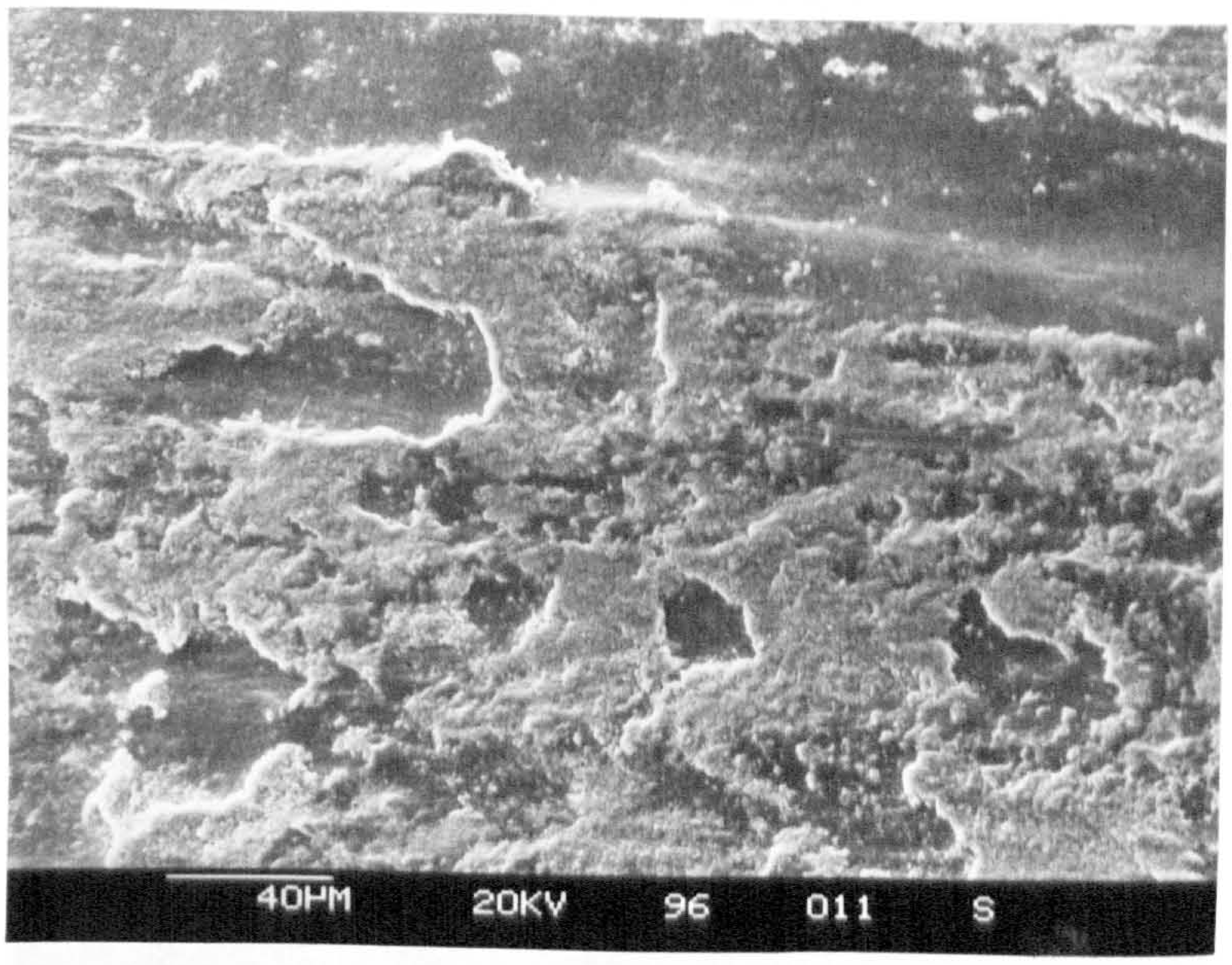

(b)

Fig.4.37 SEM of worn surface of untreated BS970,905M39 (EN41B) pin, tested in severe wear regime (sliding speed: 0.5 $m \cdot s^{-1}$, test load: 40 N)
(a) x22 **(b)** x320

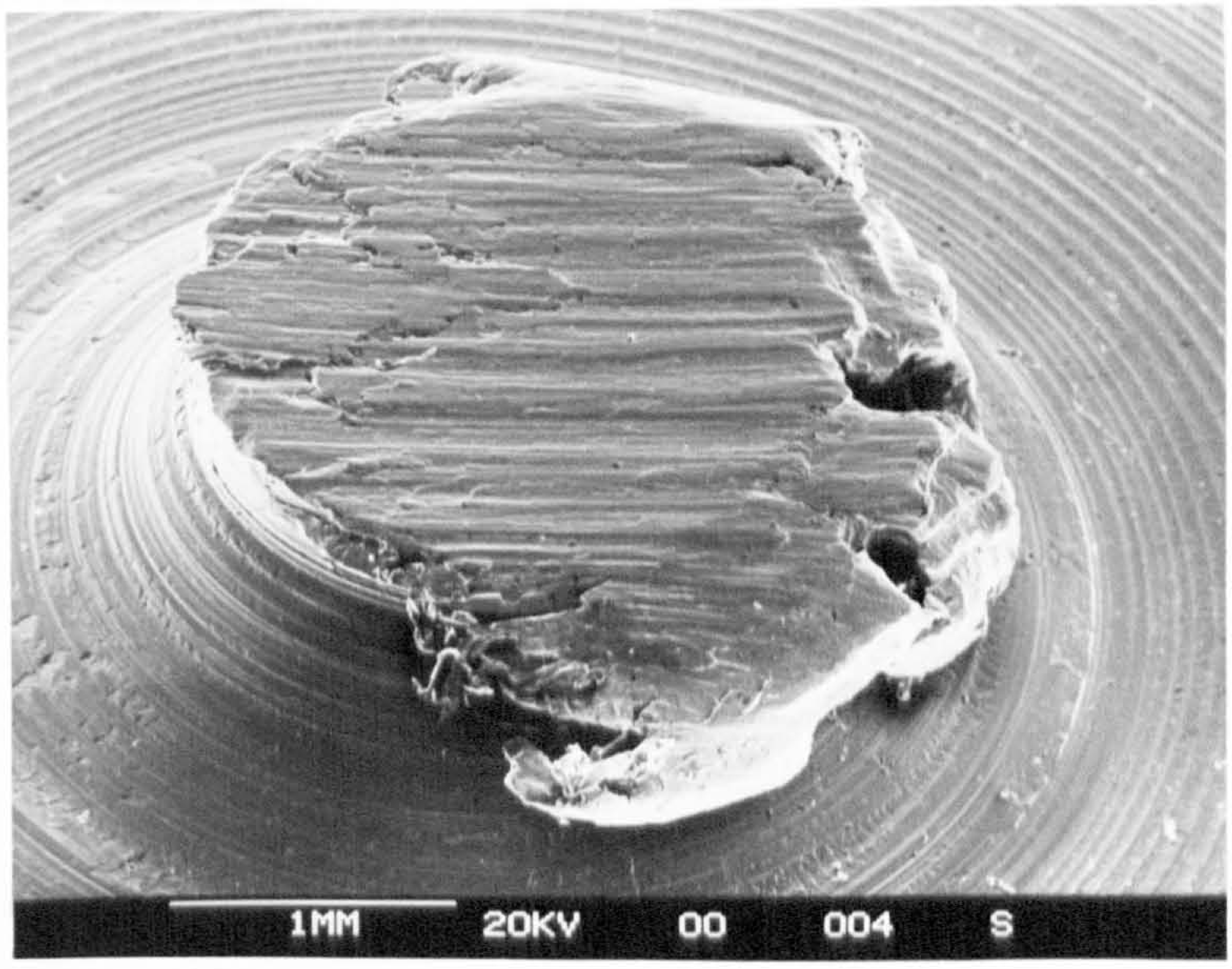

sliding
direction
of disc
→

(a)

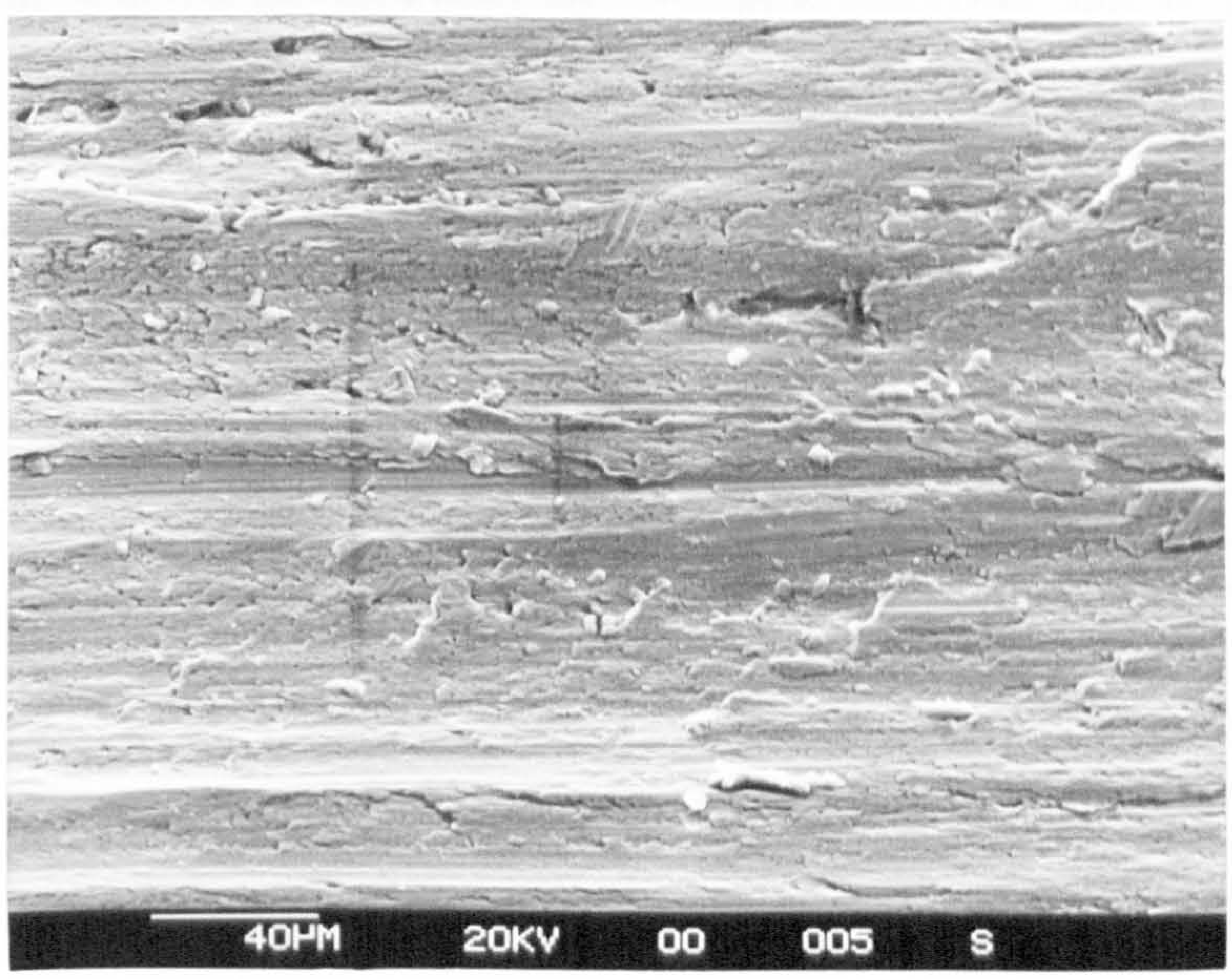

(b)

Fig.4.38 SEM of worn surface of <u>untreated</u> BS970,905M39 (EN41B) pin, tested in <u>extremely-severe</u> wear regime (sliding speed: 1 $m \cdot s^{-1}$, test load: 160 N)
(a) x22 **(b)** x320

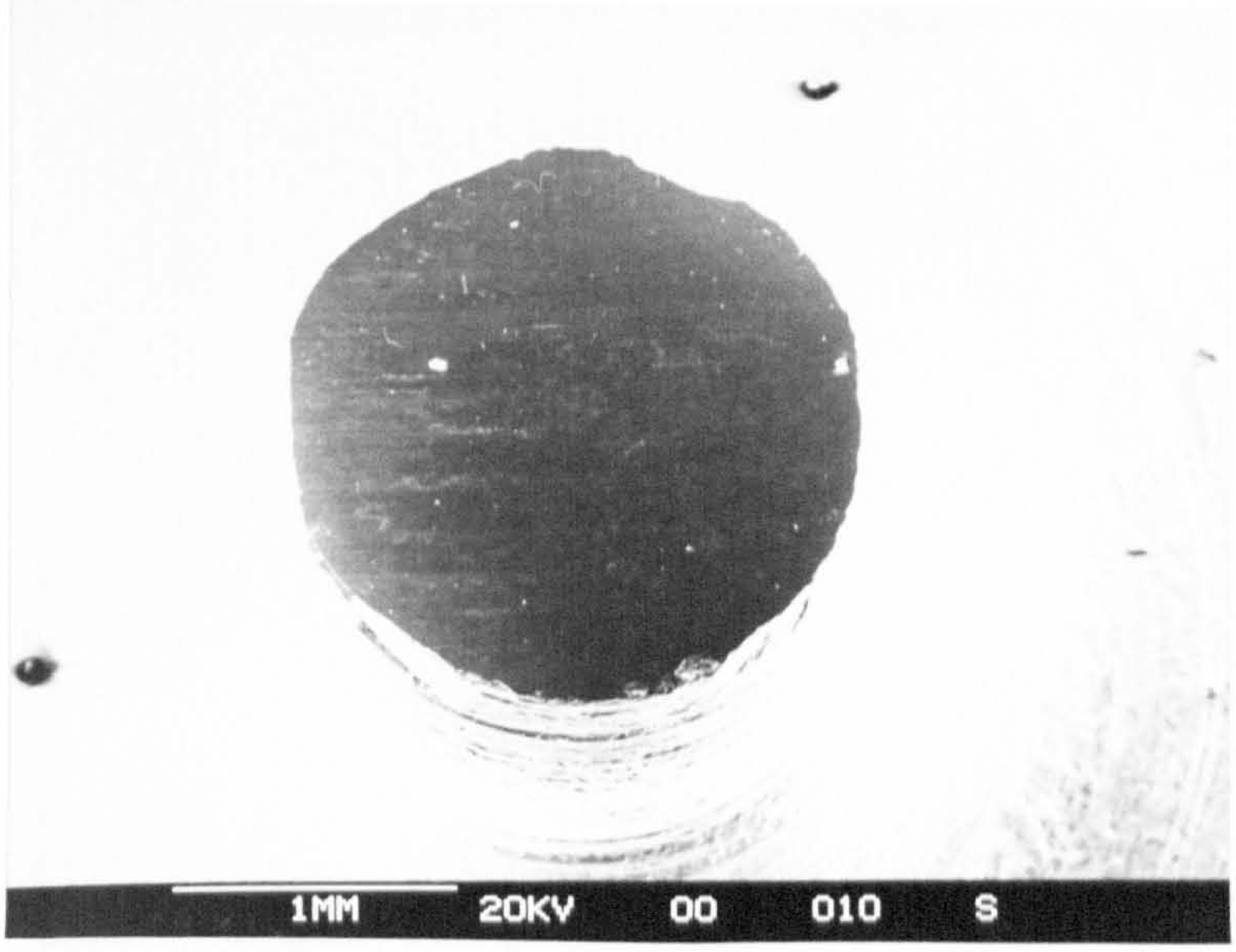

sliding direction of disc →

(a)

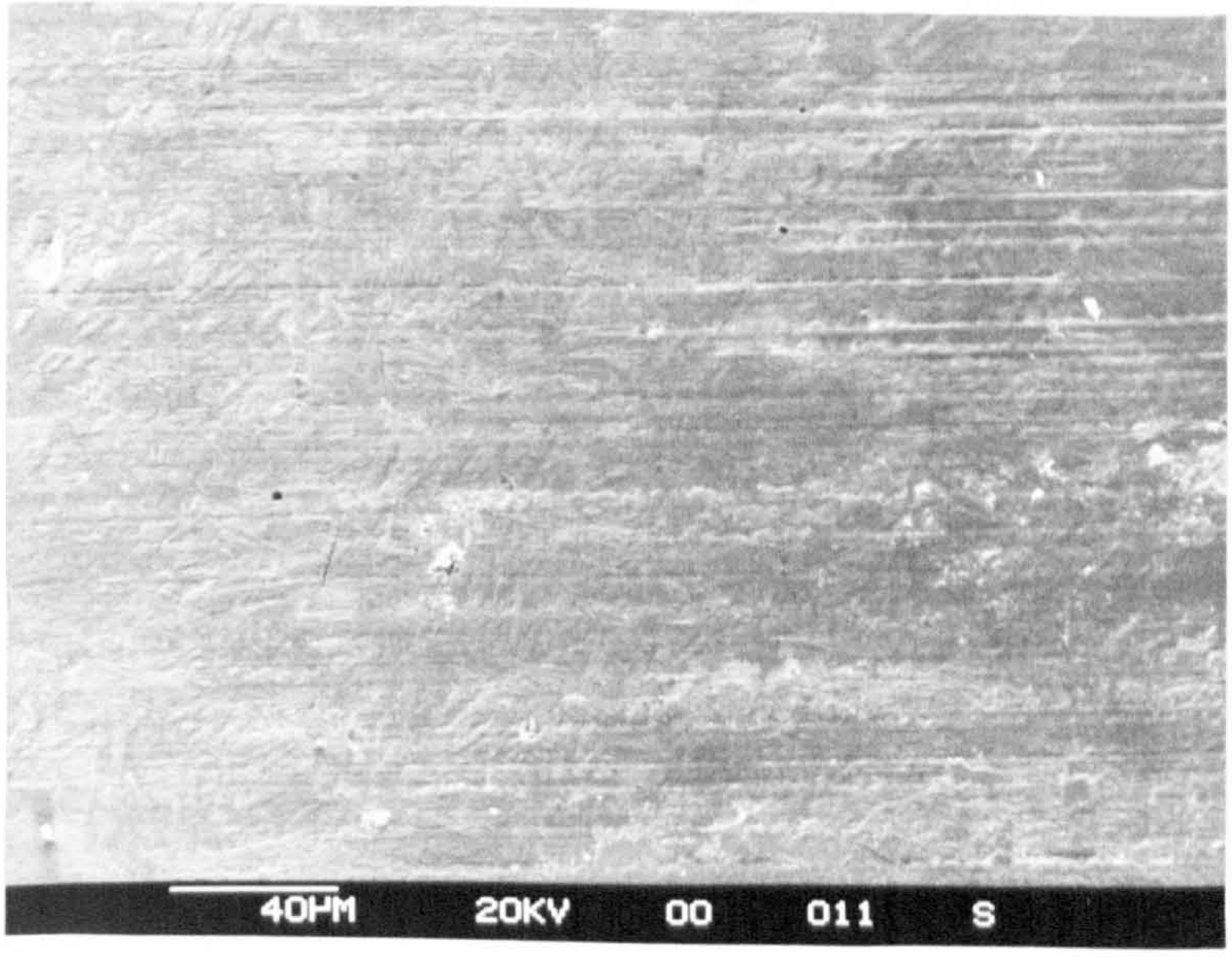

(b)

Fig.4.39 SEM of worn surface of gas nitrided BS970,905M39 (EN41B) pin, tested in mild wear regime (sliding speed: 1 $m\cdot s^{-1}$, test load: 10 N)
(a) x22 **(b)** x320

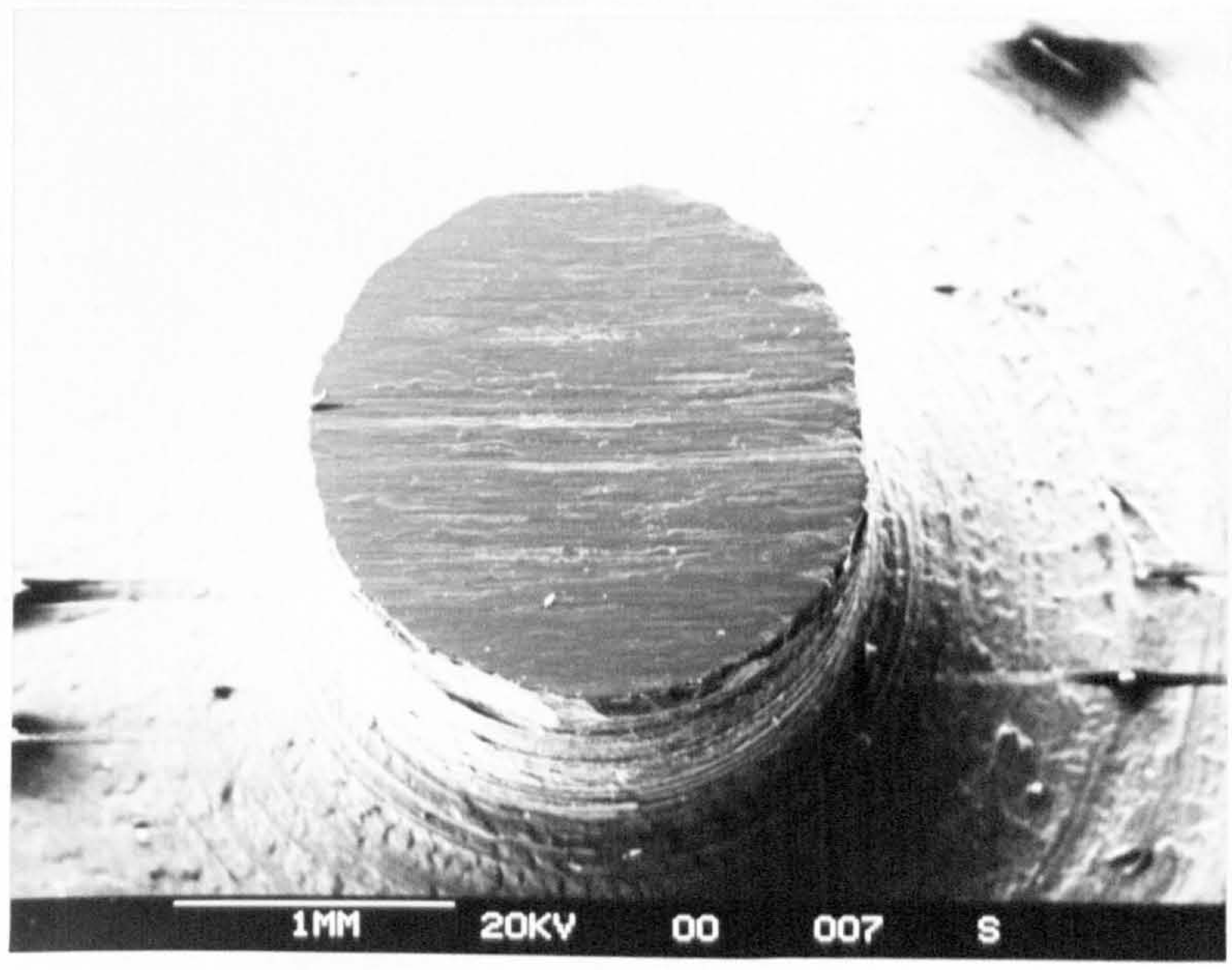

sliding
direction
of disc
→

(a)

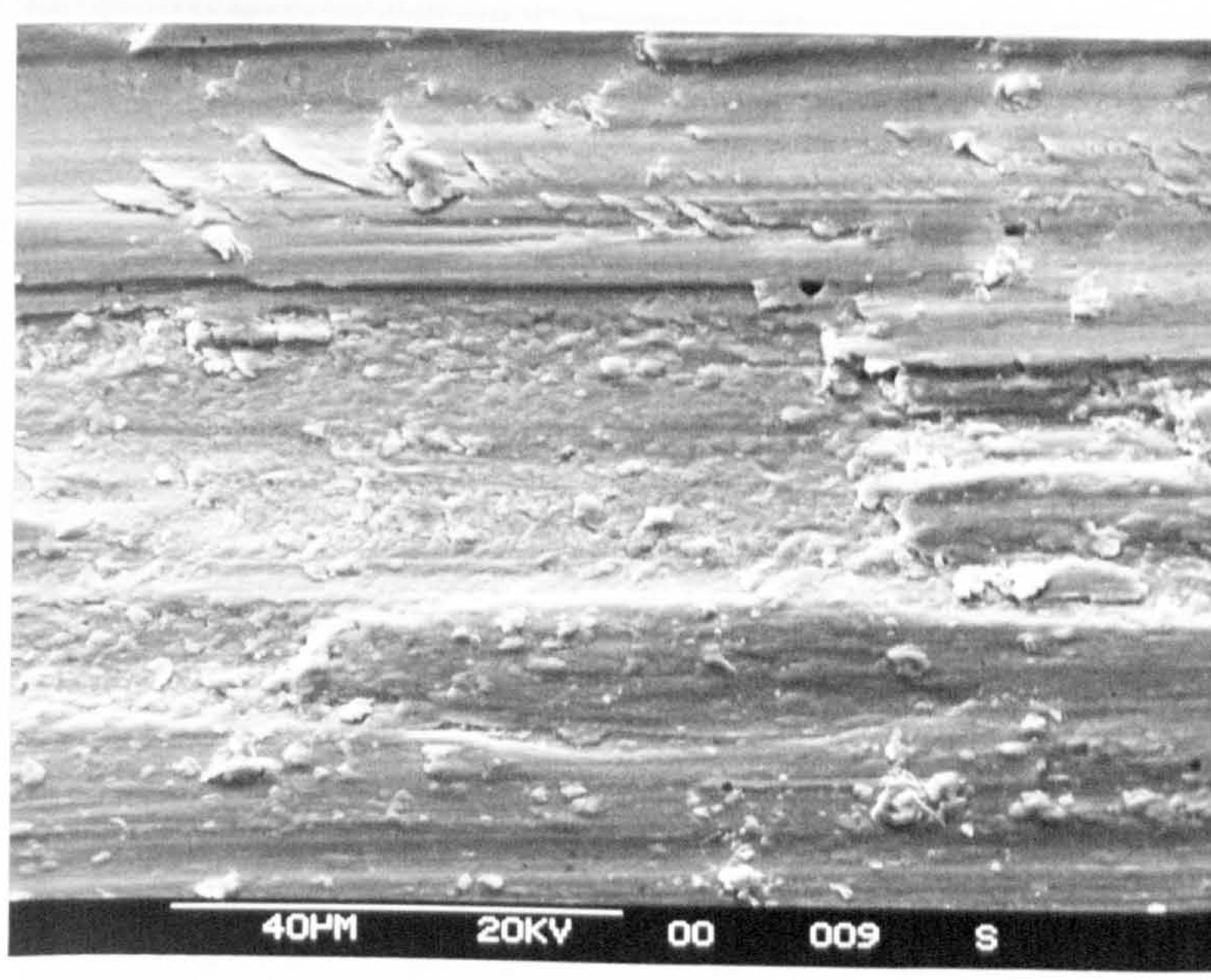

(b)

Fig.4.40 SEM of worn surface of gas nitrided BS970,905M39 (EN41B) pin, tested in severe wear regime (sliding speed: $1\ m \cdot s^{-1}$, test load: 160 N)
(a) x22 **(b)** x800

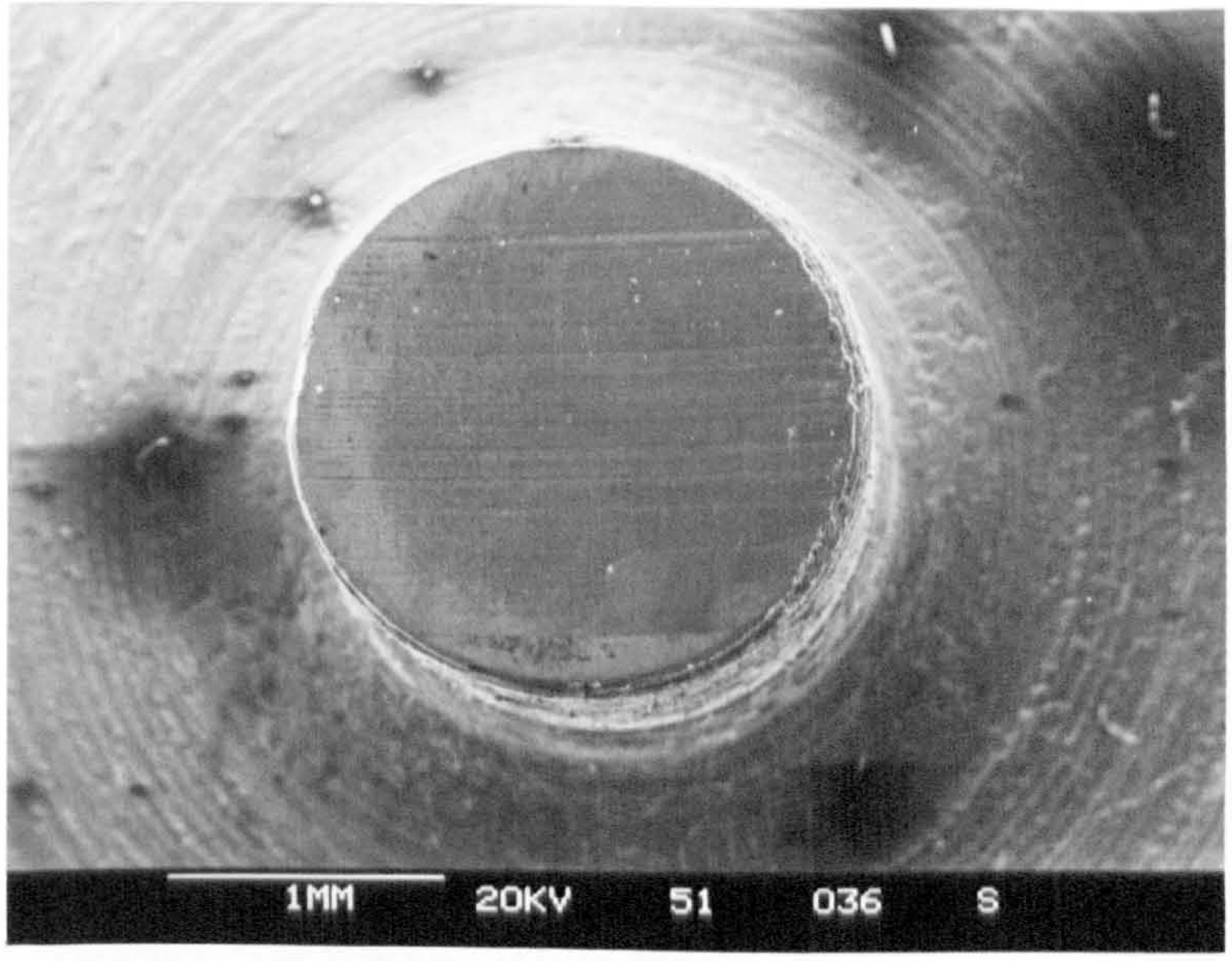

sliding direction of disc →

(a)

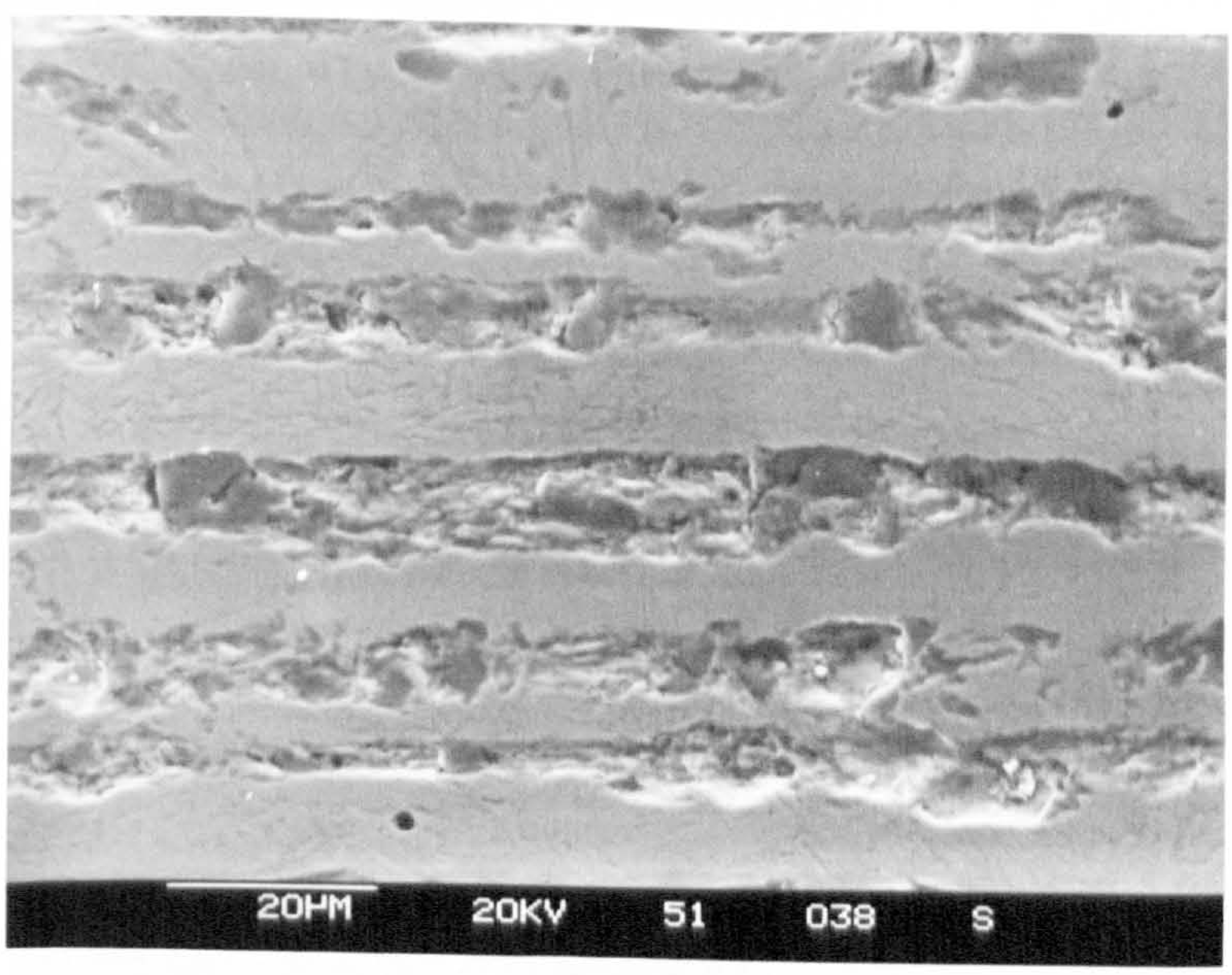

(b)

Fig.4.41 SEM of worn surface of gas nitrided BS970,905M39 (EN41B) pin. The wear test was stopped at a pin wear length within the compound layer depth. (sliding speed: 0.5 $m\cdot s^{-1}$, test load: 10 N, sliding distance: 1800m, pin wear length: 26 µm)
(a) x22 **(b)** x3500

sliding direction of disc

→

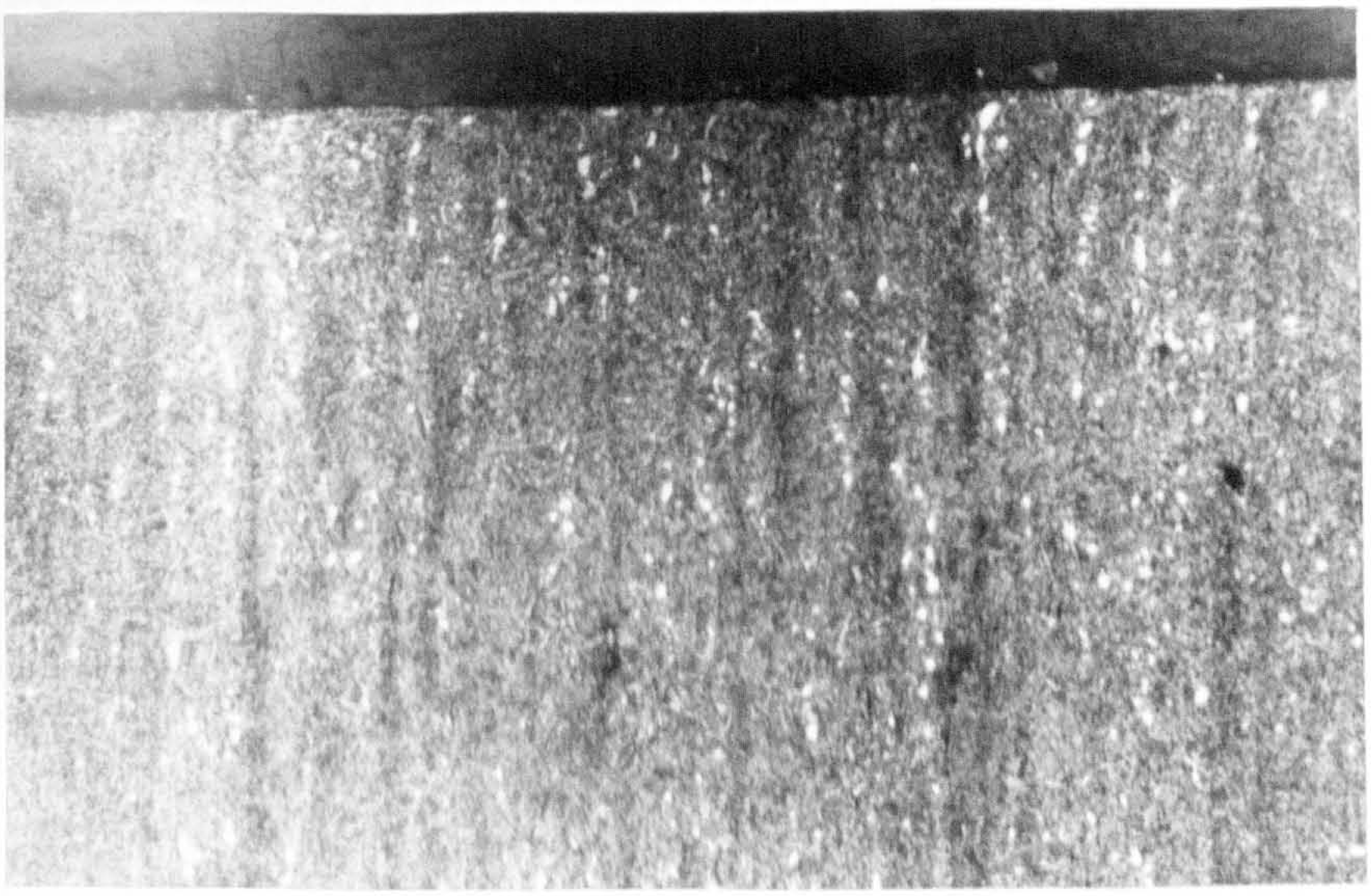

(a) 100μm

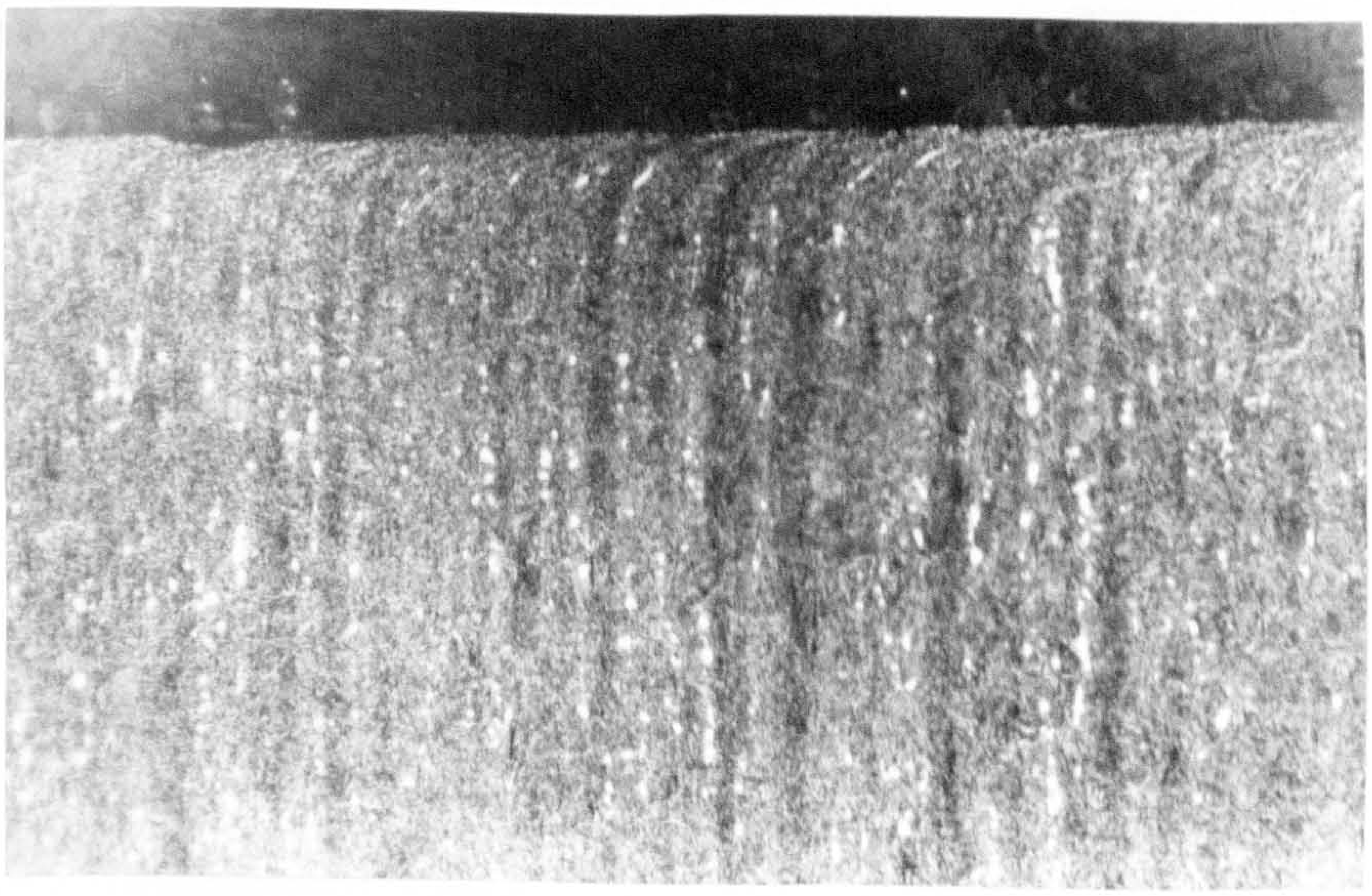

(b) 100μm

Fig.4.42 Optical microstructure of longitudinal section normal to worn surface of untreated BS970,905M39 (EN41B) pin
(a) tested in mild wear regime (sliding speed: 0.5 $m \cdot s^{-1}$, test load: 10 N)
(b) tested in severe wear regime (sliding speed: 0.5 $m \cdot s^{-1}$, test load: 40 N)

sliding direction of disc

→

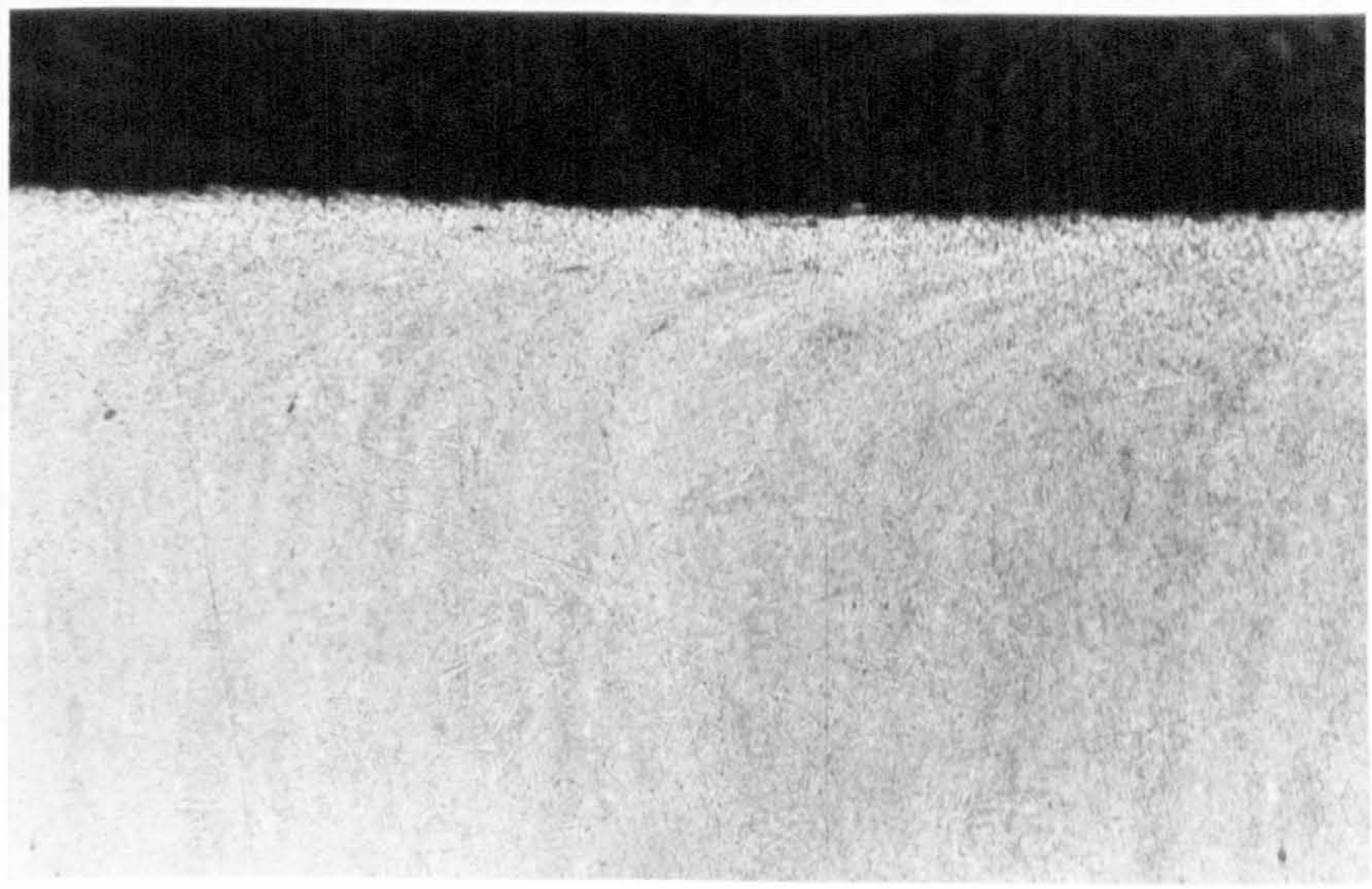

(c) 100μm

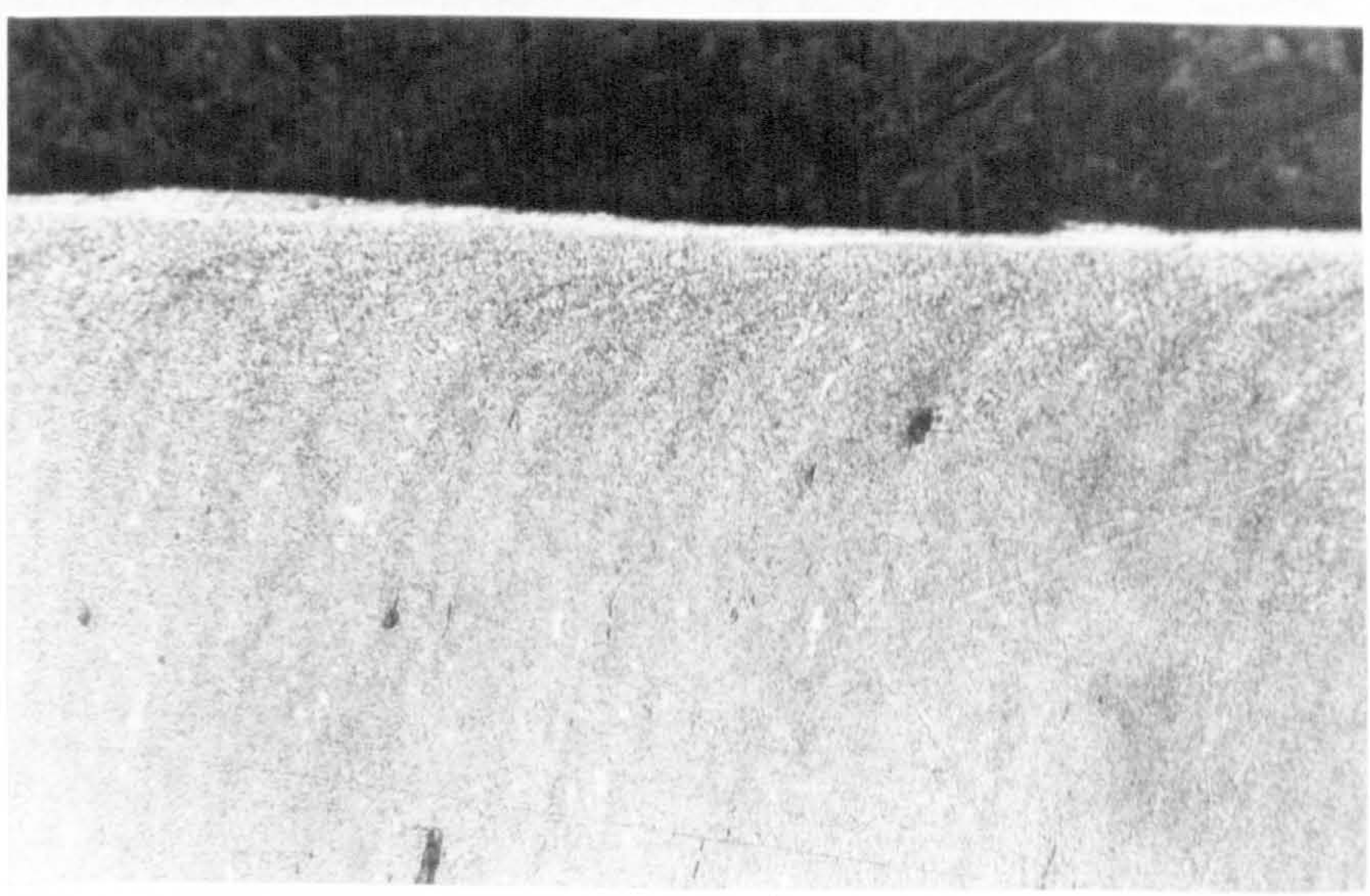

(d) 100μm

Fig.4.42 Optical microstructure of longitudinal section normal to worn surface of untreated BS970,905M39 (EN41B) pin
(c) tested in mild wear regime above T_2 (sliding speed: 0.5 $m \cdot s^{-1}$, test load: 160 N)
(d) tested in extremely-severe wear regime (sliding speed: 2 $m \cdot s^{-1}$, test load: 80 N)

sliding direction of disc

→

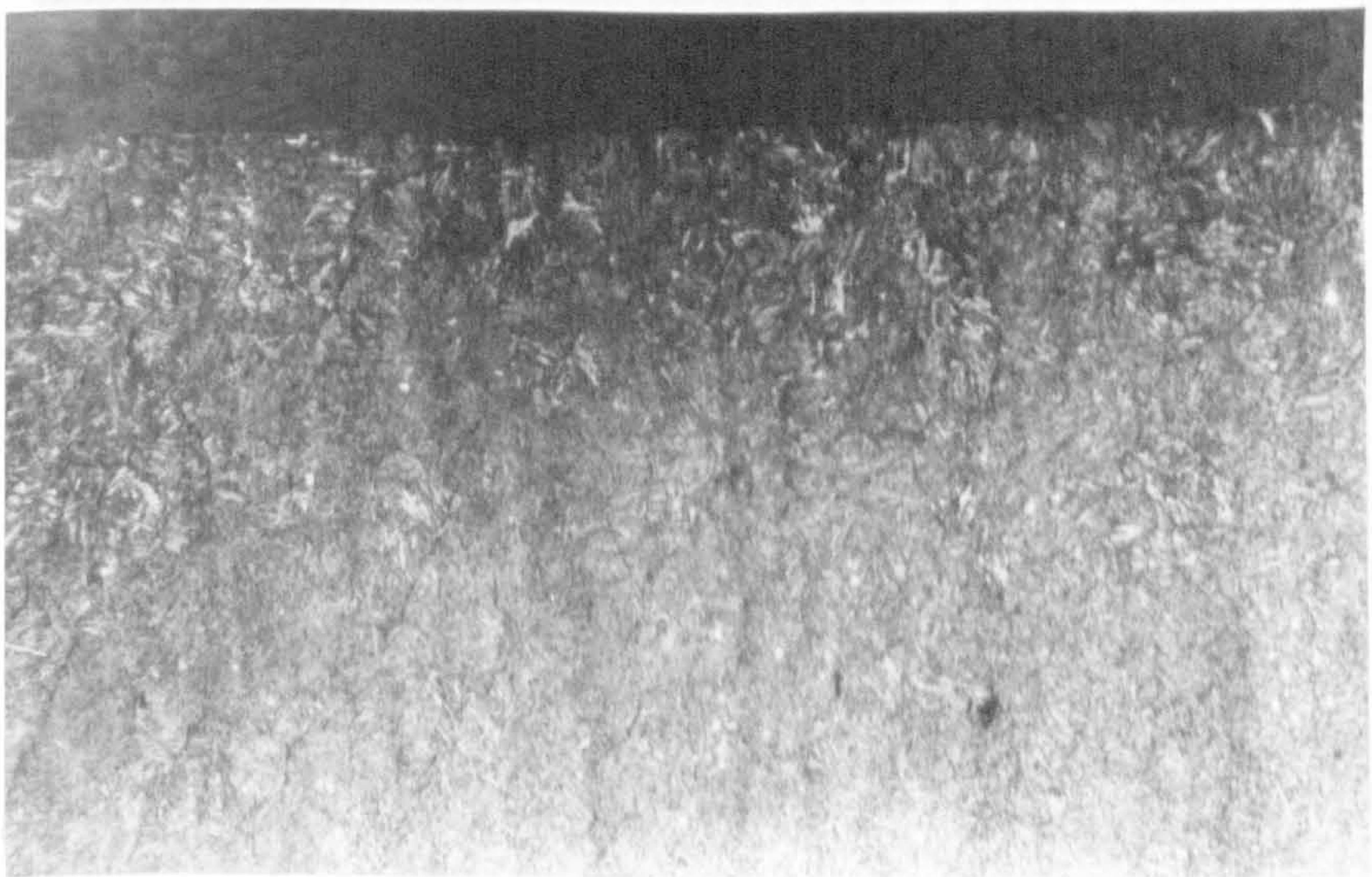

(a) 100μm

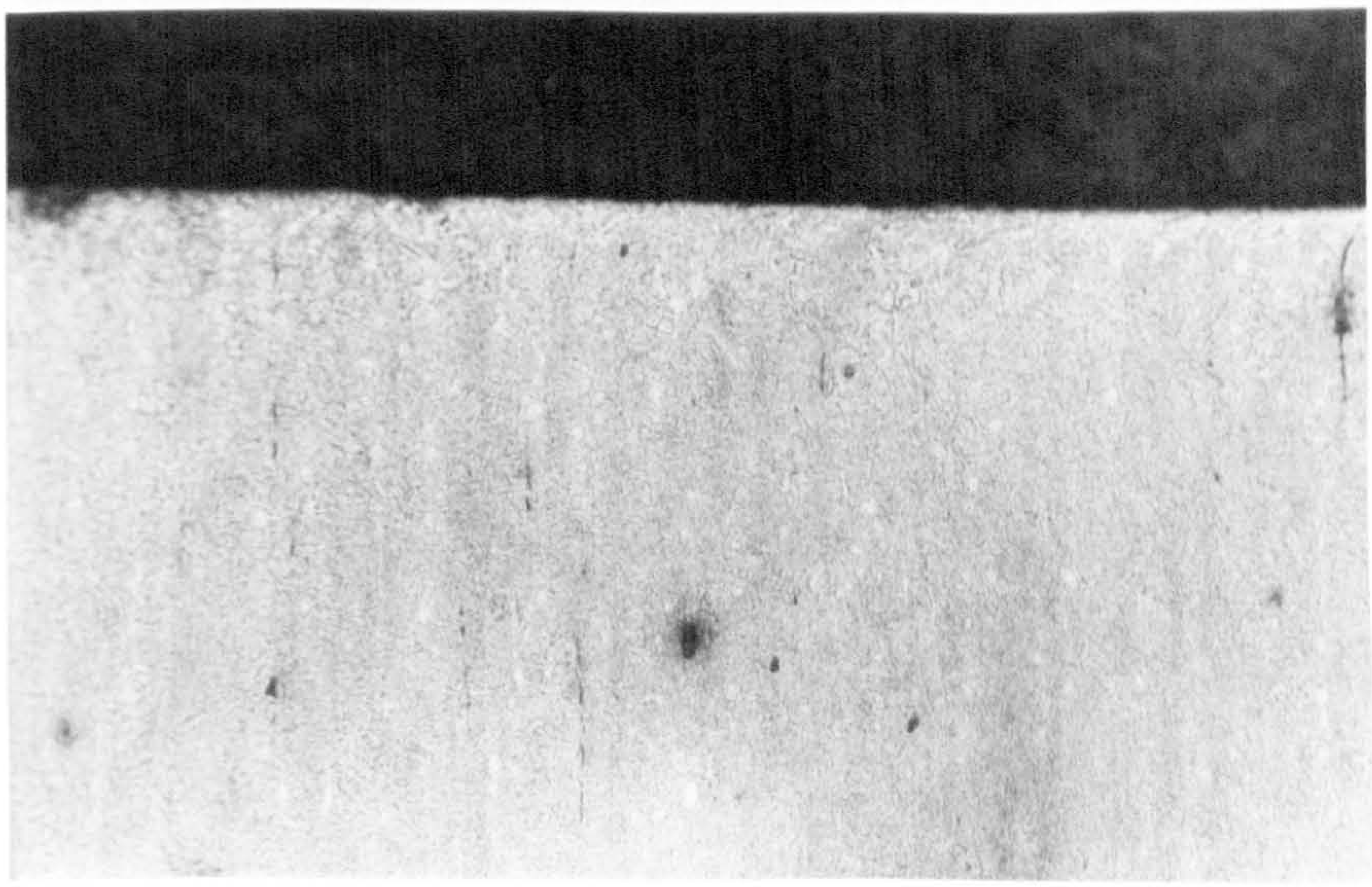

(b) 100μm

Fig.4.43 Optical microstructure of longitudinal section normal to worn surface of gas nitrided BS970,905M39 (EN41B) pin
(a) tested in mild wear regime (sliding speed: 0.5 $m \cdot s^{-1}$, test load: 40 N)
(b) tested in mild wear regime (sliding speed: 2 $m \cdot s^{-1}$, test load: 20 N)

sliding direction of disc

→

(c) 100μm

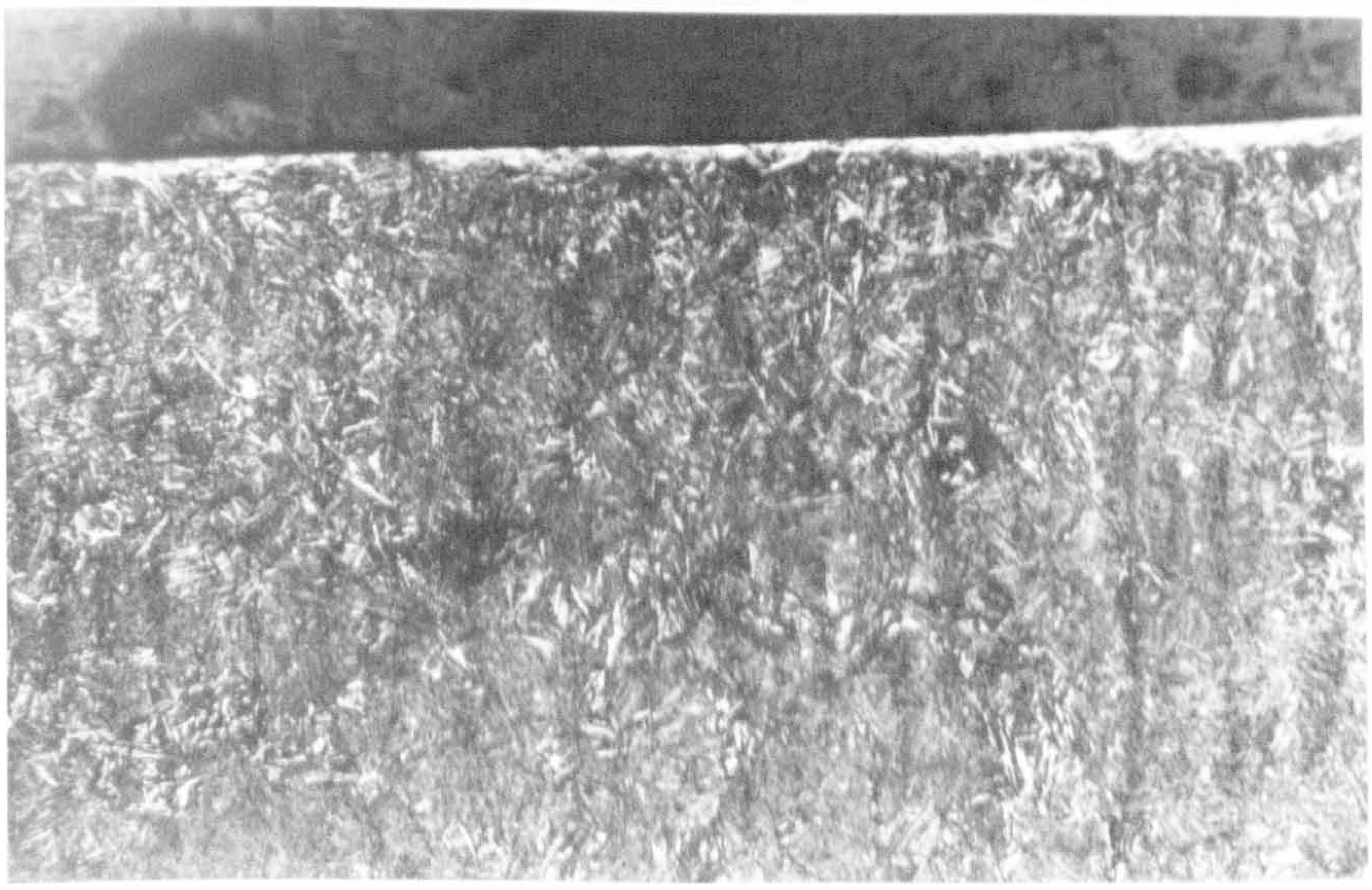

(d) 100μm

Fig.4.43 Optical microstructure of longitudinal section normal to worn surface of <u>gas nitrided</u> BS970,905M39 (EN41B) pin

(c) tested in <u>severe</u> wear regime (sliding speed: 2 $m \cdot s^{-1}$, test load: 80 N)

(d) The wear test was stopped at a pin wear length within the compound layer depth. (sliding speed: 0.5 $m \cdot s^{-1}$, test load: 10 N, sliding distance: 1800m, pin wear length: 26 μm)

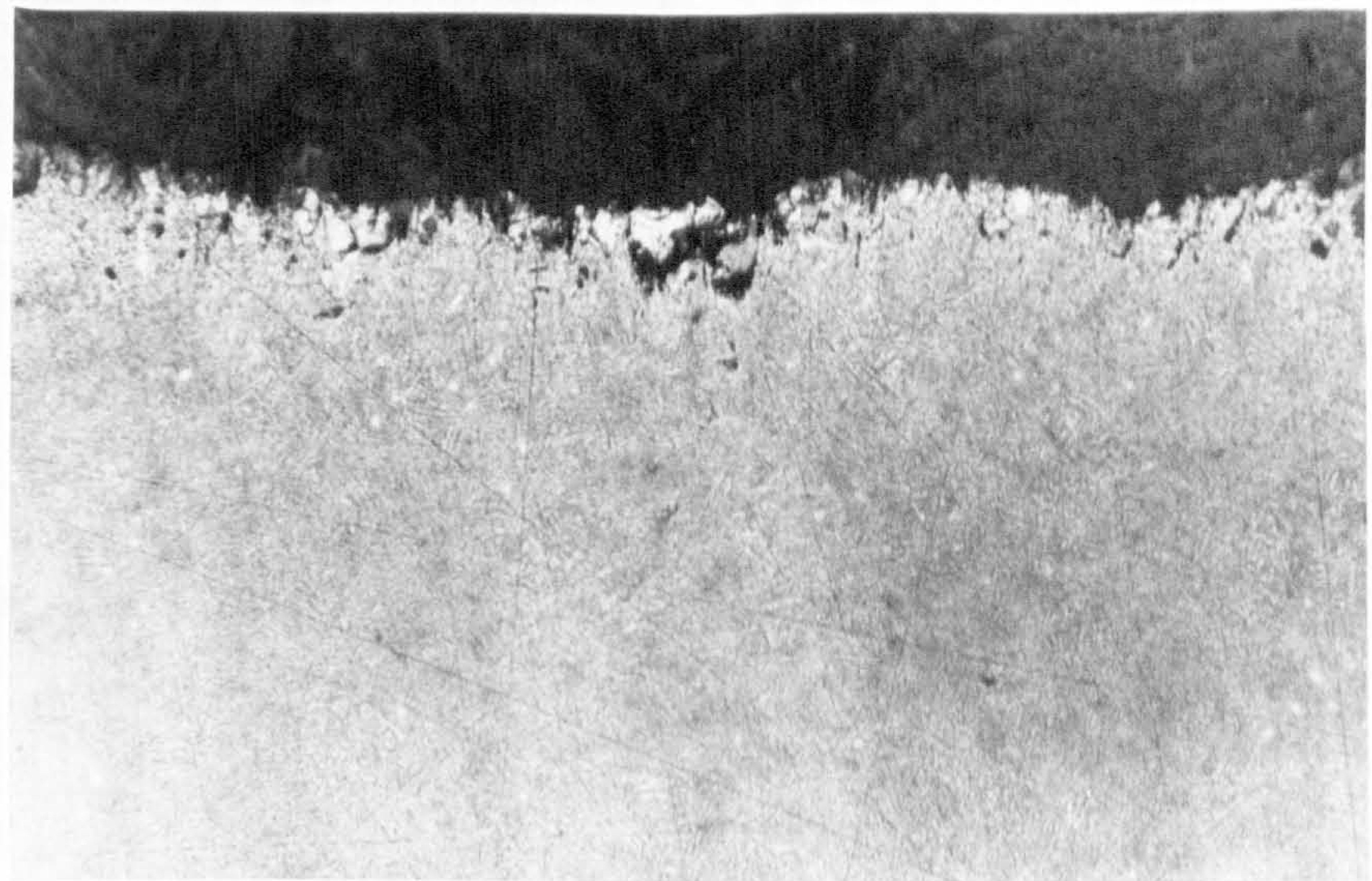

12μm

(a) 100μm

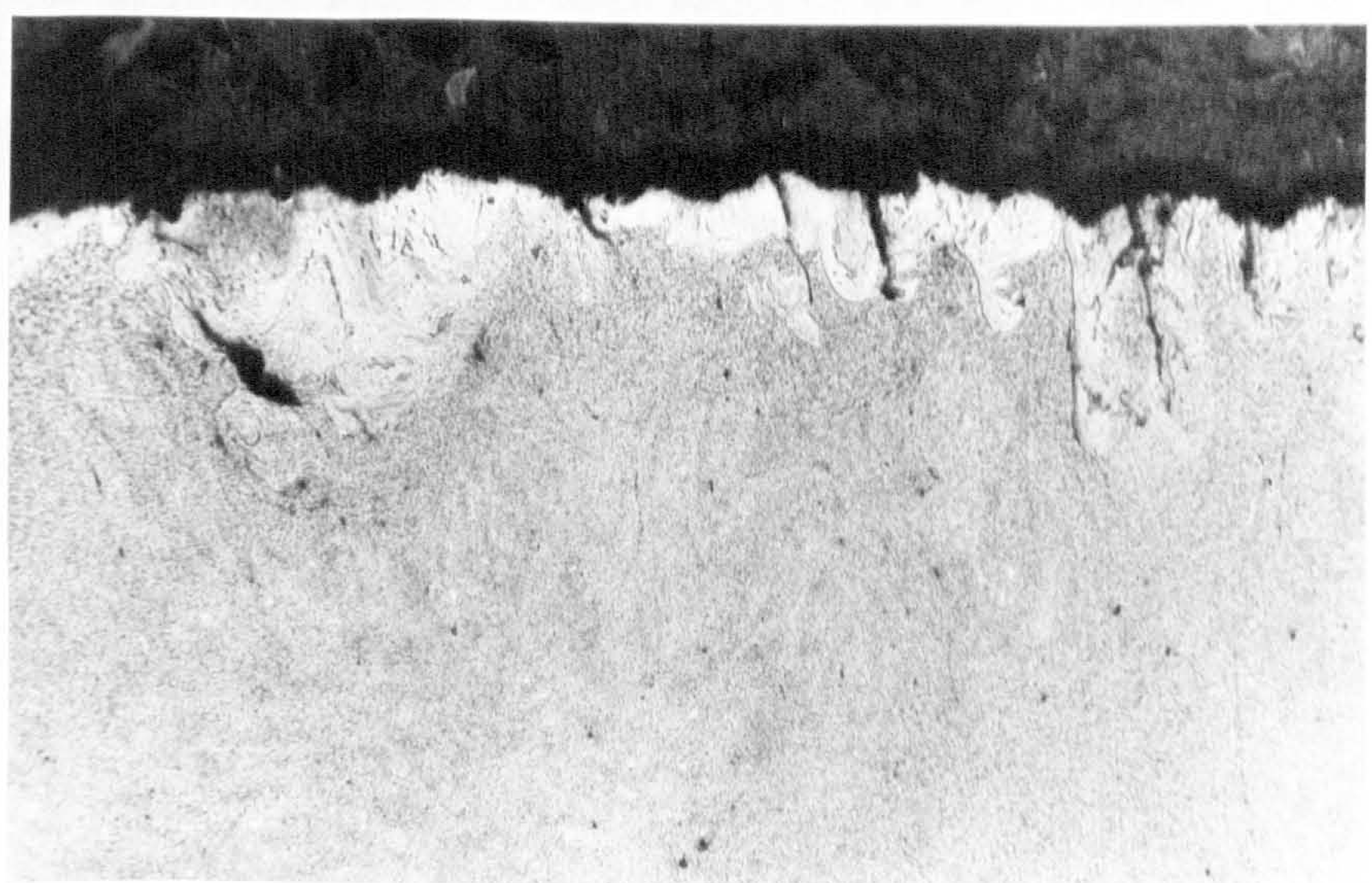

30μm

(b) 200μm

Fig.4.44 Optical microstructure of transverse taper section through worn surface of untreated BS970,905M39 (EN41B) pin
(a) tested in mild wear regime (sliding speed: 1 $m \cdot s^{-1}$, test load: 4 N)
(b) tested in severe wear regime (sliding speed: 1 $m \cdot s^{-1}$, test load: 40 N)

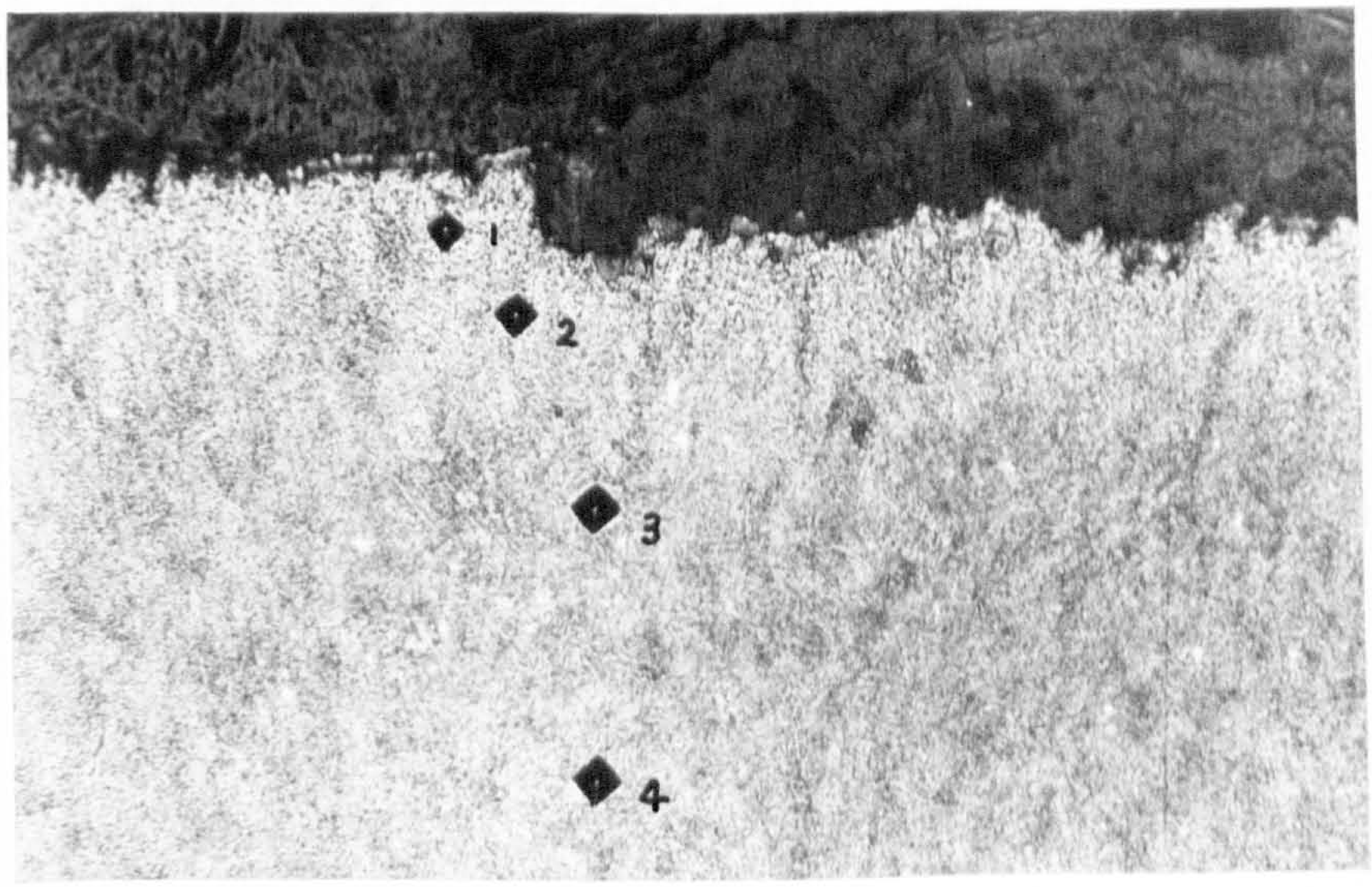

12µm

(c) 100µm

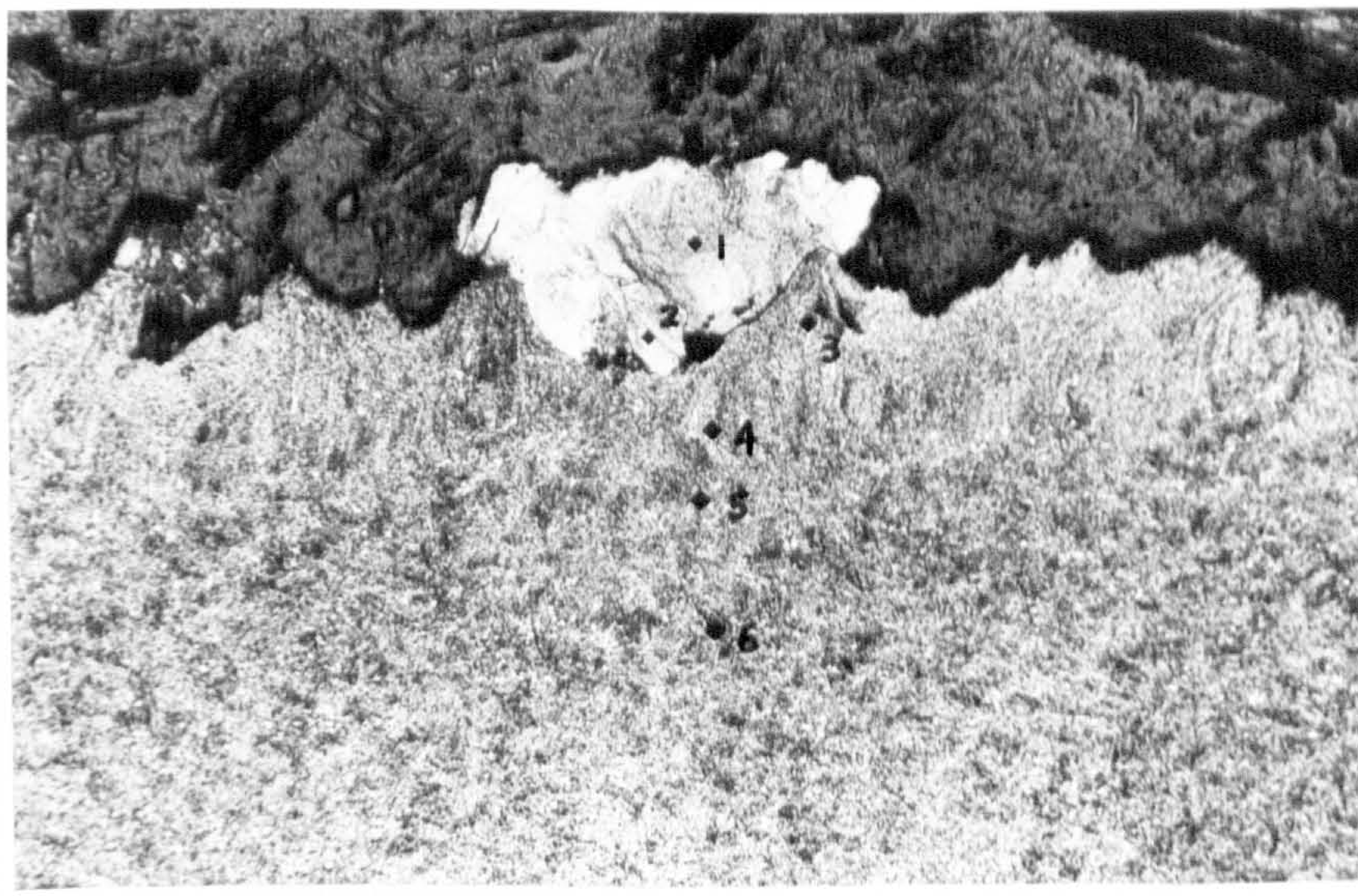

25µm

(d) 200µm

Fig.4.44 Optical microstructure of transverse taper section through worn surface of untreated BS970,905M39 (EN41B) pin
(c) tested in mild wear regime above T_2 (sliding speed: 0.5 $m \cdot s^{-1}$, test load: 80 N). Microhardness results ($Hv_{0.5N}$): 1. Hv 362, 2. Hv 299, 3. Hv 252, 4. Hv 257
(d) tested in extremely-severe wear regime (sliding speed: 1 $m \cdot s^{-1}$, test load: 120 N). Microhardness results ($Hv_{0.5N}$): 1. Hv 666, 2. Hv 739, 3. Hv 418, 4. Hv 358, 5. Hv 353, 6. Hv 310

10μm

(a) 100μm

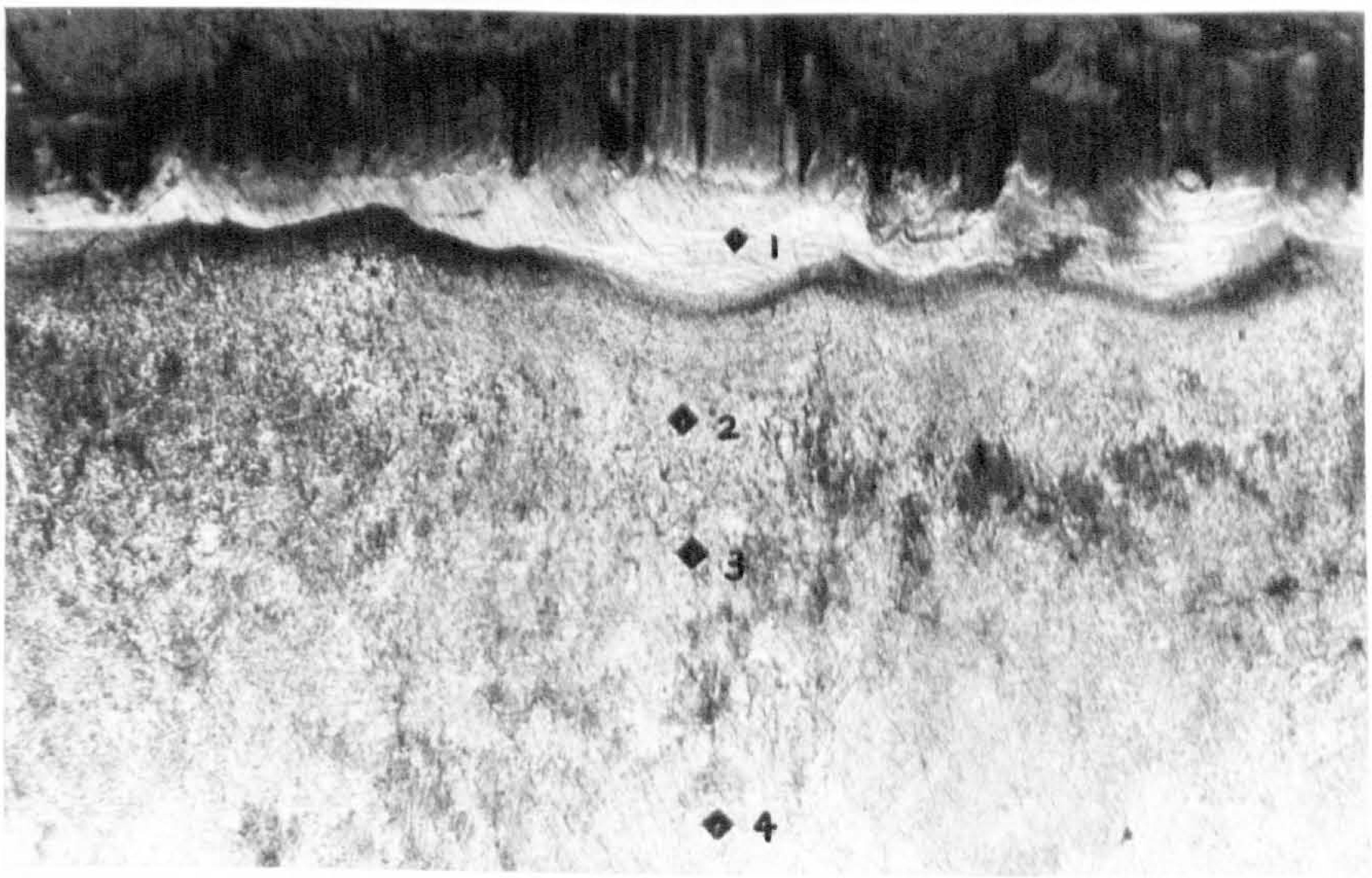

12μm

(b) 100μm

Fig.4.45 Optical microstructure of transverse taper section through worn surface of gas nitrided BS970,905M39 (EN41B) pin **(a)** tested in mild wear regime (sliding speed: 1 $m \cdot s^{-1}$, test load: 10 N) **(b)** tested in severe wear regime (sliding speed: 1 $m \cdot s^{-1}$, test load: 160 N). Microhardness results ($Hv_{0.5N}$): 1. Hv 909, 2. Hv 603, 3. Hv 566, 4. Hv 466

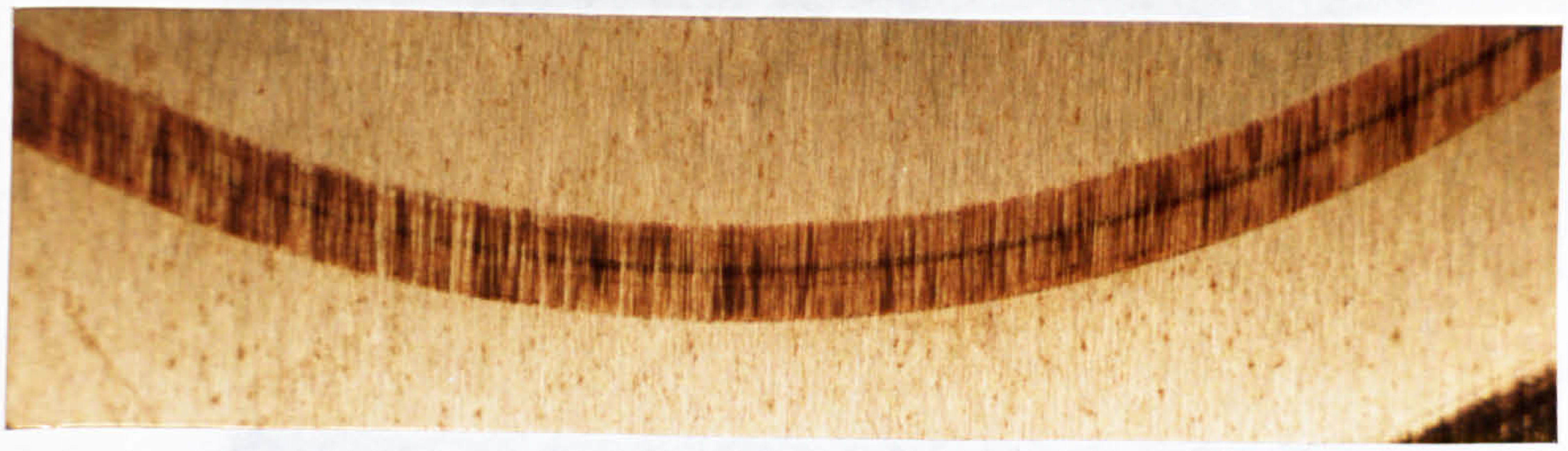

(a) 5mm

(b) 5mm

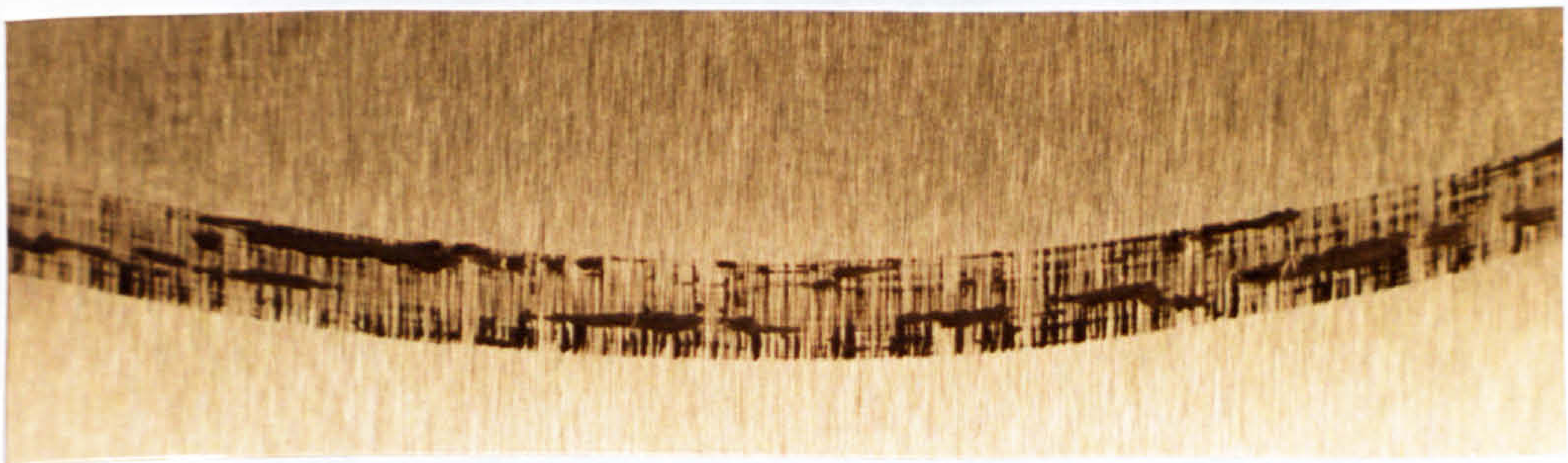

(c) 5mm

Fig.4.46 Macrograph of wear track on disc rubbed against gas nitrided BS970,905M39 (EN41B) pin
(a) tested in mild wear regime (sliding speed: 0.2 $m \cdot s^{-1}$, test load: 20 N)
(b) tested in mild wear regime (sliding speed: 1 $m \cdot s^{-1}$, test load: 40 N)
(c) tested in severe wear regime (sliding speed: 5 $m \cdot s^{-1}$, test load: 40 N)

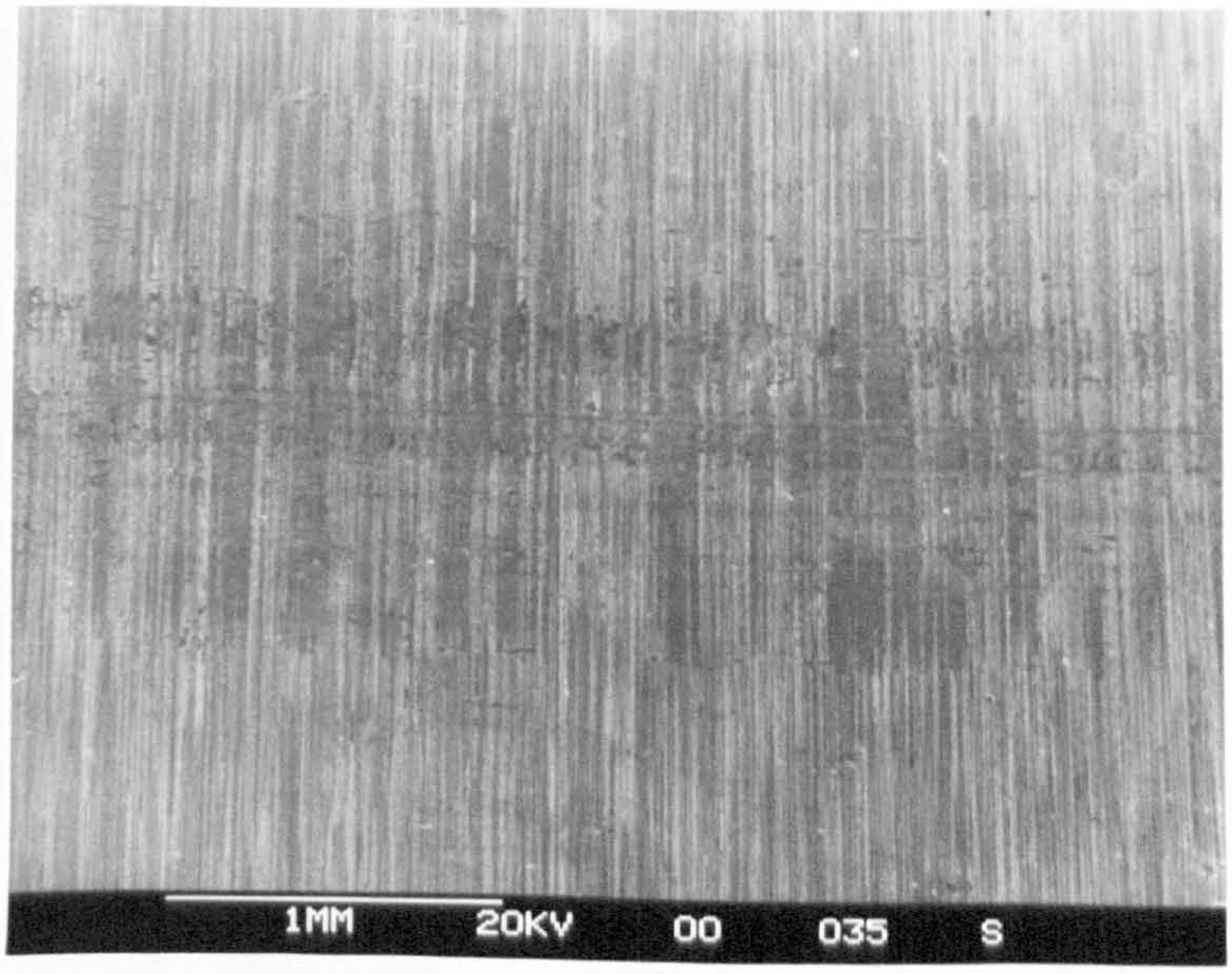

relative sliding direction of pin →

finish grinding direction of disc ⇕

(a)

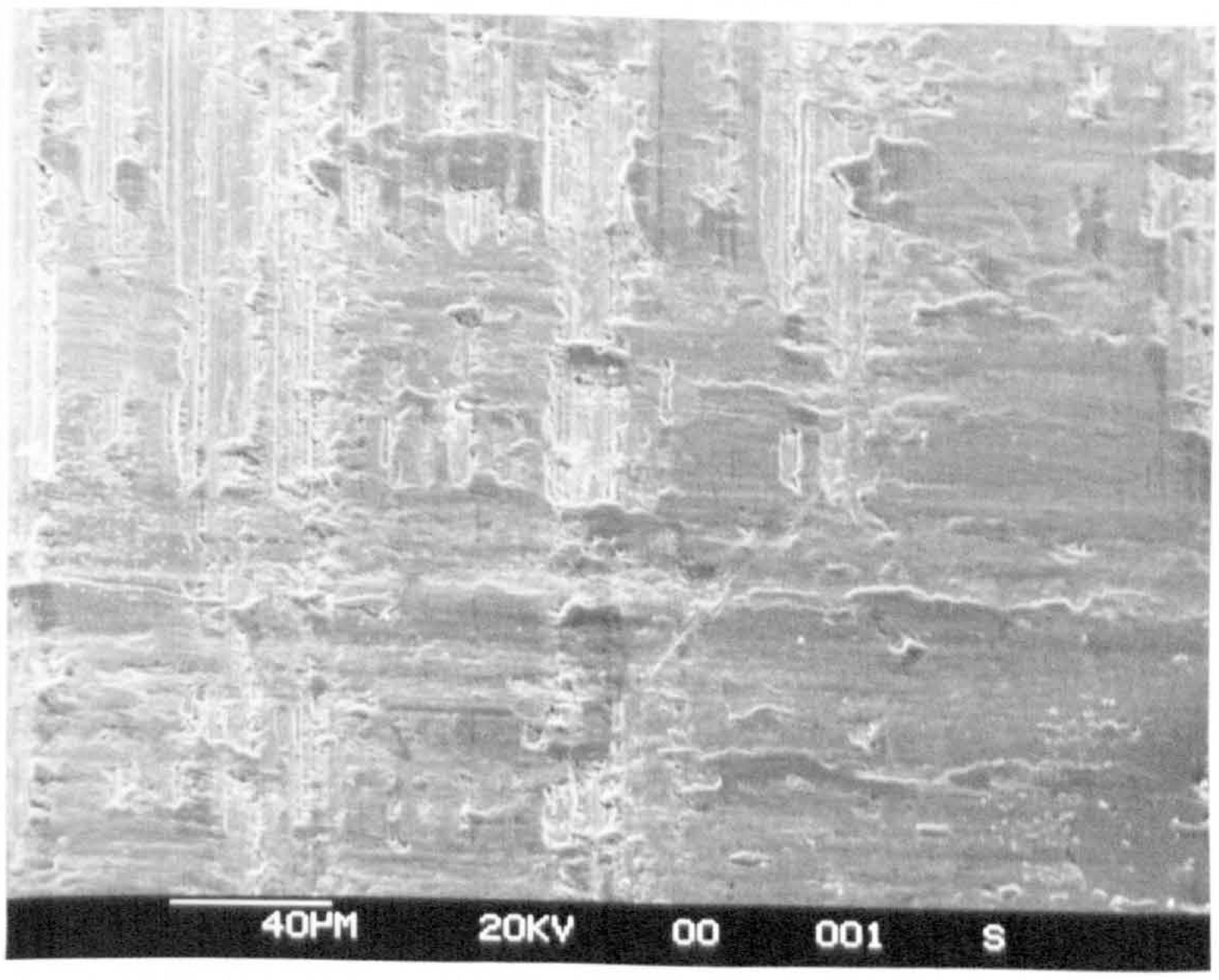

(b)

Fig.4.47 SEM of worn surface of disc tested against untreated BS970,905M39 (EN41B) pin in mild wear regime (sliding speed: 1 m$\cdot$s^{-1}, test load: 4 N)
(a) x26 **(b)** x320

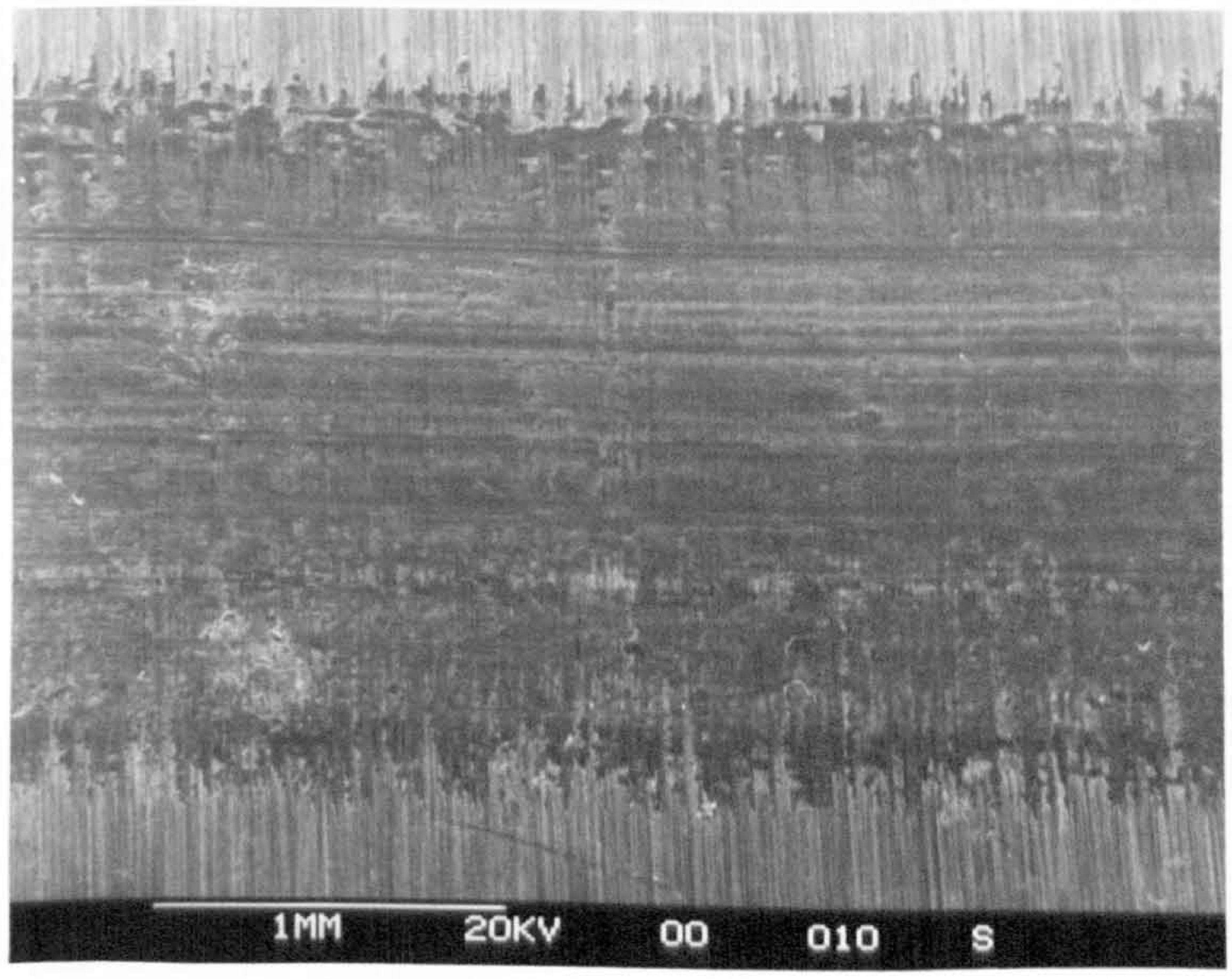

relative sliding direction of pin

→

finish grinding direction of disc

⇕

(a)

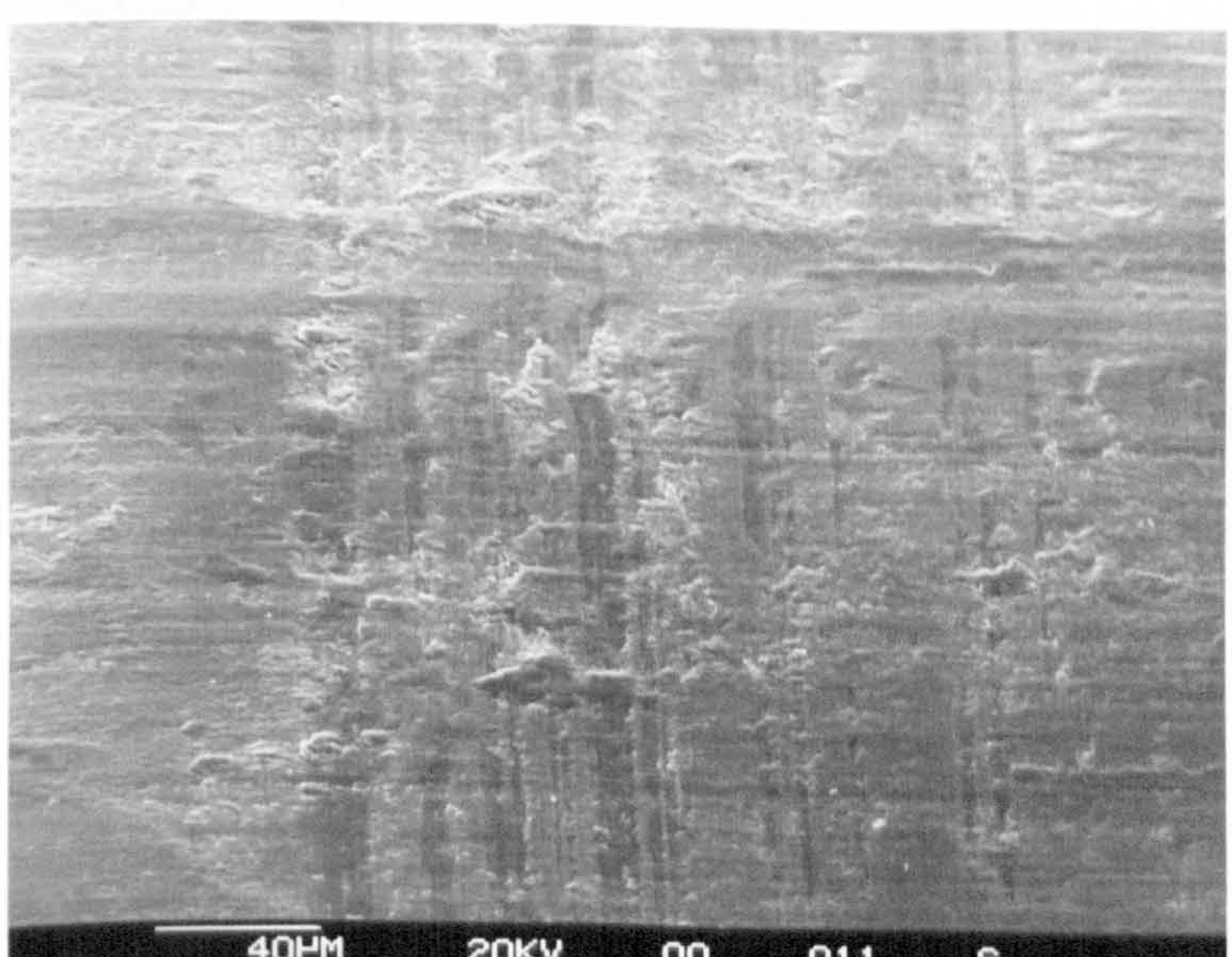

(b)

Fig.4.48 SEM of worn surface of disc tested against untreated BS970,905M39 (EN41B) pin in severe wear regime (sliding speed: 1 $m \cdot s^{-1}$, test load: 40 N)
(a) x26 **(b)** x320

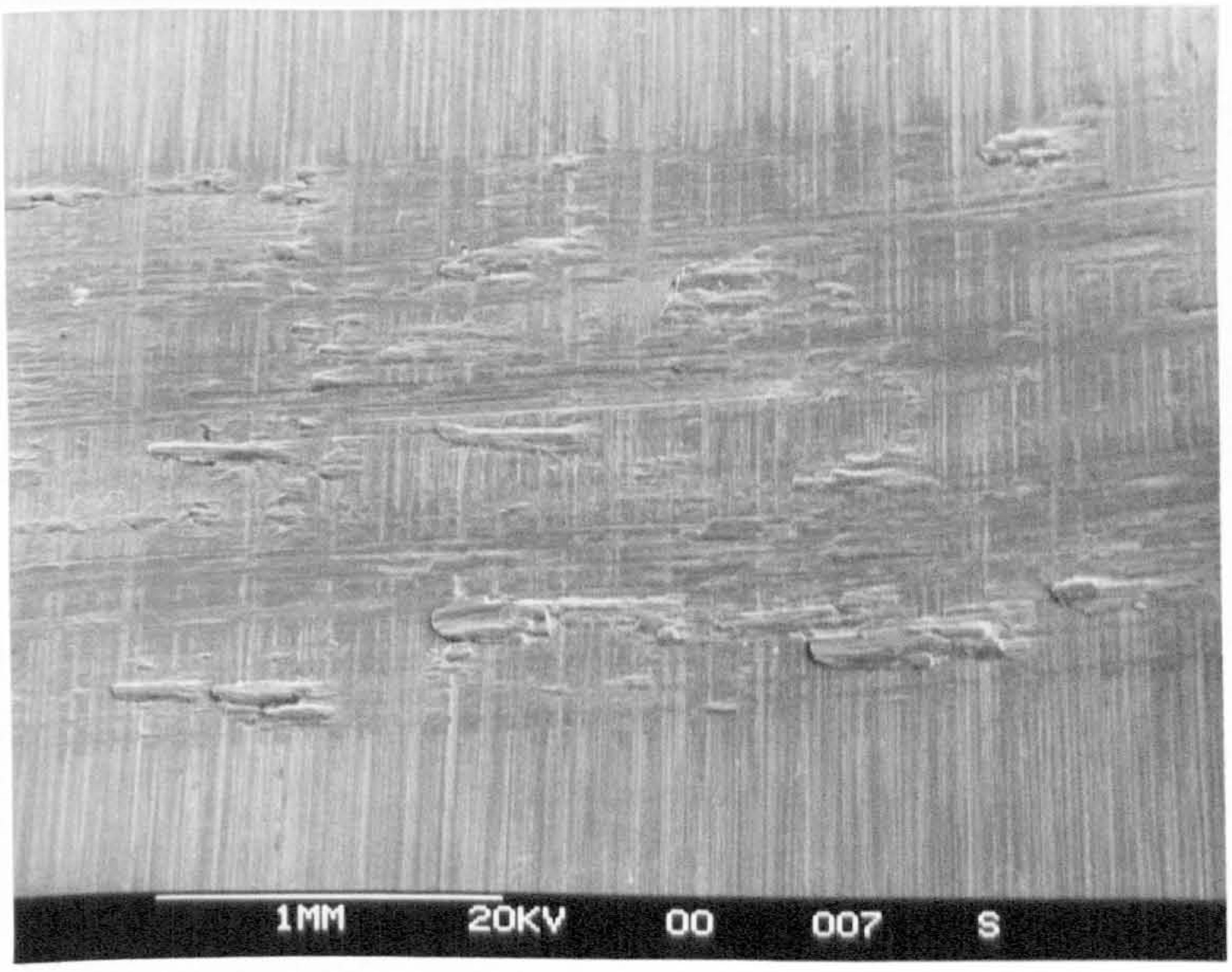

(a)

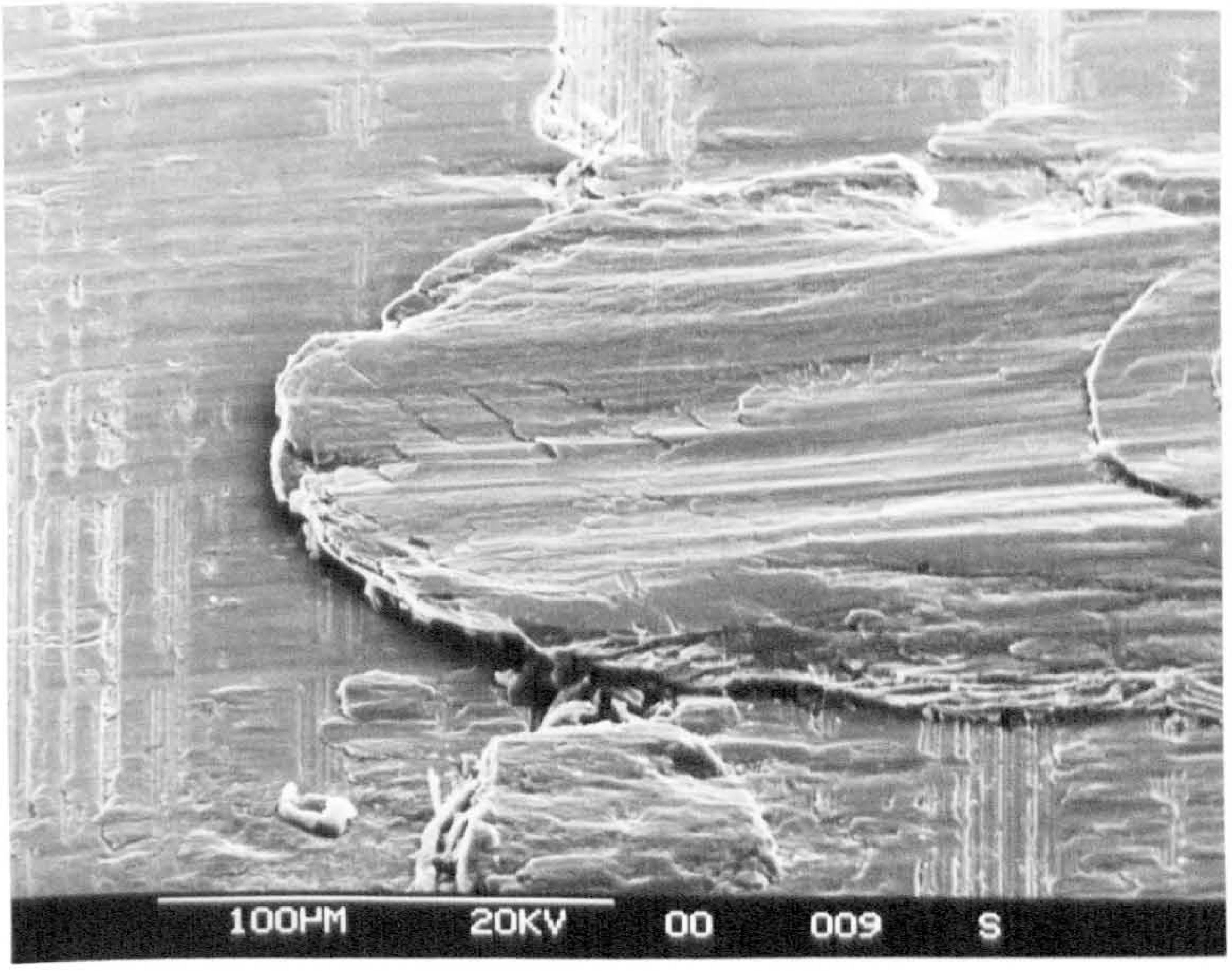

(b)

Fig.4.49 SEM of worn surface of disc tested against <u>untreated</u> BS970,905M39 (EN41B) pin in <u>extremely-severe</u> wear regime (sliding speed: 1 $m \cdot s^{-1}$, test load: 160 N)
(a) x26 **(b)** x320

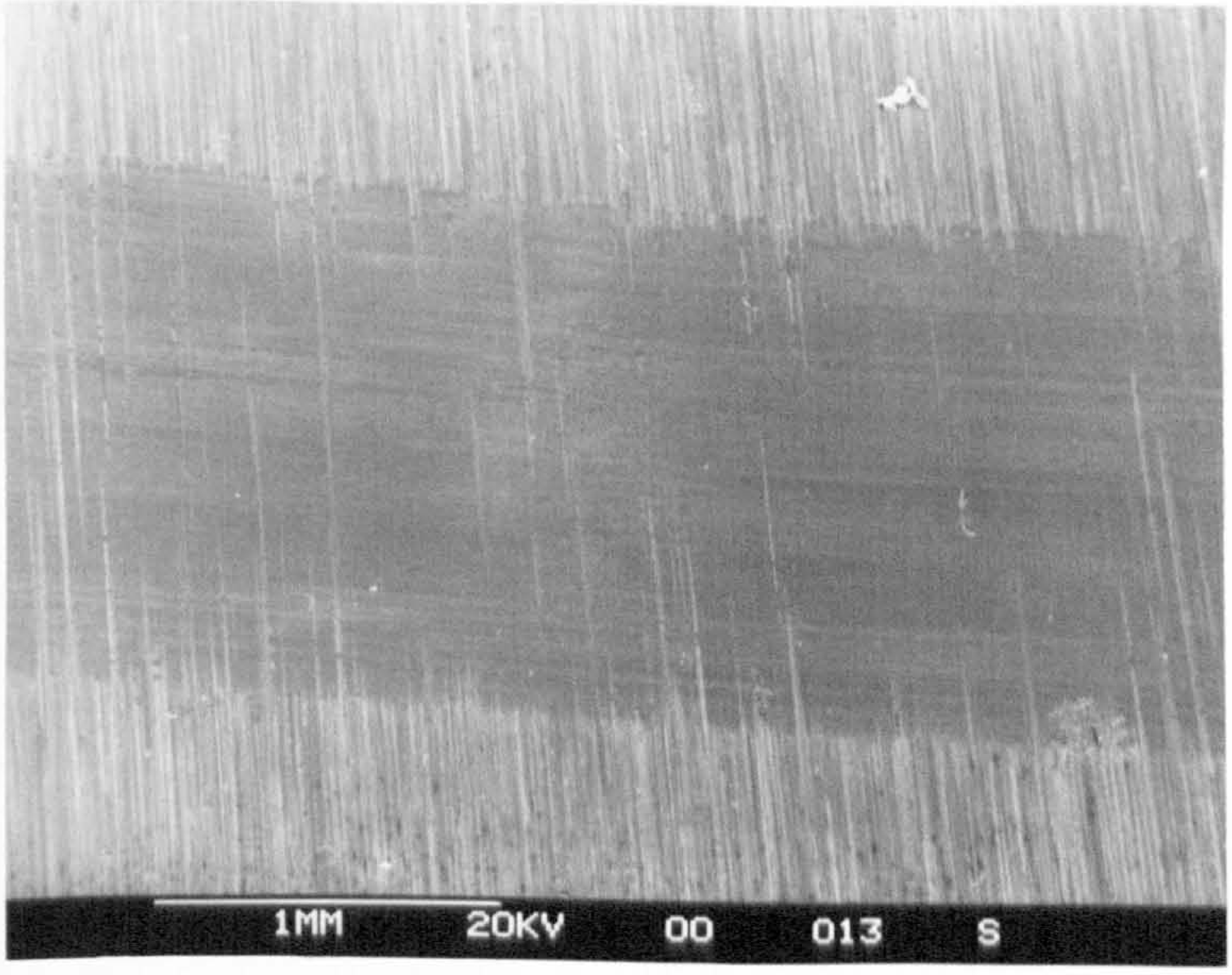

relative sliding direction of pin →

finish grinding direction of disc ⇕

(a)

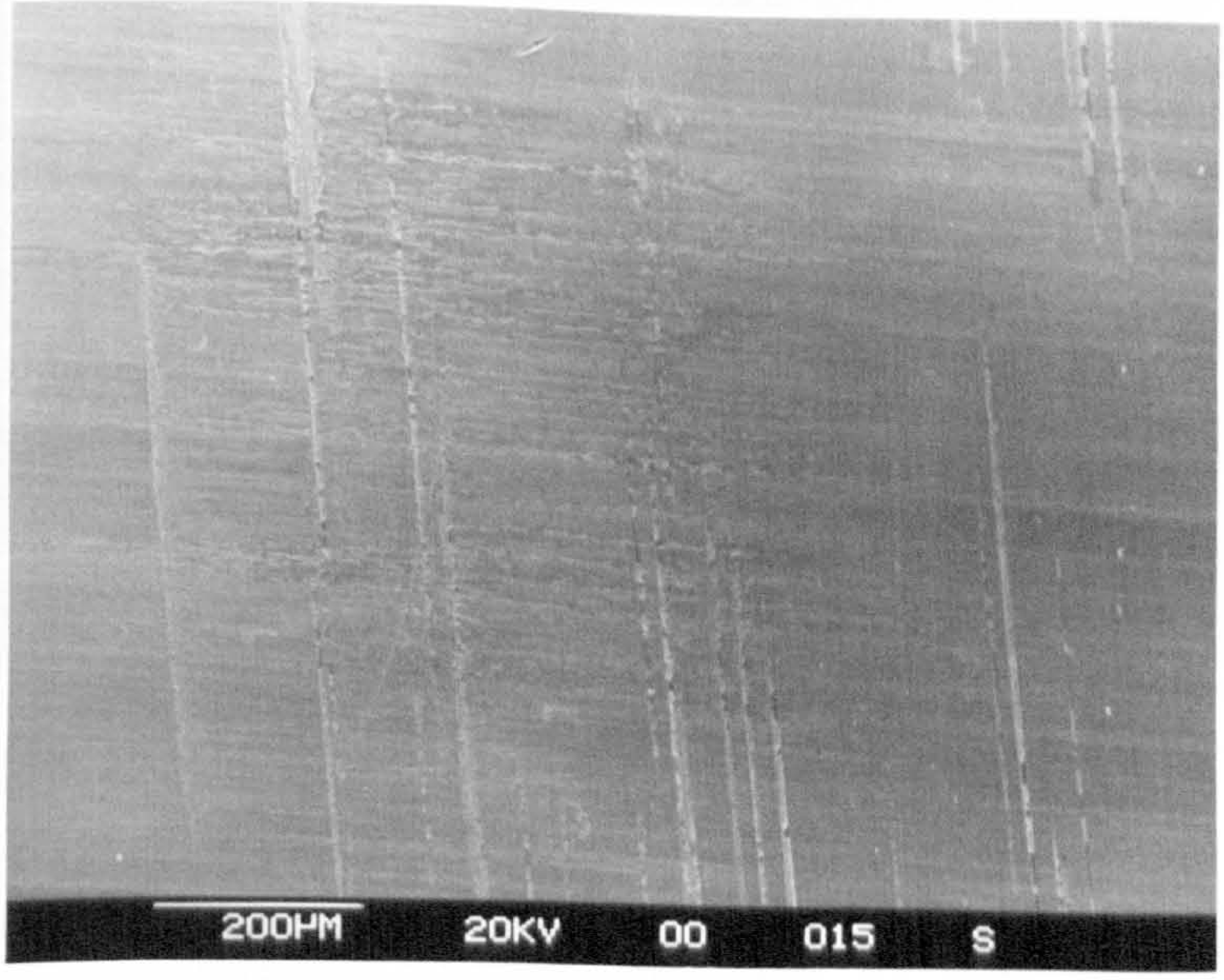

(b)

Fig.4.50 SEM of worn surface of disc tested against <u>gas nitrided</u> BS970,905M39 (EN41B) pin in <u>mild</u> wear regime (sliding speed: 1 $m \cdot s^{-1}$, test load: 10 N)
(a) x26 **(b)** x80

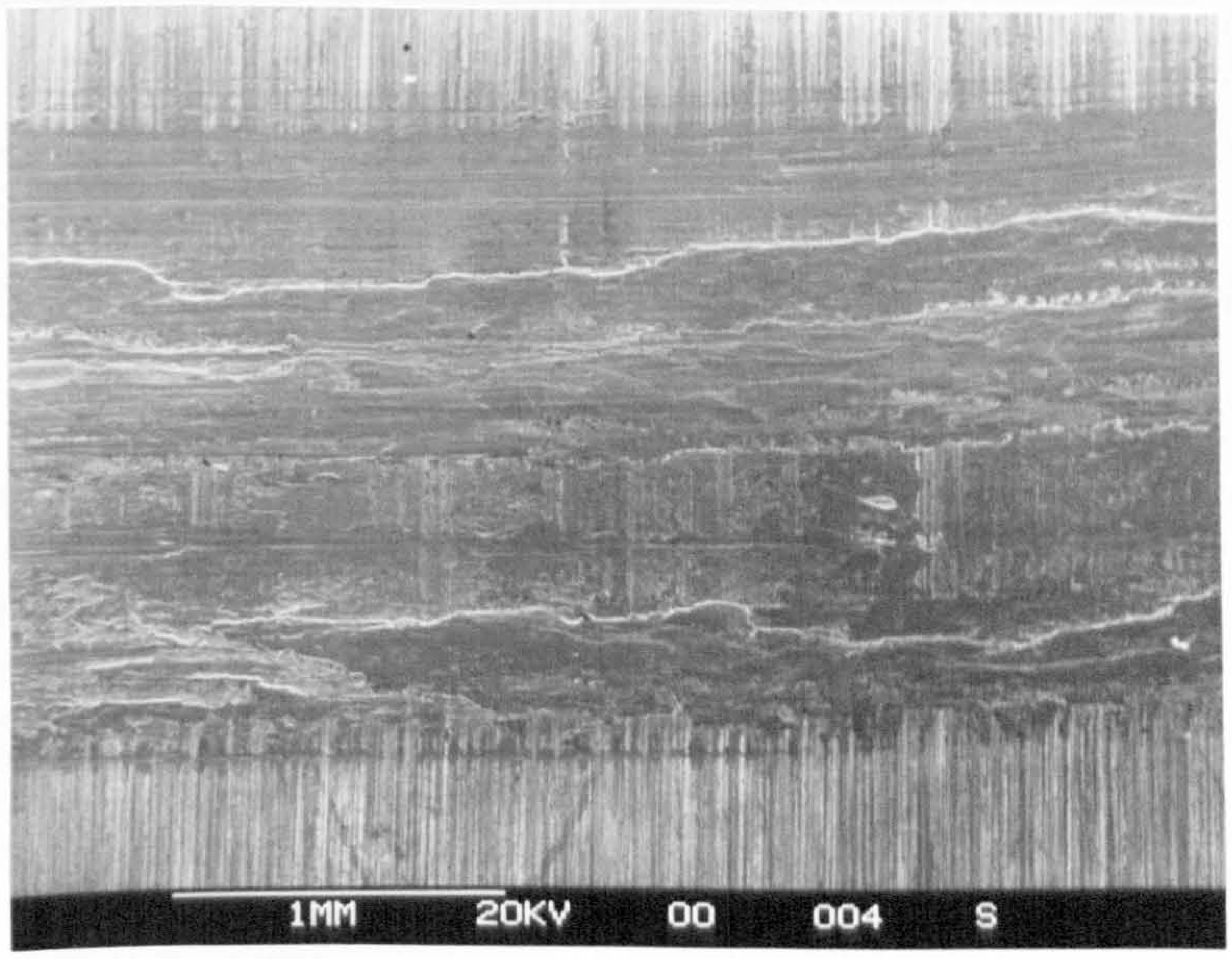

relative sliding direction of pin

→

finish grinding direction of disc

⇕

(a)

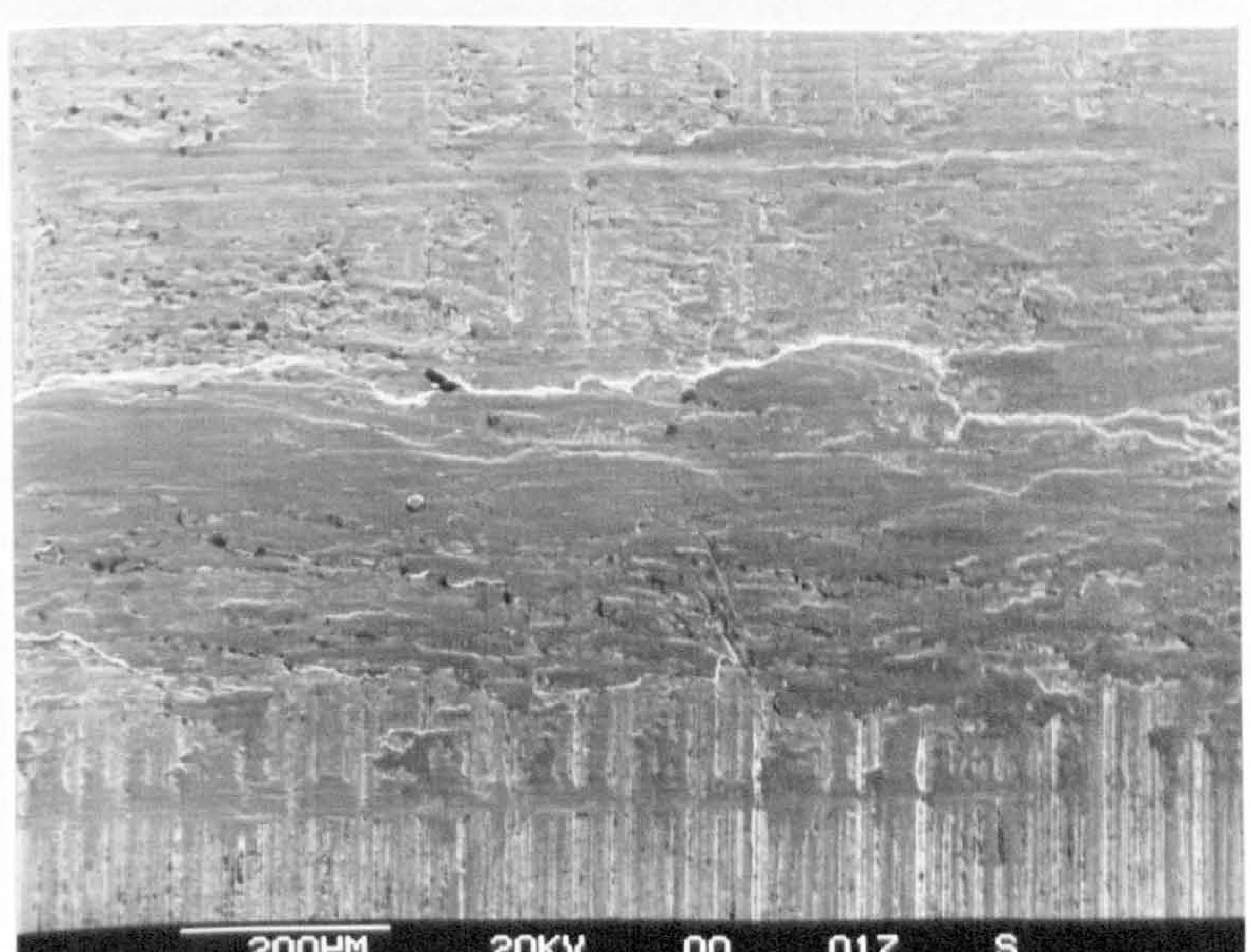

(b)

Fig.4.51 SEM of worn surface of disc tested against gas nitrided BS970,905M39 (EN41B) pin in severe wear regime (sliding speed: 1 $m \cdot s^{-1}$, test load: 160 N)
(a) x26 **(b)** x80

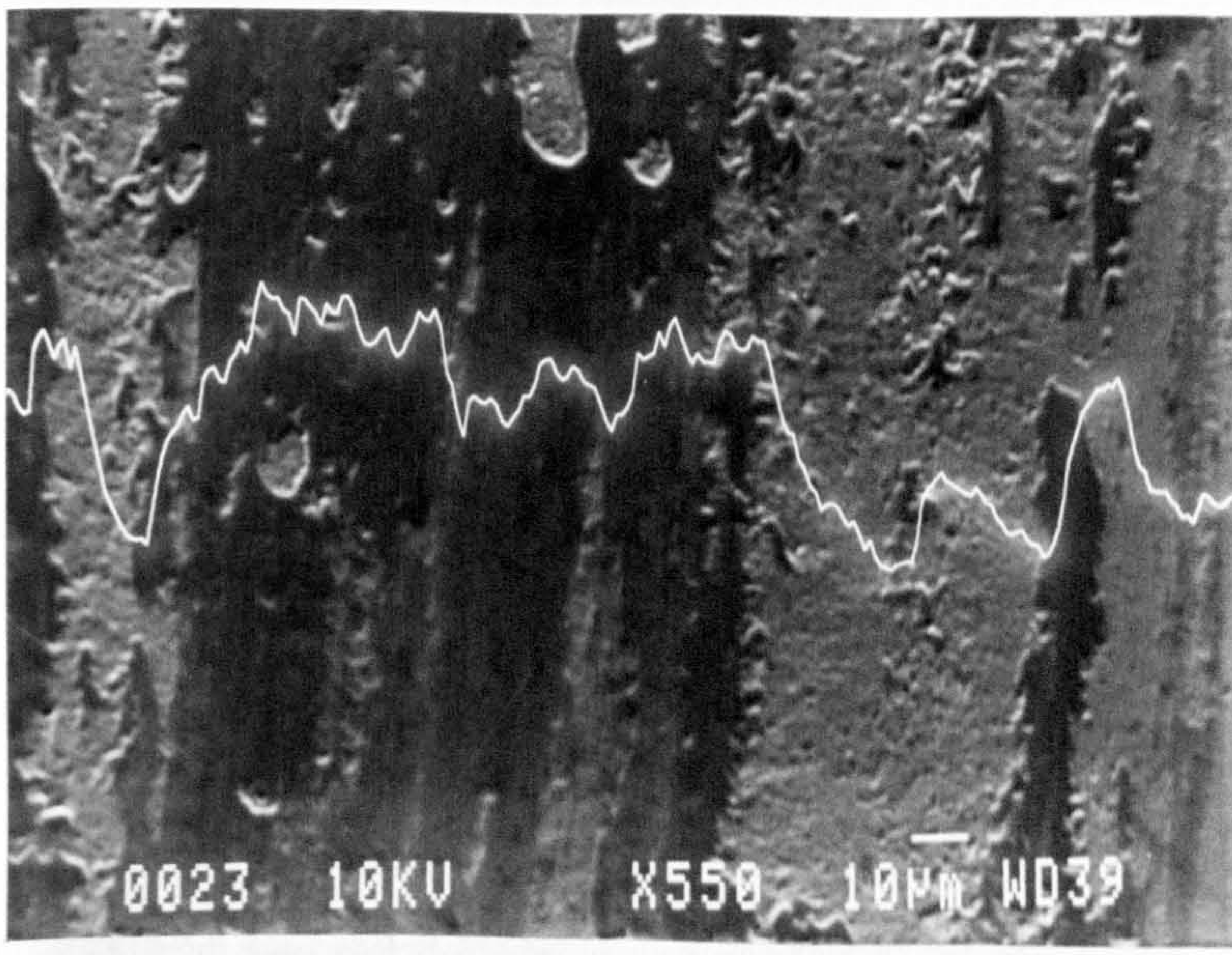

relative
sliding
direction
of pin
↓

(a)

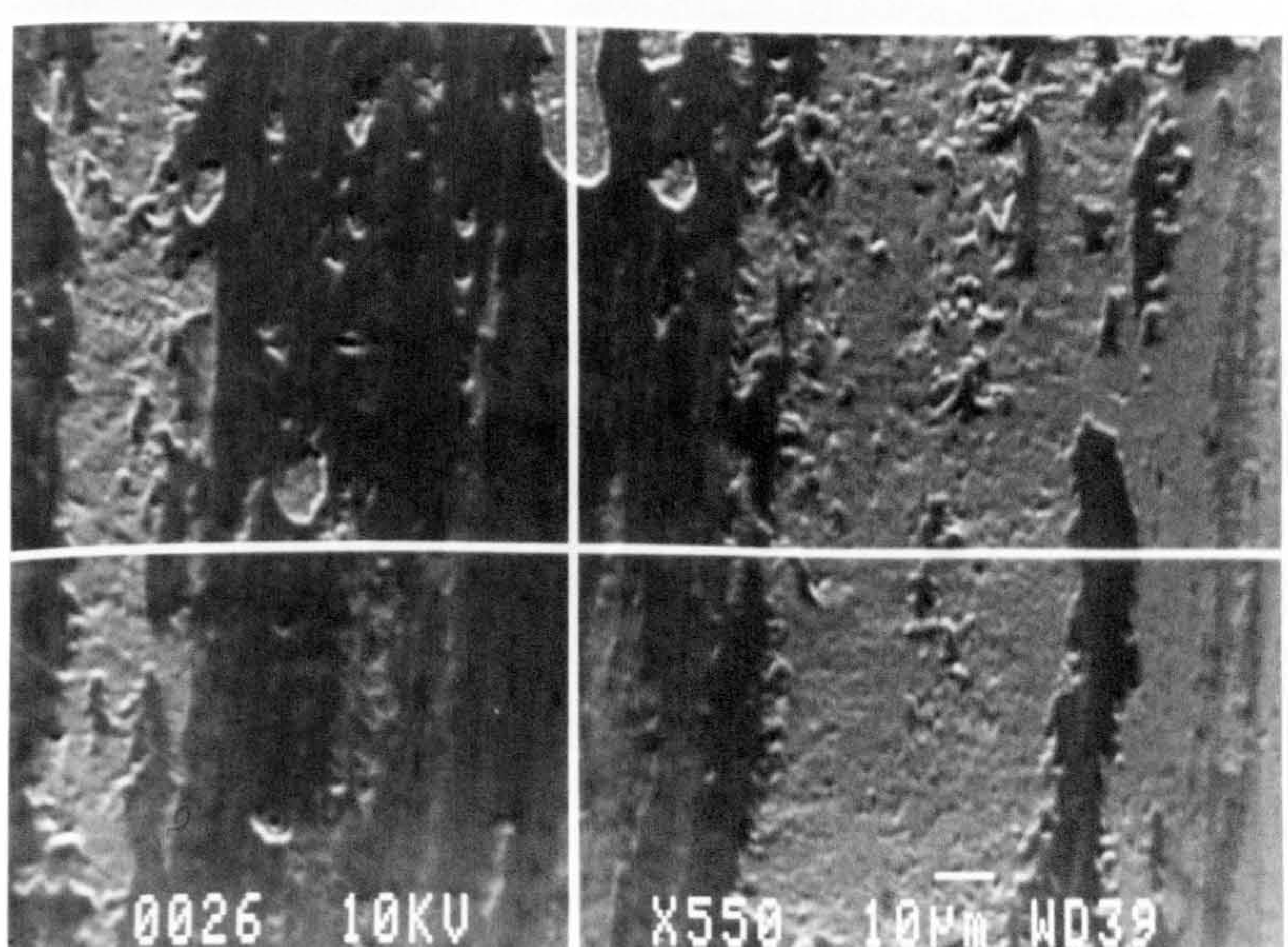

(b)

Fig.4.52 EPMA of worn surface of disc tested against <u>gas nitrided</u> BS970,905M39 (EN41B) pin in <u>mild</u> wear regime (sliding speed: 1 $m \cdot s^{-1}$, test load: 10 N)

(a) Secondary electron image and oxygen $K\alpha$ X-ray line scan analysis

(b) Line scanning position for analysis shown in Fig.4.52 (a) (horizontal line)

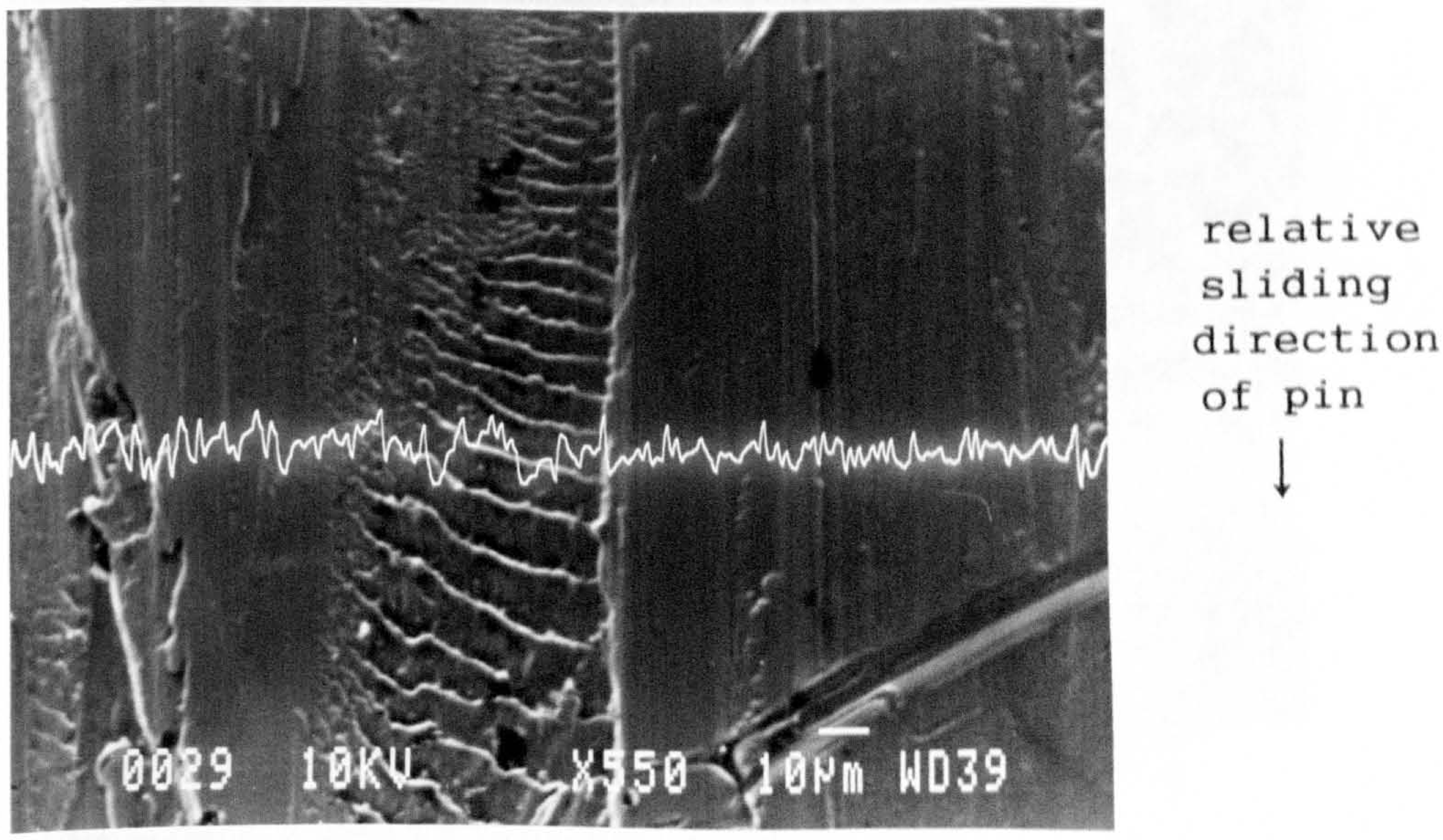

(a)

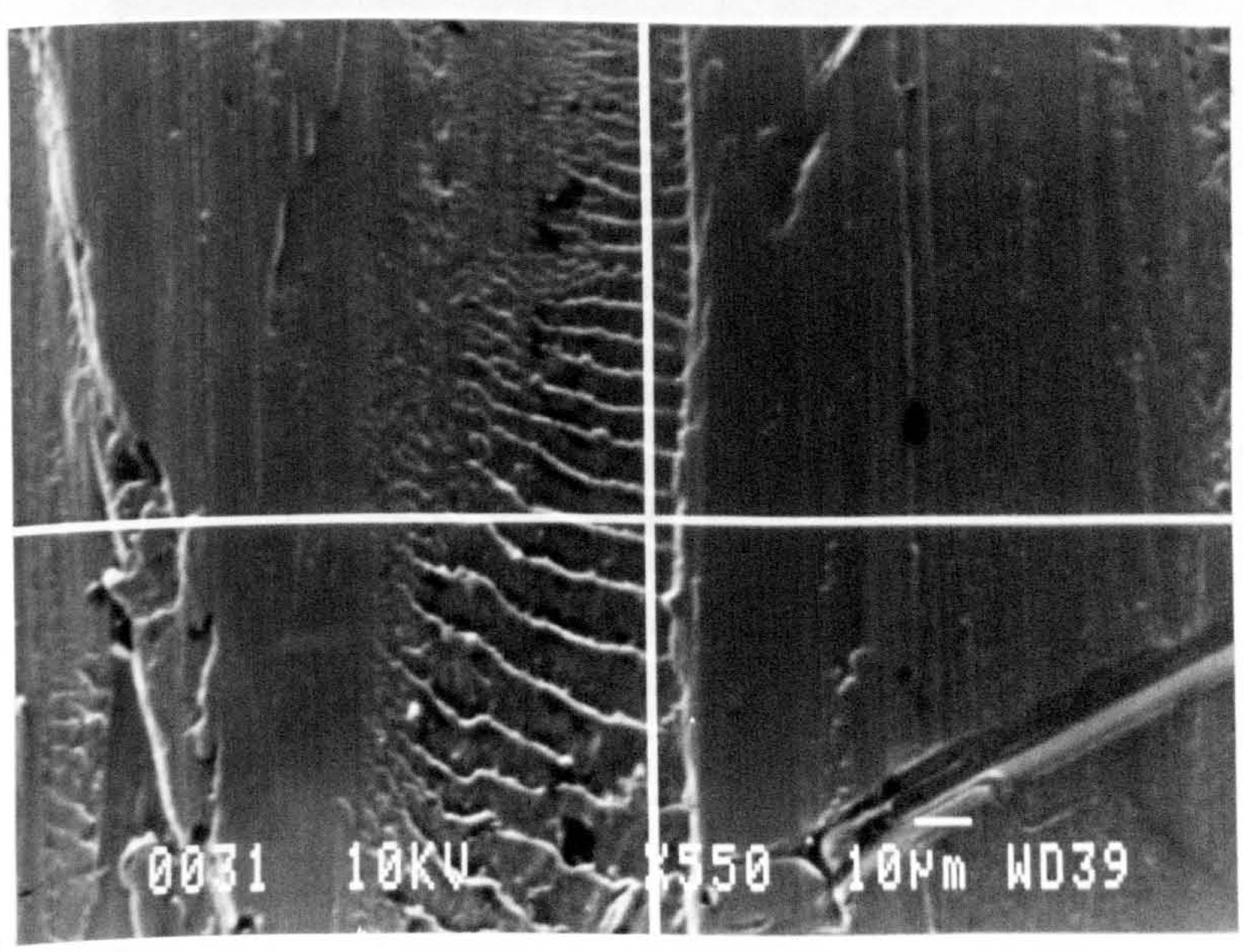

(b)

Fig.4.53 EPMA of worn surface of disc tested against <u>gas nitrided</u> BS970,905M39 (EN41B) pin in <u>severe</u> wear regime (sliding speed: 1 $m \cdot s^{-1}$, test load: 160 N)

(a) Secondary electron image and oxygen $K\alpha$ X-ray line scan analysis

(b) Line scanning position for analysis shown in Fig.4.53 (a) (horizontal line)

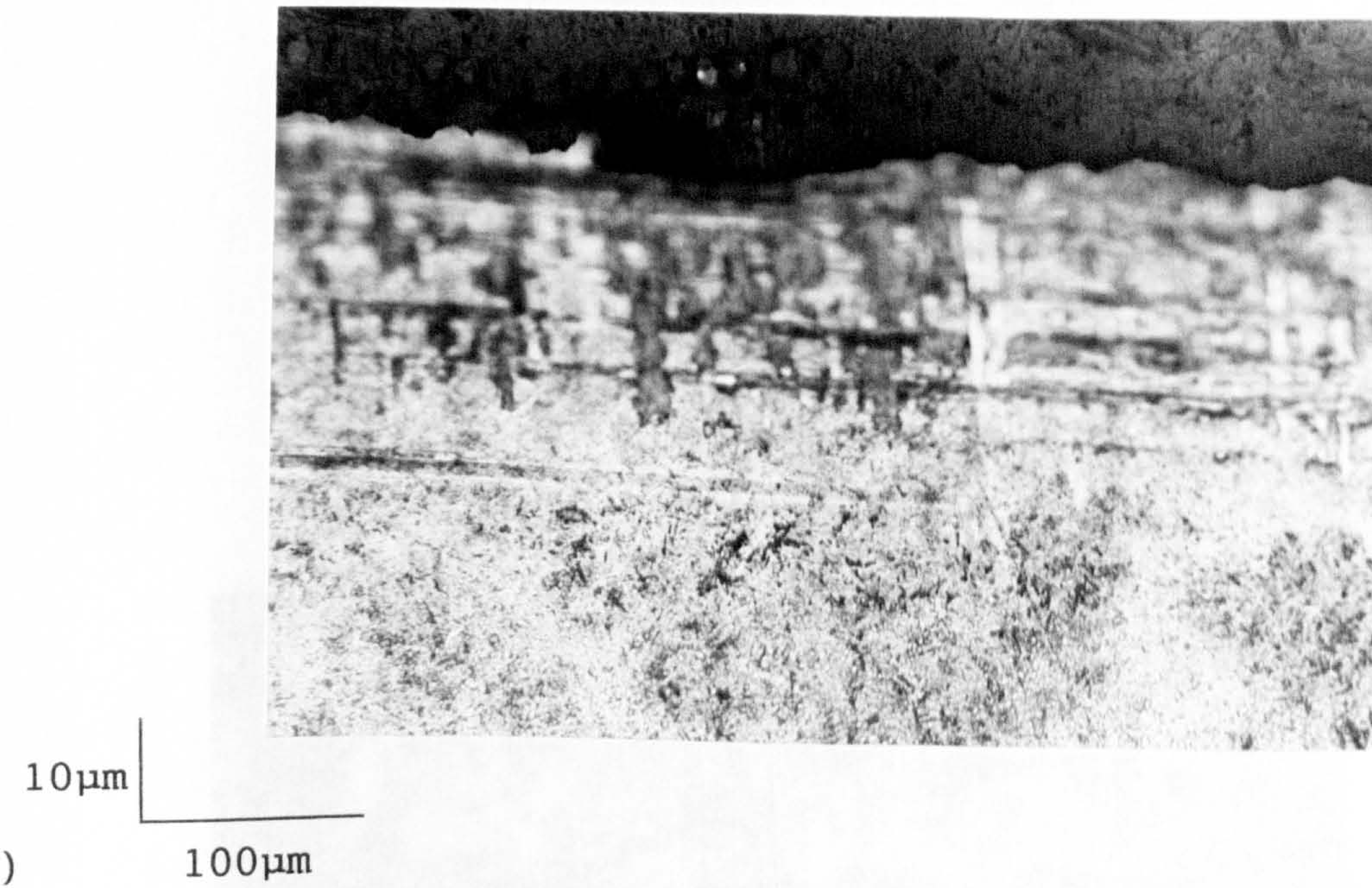

(a)

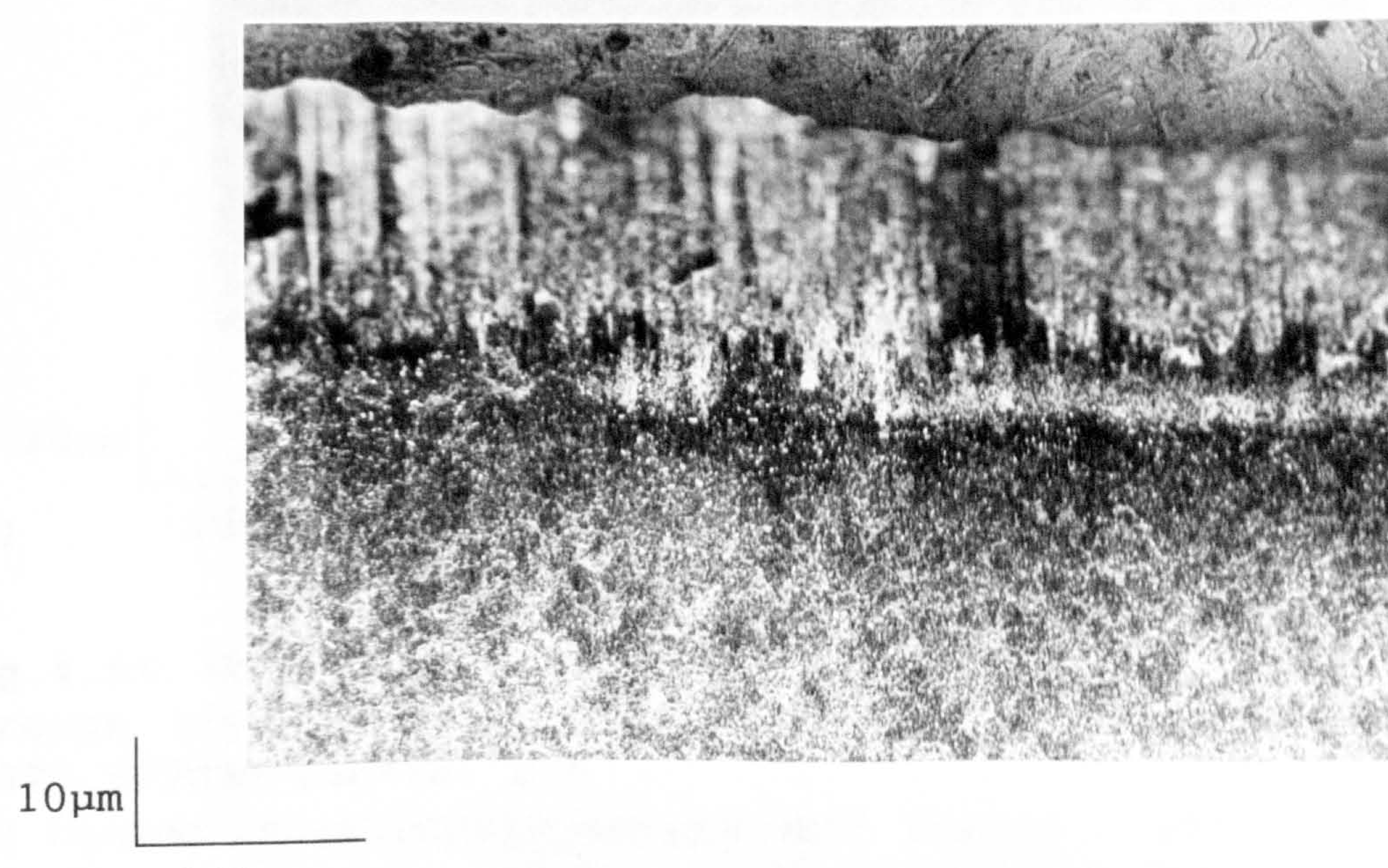

(b)

Fig.4.54 Optical microstructure of transverse taper section through worn surface of disc rubbed against untreated BS970,905M39 (EN41B) pin

(a) tested in mild wear regime (sliding speed: 1 $m \cdot s^{-1}$, test load: 4 N)

(b) tested in severe wear regime (sliding speed: 1 $m \cdot s^{-1}$, test load: 40 N)

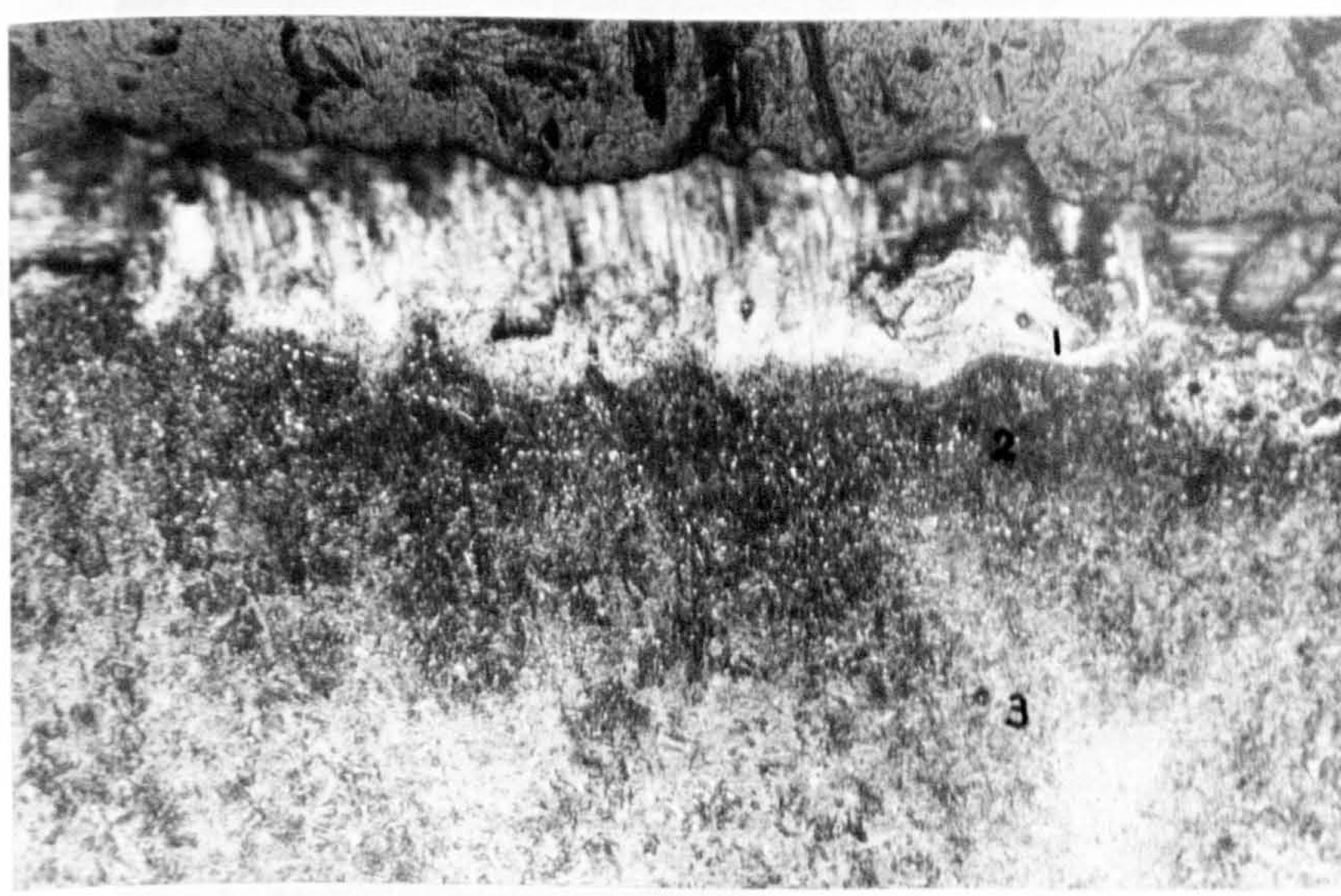

10μm

(c) 100μm

Fig.4.54 Optical microstructure of transverse taper section through worn surface of disc rubbed against untreated BS970,905M39 (EN41B) pin

(c) tested in extremely-severe wear regime (sliding speed: 1 m·s^{-1}, test load: 160 N). Microhardness results ($Hv_{0.25N}$): 1. Hv 782, 2. Hv 572, 3. Hv 612

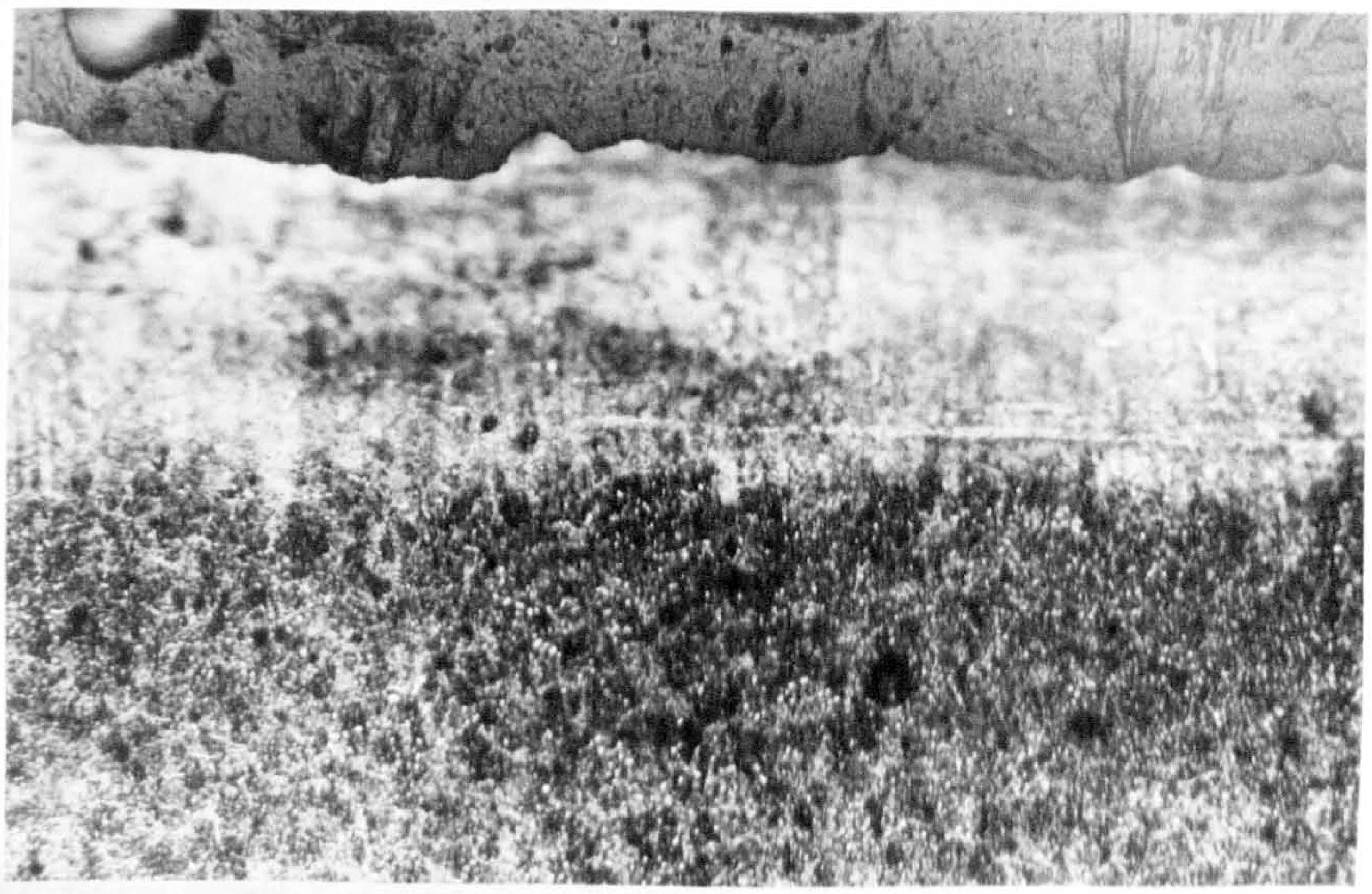

10μm

(a) 100μm

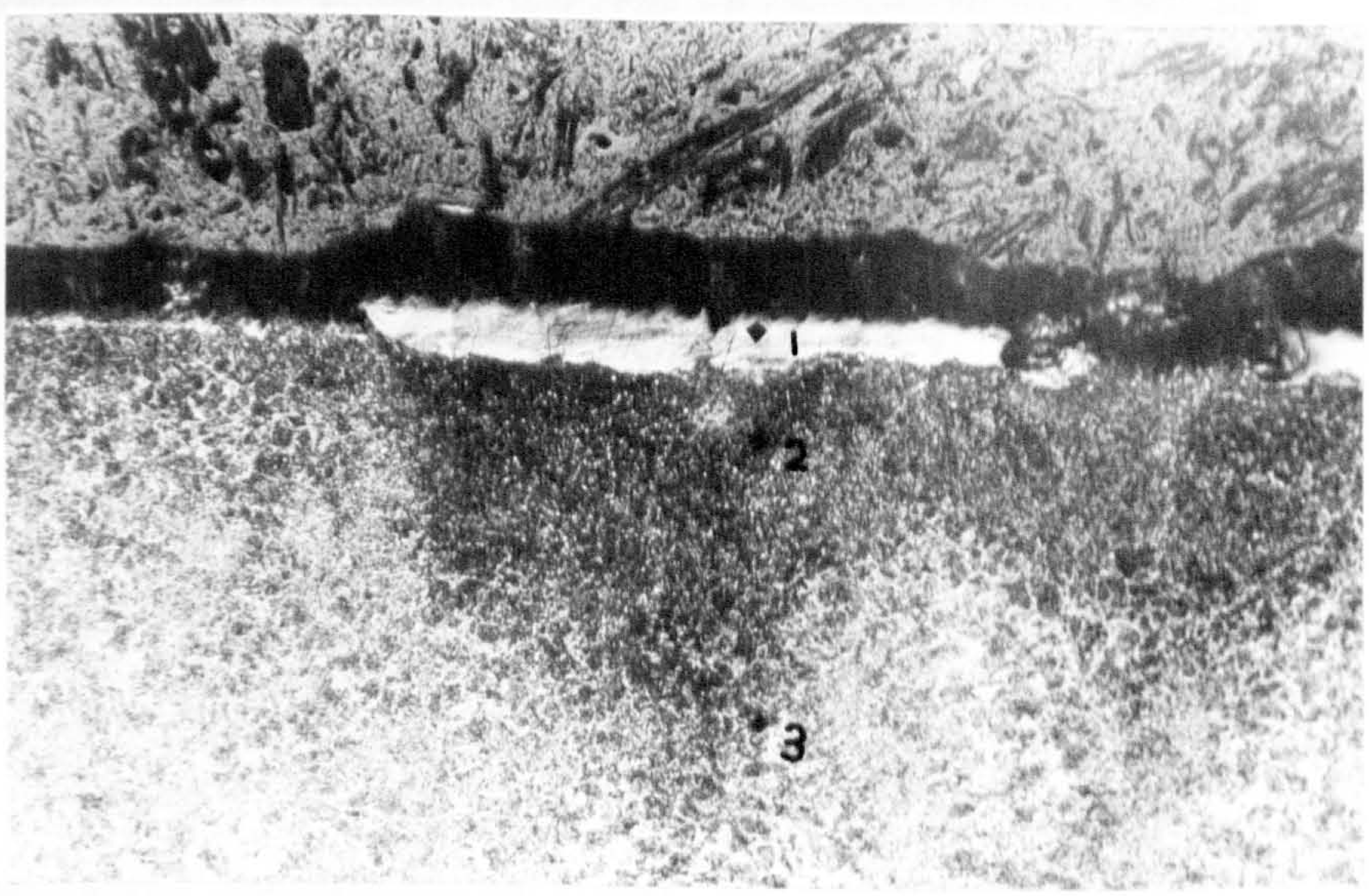

20μm

(b) 200μm

Fig.4.55 Optical microstructure of transverse taper section through worn surface of disc rubbed against <u>gas nitrided</u> BS970,905M39 (EN41B) pin

(a) tested in <u>mild</u> wear regime (sliding speed: 1 $m \cdot s^{-1}$, test load: 10 N)

(b) tested in <u>severe</u> wear regime (sliding speed: 1 $m \cdot s^{-1}$, test load: 160 N). Microhardness results ($Hv_{1.0N}$): 1. Hv 743, 2. Hv 542, 3. Hv 847

relative sliding
direction of pin

→

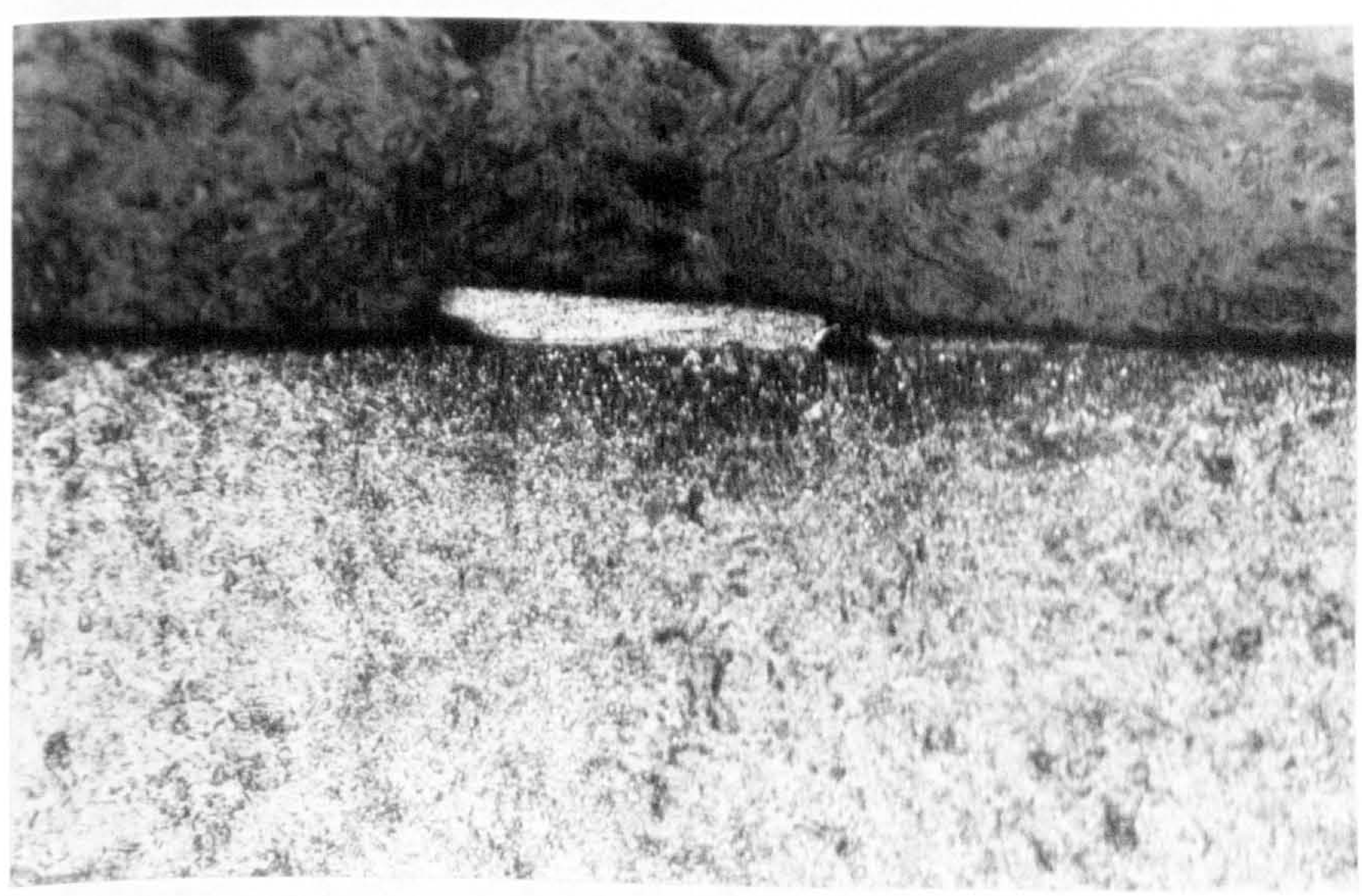

100μm

Fig.4.56 Optical microstructure of longitudinal section normal to worn surface of disc tested against untreated BS970,905M39 (EN41B) pin in extremely-severe wear regime (sliding speed: 1 $m \cdot s^{-1}$, test load: 160 N)

relative sliding
direction of pin

→

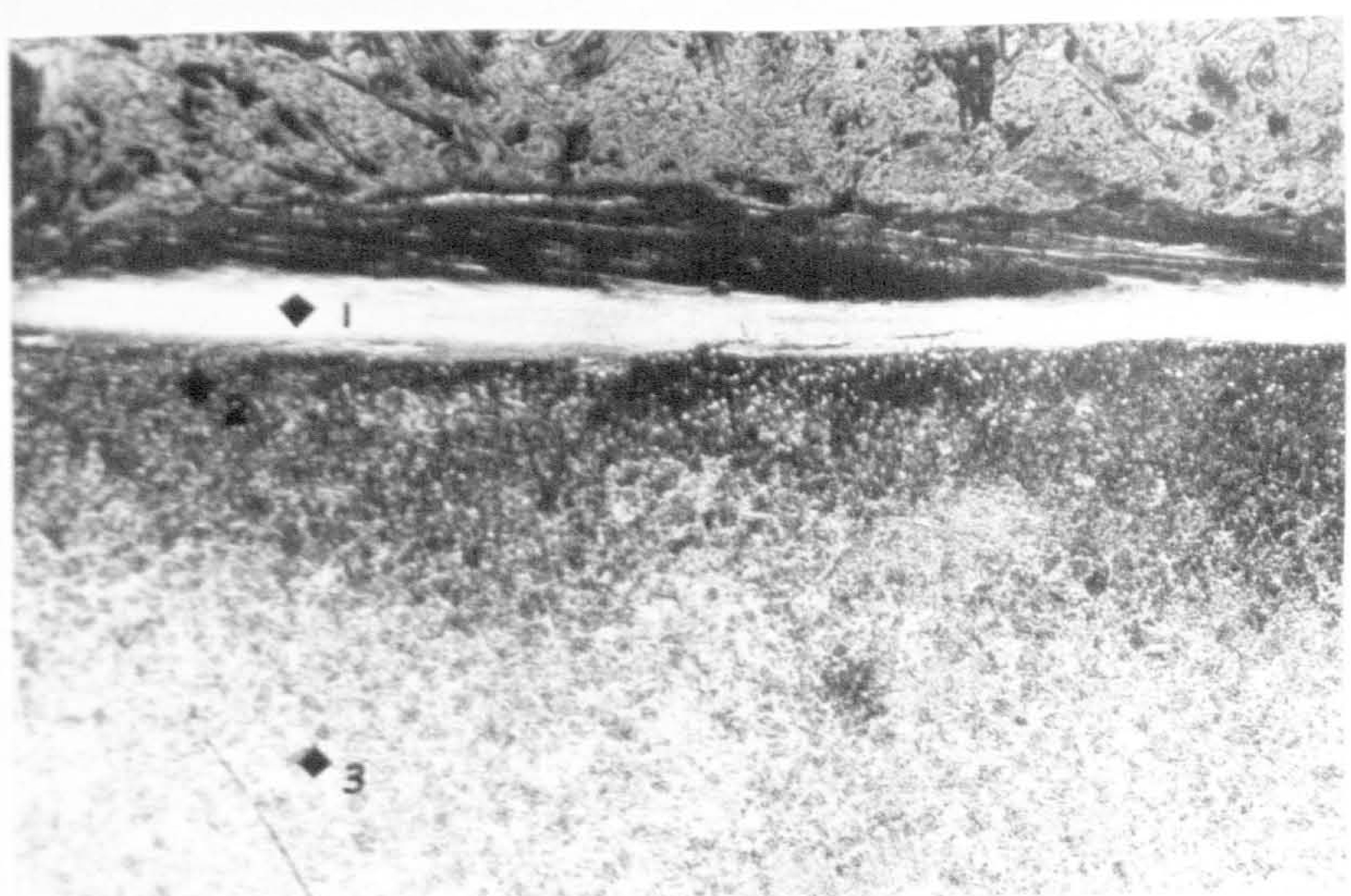

20μm

200μm

Fig.4.57 Optical microstructure of longitudinal taper section through worn surface of disc tested against gas nitrided BS970,905M39 (EN41B) pin in severe wear regime (sliding speed: 1 $m \cdot s^{-1}$, test load: 160 N). Microhardness results ($Hv_{3.0N}$): 1. Hv 720, 2. Hv 627, 3. Hv 786

(a) 5mm

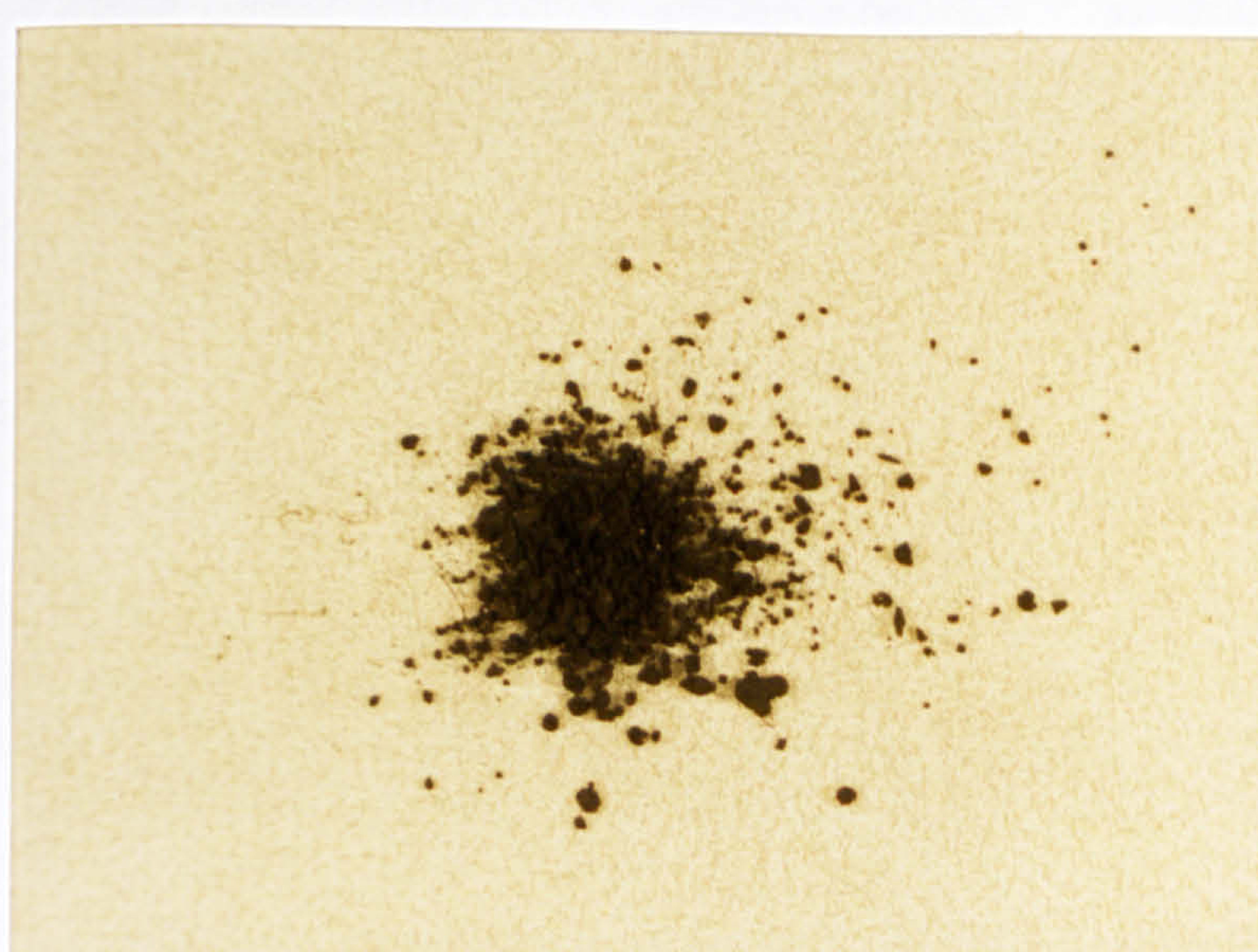

(b) 5mm

Fig.4.58 Macrograph of wear debris produced from untreated BS970,905M39 (EN41B) pin test
(a) generated from mild wear regime (sliding speed: 1 $m \cdot s^{-1}$, test load: 4 N)
(b) generated from severe wear regime (sliding speed: 1 $m \cdot s^{-1}$, test load: 20 N)

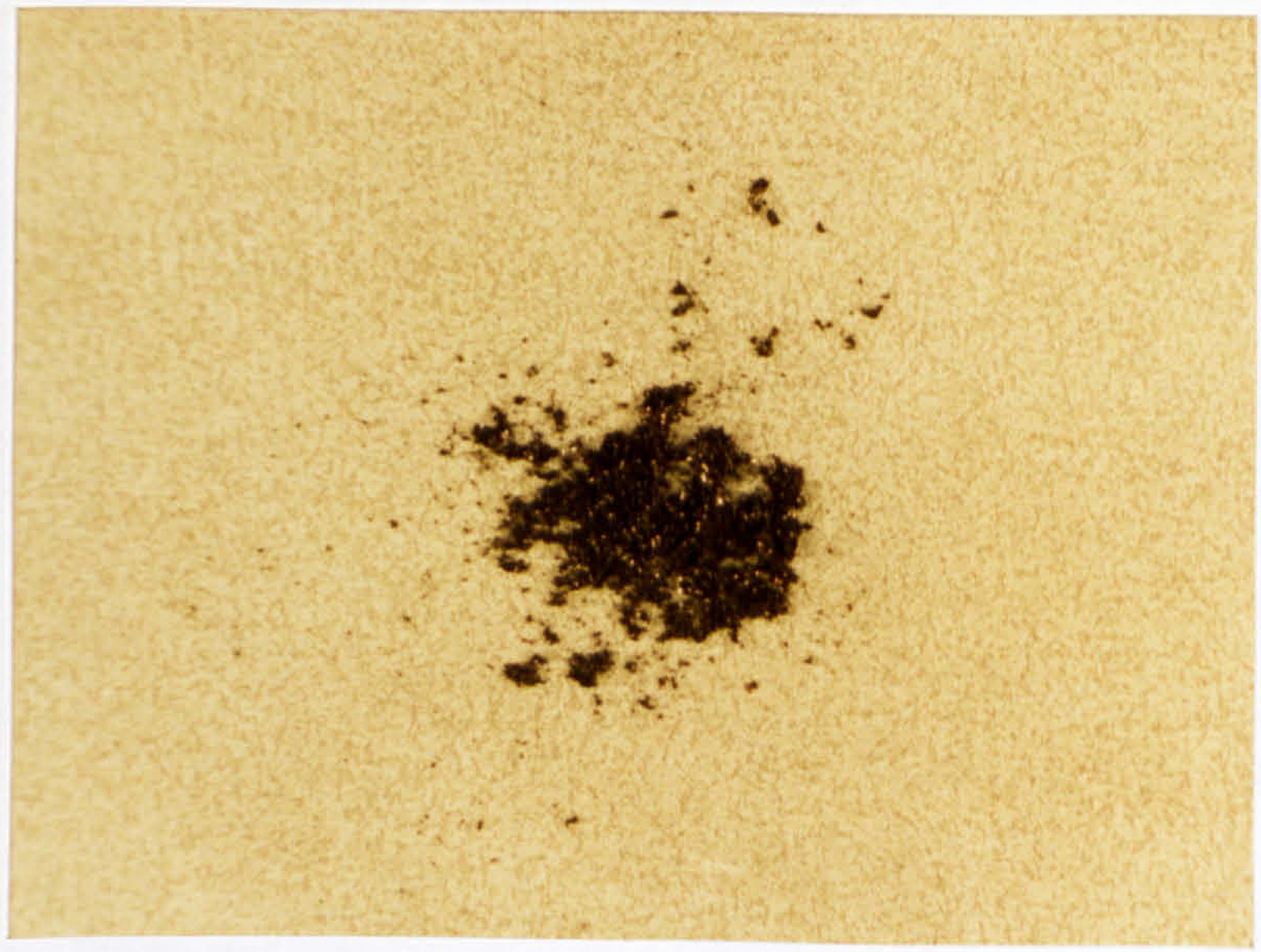

(c) 5mm

(d) 5mm

Fig.4.58 Macrograph of wear debris produced from untreated BS970,905M39 (EN41B) pin test
(c) generated from severe wear regime (sliding speed: 1 $m\cdot s^{-1}$, test load: 80 N)
(d) generated from extremely-severe wear regime (sliding speed: 1 $m\cdot s^{-1}$, test load: 160 N)

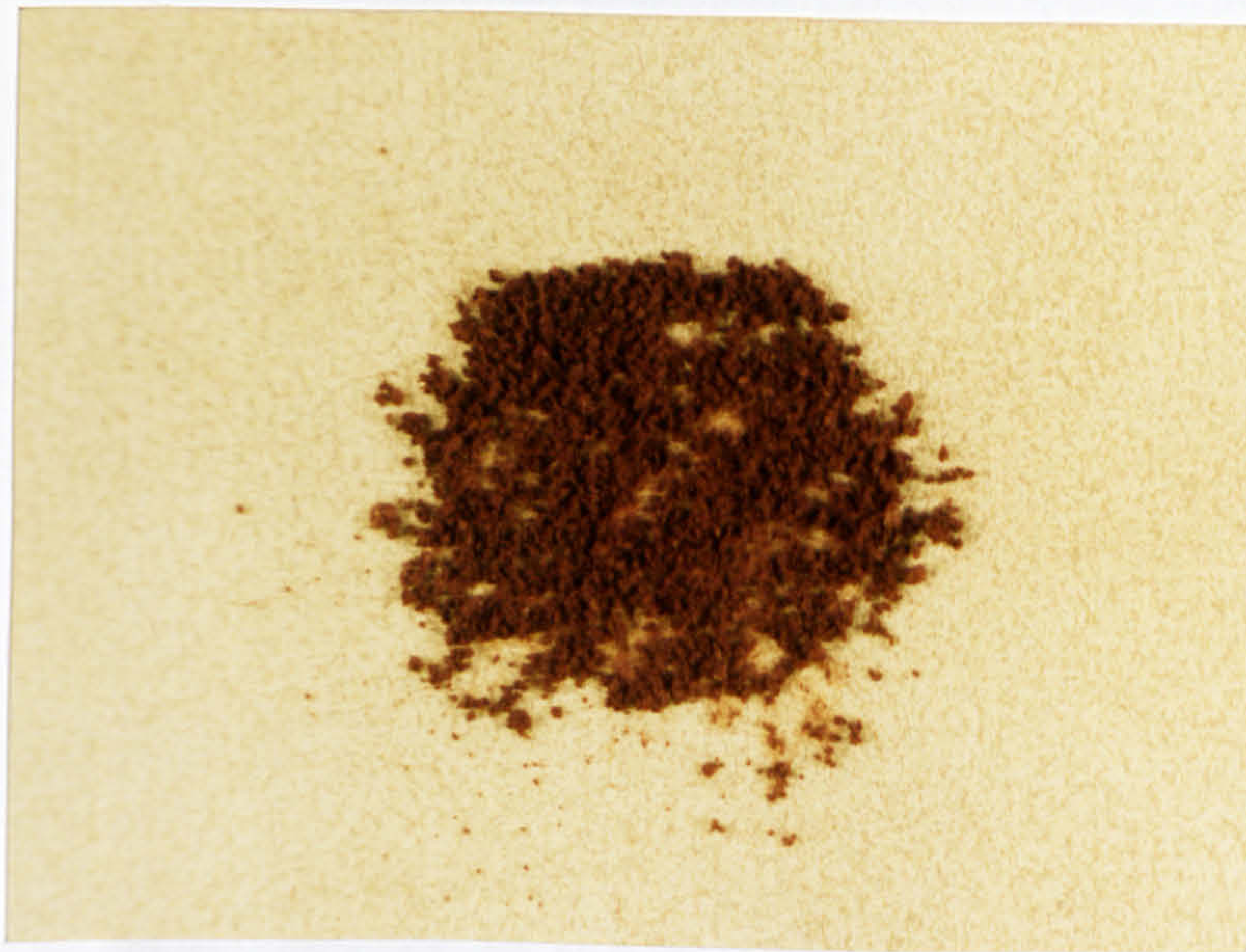

(a) 5mm

(b) 5mm

Fig.4.59 Macrograph of wear debris produced from gas nitrided BS970,905M39 (EN41B) pin test
(a) generated from mild wear regime (sliding speed: 1 $m \cdot s^{-1}$, test load: 10 N)
(b) generated from mild wear regime (sliding speed: 1 $m \cdot s^{-1}$, test load: 40 N)

(c)

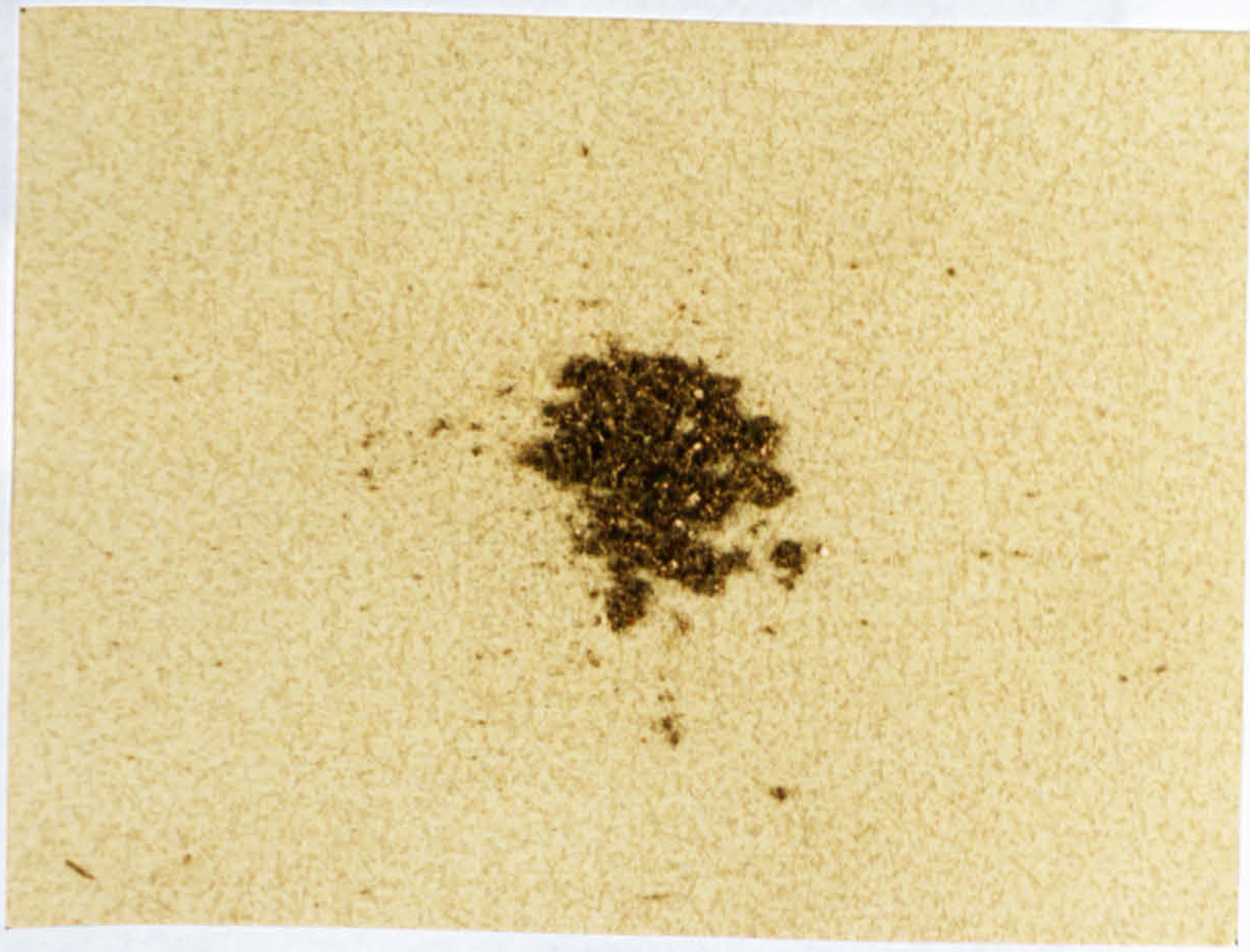

Fig.4.59 Macrograph of wear debris produced from <u>gas nitrided</u> BS970,905M39 (EN41B) pin test
(c) generated from <u>severe</u> wear regime (sliding speed: 1 $m \cdot s^{-1}$, test load: 160 N)

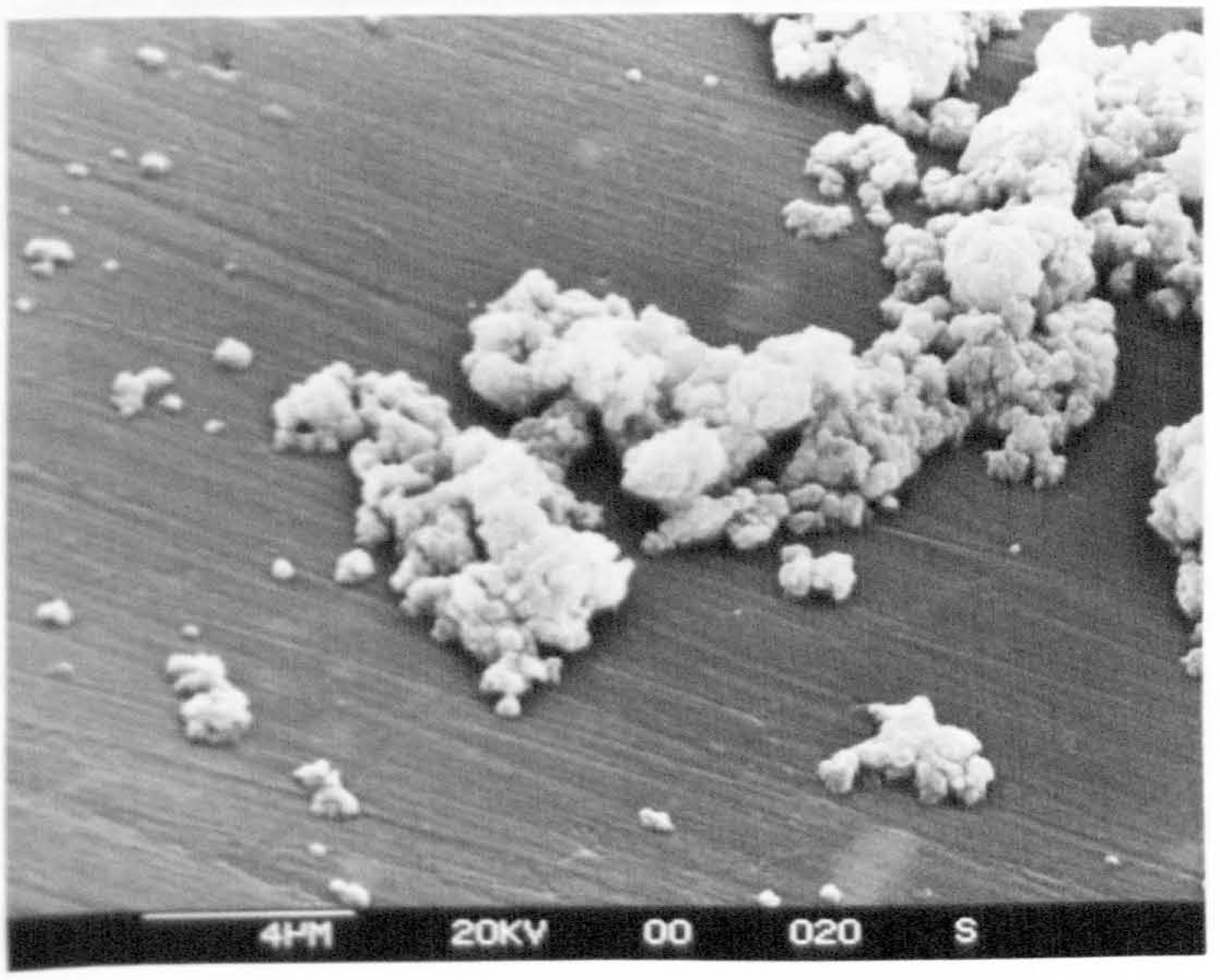

(a)

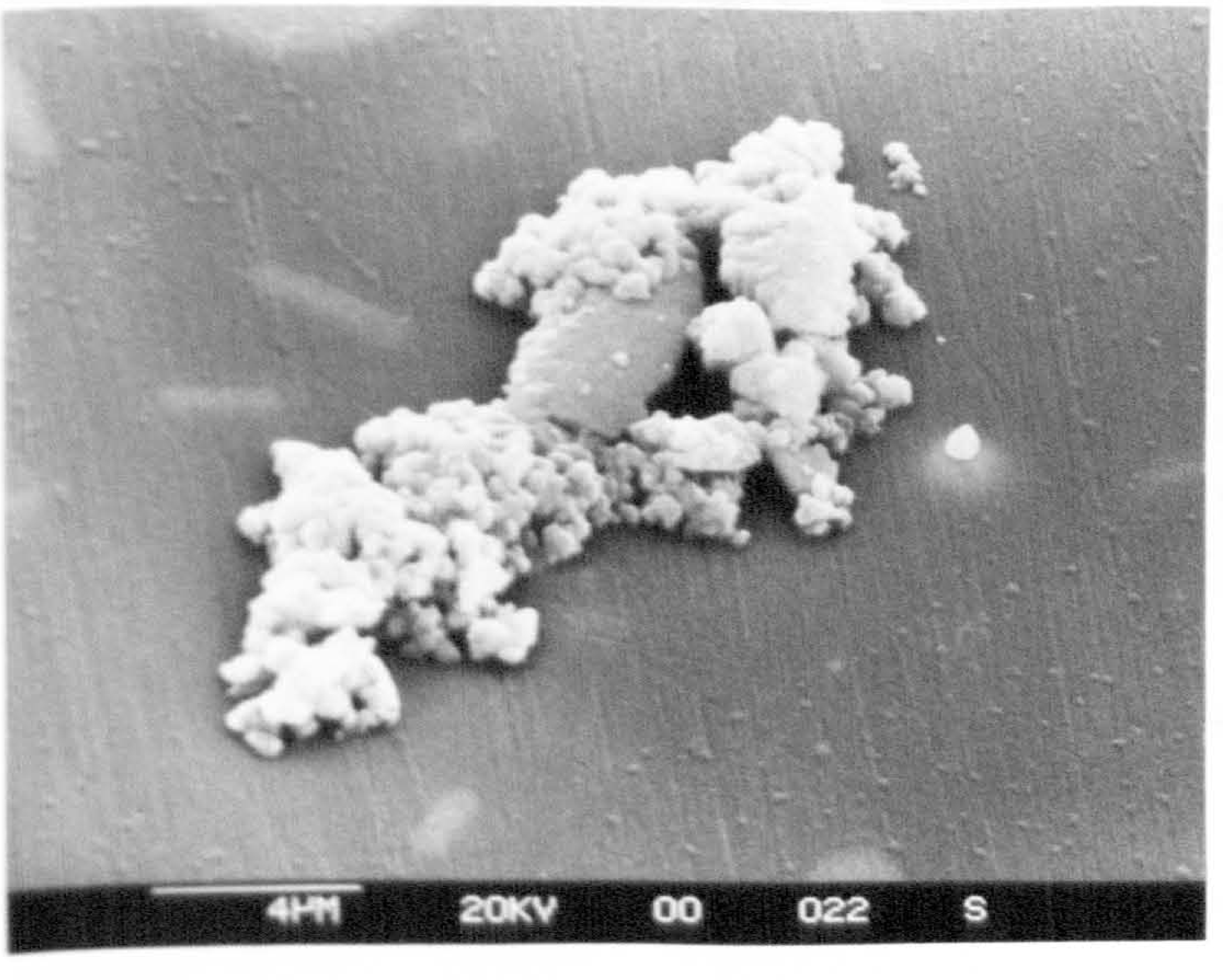

(b)

Fig.4.60 SEM of wear debris produced from untreated BS970,905M39 (EN41B) pin test
(a) generated from mild wear regime (sliding speed: 1 $m \cdot s^{-1}$, test load: 4 N)
(b) generated from severe wear regime (sliding speed: 1 $m \cdot s^{-1}$, test load: 20 N)

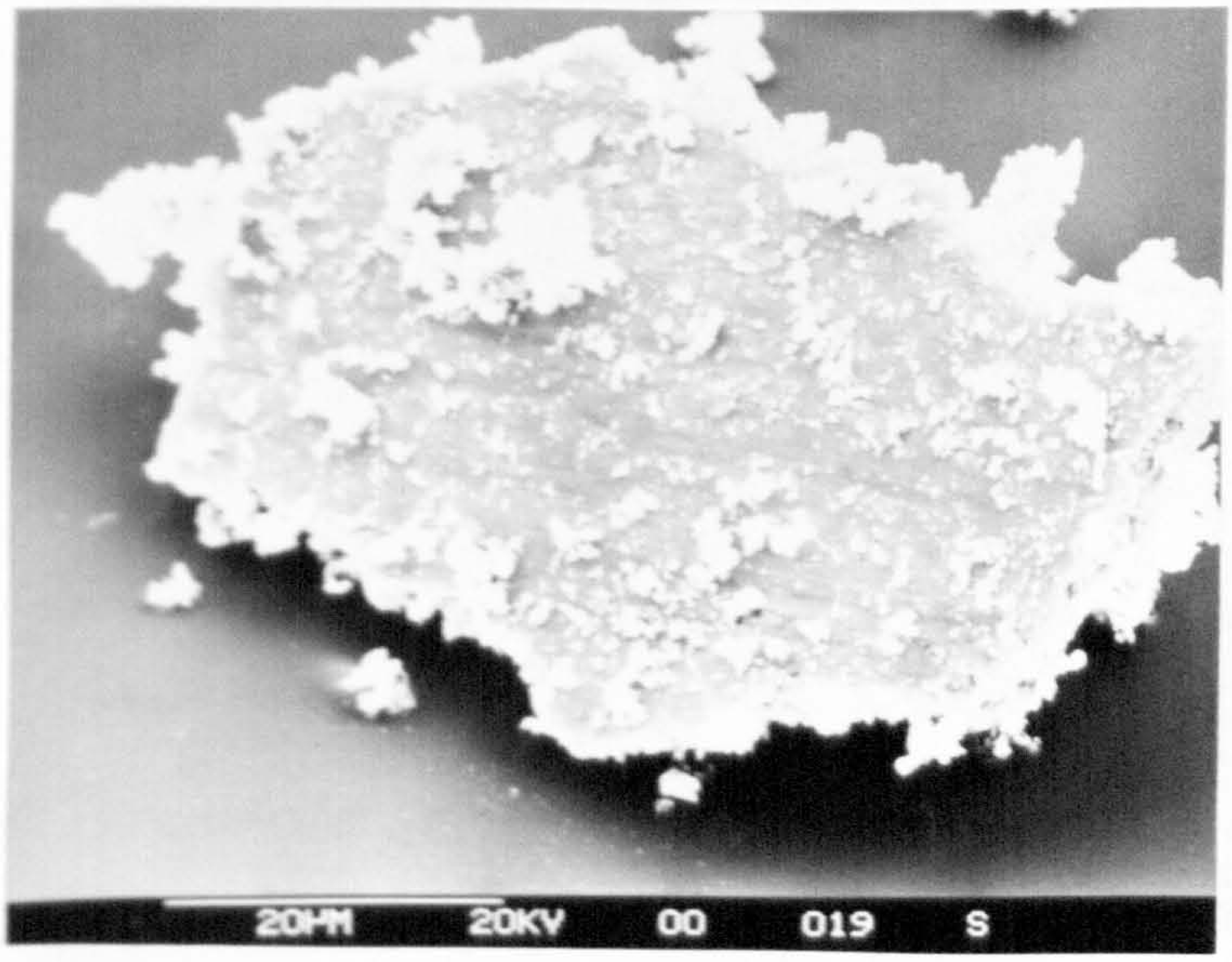

(c)

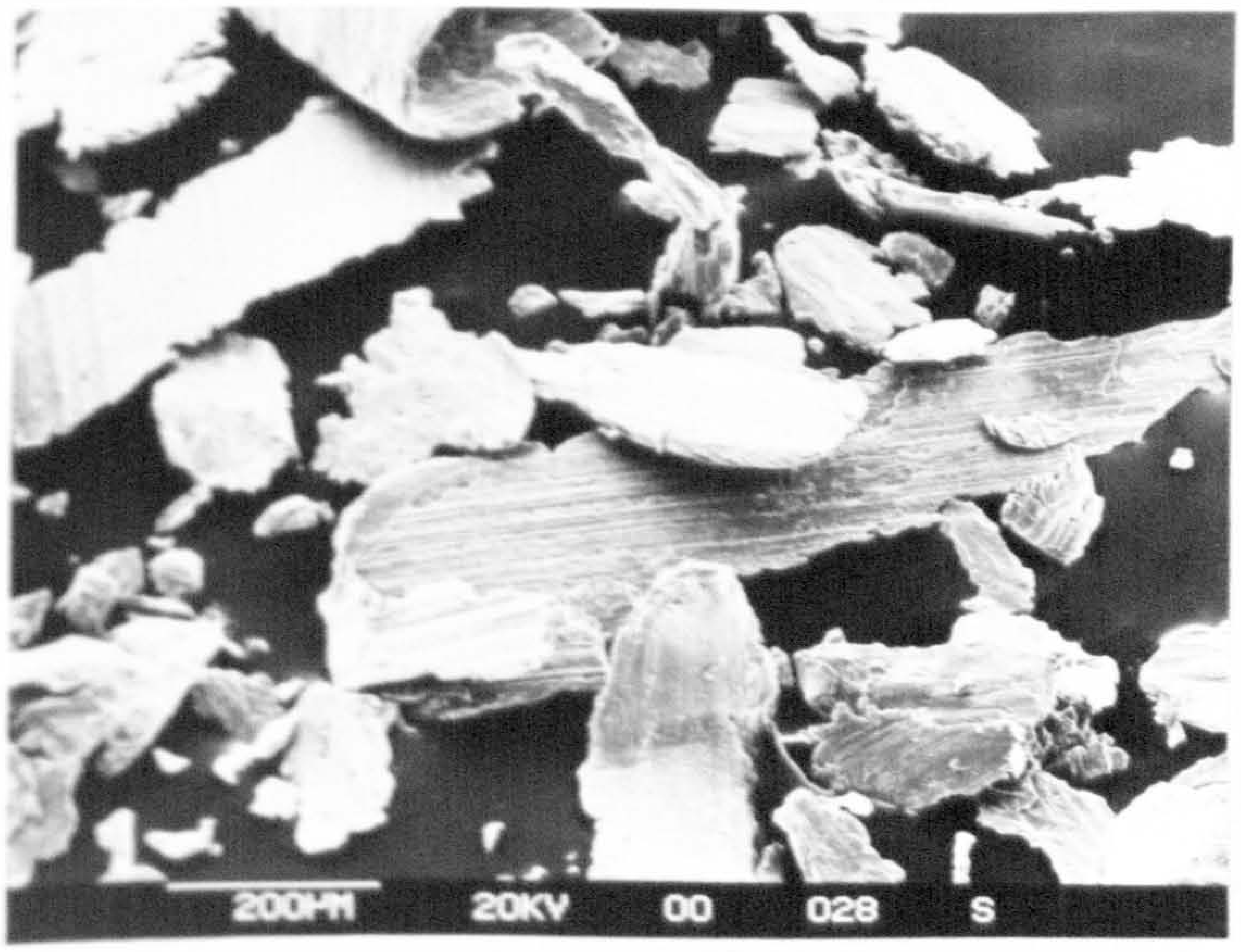

(d)

Fig.4.60 SEM of wear debris produced from untreated BS970,905M39 (EN41B) pin test
(c) generated from severe wear regime (sliding speed: 1 $m \cdot s^{-1}$, test load: 80 N)
(d) generated from extremely-severe wear regime (sliding speed: 1 $m \cdot s^{-1}$, test load: 160 N)

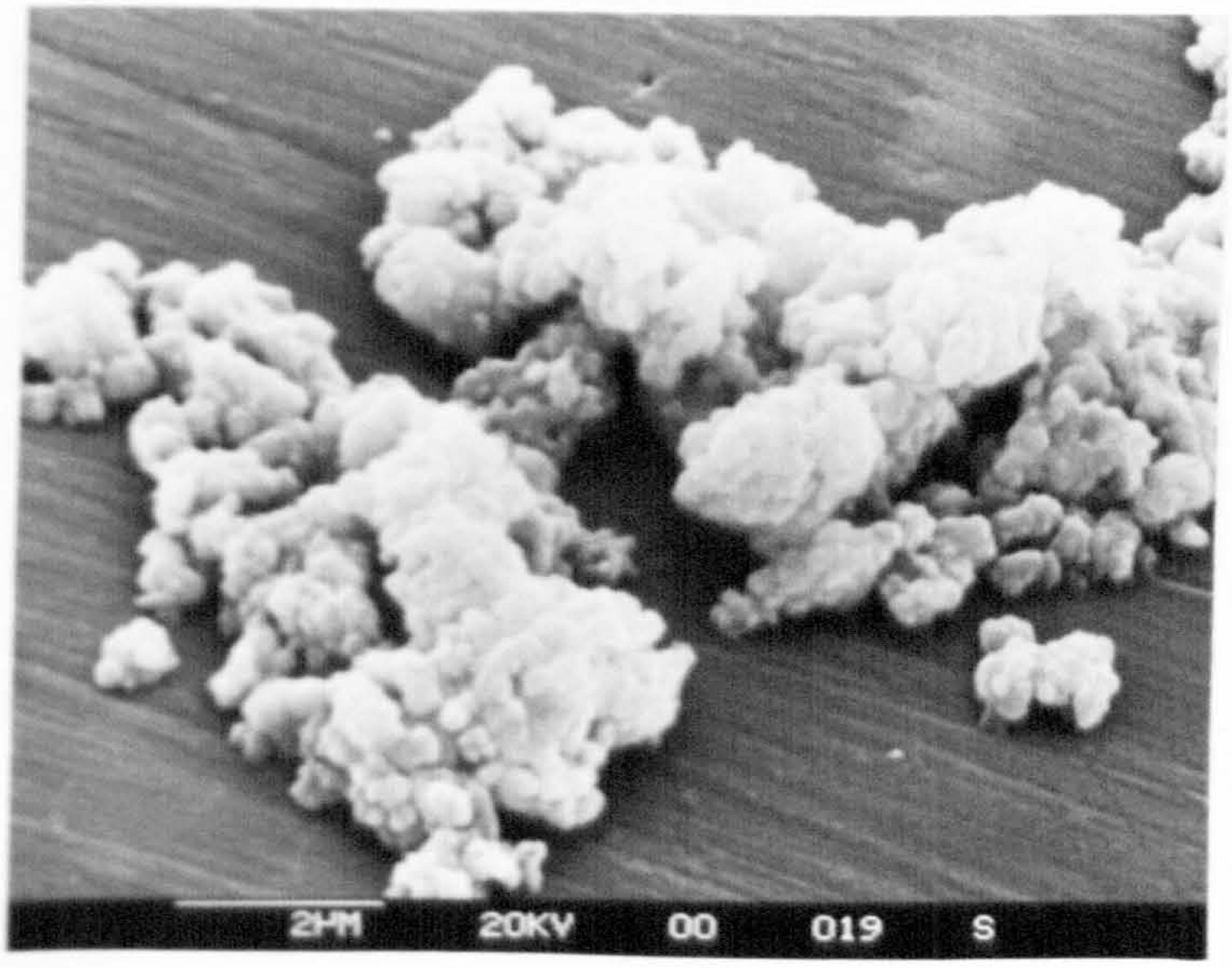

(a)

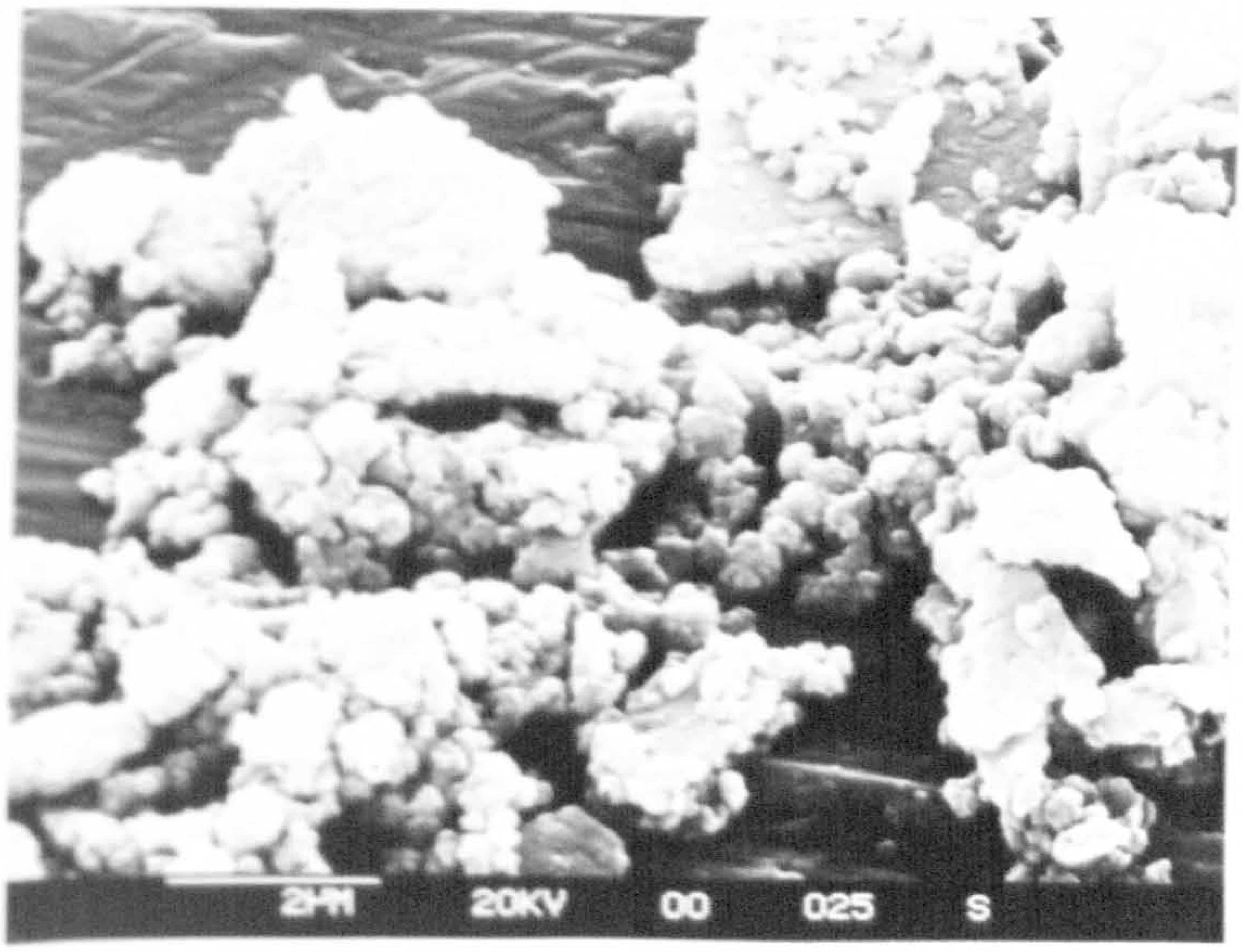

(b)

Fig.4.61 SEM of wear debris produced from <u>gas nitrided</u> BS970,905M39 (EN41B) pin test
(a) generated from <u>mild</u> wear regime (sliding speed: 1 $m \cdot s^{-1}$, test load: 10 N)
(b) generated from <u>mild</u> wear regime (sliding speed: 1 $m \cdot s^{-1}$, test load: 40 N)

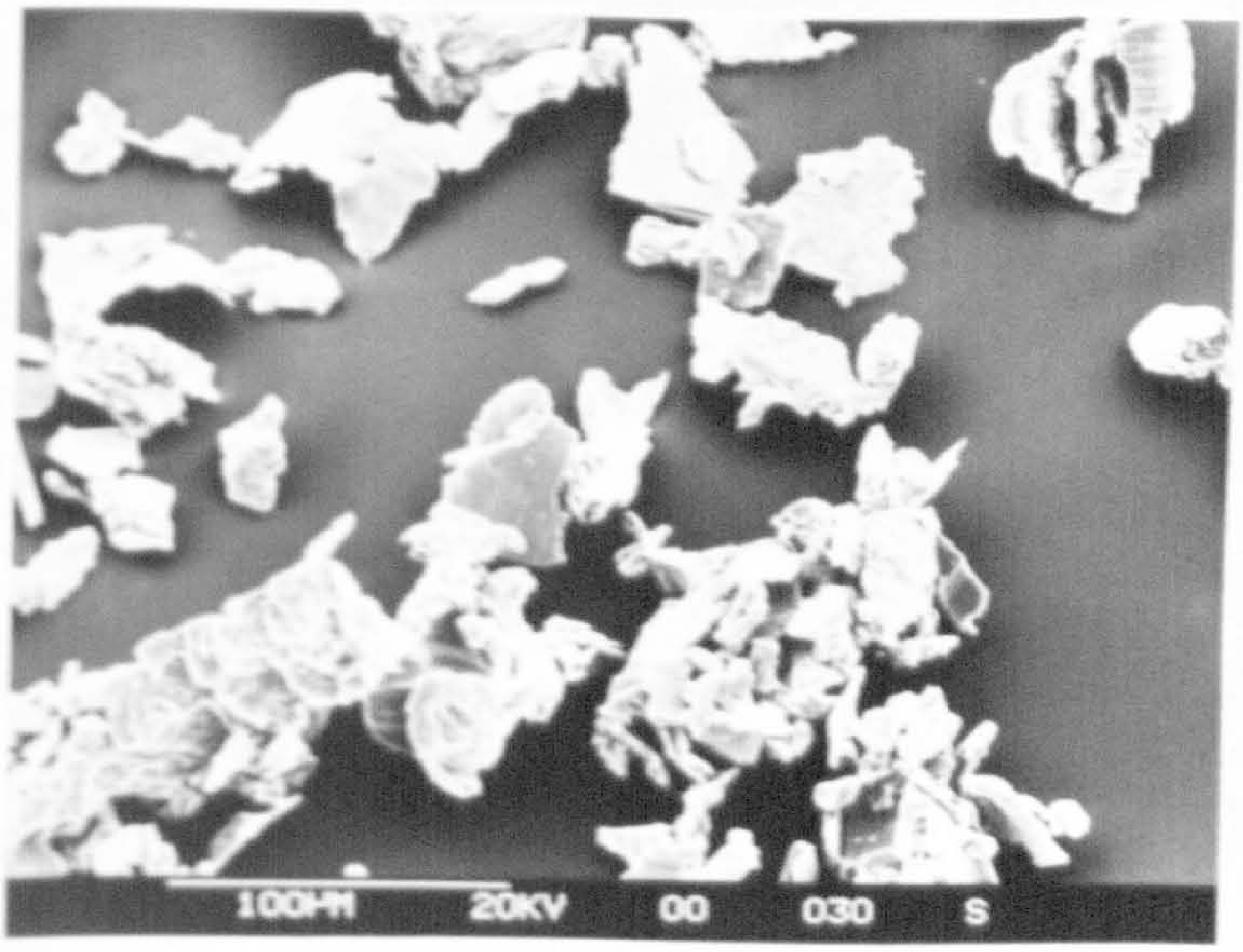

(c)

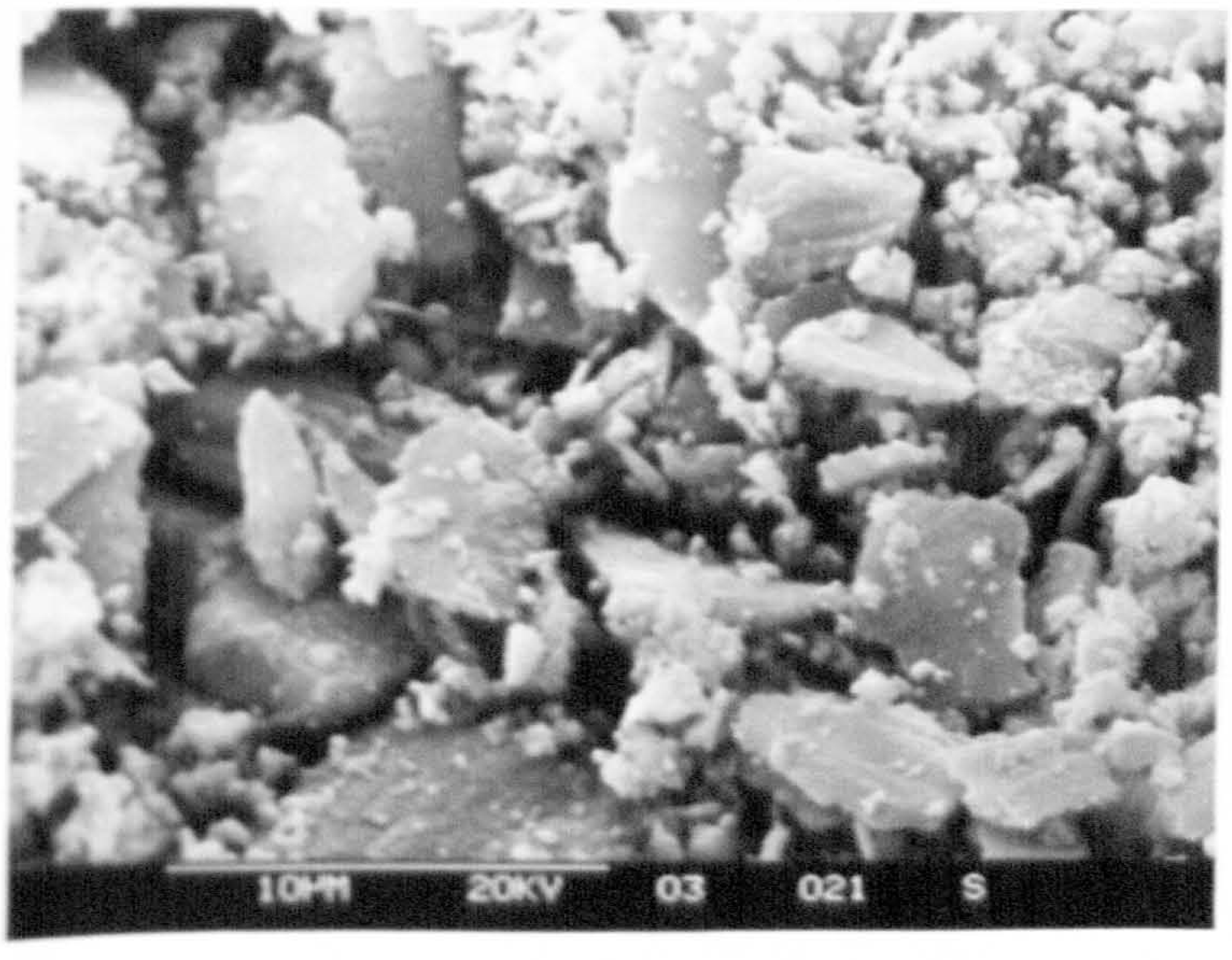

(d)

Fig.4.61 SEM of wear debris produced from gas nitrided BS970,905M39 (EN41B) pin test
(c) generated from severe wear regime (sliding speed: 1 $m \cdot s^{-1}$, test load: 160 N)
(d) The wear test was stopped at a pin wear length within the compound layer depth. (sliding speed: 0.5 $m \cdot s^{-1}$, test load: 10 N, sliding distance: 1800m, pin wear length: 26 μm)

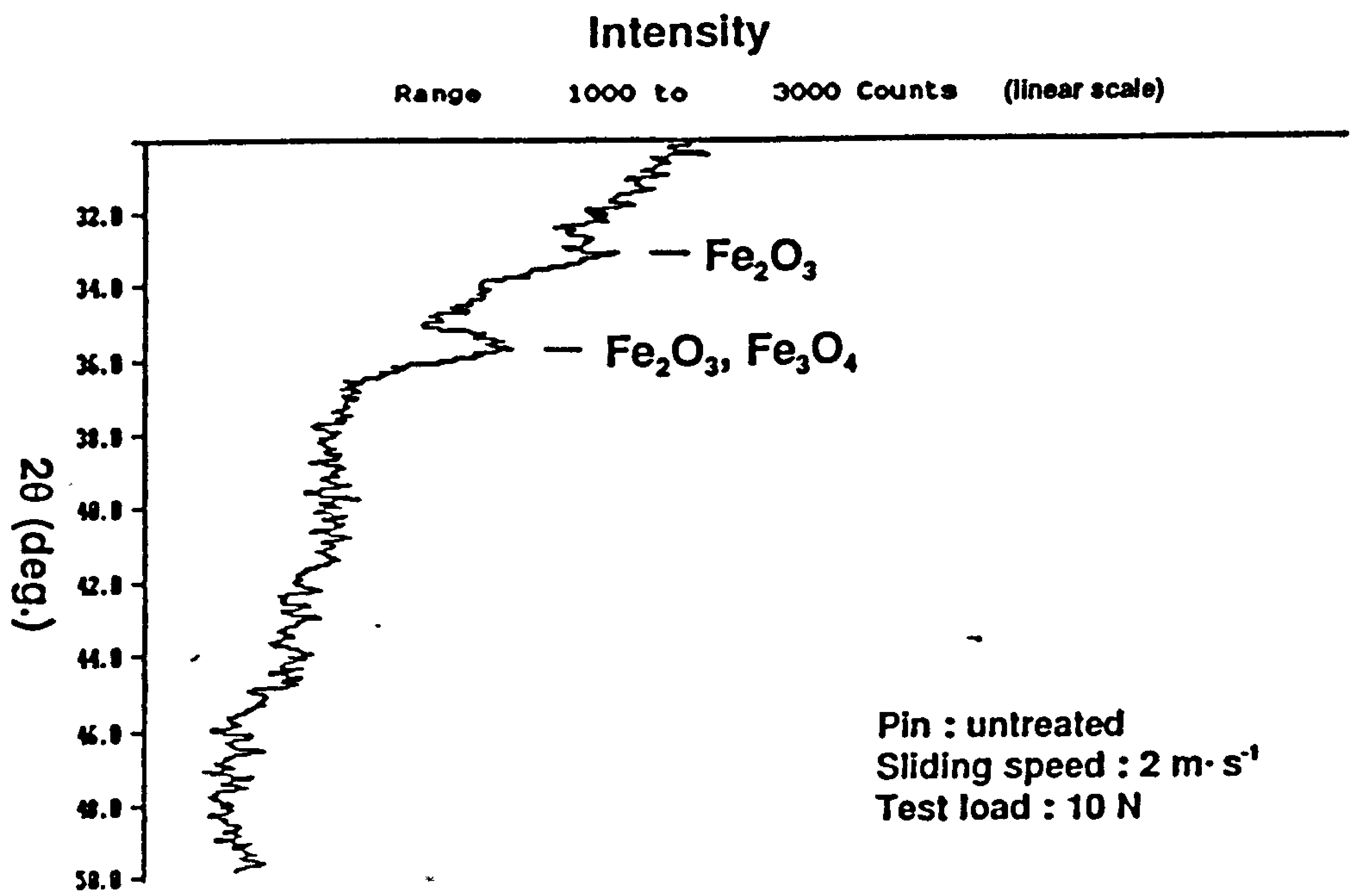

(a)

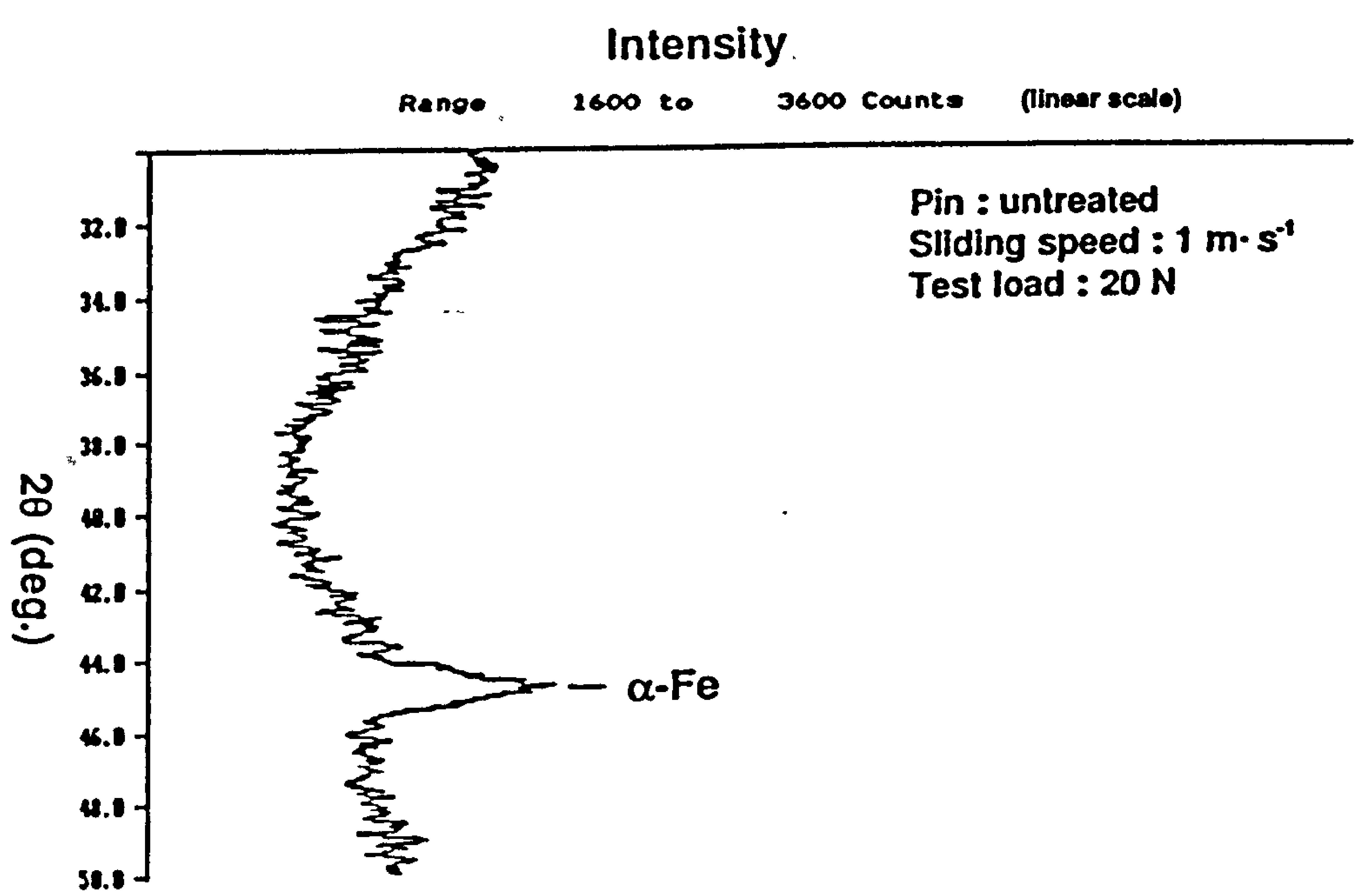

(b)

Fig.4.62 X-ray diffraction diagram of wear debris produced from <u>untreated</u> BS970,905M39 (EN41B) pin test
(a) generated from <u>mild</u> wear regime (sliding speed: 2 m·s^{-1}, test load: 10 N, debris appearance: red powder)
(b) generated from <u>severe</u> wear regime (sliding speed: 1 m·s^{-1}, test load: 20 N, debris appearance: black powder)

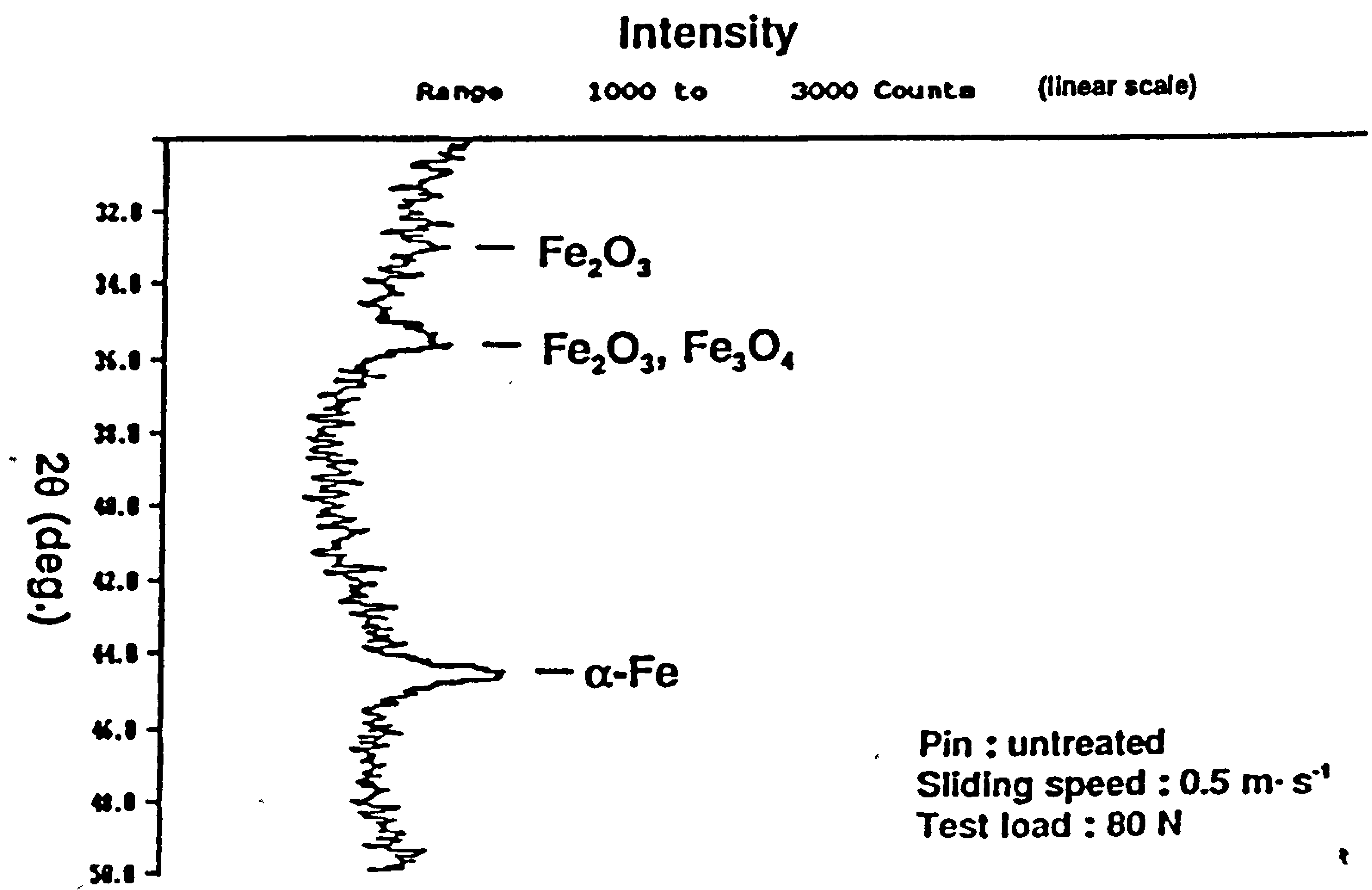

(c)

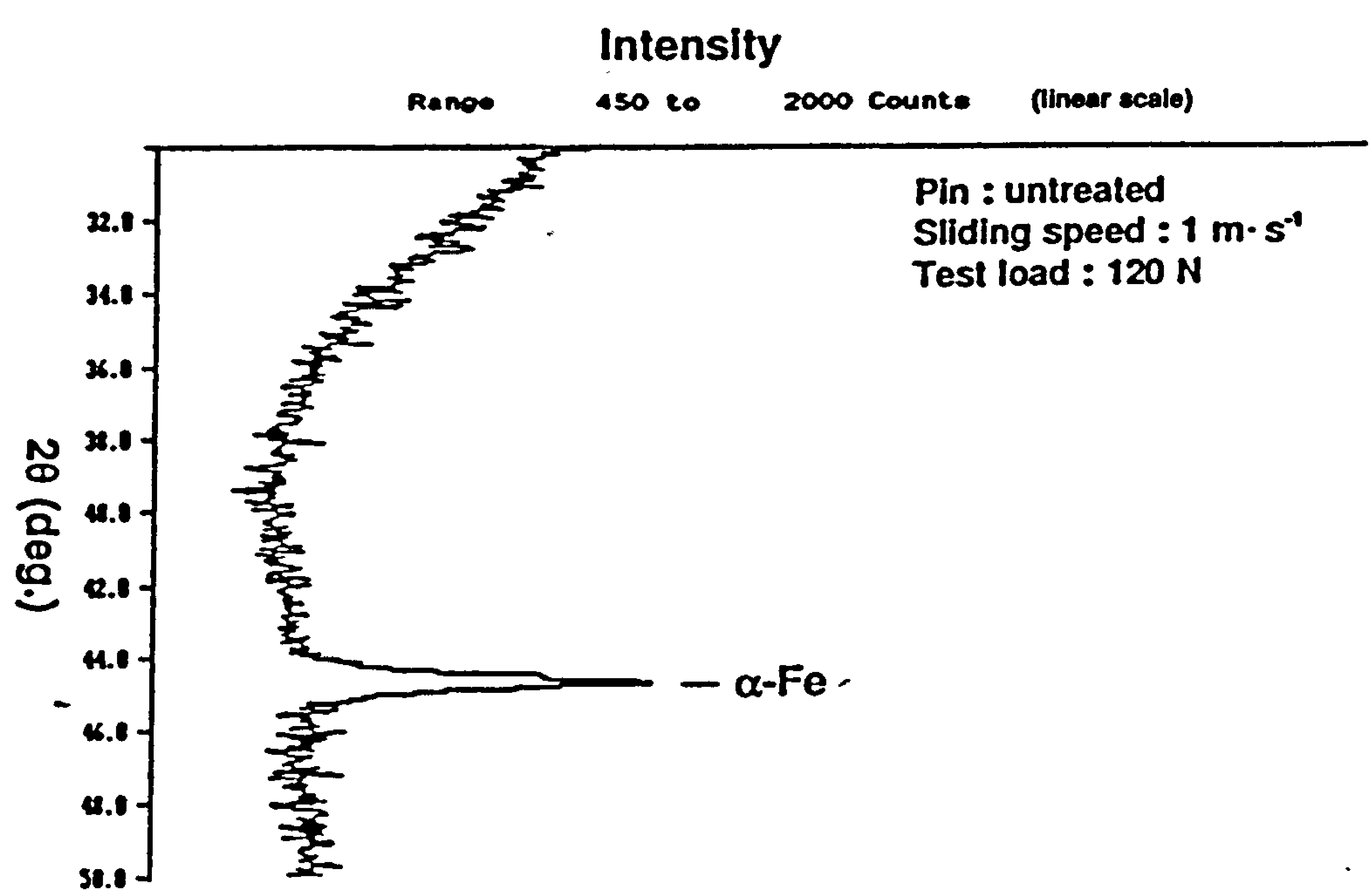

(d)

Fig.4.62 X-ray diffraction diagram of wear debris produced from <u>untreated</u> BS970,905M39 (EN41B) pin test
(c) generated from <u>mild</u> wear regime above T_2 (sliding speed: 0.5 $m \cdot s^{-1}$, test load: 80 N, debris appearance: black powder)
(d) generated from <u>extremely-severe</u> wear regime (sliding speed: 1 $m \cdot s^{-1}$, test load: 120 N, debris appearance: large metallic)

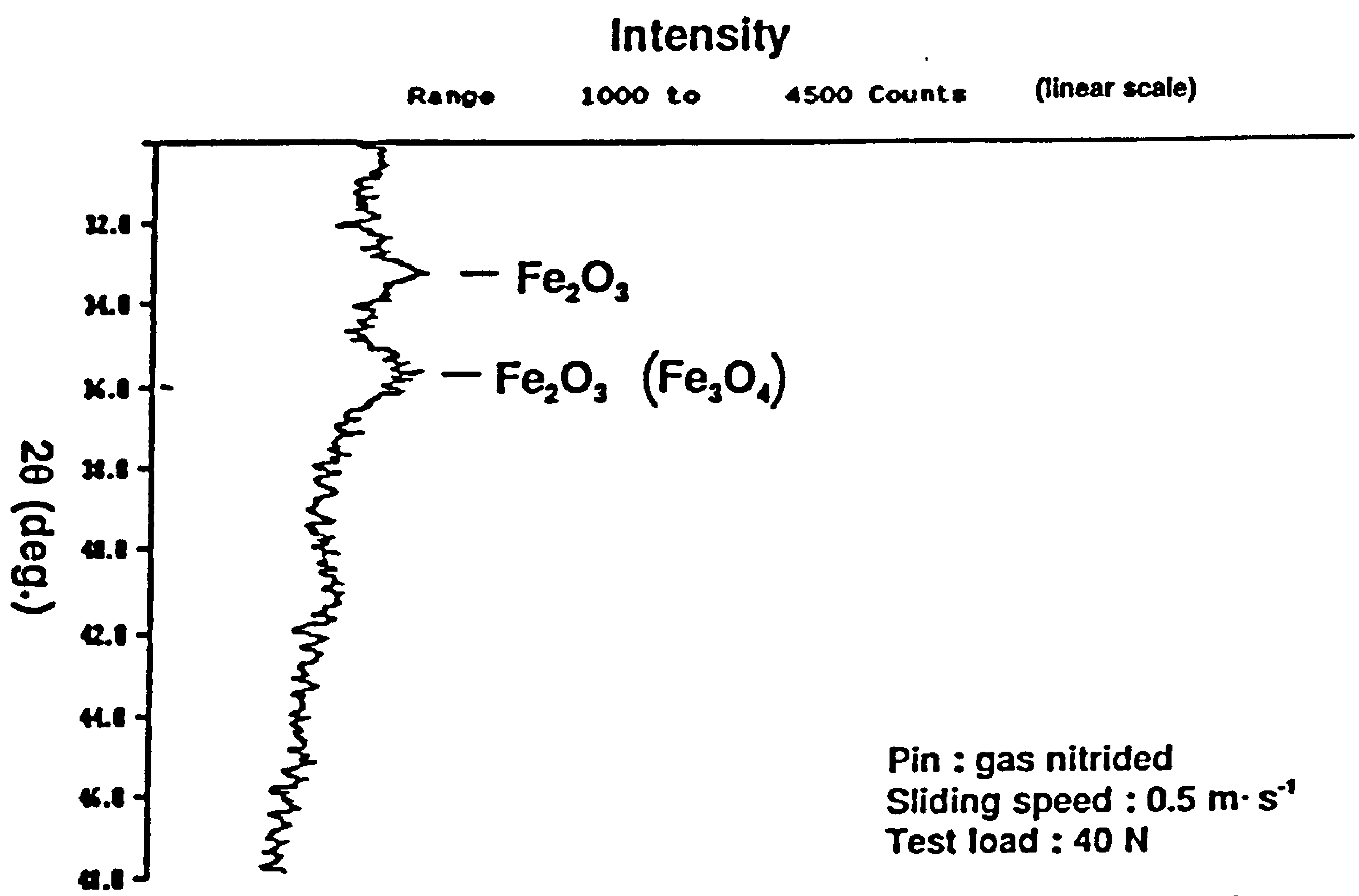

(a)

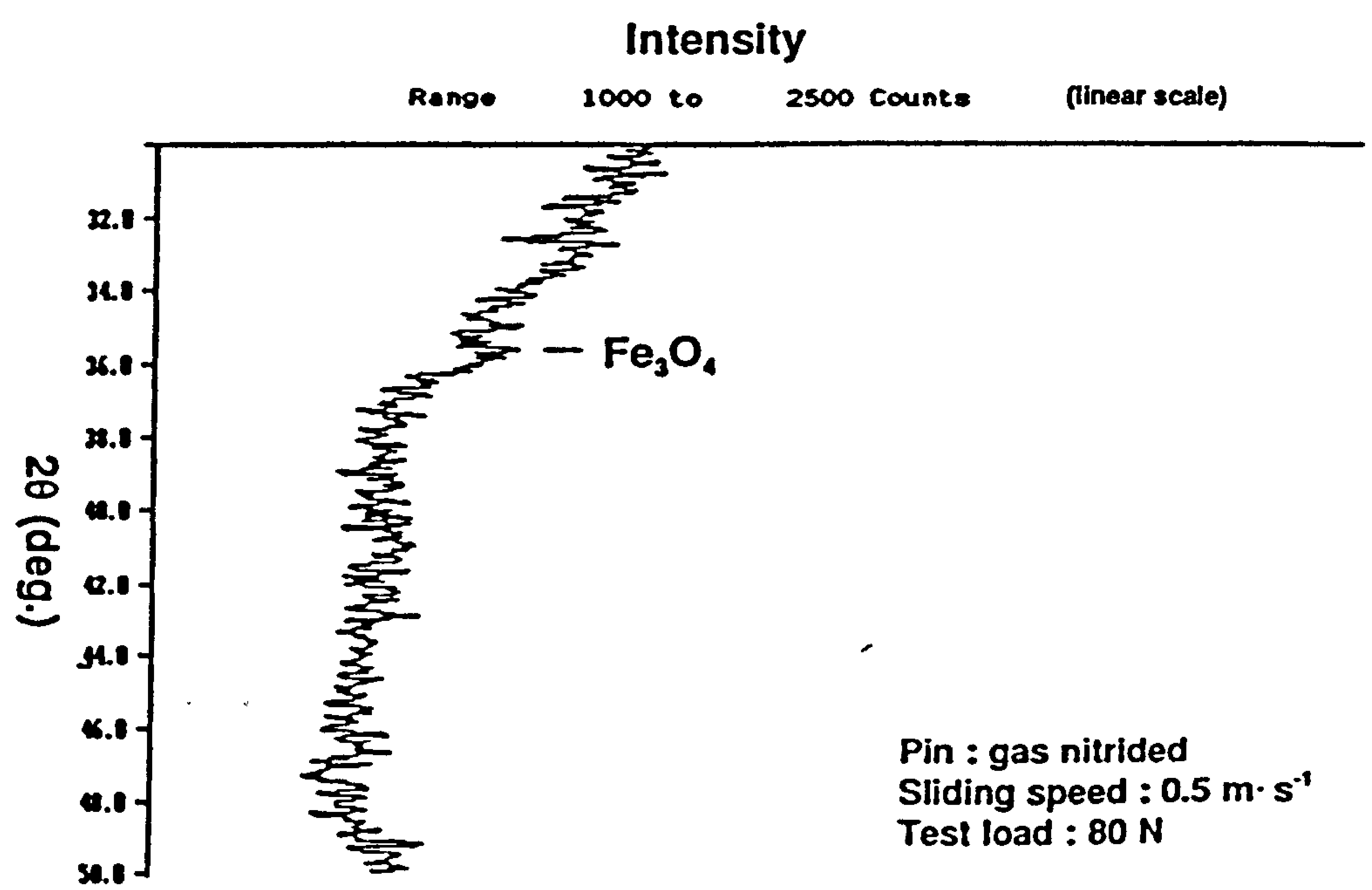

(b)

Fig.4.63 X-ray diffraction diagram of wear debris produced from <u>gas nitrided</u> BS970,905M39 (EN41B) pin test
(a) generated from <u>mild</u> wear regime (sliding speed: 0.5 $m \cdot s^{-1}$, test load: 40 N, debris appearance: red powder)
(b) generated from <u>mild</u> wear regime (sliding speed: 0.5 $m \cdot s^{-1}$, test load: 80 N, debris appearance: black powder)

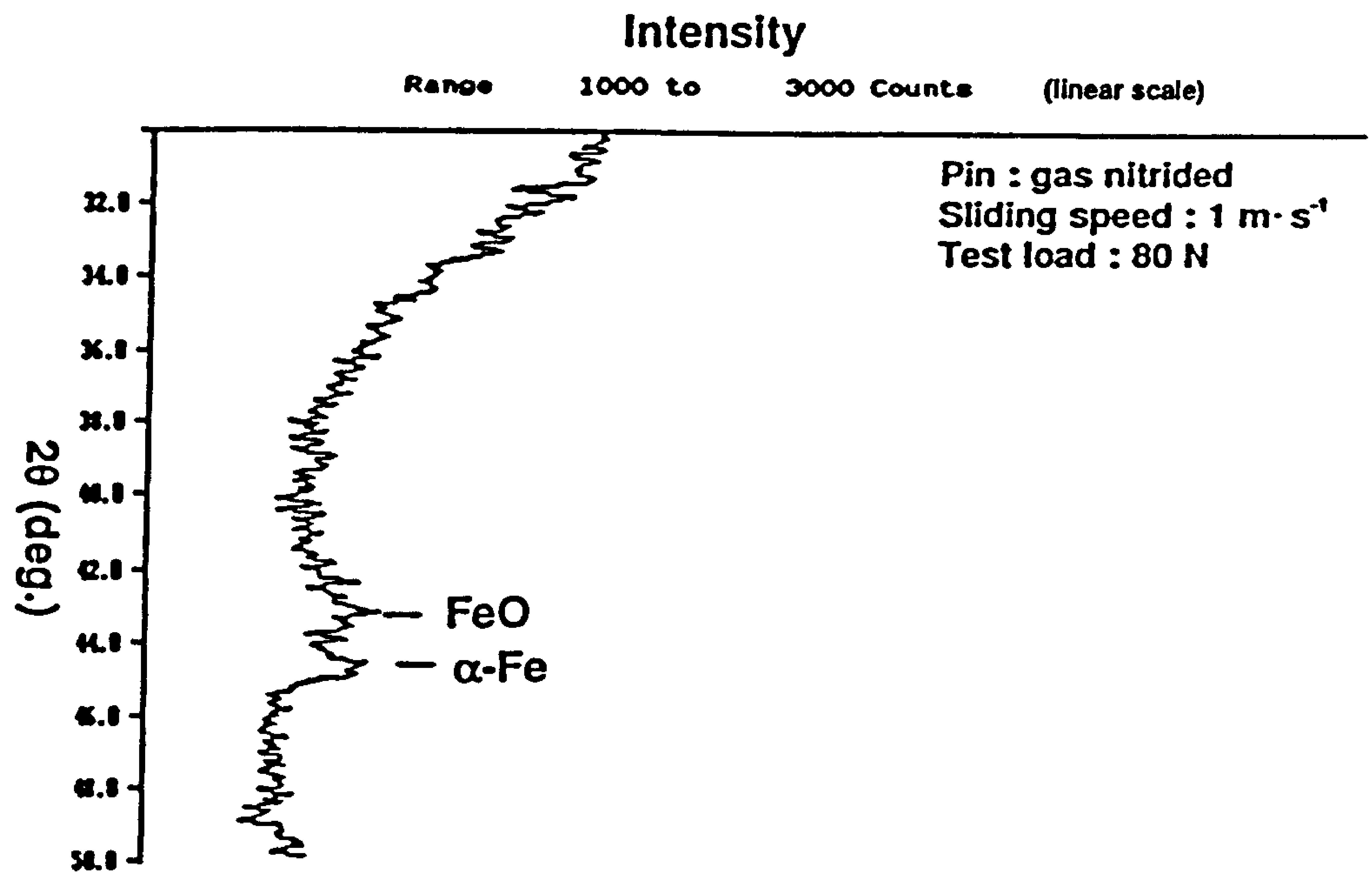

(c)

Fig.4.63 X-ray diffraction diagram of wear debris produced from <u>gas nitrided</u> BS970,905M39 (EN41B) pin test
(c) generated from <u>severe</u> wear regime (sliding speed: 1 $m \cdot s^{-1}$, test load: 80 N, debris appearance: black and metallic particles)

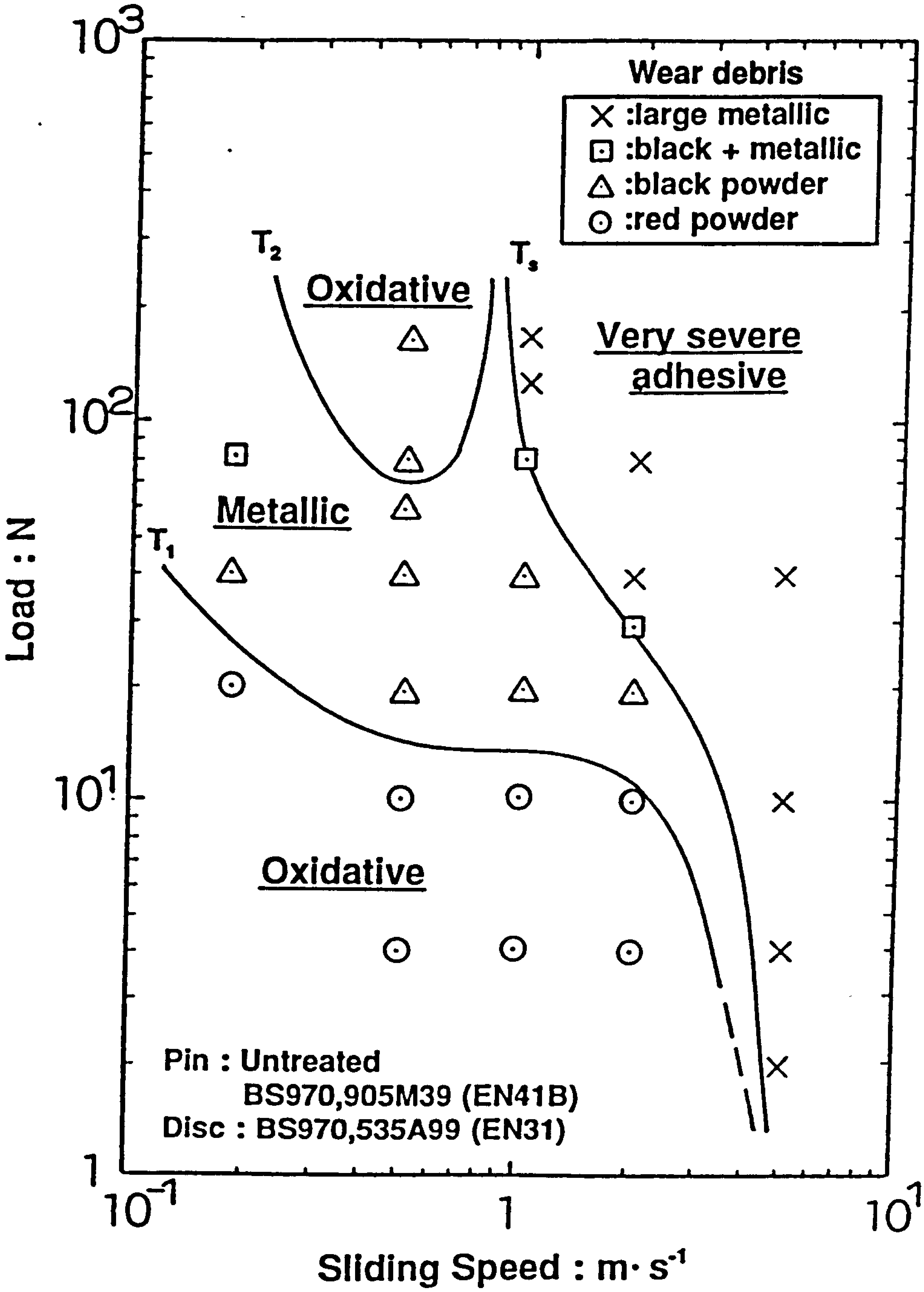

Fig.5.1 (a) Wear map for untreated BS970,905M39 (EN41B)

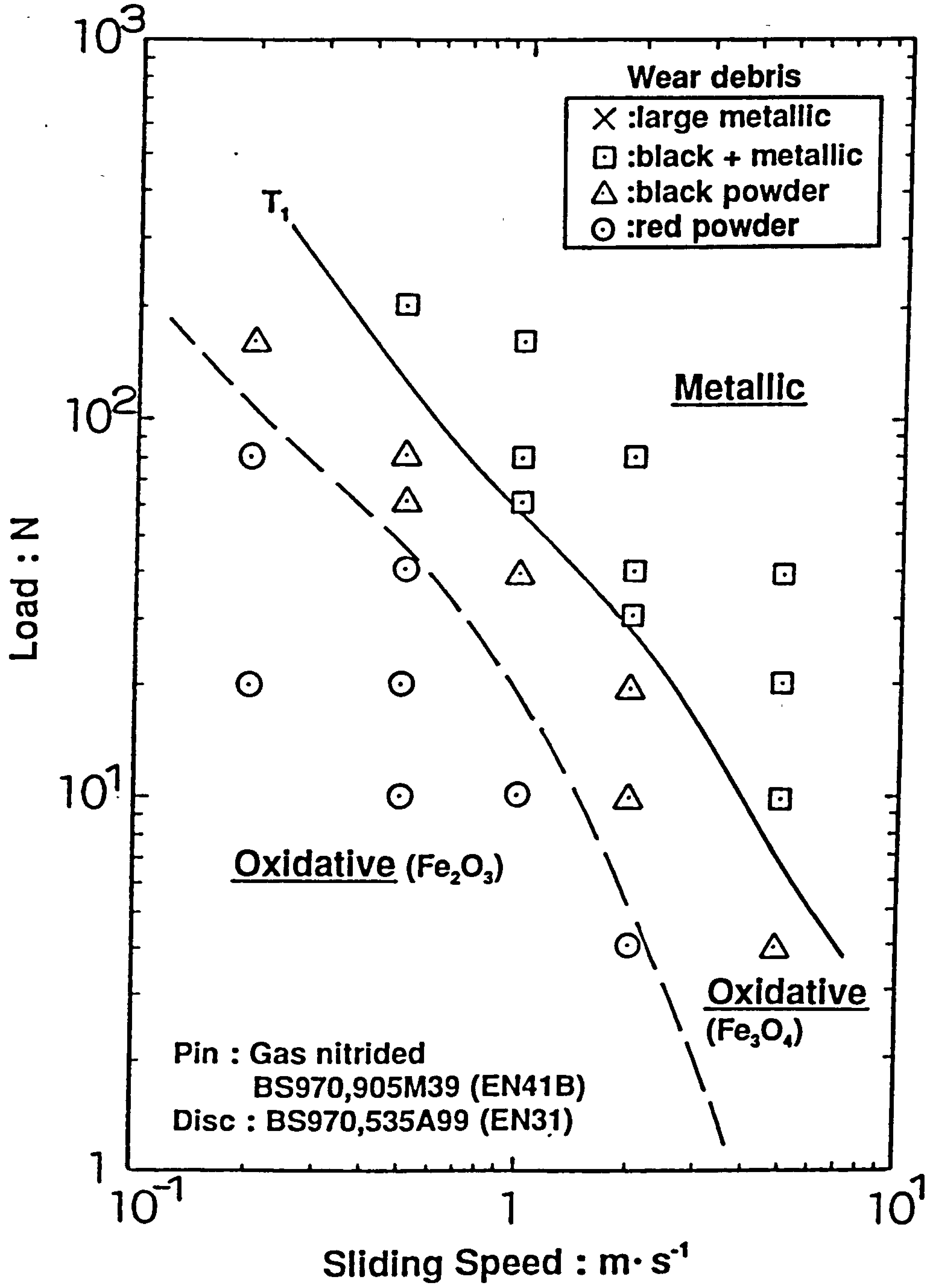

Fig.5.1 (b) Wear map for gas nitrided BS970,905M39 (EN41B)

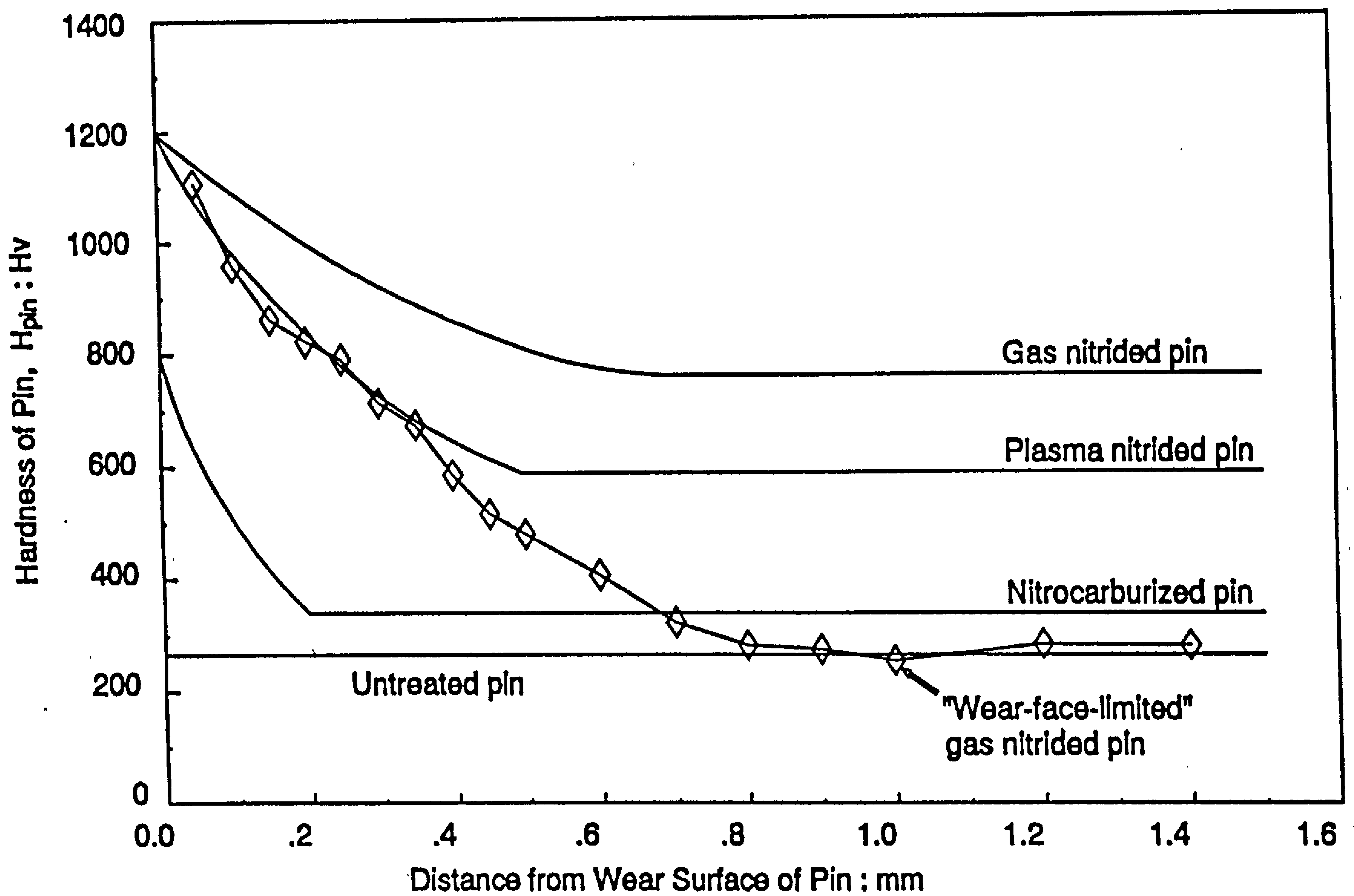

Fig.5.2 Relationship between apparent mean value of hardness of surface treated pin and distance from pin wear surface

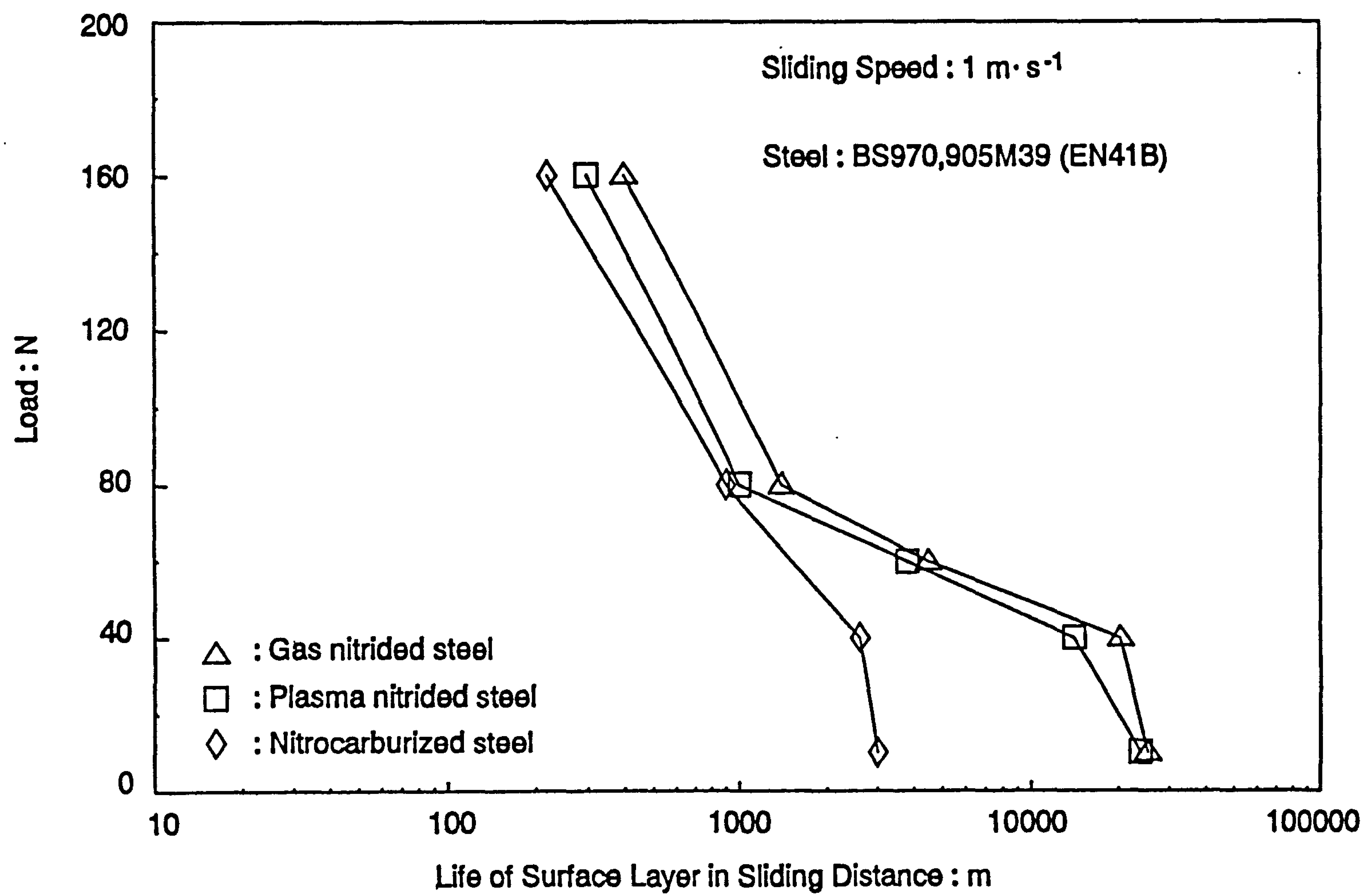

Fig.5.3 Relationship between load and wear life of surface layer (= sliding distance at which the effective case layer was worn away) for variously nitrided BS970,905M39 (EN41B) steels (sliding speed: 1 $m \cdot s^{-1}$)